Deciphering the Contribution of RhoGTPases Dependent Signaling Pathways to the Collective Invasion of Colorectal Carcinoma

Fotine Libanje

université
PARIS-SACLAY

NNT : 2017SACLS503

THESE DE DOCTORAT
DE
L'UNIVERSITE PARIS-SACLAY
PREPAREE A
L'UNIVERSITE PARIS-SUD

ECOLE DOCTORALE N° 582
CBMS Cancérologie : biologie - médecine - santé

Spécialité de doctorat : Aspect moléculaire et cellulaire de la biologie

Par

Mme Fotine LIBANJE

Deciphering the contribution of Rho-GTPases dependent signaling pathways to the collective invasion of colorectal carcinoma

Etude de la contribution des voies de signalisation dépendantes des Rho-GTPases à l'invasion collective des carcinomes colorectaux

Thèse présentée et soutenue à Villejuif, le 8.12.17 :

Composition du Jury :

Dr, Boucheix, Claude	Directeur de Recherche, Institut Andre Lwoff	Président du Jury
Dr, Etienne-Manneville, Sandrine	Directrice de Recherche, Institut Pasteur	Rapportrice
Dr, Wang, Xiaobo	Chargé de Recherche, Centre de Biologie	Rapporteur
Dr, Matic Vignjevic, Danijela	Directrice de Recherche, Institut Curie	Examinatrice
Dr, Jaulin, Fanny	Chargée de Recherche, Gustave Roussy	Directrice de thèse
Dr, Bertoglio, Jacques	Chercheur Emerite, Gustave Roussy	Co-directeur de thèse

A Félicien LIBANJE, 14 Février 2017

Je souhaite adresser mes sincères remerciements aux membres de mon jury de thèse :

Le Dr Claude Boucheix pour avoir accepté de présider le jury.

Le Dr. Sandrine Etienne-Manneville, le Dr. Daniela Vignjevic-Matic et le Dr. Wang Xiaobo pour avoir accepté d'être rapporteur et examinateur de ma thèse et de prendre le temps de lire et juger mon manuscrit et mon travail de thèse.

Je suis honorée de votre participation à la finalisation de mon travail de thèse.

I would like to sincerely thank the members of my thesis committee :

The Dr. Claude Boucheix for accepting to chair the committee.

The Dr. Sandrine Etienne-Manneville, the Dr. Vignjevic-Matic Daniela and the Dr. Wang Xiaobo for agreeing and devoting time to the task of reviewing my thesis manuscript and my PhD work.

I am grateful for your contribution to the completion of my PhD work.

Je souhaite remercier ma directrice de thèse, le Dr. Fanny Jaulin, pour m'avoir accueillie dans son laboratoire et m'avoir donnée l'opportunité de réaliser ce travail de thèse. Cette expérience a été riche autant au point de vue scientifique qu'au point de vue personnelle.

Je souhaite remercier le Dr. Jacques Bertoglio pour avoir accepté de co-diriger mon travail de thèse.

Je remercie les membres actuels du Laboratoire le Dr. Joel Raingeaud et Zajac Olivier et Charlotte Canet Jourdan, et les anciens membres qui ont contribué à la conduite de mon travail de thèse.

Je remercie mes collaborateurs, dont les membres de l'équipe du Dr. Geri Kreitzer.

J'adresse ma profonde gratitude à Olivier Zajac, Nadia Elkhatib, Francesco Baschieri, Enzo Bresteau, Joel Raingeaud et Charlotte Canet-Jourdan sans qui ce manuscrit n'aurait jamais vu le jour.

Abbreviations

2D	Two dimensions
3D	Three dimensions
ADAMs	A disintegrin and metalloproteinase
ADF	Actin-Depolymerising Factor
AGC	Protein kinase A, G, and C families
AJ	Adherens Junctions
AJC	Apical Junctionnal Complex
ANOVA	ANalysis Of VAriance
APC	Adenomatous Polyposis Coli
aPKC	Atypical Protein Kinase C
Arp	Actin Related Protein
Asef	APC-stimulated guanine nucleotide exchange factor
ATP	Adenosine Triphosphate
ATPase	Adenosine Triphosphatase
AVE	AnteroVisceral Endoderm
BLAST	Basic Local Alignment Search Tool
B-RAF	Rapidly Accelerated Fibrosarcoma
β –Pix	PAK-Interacting Exchange Factor Beta
Casp3	Caspase 3
CD133	Cluster of Differentiation 133
Cdc42	Cell Division Control Protein 42 homolog
CDEP	Chondrocyte Derived Ezrin-like Protein
cDNA	complentary DeoxyriboNucleic Acid
CIMP	CpG Island Methylator Phenotype
CIN	Chromosomal Instable
CIT	Carte d'Identité des Tumeurs
CK20	Cytokeratin 20
CRB	Crumbs proteins
CRC	Colorectal Cancer
CRIB domain	Cdc42- and Rac-interactive binding
CRIB/MPP	Cribriform / Micropapillary
CRIK	Citron Rho-Interacting Kinase
CRMP	Collapsin Response Mediator Protein
CXCR	CXC chemokines receptor
CytoC	Cytochrome C
DAPI	4',6-diamidino-2-phénylindole
Dbl	Diffuse B-cell lymphoma
DDR	Discoidin domain receptor
DH	Dbl homology
DH-PH	Dbl homolgy-Peckstrin homology
DHR	DOCK Homology Region
DIC	Differential interference contrast
DLG	Disc Large
DMPK	Dystrophia myotonica protein kinase
DNA	DeoxyriboNucleic Acid
DOCK	Dedicator of Cytokinesis
DRF	Diaphanous Related Formin
dSC	Dissociated single cells
EB1	End Binding 1

E-Cadherin	Epithelial Cadherin
ECM	Extracellular matrix
ECT2	Epithelial cell transforming 2
EDTA	Ethylenediamine tetraacetic acid
EEF1	Eukaryotic elongation factor
EGF	Epidermal Growth Factor
EMT	Epithelial-to-Mesenchymal Transition
ENA/VASP	Enabled/Vasodilator-stimulated phosphoprotein
EpCam	Epithelial Cell Adhesion Molecule
ERM	Ezrin, Radixin and Moesin
ETA	Endothelin A
F-actin	Filamentous Actin
FAK	Focal adhesion kinase
FAP	Familial Adenomatous Polyposis
FARP	FERM, arhgef and pleckstrin domain-containing protein
FERM	4.1 protein, ezrin, radixin and moesin
FFPE	Formalin-Fixed Parafin Embeded
FH domain	Formin Homology domain
FilGAP	Filamin A (FLNa)-binding RhoGTPase-activating protein
FIR	FERM domain including RhoGEF
FRET	Förster resonance energy transfer
FRG	FGD1-Related Cdc42-GEF
G-actin	Globular actin
GAP	GTPase activating proteins
GAPDH	Glyceraldehyde 3-phosphate dehydrogenase
GDI	Guanine nucleotide Dissociation Inhibitors
GEF	Guanine nucleotide exchange factors
GFAP	Glial Fibrillary Acidic Protein
GFP	Green Fluorescent Protein
GM 130	Golgi Matrix 130
GP130-IL6ST	Glycoprotein 130 - Interleukin 6 Signal Transducer
GSEA	Gene Set Enrichment Analyses
GTP	Guanosine triphosphate
HEK	Human Embryonic Kidney
HES	Haematoxylin/Eosin/Saf r n
HIPEC	Hyperthermic Intraperitoneal Chemotherapy
HNPCC	Hereditary nonpolypous colorectal cancer
HSC70	Heat shock cognate 70
Hsp90	Heat shock protein
ITGA2	Integrin subunit alpha 2
JAK/STAT	Janus Kinase/Signal Transducer and Activator of Transcription
JAM	Junction adhesion molecule
KD	Kinase Dead
Kif17	Kinesin family member 17
KRAS	Kirsten rat sarcoma
LBK	Lieberkuhnian
LGL	Lethal giant larvae
LIMK	LIM domain kinase
LOH	Loss of Heterozygosis
MAPRE1	Microtubule Associated Protein RP/EB Family Member 1
MARCKs	Myristoylated alanine-rich C-kinase substrate

MBS	Myosin binding subunit
M-cadherin	Myotubular cadherin
mCh	mCherry
MDCK	Madin-Darby canine kidney
mDia	mammalian diaphanous
MET	Mesenchymal-to-Epithelial Transition (MET)
MG	Matrigel
MHC	Major histocompatibility complex
MLC	Myosin light chain
MMPs	Matrix metalloproteinases
MMR	Mismatch Repair
MPP	Micropapillar
MRCK	Myotonic dystrophy kinase-related CDC42-binding kinase
MSI	Microsatellite instability
MSS	Microsatellite stable
MUC	Mucinous carcinoma
MUC	Mucinous
MYPT1	Myosin phosphatase target subunit 1
N-cadherin	Neural cadherin
NEDD9	Neural precursor cell expressed developmentally down-regulated protein 9
NF-L	Neurofilament light
NHE1	Sodium- hydrogen exchanger
NHERF1	Na+/H+ Exchanger Regulatory Factor
NMHC	Nonmuscle myosin heavy chain
NM-II	Non-Muscle MyosinII
NPFs	Nucleation Promoting Factors
NSCLC	Non-small-cell lung carcinoma
NT	Non treated
N-WASP	Neural Wiskott-Aldrich syndrome protein
NZ	Nocodazol
PAK	p-21 activated kinase
PAR	Partitioning defective proteins
ParD6A	Partitioning defective 6 homolog alpha
PATJ	Pals1-associated tight junction
PC	Peritoneal carcinomatosis
P-cadherin	Placental Cadherin
PCI	Peritoneal Cancer Index
PDX	Patient derived xenograft
PH domain	Pleckstrin homology domain
PI	Propidium iodide
PI	Phosphoinositide
PIK3CA	Phosphatidylinositol 4,5-bisphosphate 3-kinase catalytic subunit alpha isoform
PIP2	Phosphatidylinositol 4,5-bisphosphate
PIP3	Phosphatidylinositol 3,4,5-trisphosphate
PP1	Protein phosphatase 1
PP1c	Protein phosphatase 1 catalytic subunit
Ptdlnst	Phosphatidylinositol
PTEN	Phosphatase and tensin homolog
PVF	PDGF/VEGF Factor
PVR	PDGF/VEGF receptor
PDGF	Platelet derived growth factor

Rac1	Ras-related C3 botulinum toxin substrate 1
Ras	Rat sarcoma
R-cadherin	Retinal cadherin
Rho	Ras homolog
RhoA	Ras homolog gene family, member A
RhoGDI	Rho GDP-dissociation inhibitor
RICH	RhoGAP interacting with CIP4 homologues
RNA	Ribonucleic acid
RNAi	RNA interference
ROCK RB-PH	ROCK RhoBinding–Pleckstrin homology domain
ROCK	Rho-associated protein coiled -coil kinase
ROIs	Regions of interest
ROK	Rho associated kinase
RTK	Receptor tyrosine kinase
s.e.m	Standard error of the mean
SCC	Squamous cell carcinoma
SCRIB	Scribble
Sdf1	Stromal cell-derived factor 1
SH3	SRC Homology 3 Domain
shNC	short hairpin negative control
shRNA	small hairpin RNA
SMAD	Sma and Mad (Mothers against decapentaplegic)
SMIFH2	Small Molecule Inhibitor of Formin Homology 2
Stat3	Signal transducer and activator of transcription
STK11	Serine/threonine kinase 11
SynCAM1	Synaptic cell adhesion molecule 1
TAU	Tubulin associated unit
TCGA	The Cancer Genome Atlas
TfR	Transferrin receptor
TGFβR	Transforming growth factor-β receptor
TGFβ	Transforming Growth Factor-β
Tiam1	T-Cell Lymphoma Invasion And Metastasis 1
TIAM1	T-lymphoma invasion and metastasis-inducing protein 1
TJ	Tight Junction
TP53	tumor protein 53
TSIP	Tumour Sphere with Inverted Polarity
VCA	Verprolin homology, cofilin homology, and acidic region
VEGF	Vascular endothelial growth factor
WASP	Wiskott–Aldrich Syndrome protein
WAVE1	WASP-family verprolin homologous protein 1
WNT	Wingless and Integration site contraction
WRC	Wave Regulatory Complex
YAP	Yes-associated protein
TAZ	transcriptional coactivator with PDZ-binding motif
ZEB1	Zinc finger E-box-binding homeobox 1
ZO	Zonula occludens

CHAPTER 1: INTRODUCTION

CHAPTER 2: RESULTS

CHAPTER 3: DISCUSSION

CHAPTER 1: INTRODUCTION

1 Colorectal Carcinoma (CRC): cancer of the intestinal epithelium

Introduction

Tumors arise from various specialized cell types throughout the body. Epithelial borne cancers, the carcinomas, represent the majority of them. These tumors are responsible for more than 80% of the cancer related deaths (Weinberg, 2013). Epithelia are sheets of highly cohesive cells that line the walls of cavities and channels or serve as the covering of the outside of the body (the skin).

The rest of tumors arise from different tissues in the body, composed of individual or loosely connected cells. The major ones are the sarcoma tumors, originating from connective tissue (mainly mesenchymal cells), the hematopoietic tumors arising from blood cells, the melanoma, which arise from the pigmented cells of the skin and tumours of the nervous sytem.

The intestinal epithelium, which lines the colon and the rectum spawns colorectal carcinomas (CRC), the third most common cancer worldwide (Ferlay et al., 2015) (Figure 1). CRC tumor biology is closely related to the intestinal epithelium biology as the biology of a tumour is conditioned, in part, by the biology of the tissue it arises from (Weinberg, 2013).

1.1 Architecture of the intestinal epithelium

1.1.1 Overview

The intestinal wall, formed by four layers of distinct tissues, surrounds the lumen of the intestinal tract. The different layers are the muscularis mucosae, composed of the epithelium, the lamina propria, a connective tissue and the muscular mucosae, a thin muscular layer. Underneath is the submucosa, a connective tissue containing blood, lymphatic vessel and nerves. Follows the muscular layer and the peritoneum, a serous membrane (Figure 1)

The colon and the rectum epithelium is monolayered. It insures water and nutrient absorption and forms a barrier against luminal pathogens. It is organized into invaginations called colonic glands, glands of Lieberkühn or colonic crypts. It is composed of differentiated cell

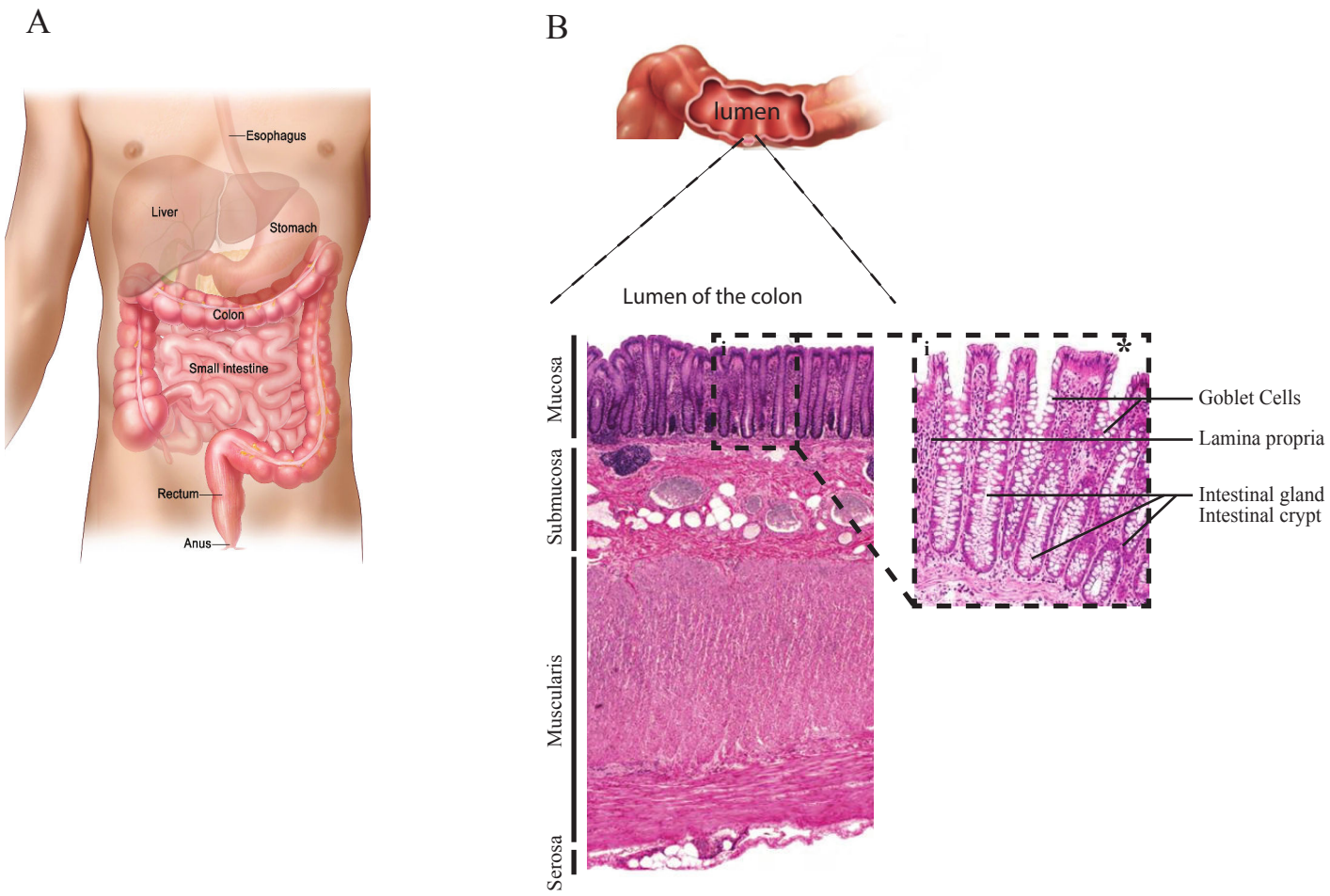

Figure 1

A. Anatomy of the gastrointestinal system.
B. Representative histological section of the colon. Stars show the luminal cavity.
C. Schematic representation of a monolayered glandular epithelium. AJ : adherens junctions, TJ:tight junctions

types: the absorptive enterocytes, the mucus secreting goblet cells, the hormone secreting enteroendorine cells and stem cells (figure 1B) (van der Flier and Clevers, 2009) (figure 1B).

Intestinal epithelium like all monolayered epithelia display a specific architecture characterized by strong cell-cell junction and an apico-basolateral polarity (figure 1C). The apical and basolateral membranes have very different compositions, which allow them to insure their specific function. The apical pole controls absorption, allows mucus secretion and protection against pathogens and displays microvilli. The basal pole of these cells contacts the underlying basement membrane composed of laminin-rich extracellular matrix (ECM). The lateral membranes of these cells contact adjacent cells and display specialized junctions and cell–cell adhesion structures, which delimits the apical and the basal pole. The basal and lateral membranes are similar in composition and organization and are often referred to as the basolateral pole. The epithelial cytoskeleton is composed of the actin, the microtubules and the intermediate filaments. Intermediate filaments are assembled from a diverse group of fibrous proteins, Keratins in the case of epithelial cells and vimentin in the case of mesenchymal cells. The actin and microtubule filaments will be described in detail (1.1.4-1.1.5)

1.1.2 Cell-cell junctions

Structure

Four specialized intercellular junctions can be found distributed along the lateral membrane of epithelial cells (figure 2): The most apical of these are the tight junctions (TJs), a complex of transmembrane proteins of the occludin, junctional adhesion molecule (JAM), and claudin family (Niessen, 2007). Cytoplasmic scaffold proteins zonula occludens (ZO) family members (ZO-1, ZO-2, ZO-3) and cingulin link these molecules to the actin cytoskeleton. Tight junctions function as a barrier as they seal the neighbouring cells and insure the impermeability of the epithelium by preventing the paracellular passage of ions or molecules. They also segregate the apical plasma membrane from the basolateral membrane by preventing transmembrane protein diffusion (figure 2) (Koch and Nusrat, 2009).

Directly below the TJs are the adherens junctions (AJs), which comprise E-cadherin and nectins (figure 2). AJs are composed of clusters of the trans-membrane molecule E-cadherin

A

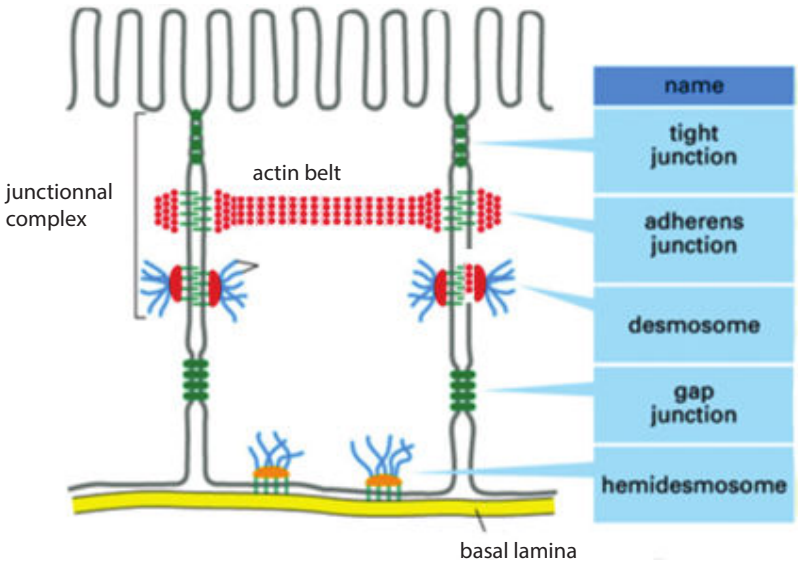

B

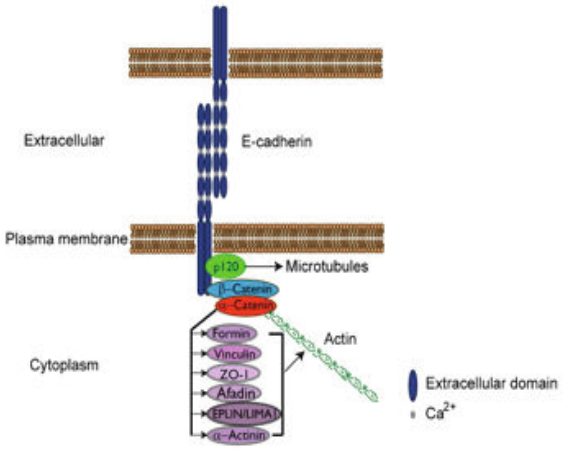

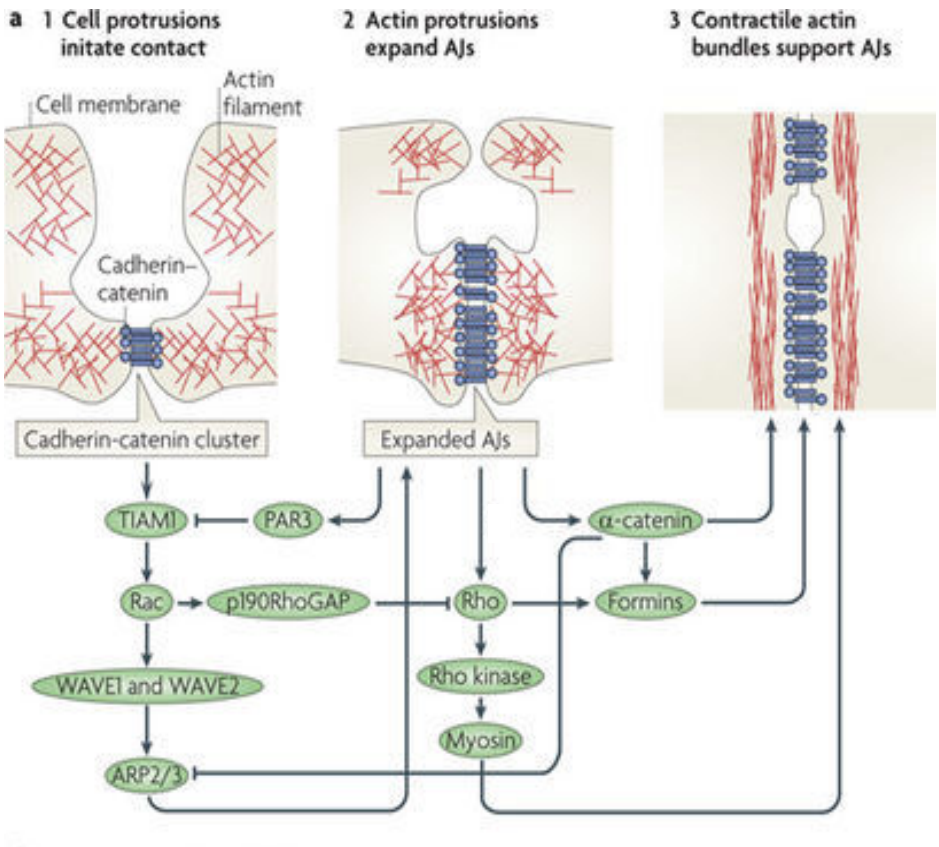

Figure 2 . Cell-cell junctions

(A) Differents types on cell-cell junction in epithelial cells.

(B) E-Cadherin can dimerize and form trans-homophilic interactions to form cadherin clusters. Ca2+ ions are required to stiffen the extracellular domain and are essential to form homophilic interactions. The E-cadherin intracellular domain contains binding sites for the catenins p120 and β-catenin, thereby forming the cadherin–catenin complex. p120 catenin links cadherin to microtubules and is also important to prevent cadherin endocytosis and degradation. β-Catenin binds α-catenin, which in turn binds actin and several actin-associated proteins, including α-actinin, vinculin, and formin-1. The cadherin–catenin complex also binds many other proteins, including signaling proteins, and cell surface receptors and forms a hub for protein–protein interactions. C- cell-cell junction dynamics and control by RhoGTP signling pathway Adapted from Baum and Georgiou, 2011.

(for epithelium-cadherin). E-cadherin is a member of the classical cadherin family of transmembrane proteins, which also includes M- (myotubule), N- (neuronal), P- (placental), R- (retinal) cadherin, expressed in distinct cell types (Gassama-Diagne et al., 2006; Martin-Belmonte et al., 2007, 2007). They are calcium Ca2+ dependent adhesive proteins with five repeats in their extracellular domain, which upon binding of Ca2+ engage homophilic interactions with the cadherin ecto-domains of neighboring cells. The cytoplasmic domain of E-cadherin binds to cytoplasmic beta-catenin and p120 catenin. Alpha-catenin links the cadherin-catenin complex to F-actin, this interaction necessitates a conformational change of the protein, generated by mechanical of the actin cytoskeleton (Buckley et al., 2014). Adherens junctions are thought to act as dynamic connectors of the actin cytoskeleton of adjacent cells and are a defining feature of the epithelium architecture (Perez-Moreno et al., 2003)**.** They initiate and stabilize cell-cell junctions and the tissues organization, preventing dissociation into single cells.

The third big group of cell-cell contacts, the desmosomes, are composed of transmembrane desmosomal cadherins, desmoglein and desmocollin, which bind to the cytoplasmic scaffold proteins plakoglobin and desmoplakin, which in turn link the protein complexes to intermediate filaments to provide structural strength (Dusek et al., 2007) (figure 2).

Finally, Gap junctions are sites of direct communication of neighboring cells. Multimers of connexin and pannexin proteins form transmembrane channels termed connexons, which allow the exchange of small molecules and ions between neigbouring cells (Meşe et al., 2007).

1.1.3 Apico-basolateral polarity

Polarity protein

The epithelium polarity is regulated by three groups of polarity proteins, the partitioning defective (PAR) proteins, the Crumbs (CRB) proteins and the Scribble (SCRIB) proteins. The localization of these proteins at different localization establishes the apico-basolateral asymmetry of the cell (Goldstein and Macara, 2007; Nelson, 2003).

The PAR group of protein was identified in a C.elegans embryo screen (Kemphues et al., 1988):it is composed by Par3, Par6, aPKC and Cdc42 small RhoGTPase.

Later on, screening in D.melanogaster uncovered the CRB group which consists of the CRB protein, the PALS1 and PATJ (Tepass et al., 1990) and the SCRIB group composed of the

A

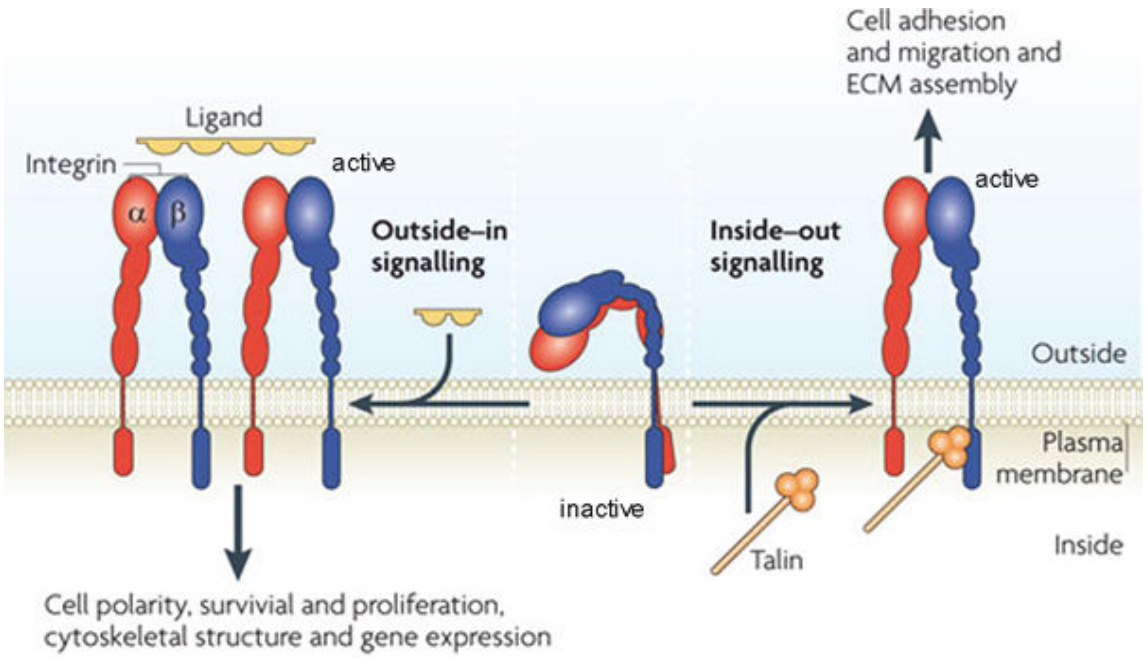

B

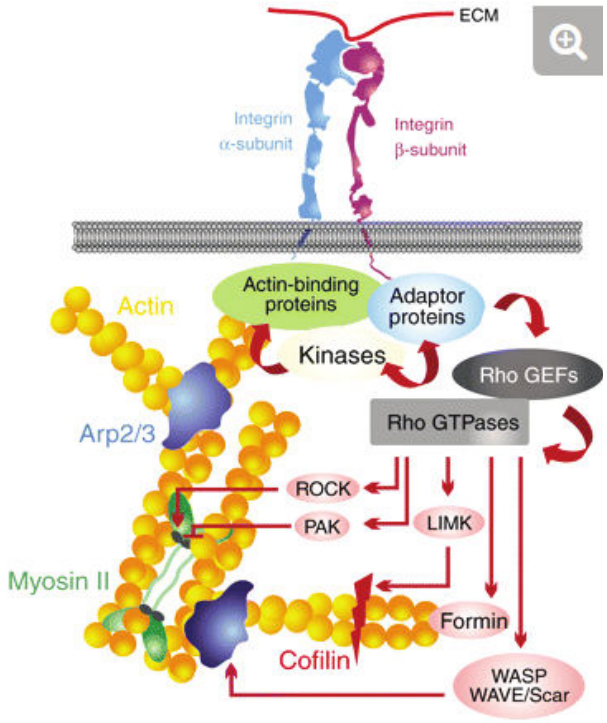

Figure 3. Integrin architecture and schematic representation of integrin activation

(A)The contacts between the extracellular, the transmembrane and cytoplasmic domains keep the integrin in its bent inactive conformation. Separation of the integrin extracellular, transmembrane and cytoplasmic domains occurs during integrin activation, resulting in an extended integrin conformation. There are two directions of activating integrins. In "inside-out" signaling, an intracellular activator, such as talin or kindlin, bind to the cytoplasmic integrin tail, leading to conformational changes that increase the affinity of integrin for the extracellular ligands. Integrins also serve to transmit the information from the extracellular environment into the cell via "outside-in" signaling. Binding of integrins to the extracellular ligands change the conformation of integrin and contributes to integrin clustering. Adapted from Shattil et al, Nature Reviews Mol Cell Biol 2010.

(B)Outline of adhesive signaling in migration. Integrin ligation induces the nucleation of different signaling elements. The major categories (kinases, non-catalytic adaptor proteins and actin-binding proteins) are shown. These categories can influence the recruitment and/or activation of other components of adhesions (represented by red arrows). Most migratory signaling converges on the Rho GTPases, which regulate actin polymerization and stability (via nucleators such as the Arp2/3 complex and formins, or actin-filament-severing proteins such as cofilin), actomyosin contractility (via MLC phosphorylation), and microtubules (not shown). Adapted from Vicente-Manzaranes

SCRIB, Disc large (DLG) and the LGL (lethal giant larvae) (Bilder et al., 2000). To achieve polarized domains, reciprocal exclusion occurs between members of the polarity proteins. While the PAR3/PAR6/aPKC/Cdc42-GTP complex and the CRB protein determine the apical pole, the SCRIB proteins localize at the basolateral pole (Goldstein and Macara, 2007).

Polarity lipids

The other determinant of apical–basolateral is the asymmetric segregation of protein and lipids in apical and basolateral membrane domains. In mammalian epithelial cells phosphatidylinositol 4,5-bisphosphate (PIP2) is a key determinant of the apical surface, whereas phosphatidylinositol 3,4,5 triphosphate (PIP3) is a key determinant of the basolateral membrane (Gassama-Diagne et al., 2006; Martin-Belmonte et al., 2007). PIP3 results from activation of the protein kinase PI3K whereas PTEN phosphatase promotes PIP2 formation from PIP3. They interact with various proteins through their Pleckstrin homology (PH) domain and play a docking role for apical or basal specific proteins.

Adhesion to the extracellular matrix (ECM)

Adhesion of epithelial cells to the ECM orientates the apico-basolateral polarity of the cells. Epithelial cells sit on a specialized ECM, the basement membrane and adhere to it through integrins and hemidesmosomes (figure 2-3).

The basement membrane is a specialized type of extracellular matrices that lines the basal pole of epithelial sheets. It is composed of collagen IV, laminin, nidogen and proteoglycans. The basement membrane signals to the cells through βintegrin and initiates a cross-talk between Rac1 and ROCK kinases to properly orient the apical and the basal pole (Bryant et al., 2010; Liu et al., 2007; O'Brien et al., 2001). Beta-1 integrin was shown to promote Rac1 activation to induce laminin assembly at the basal pole of 3D MDCK cysts, this mechanism required ROCK1 inhibition and allowed normal apical-basal orientation of the polarity axis. Inhibition of Beta-1 integrin by blocking antibodies or of Rac1 by its dominant negative mutant was found to induce an inverted polarity axis, with the apical pole at the periphery of the cysts. The phenotype was due to a misassembled laminin network and could be rescued by providing exogenous laminin. This study from Mostov lab showed the importance of the ECM in the orientation of the polarity axis.

1.1.4 Actin cytoskeleton

Actin filament structure and dynamics

The actin filaments (F-actin) is a polymers of monomers of globular actin (G-actin) molecules. F-actin is polarized with a fast growing barbed end and a slow growing pointed end. F-actin polymerization occurs after a limiting step of nucleation of three (G-actin). Nucleation primes the elongation phase where G-actin monomers, are added to the growing filaments (Blanchoin et al., 2014). While *in vitro* elongation of F-actin is conditioned by the concentration of G-actin, F-actin dynamics is regulated by actin binding proteins (figure 4).

These proteins act on F-actin assembly by 1) maintaining a large pool of actin monomers available for polymerization, 2) by nucleating new filaments, 3) by promoting elongation, 4) by preventing elongation through capping of the F-actin ends, 5) by severing filaments, and crosslinking filaments (figure4).

Profilin binds to G-actin monomer and inhibits its nucleation. Profilin-bound G-actin are added to uncapped barbed ends by the elongation factor formin (Blanchoin et al., 2014). This makes of Profilin a major regulator of F-actin growth (figure 4).

Nucleators catalyze the formation of the core G-actin oligomers used for progressive elongation of F-actin. They are three main categories: Formins, Arp2/3 and the WH2 domains containing proteins (Pollard, 2016) (figure 4). Formins stabilize the core of G-actin monomer and bind to the barbed end of actin filament to promote linear elongation of the filament. Proteins belonging to this group all share the highly conserved formin homology domain (FH2) which is necessary and sufficient to nucleate actin filaments in vitro. To date, three types of formins have been identified in humans: Diaphanous Related Formin-1 (DRF1= mouse homologue of *Drosophilia* Diaphanous 1 or mDia1), DRF2 (mDia3) and DRF3 (mDia2). Arp2/3 binds to the lateral side of a preformed actin ("mother" filament) and nucleates the polymerization of a new "daughter" filament, which results in branched actin network. The Arp2/3 complex is composed of seven subunits (Arp2, Arp3, p34, p16, p20, p21 and p40). The Arp2/3 complex is intrinsically inactive and is activated by Nucleation Promoting Factors (NPFs), such as the WASP/Scar family including (N-WASP, WAVE, Scar). Spire, Cordon Bleu and JMY are tandem WH2 domains containing proteins and

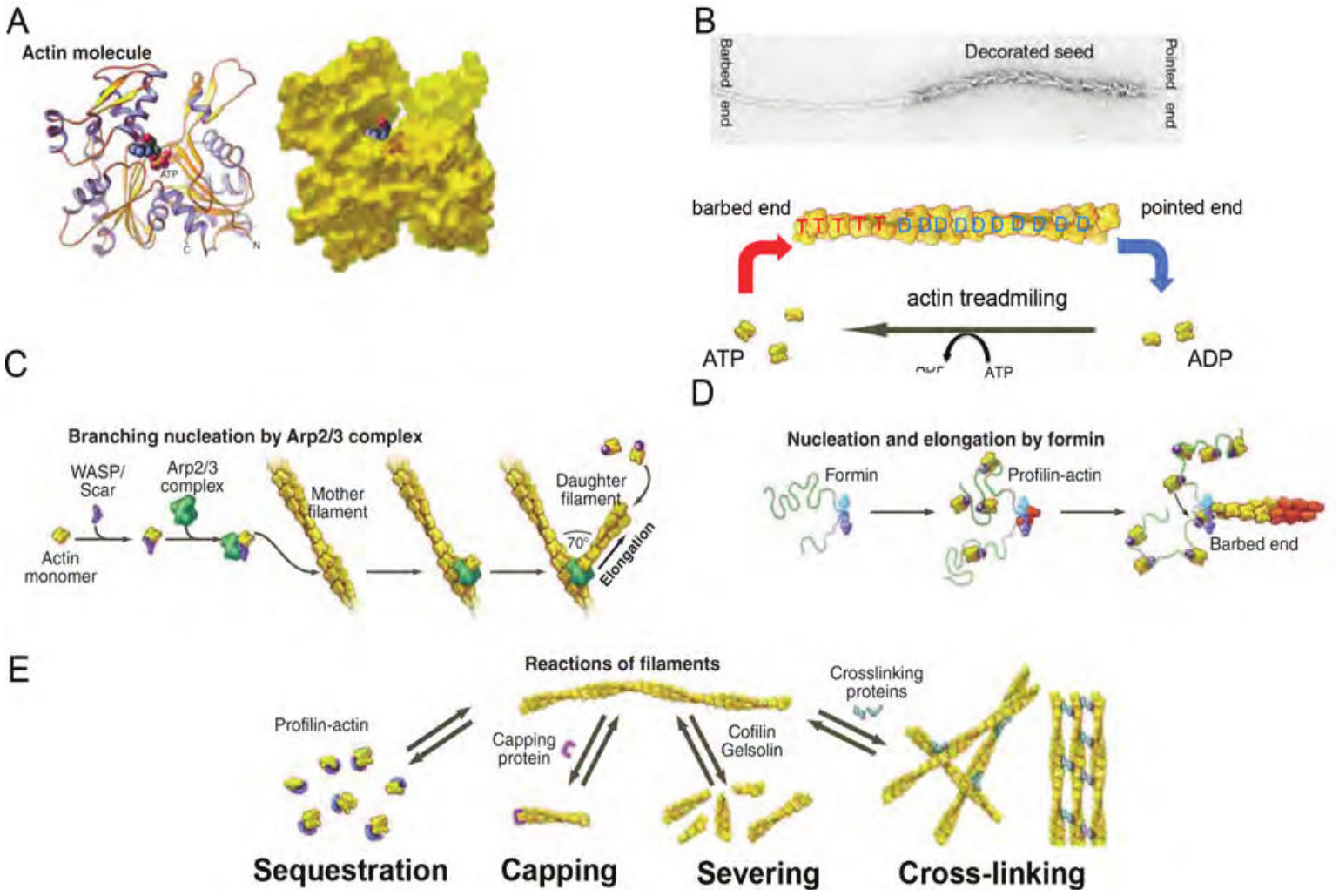

Figure 4 . The actin cytoskeleton. Actin polymerization and regulatory proteins

(A) Ribbon and space-filling models of the actin molecule. Binding site for ATP is depicted in blue in the center of the molecule.

(B) The electron micrograph shows an actin filament seed decorated with myosin II heads and elongated with ATP-actin. Schematic view of the actin filament polymerization and treadmilling. Actin monomers coupled with ATP are preferentially added to the barbed end, while monomers coupled with ADP disassociate from the filament at the pointed end.

(C) Nucleation of actin filaments by Arp2/3 complex. Nucleation-promoting factors such as WASP bind an actin monomer and the Arp2/3 complex. Binding to the side of filament completes activation, and the barbed end of the daughter filament grows from Arp2/3 complex.

(D) Nucleation and elongation by formins. Formins initiate polymerization from free actin monomers and remain associated with the growing barbed end. Profilin-actin binds to formin and transfers actin onto barbed end of the filament.

(E) Actin-binding proteins and their function. ADF/cofilin and profilin bind monomers and regulate actin polymerization; capping proteins bind to and block addition of monomers at barbed ends; cofilin and gelsolin sever filaments; cross-linking proteins assemble networks and bundles actin filaments.

Adapted from Pollard and Cooper, 2009.

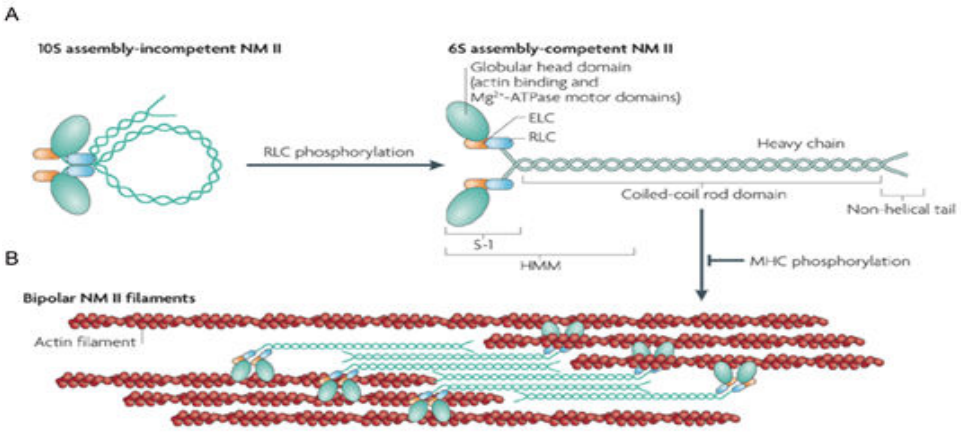

Figure 5. Structure of myosin II

A. The subunit and domain structure of non-muscle myosin II (NM II), which forms a dimer through interactions between the α-helical coiled-coil rod domains. The globular head domain contains the actin-binding regions and the enzymatic Mg2+-ATPase motor domains. The essential light chains (ELCs) and the regulatory light chains (RLCs) bind to the heavy chains at the lever arms that link the head and rod domains. In the absence of RLC phosphorylation, NM II forms a compact molecule through a head to tail interaction. This results in an assembly- incompetent form (10S; left) that is unable to associate with other NM II dimers. On RLC phosphorylation, the 10S structure unfolds and becomes an assembly-competent form (6S). S-1 is a fragment of NM II that contains the motor domain and neck but lacks the rod domain and is unable to dimerize. Heavy meromyosin (HMM) is a fragment that contains the motor domain, neck and enough of the rod to effect dimerization. B. myosin II molecules assemble into bipolar filaments through interactions between their rod domains. These filaments bind to actin through their head domains and the ATPase activity of the head enables a conformational change that moves actin filaments in an anti-parallel manner. Bipolar myosin filaments link actin filaments together in thick bundles that form cellular s tructures such as stress fibers. Adpated from Vicentre-Manzaranes et al, 2009.

promote nucleation by favoring the association of dimers or trimers of G-actin. Ena/VASP family and formins antagonize with capping protein by preventing its capping they promote elongation of actin filaments (Pollard, 2016).

To destabilize and disassemble F-actin, ADF/cofilins and Gesolin binds to the side of F-actin and promote severing and depolymerisation (Pollard and Borisy, 2003; Revenu et al., 2004).

Actin filament organization

In cells, F-actin organizes in different structures: branched actin networks, cross-linked meshwork, bundles of parallel actin filaments, and bundles of antiparallel actin filaments. Arp2/3 is responsible for the branched actin network organization. Crosslinkers connect already polymerized actin filaments. Non-muscle myosin II motor protein can act as a cross linker of anti-parallel F-actin.

Actin-myosin complex

Actin filaments serve as a scaffold to non muscle myosin II (NM-II). The resulting acto-myosin network generates the contractile forces necessary for all types of cell motility (figure 5). The non-muscle myosin-II (NM-II) that will be referred to as Myosin-II is an actin-dependent ATP motor protein. It is a hexamer composed of 2 heavy chains (NMHC) and four light chains (MLC): two structural light chains and two regulatory light chains. The regulatory chains are responsible for NM-II regulation by signaling; therefore MLC will be used to refer to these important regulatory chains. The heavy chain harbors three domains: a globular head that interact with F-actin and binds ATP nucleotides, a supercoiled long domain that mediates dimerization of the MHCII, and a non-helical tail domain (Vicente-Manzanares et al., 2009).
Mammalian cells possess three isoforms of Non-Muscle Myosin II (NMII), II-A, II-B and II-C, which harbor specific and distinct MHC. Their ability to generate mechanical forces is context-dependent; thereby each isoform regulates specific cellular functions. NM IIA has the highest rate of ATP hydrolysis of the three NM II isoforms meaning that it contracts actin more rapidly, while NM-IIB which remains bound to actin in a force-generating state contracts the acto-myosin network more slowly (Juanes-García et al., 2016; Vicente-Manzanares et al., 2011).

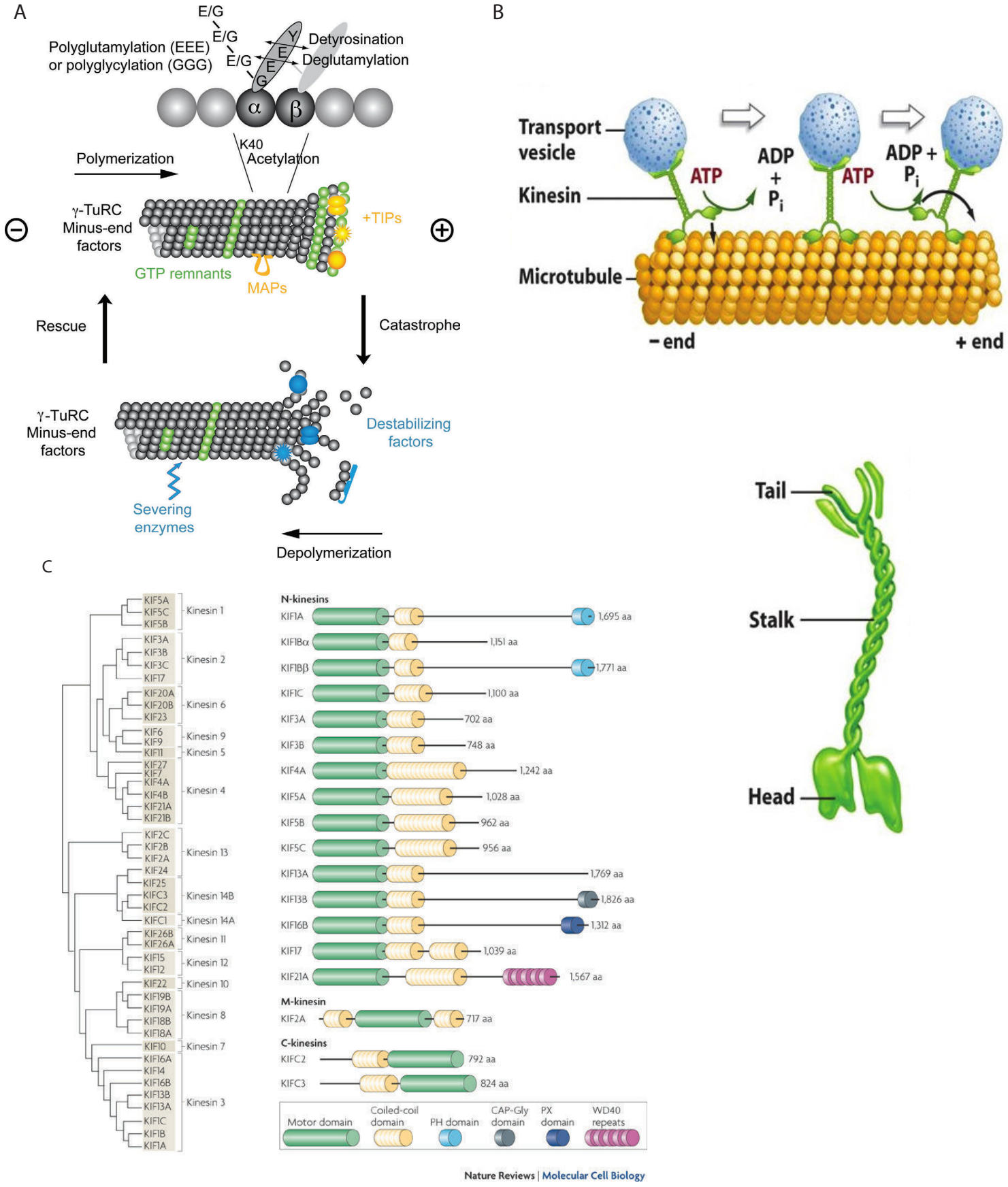

Figure 6 . Microtubules and microtubule motor proteins
A-Microtubule dynamic
B- Motor protein walking on microtubule
C-members of the kinesin superfamily
Adapted from Hirokawa 2009, Vale 2003, De Forge 2012

In a non-activated form NM-II is folded in a compact conformation and it is not able to bind actin filaments. Upon its phosphorylation on Ser19, NM-II extends and polymerizes to form bipolar filaments. This allows the binding of the myosin head to F-actin and triggers the « walking » of the head along the actin filament in an ATP-hydrolysis dependent manner. NM-II can be phosphorylated on Thr18, which in association with Ser19 phosphorylation increases the rate of ATPase activity.

1.1.5 Microtubule cytoskeleton

Microtubules structure and organization

Microtubules are hollow microfilaments assembled from 13 parallel protofilaments, that result from the head-to tail polymerization of α-β-tubulin heterodimers along the longitudinal axis of the microtubule. These microfilament are intrinsically robust and resist compression and bending and can reach several micrometer long. Microtubules are polarized minus end and plus end hollow microfilament (figure 6).

In most cells, microtubules nucleate from the microtubules organizing center (MTOC) at centrosomes where the minus-end is tethered and radiate to the periphery where plus-ends are captured and stabilized. However in apico-basolateral polarized epithelial cells, microtubules are mostly non-centrosomal. They either polarize along the apical-basal axis, and mainly localize at the cell cortex with minus end tethered at the apical pole or in some cases at cell-cell adhesion, while plus ends are found at the basal pole (Bacallao et al., 1989; Ligon and Holzbaur, 2007; Meng et al., 2008). Another group of centrally localized microtubules in epithelial cells nucleate from the centrosome and extend to apical periphery of the cell, in this case stabilizing their plus end at the apical pole of the cell (Jaulin et al., 2007)

Microtubules dynamics and their regulation

Microtubule nucleation begins from the minus end and is mostly dependent on the γ-tubulin ring complexes (γ-TuRCs) formed at MTOC (Moritz and Agard, 2001). Alpha and β tubulin are able to bind to GTP, however only the GTP bound to beta-tubulin is hydrolysed. The binding of beta- tubulin to GTP and its hydrolysis drive the assembly and disassembly of microtubules. GTP-loaded tubulin are added at the plus end tip of microtubules and GTP

hydrolysis induces depolymerization by promoting an unstable state of the microtubule which was proposed to be the result of the protofilament‘s conformational change (Wang and Nogales, 2005). Microtubules are stabilized by a ‘GTP cap’, a region at the end of a polymerizing microtubule where GTP hydrolysis has not yet occurred (Brouhard and Sept, 2012) (figure 6).
Microtubules alternate episodes of growth, pause and shrinkage in a mechanism called dynamic instability (Gardner et al., 2008). The dynamic instability can be defined by the growth rate, the shrinkage rate as well as the frequency of catastrophes (transition from growth to shrinkage) and the rescues (transition from shrinkage to growth).

Microtubules dynamics can be regulated by microtubule-associated proteins by tubulin post-translationnal modifications, and can be modulated by exogenous microtubule targeting agents (MTA). The microtubule dynamics can be modulated in different ways : by regulating polymerization and depolymerization, by affecting catastrophes and rescues, or by capping the microtubules plus end (de Forges et al., 2012) (figure 6).

Microtubules post-translational modifications are linked to the regulation of microtubule dynamics and mostly linked to microtubule stability. Microtubule modifications can be detyrosination, glutamylation, glycylation and acetylation. These modifications are recognized by MAPs or motor proteins (Janke and Kneussel, 2010)

Microtubule-targeting agents constitute a class of chemotherapeutic drugs that target microtubules dynamics and disrupt the normal function of the mitotic spindle to cause cancer cell death (MTA) can be classified in microtubule stabilizing and destabilizing drugs. Examples of microtubule destabilizing agents are colchicine and Nocodazole. Microtubule stabilizing agents are mainly composed by Taxanes and epothilones. Taxanes bind tubulin to inhibit depolymerization, enhance assembly, and thereby bundling and stabilizing microtubules (Fojo and Menefee, 2005)

Microtubule associated proteins (MAPs)

There are two main groups of MAPs: proteins that stabilize microtubules and proteins that destabilize them. The stabilizing group is composed of classical MAPs such as Tau, MT assembly promoters, MT stabilizers with mitosis-specific functions, MT stabilizers through

cell cortex interaction, and other MT-stabilizing proteins (Lyle K et al. 2009a; Lyle K et al. 2009b). MT-destabilizing proteins include microtubule-associated proteins, microtubule-severing proteins, microtubules plus-ends tracking proteins (+TIPs) such as EB1 and some microtubule motor proteins.

Microtubule motor proteins and function

Motor proteins use microtubules as tracks to transport the vesicle in the form of cargo.
There are two types of motor proteins, which navigate on microtubules in ATP hydrolysis dependent manner: the kinesins and the dyneins (figure 6).
Kinesins superfamily (KIF) of microtubule-based ATPase motor proteins are 45 mammalian KIF which are divided into 15 kinesins families, : kinesin 1 to kinesin 14B according to the results of phylogenetic analyses. In general, kinesins with an amino-terminal motor domain (N-kinesins) move towards MT plus ends, whereas kinesins containing a carboxy-terminal motor domain (C-kinesins) move in the opposite direction, and kinesins with a central motor domain (M-kinesins) often destabilize MTs rather than move along their surface.
They are composed of a motor domain also called head domain, which interacts and move along the microtubule thanks to its ATPase activity. The stalk domain is composed of coiled-coilded domains used by the kinesin to dimerize. Finally they possess a tail domain, which interacts with cargo and which in some cases has been shown to have an autoinhibitory effect of the protein ATPase activity (Acharya et al., 2013).

Although best known for their role in vesicle transport many kinesin modulate microtubule dynamics. It can be mediated by direct effects of motors on MTs, usually at MT ends, or indirectly by transporting cargoes to microtubule ends that affect microtubule dynamics.

Kif17 motor protein Kif17 is a member of the Kinesin2A family and function as a homodimeric motor in the transport of cargoes along toward the +enf microtubules. It was found to interact with the EB1 protein and APC at plus end of microtubule and stabilize them at the apical membrane of epithelial cells (Jaulin and Kreitzer, 2010) The Tail domain of Kif17 was shown to regulate its motor domain (Acharya et al., 2013)

A

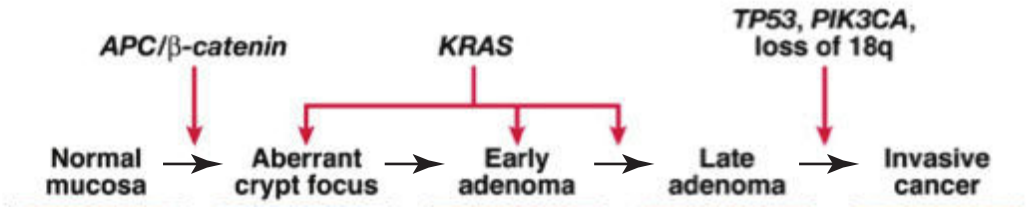

B

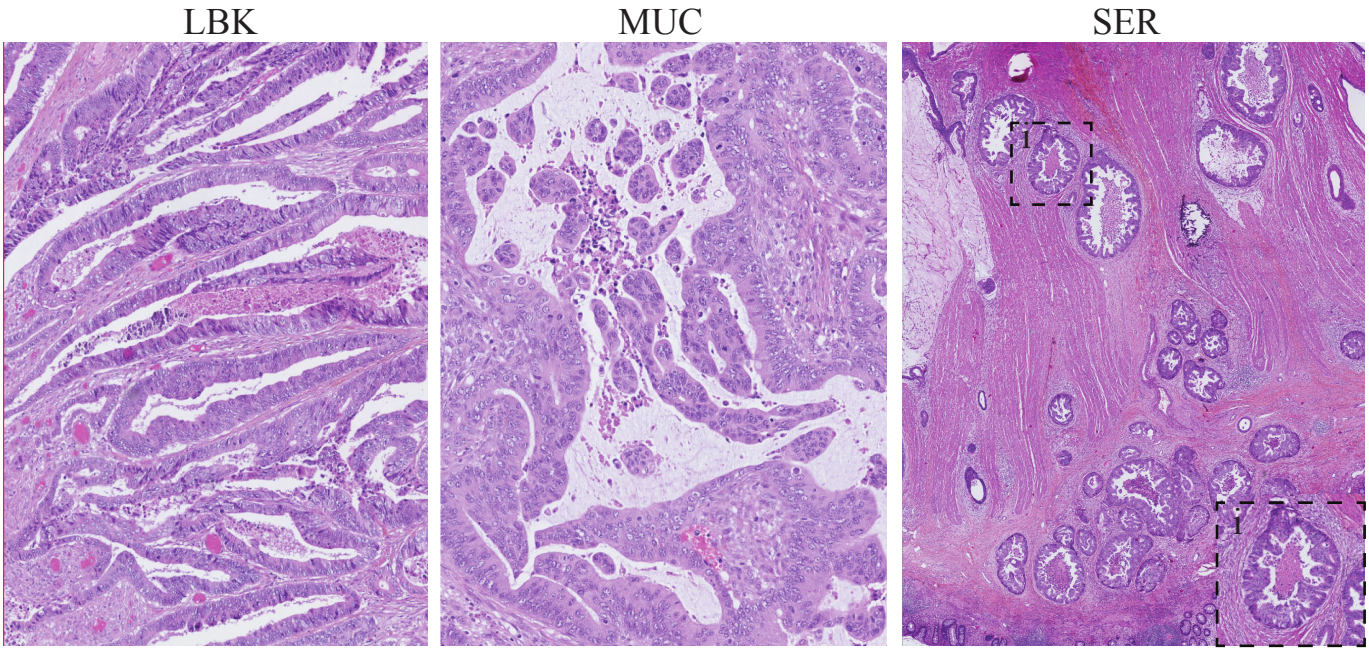

Figure 7 . Progression and classification of CRC

A. Schematic representation of the mutations progression cascade that commonly lead to colorectal cancer. B. Representative tumour specimens of Lieberkunhian (LBK), Mucinous (MUC) and Serrated precursor gland (Ser) stained with haematoxylin/eosin/safran (HES). (i) shown a high magnification of a serrated neoplasic gland.

Microtubule function in epithelial cells

The epithelial microtubule organization mediates the typical supra-nuclear localization of the Golgi, common recycling endosomes (CREs) and AREs, and the peripheral localization of apical and basolateral sorting endosomes. The microtubule serves as track for the polarized secreation of molecules or vesicles along them.

Some microtubules under the apical surface may be released and captured by the developing apical junctional complex (Meng et al., 2008). In turn, these captured microtubules contribute to the development of the apical junctional complex (Chausovsky et al., 2000) It has been shown that E-cadherin expression has microtubule-stabilizing properties, which is consistent with the higher stability of epithelial micro- tubules. Kinesin family 17 (KIF17), end-binding 1 (EB1) and APC stabilize microtubules at the basal plus ends, which contributes to establishing the height of epithelial cells (Jaulin and Kreitzer, 2010).

1.2 Colorecatal carcinoma

90% of CRC are the result of sporadic somatic genetic and epigenetic alteration, whereas inherited syndromes cause the remaining 10%: the familial adenomatous polyposis (FAP) or the hereditary non-polypus colorectal cancer (HNPCC). While sporadic and FAP CRC are initiated by inactivating mutation of APC (adenomatous polyposis coli), HNPCC CRC are the result of Mismatch repair (MMR) system deficiency. (Fearon and Vogelstein, 1990) (figure 7).

1.2.1 Molecular classification

90% of CRC are the result of sporadic somatic genetic and epigenetic alteration, whereas inherited syndromes cause the remaining 10%: the familial adenomatous polyposis (FAP) or the hereditary non-polypus colorectal cancer (HNPCC). While sporadic and FAP CRC are initiated by inactivating mutation of APC (adenomatous polyposis coli), HNPCC CRC are the result of Mismatch repair (MMR) system deficiency. (Fearon and Vogelstein, 1990) (figure 7).

In 1990 Fearon and Vogelstein have proposed a multi-step genetic model for the progression of sporadic CRC from benign adenoma to adenocarcinoma, which is initiated by the APC

gene mutation and relies on accumulation of genetic alterations (Fearon and Vogelstein, 1990). The APC loss dependent Wnt/Beta-catenin activation is followed by KRas mutations and subsequent mutations in driver signaling pathways.

However it was later found that CRC is a heterogeneous presenting three different genomic instability which generate multiple genetic alterations. The best-characterized genomic instability inducer is the chromosomal instability (CIN) (75% of CRC), which leads to loss of big arrays of chromosomes and Loss of Heterozygosis (LOH). It is believed to be a direct consequence of APC mutation gene.
The Microsatellite instability (MSI) is due loss of the DNA repair system MMR and leads to DNA breakage at site of microsatellite repeated sequences.
The CpG island methylator phenotype (CIMP) group leads to methylation of long arrays of chromatin inducing gene silencing. This deficiency can lead to MSI, by silencing of the MMR genes. Therefore the status of CRC CIMP can be MSI-high, MSI-low or MSS (Fearon, 2011).

About 15 gene mutations have been identified as recurring in CRC and thought to drive tumor progression. They include the oncogenes *APC, KRAS, PIK3CA, BRAF, SMAD4, TGFb*R and tumour suppressors *TP53*. *TGFBR, SMAD2* and *SMAD4.* SMAD2 and SMAD4 are activated downstream of the TGF-β receptor complex. Inactivating mutations in the TGF-β type II receptor gene are found in approximately 25% of CRCs. Mutations that inactivate *SMAD4* are found in ~10–15% of CRCs, and SMAD2 mutations are found in ~5% of CRCs. Recent findings suggest that mutations inactivating the *SMAD3* gene are found in ~5% of CRCs. TGFβRII is mutated in up to 90% of colon cancer tumors with MSI. TGFβ signals through a canonical and a non-canonical pathway (Fearon, 2011).

1.2.2 Histological classification

90% of CRC are adenocarcinoma. At diagnosis around 70% of adenocarcinoma form gland which recapitulate the architecture of normal tissue (Fleming et al., 2012) (figure 7). Different histological variants are found; the mucinous CRC subtype is the most common and represents 10 to 15% of diagnosed CRC. Mucinous CRC are characterized by tumor mass composed by over 50% of mucus. This subtype accounts for 10% of CRC. Less common histological subtypes are the signet ring cell carcinoma, the neuroendocrine carcinoma, the medullary carcinoma and the micropapillary carcinoma. These distinct histologies are thought

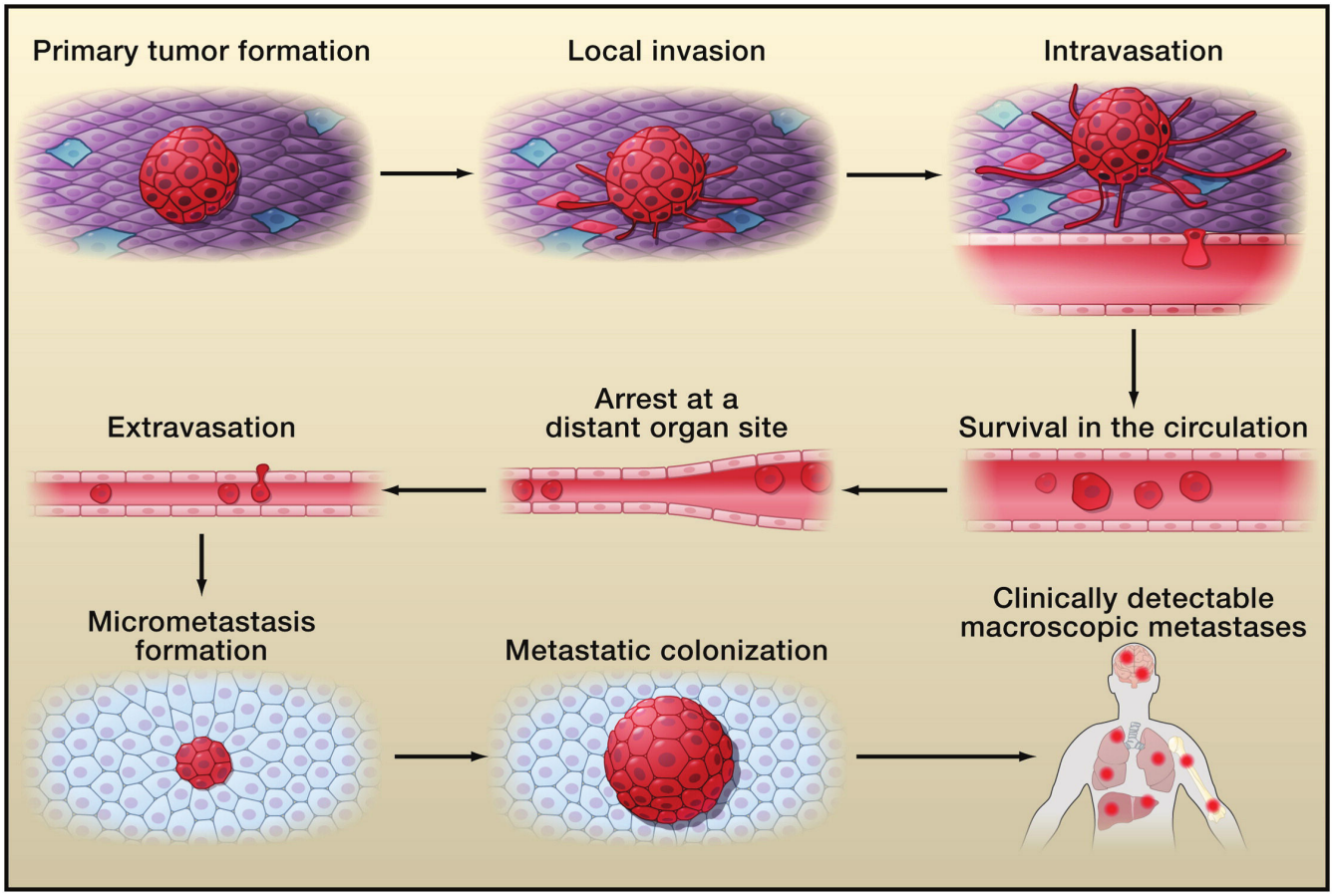

Figure 8 . The Invasion-Metastasis Cascade
Clinically detectable metastases represent the end products of a complex series of cell-biological events, which are collectively termed the invasion-metastasis cascade. During metastatic progression, tumor cells exit their primary sites of growth (local invasion, intravasation), translocate systemically (survival in the circulation, arrest at a distant organ site, extravasation), and adapt to survive and thrive in the foreign microenvironments of distant tissues (micrometastasis formation, metastatic colonization). Carcinoma cells are depicted in red. Adapted from Chaffer, 2016

to result from intrinsic molecular programs or from microenvironmental factors (Fleming et al., 2012; Nagtegaal and Hugen, 2015).

1.3 CRC dissemination: a collective route to metastasis?

1.3.1 The metastatic cascade

Metastatic dissemination is the process used by the primary tumor cells to disseminate throughout the organism and colonize distant organs in order to form secondary tumors termed metastasis. The metastatic cascade is a complex multi-step process: tumor cells invade the surrounding peritumoral stroma to reach the blood or lymphatic stream where they travel in the liquid environment before extravasation, and eventually invade the stroma of a distant organ where they grow a secondary tumor, termed metastasis (Chaffer et al., 2016) (Figure 8). Alternative routes of dissemination are nerve (perineural invasion) or the transcoelomic invasion to reach the peritoneum. Whereas surgical resection and adjuvant therapy can cure confined and detectable primary tumors, metastatic disease is largely incurable because of its systemic spread and because of the difficulty to detect the secondary tumors. In addition, disseminated tumors often display resistance to existing therapeutic agents. This explains why over 90% of mortality from cancer is attributable to metastases (Duchek et al., 2001) (Gupta and Massagué, 2006, Steeg, 2006). Thus, our ability to effectively treat cancer relies on our capacity to prevent metastatic progression.

1.3.2 CRC site of metastasis

CRC tumors are considered invasive once they have reached the submucosa layer of the intestinal wall (Fleming et al., 2012). They can either go through all the layers of the wall to colonize to the peritoneum (3rd site of CRC metastasis) or they can use the common routes of dissemination to reach the organ they have a strong tropism for: the Liver (first metastatic site) and the lung (the second CRC metastatic site). Bone, spleen, brain and distant lymph nodes and more rarely pancreas and heart can also be CRC metastasis sites.

The peritoneum is a serous membrane, which covers the visceral organs composed of two layer or mesothelial cells surrounding a thin cavity filled with serous fluids.

1.3.3 EMT program promotes CRC individual cell dissemination

It was long believed that single cells that have travelled from the primary tumor seed metastases. To achieve this single mode of invasion carcinoma cells would require a mechanism leading to the loss of their epithelial features and most importantly loss of their cell-cell junction leading to their individualization. The EMT (epithelial to mesenchymal transition) is a transcriptional program that was proposed to fulfill that role, as it leads to loss of epithelial features and promotes the acquisition of mesenchymal traits.

The EMT program, which involves dissolution of adherent junction and a loss of cell polarity, dissociates the cells within the epithelial tissue into individual cells that exhibit multiple mesenchymal features, including increased motility and invasiveness (Thiery et al., 2009). This program was first observed in embryo development and was then demonstrated to contribute to carcinoma cell individualization and invasion (Cano et al., 2000).

The EMT program is orchestrated by various transcription factors, including Slug, Snail, Twist, ZEB1, and ZEB2, which promote a mesenchymal state by suppressing the expression of epithelial markers, such the junctional protein E-cadherin and by inducing expression of other markers associated with the mesenchymal state, like the mesenchymal N-cadherin or vimentin (Thiery et al., 2009). Indeed, several of these transcription factors directly repress levels of E-cadherin, the hallmark of the epithelial state (Cano et al., 2000).

Given the growing evidence contradicting the concept of full phenotype switch form epithelial to mesenchymal state in cancer invasion, the EMT concept has evolved to describe a cell plasticity promoter program (Chaffer et al., 2016; Nieto et al., 2016). In this new definition, epithelial cells acquire some or lose some epithelial features allowing them to disseminate and form metastasis, but they do not completely lose their epithelial identity (Bronsert et al., 2014; Krebs et al., 2017). In human CRC, Bronsert et al have performed a serial 3D reconstruction of histological slides of the invasive front of tumors from various human carcinomas, including CRC. They found no single cells in the peritumoral stroma but only CRC clusters characterized by Zeb-1 expression and decreased but still present E-cadherin expression. They suggested this expression pattern to promote a collective mode of invasion (Bronsert et al., 2014), thus supporting the hypothesis that cancer cells may undergo partial EMT and present a mixed phenotype with mesenchymal and epithelial features (Nieto et al., 2016). However, two recent studies in preclinical models of pancreatic cancers and breast cancer have shown that EMT was not required for dissemination but was instead

necessary for resistance to chemotherapy, questioning the contribution of EMT to cell invasion (Fischer et al., 2015; Zheng et al., 2015).

1.3.4 Do CRC retain their epithelial architecture during metastatic dissemination?

Clinical evidence keep emerging in which cohesive and/or glandular organized carcinoma cells are observed at peritumoral site of carcinoma (Brabletz et al., 2001; Khalil et al., 2017; Prall et al., 2009). In these reports, 3D reconstruction of the histological sections allow to identify cancer cells clusters, which could be missed by simply analyzing 2D sections. Patient histological specimens reveal that peritumoral stroma was invaded by carcinoma clusters that retained their cell-cell junction through E-cadherin in CRC as well as breast or pancreas carcinoma (Brabletz et al., 2001; Bronsert et al., 2014; Khalil et al., 2017; Prall et al., 2009). Unexpectedly, invasive CRC were found to retain a more complete epithelial architecture, as well-differentiated glandular CRC clusters were observed in the peritumoral stroma: in addition to cell-cell adhesions, the cancer cells surrounding a luminal cavity, displayed an apico-basolateral polarity (Prall et al., 2009). All these studies demonstrate the maintenance of epithelial features, at least during invasion, the first step of tumor metastasis.

Further supporting the maintenance and contribution of epithelial features to tumor cell dissemination, cancer cell clusters were demonstrated to be more efficient metastasis seeders than single cells in breast carcinoma (Aceto et al., 2014; Cheung et al., 2016). Using mouse models with primary carcinoma containing cancer cells with mixed expression of fluorescent proteins, two studies were able to demonstrate that metastasis arise from multicellular carcinoma cell clusters. These two studies, elegantly proved that these carcinoma cluster cells were not the result of cell aggregation, but that they had maintained their cell-cell junctions from the primary tumor and through the dissemination process (Aceto et al., 2014; Cheung et al., 2016). Hence these studies prove that carcinoma cells maintain their epithelial features to disseminate, which may be a selective advantage.

All in all, emerging evidence point to a mode of dissemination in which carcinoma cells remain cohesive and retain some of their epithelial features. EMT has for long been thought to be the main player of carcinoma dissemination, but strong evidence now supports a predominant role for other dissemination processes that do not require EMT. Therefore the challenge is now to better understand what are the molecular and cellular mechanisms of this

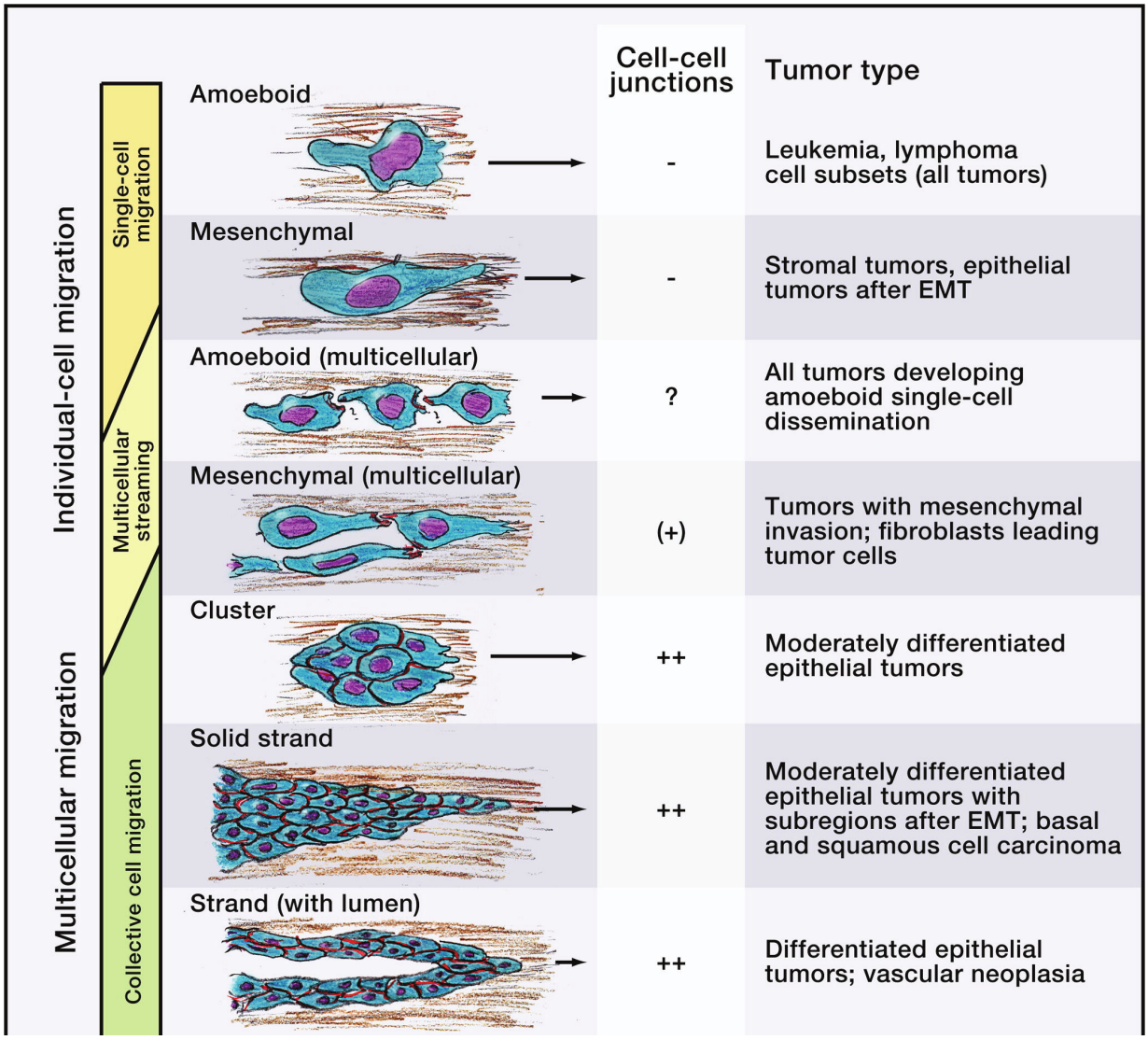

Figure 9.

Cancer cells modes of invasion

Adapted from friedl, 2009

A

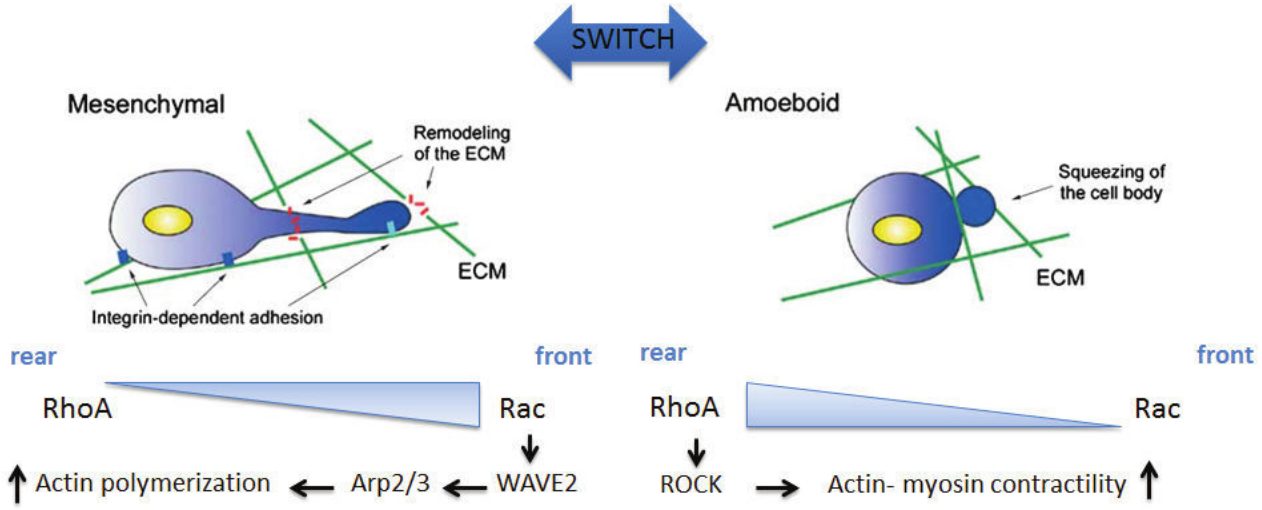

B

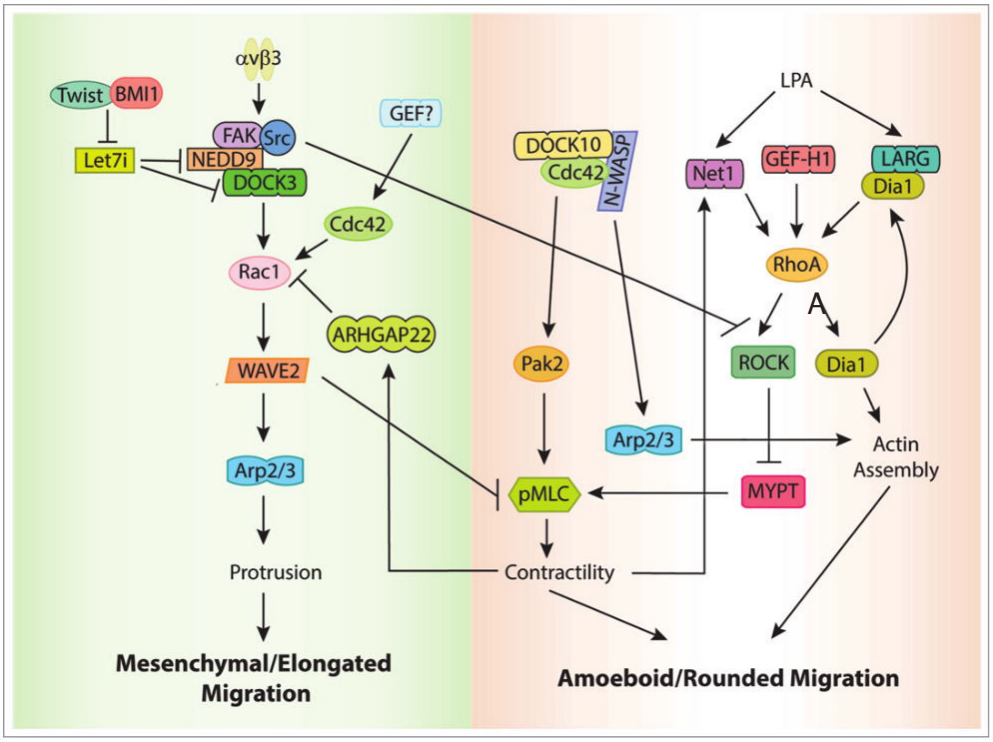

Figure 10 .

A-Schematic representation of the switch between Mesenchymal and Amoeboid cell invasion depending on RhoA and Rac sigaling pathway. Mesenchymal invasion is depending on a high actin polymerisation and amoeboid invasion is depending on a high acto-myosin contractility.

B- Rho-GTPase signaling regulating single cell invasion

Adapted from Goicoechea SM, 2014

epithelial-based dissemination modes.

2 Cancer cell invasion

Given that metastasis account for 90% of all cancer related deaths, identifying the mechanisms at the basis of this process is critical to allow the establishment of efficient therapeutical treatments. As cell invasion is the first, and therefore critical step to the metastatic progression of cancer, key mechanisms driving its process are suitable targets for therapeutics.

2.1 Cell motility in the organism

Cell invasion is related to cell migration, which is the physiological mechanism that allows cells to actively move. While migration defines cells movement on 2D substrates, invasion refers to the navigation of cells through 3D matrices. In physiological conditions, cell motility contributes to the early development of tissues during embryogenesis and participates to adult tissue processes such as tissue regeneration and healing or immune cells surveillance. Cancer cells hijack this physiological processes to achieve their dissemination. Therefore, the understanding of molecular and cellular of cancer cell invasion comes essentially from the study of normal cells as well as neoplastic cells(Friedl and Gilmour, 2009; Friedl and Wolf, 2010)

2.2 Cancer cell invasion

Cancer cells can adopt different modes of invasion to adapt to the microenvironment they encounter throughout dissemination. Depending on their nature and differentiated state, cancer cells can either invade individually (mesenchymal cancer or carcinoma cancer cells that have undergone EMT) or in a collective manner (carcinoma), in which the cells are cohesive through maintenance of cell-cell junctions (Figure 9).

2.2.1 Individual mode of invasion

Mechanistically, there are two modes of single cell invasion relying on distinct requirements of adhesion, proteolysis of the extracellular matrix (ECM) and F-actin dynamics (Friedl, 2004; Wolf et al., 2003). Individually disseminating cells originate from sarcoma or carcinoma that have undergone EMT (figure 10).

The mesenchymal mode of invasion is a traction-based locomotion relying on integrin/ECM interaction and Rac1-dependent polymerization of branched actin at the protrusive leading edge. At the rear, RhoA/ROCK/Myosin signaling is necessary for the cell retraction but do not directly contribute to the forward force generation (Ridley et al., 2003) (figure 10).

The amoeboid mode of invasion is a propulsion-based mode that relies on high acto-myosin contractility. Cells undergoing amoeboid migration use propulsive forces to squeeze between the fibers of 3D environments. The locomotion relies on the friction forces generated by myosin contractility and F-actin retrograde flow while integrin adhesion and ECM proteolysis are negligible (Orgaz et al., 2014; Paluch and Raz, 2013; Sanz-Moreno et al., 2011) (figure 10).

2.2.2 Collective mode of invasion

Collective invasion is the mode by which cells move throughout the matrix as a cohesive unit, with a supracellular coordination of their cytoskeleton and of the forces generated to drive movement. The invading group harbors a supracellular front/rear polarization, with the presence of two functionally distinct cell subtypes: the leaders at the front and the followers at the rear. Contribution of collective invasion to cancer cell dissemination depends on tumor type and tumor stage. Friedl et al., made the first observation of collective invasion of cancer cells, using explants of squamous cell carcinoma, ductal breast cancer. Further work reported prostate, breast and pancreas cancers to invade collectively and to retain an epithelial architecture (Brabletz et al., 2001; Bronsert et al., 2014; Christiansen and Rajasekaran, 2006; Giampieri et al., 2009)

2.2.3 Multicellular streaming

Multicellular streaming describes a mode of group movement, in which cell coordination

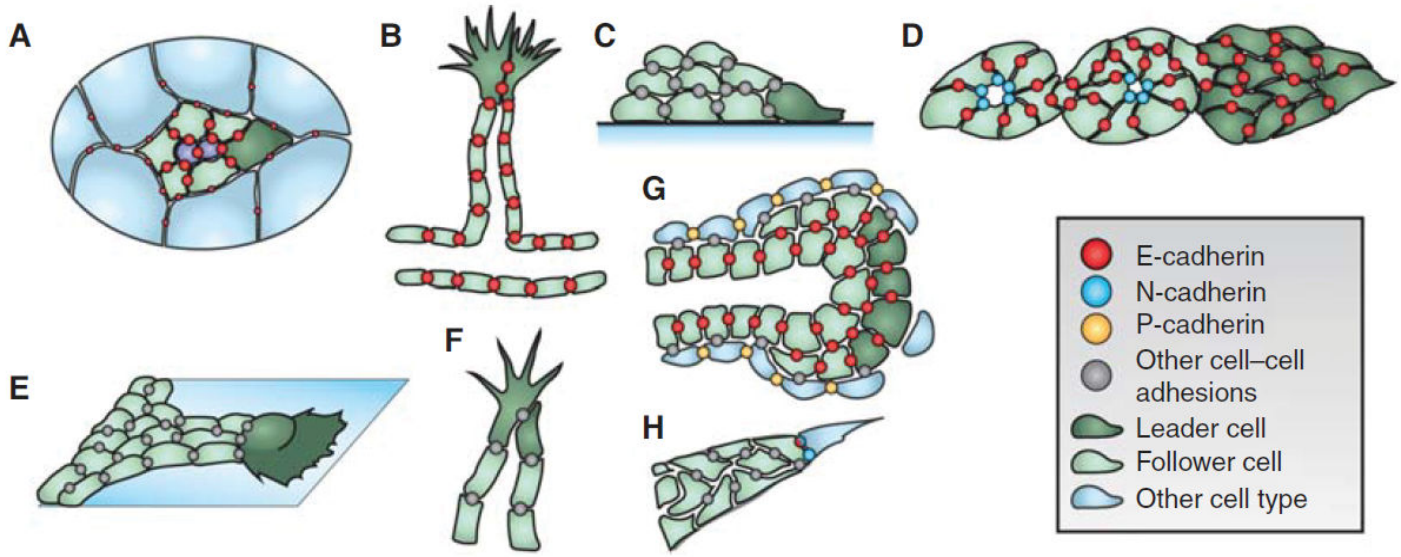

Figure 11. Models of collective cell migration

Models of collective migration. (A) Drosophila border cell cluster. Cluster of two polar cells (purple) surrounded by epithelial cells migrating between nurse cells (blue). Main adhesion molecule: Drosophila epithelial (DE)-cadherin (in order of decreasing expression: polar cells, border cells, nurse cells) (B) Drosophila tracheal branching. Branches sprout from dorsal trunk by active migration of the leader cell and elongation and intercalation of follower cells. Follower cells are also polarized apicobasally toward the lumen .Main adhesion molecule: DE-cadherin (C) Xenopus mesendoderm. Migrates as a multilayered sheet over fibronectin-rich extracellular matrix (ECM). Leader and follower cells in contact with the ECM show front–rear polarization and extend lamellipodia. Main adhesion molecule: C-cadherin (D) Zebrafish lateral line. Leading zone is polarized in the direction of migration. Behind the leading zone, there is a transitional zone in which cells acquire apicobasal polarity and are organized into rosette-like sensory organs. Main adhesion molecules: E-cadherin (throughout), N-cadherin (accumulates apically at rosette) (E) Wound healing assay. 2D sheet migration assay, in which a gap is created in a confluent monolayer. Leader cells extend lamellipodia and migrate into the wound area. Main adhesion molecules: cell-type dependent. (F) Vascular sprouting. Migrates as cord with lumen led by two leader cells. The trailing cells elongate parallel but polarize apicobasally perpendicularly to the direction of migration . Main adhesion molecule: vascular endothelial (VE)-cadherin. (G) Mammary branching. Migration of multilayered structure called terminal end bud (TEB) consisting of luminal epithelial cells that lose apicobasal polarity but retain E-cadherin and are partially covered by myoepithelial cells (blue). Leader cell in the TEB lack protrusive structures. Main adhesion molecules: myoepithelial cells, P-cadherin; luminal epithelial cells, E-cadherin . (H) Heterotypic cancer cell migration. Cancer cohorts may recruit other cell types (blue), such as fibroblasts or myeloid cells as leader cells. Main adhesion molecules: Heterotypic E-N-cadherin contacts or homotypic N-N and tight junctions .Adapted from Venhuizen and Zegers 2017.

results from the fact that the cells are attracted towards the same guiding cues and navigate through the same preformed tracks. Cell-cell adhesions are loose, (short-lived or weak) and the cells organize their cytoskeleton and generate forces toward the ECM independently. This individual behavior in a group movement is distinguished from the collective invasion of cohesive cells (Clark and Vignjevic, 2015; Friedl and Alexander, 2011; Friedl et al., 2012).

2.3 Molecular and cellular mechanisms of collective invasion

2.3.1 Studying collective invasion using different models and experimental settings

Different experimental designs exist to study collective invasion, while they do not recapitulate at the same time the features of the type of collective invasion, they come closer to some of them and they are great tools that have allowed us to better study the molecular mechanisms of collective invasion. Of course they all present some caveats and the mechanisms that are true for one model can not always be translated to another model. It is therefore essential to acknowledge how different parameters of the experimentation can impact on the broadness of the described mechanism described (Figure 11).

2D monolayers migration assays have been the most-widely used to study collective migration. When using epithelial cells, they allow the study of signaling pathways related to the multicellular mechanocoupling, force sensing and generation (Das et al., 2015; Omelchenko et al., 2003; Reffay et al., 2014). Use of astrocytes cells in these assays uncovered the mechanism of leader cell polarization (Etienne-Manneville and Hall, 2001; Osmani et al., 2006, 2010). Cell-cell junction contribution to collective invasion were deciphered thanks to the 2D monolayer assays (Camand et al., 2012; Etienne-Manneville, 2014; Hidalgo-Carcedo et al., 2011; Omelchenko and Hall, 2012; Plutoni et al., 2016a) (figure 11).

3D *in vitro* assays allow the tuning of ECM to mimic the environment in which the cells evolve and adapt stiffness, geometry, and pore sizes. Multicellular structure can be generated artificially by forming aggregation spheres, or by morphogenesis of epithelial cells.

Border

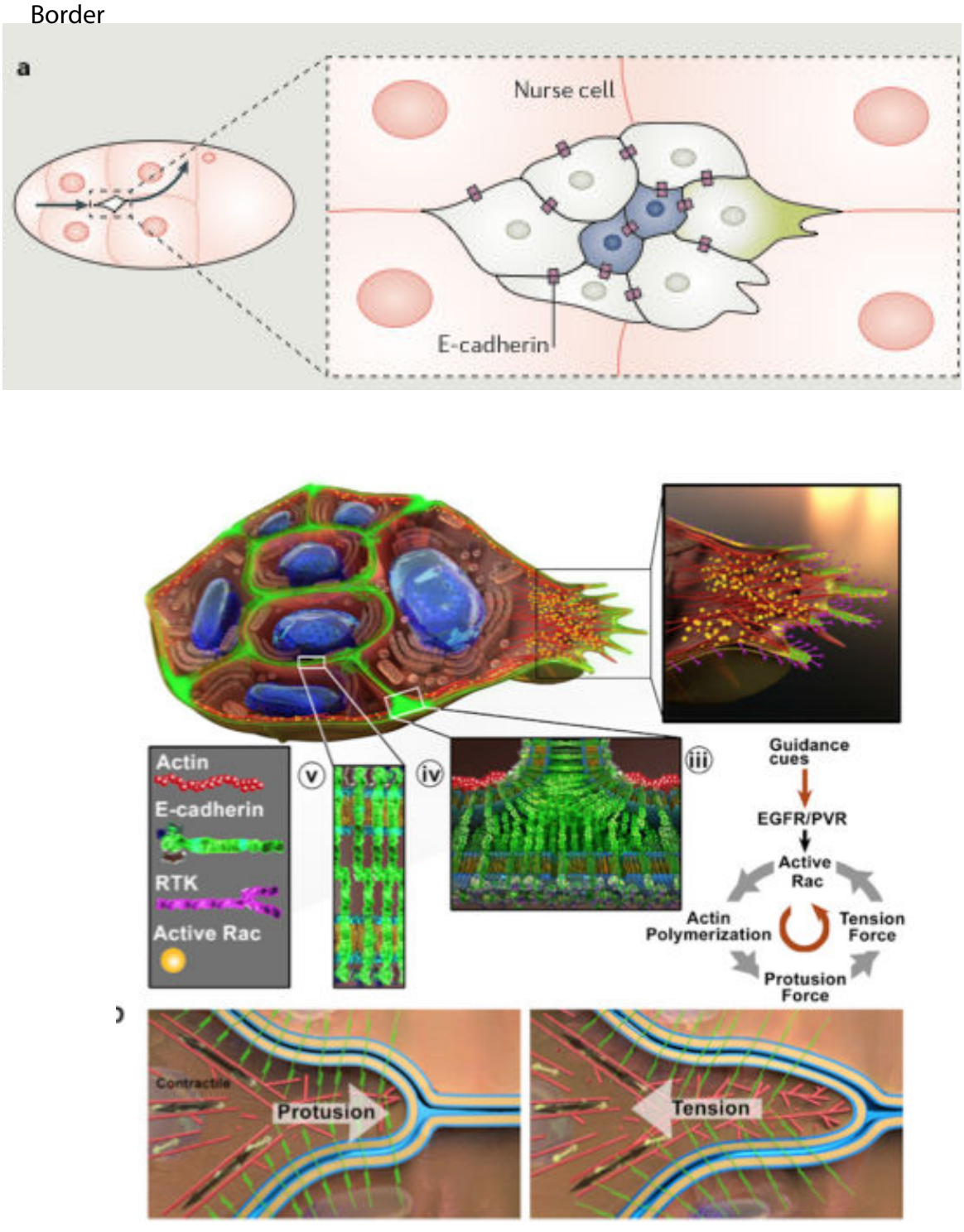

Figure 12. Border cells collective migration in the Drosophila ovary chamber

Adapted from Friedl 2009 and Cai, 2014

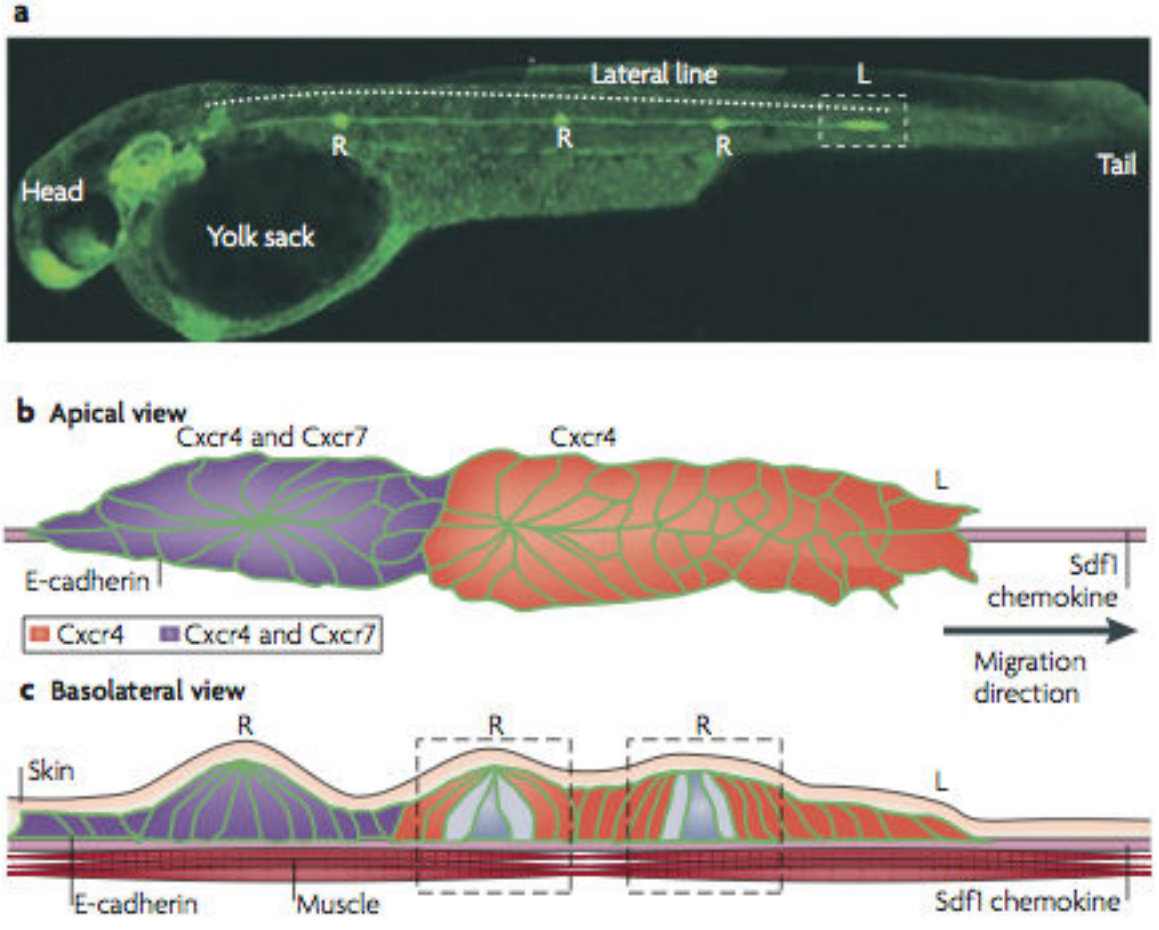

Figure 13. Collective migration of the lateral line of the Zebrafish.
Schematic representation of the collective migration observed at the lateral line of the Zebrafish, (adapted from Friedl et al., 2009).

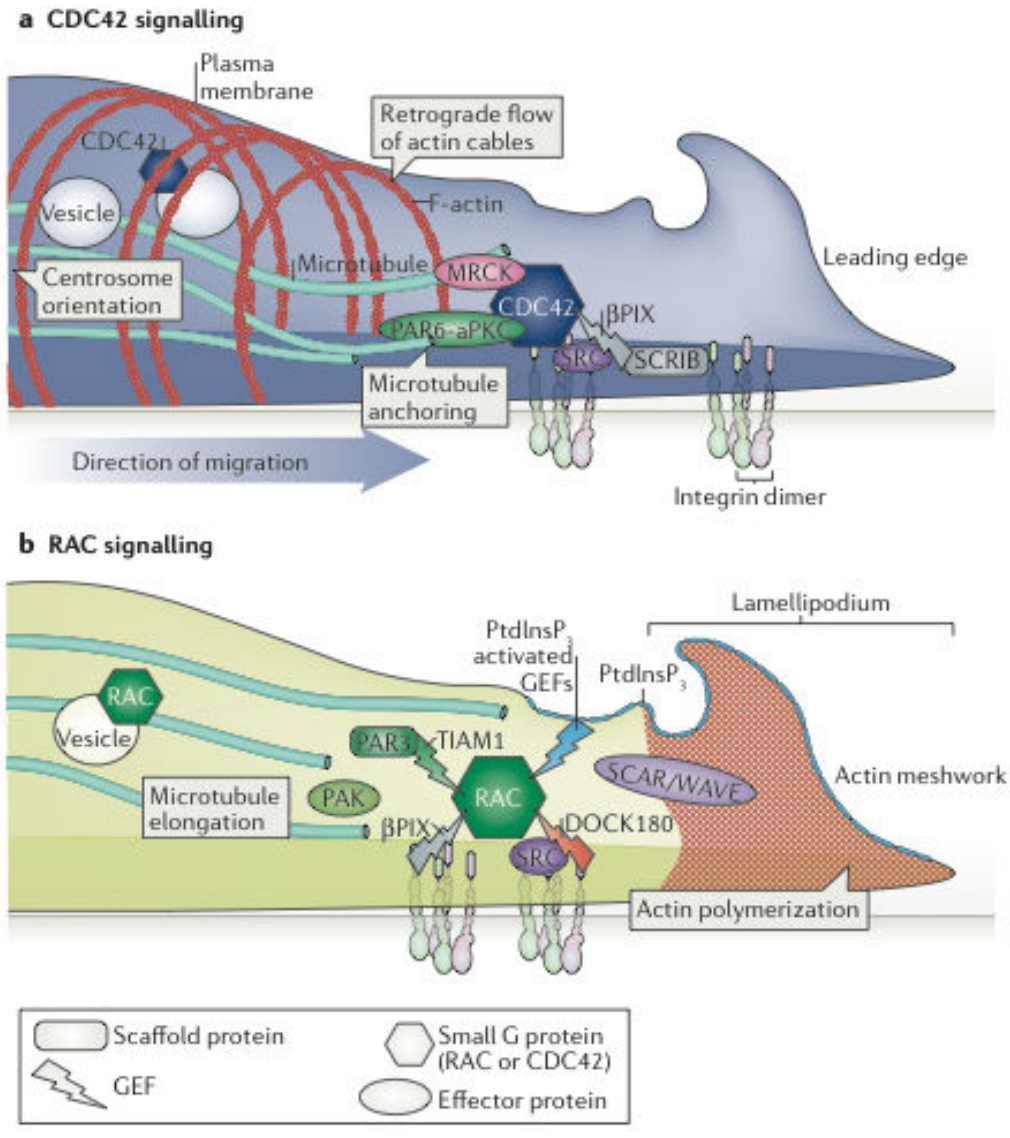

Figure 14. Cdc42 and Rac1 activity polarization in the leader cells.

Adapted from Roberto Mayor, 2009

Cell lines, explants from animal model or patients or more physiological PDX can be used (Cheung et al., 2016; Friedl et al., 1995; Julien et al., 2012) (Figure 11).

Physiological 3D *in vivo* collective migration is observed in many developmental processes. The most studied are the Border cells from Drosophila and the primordium lateral line (pLL) of Zebrafish (Friedl and Gilmour, 2009; Montell et al., 2012; Wang et al., 2010) (figure 12 and 13). The pLL is a cohesive cohort of more than 100 cells that migrate along the antero-posterior axis. The group is formed of a less organized leading region and a rear tightly packaged, rosette-like mechanosensory organ progenitors, that are deposited during migration (Haas and Gilmour, 2006). Border cells are a cohesive group of 6 to 8 cells that migrate in the ovary chamber of Drosophila between the nurse cells. Two distinct cell types: 4 to 8 migratory cells surround two central non migratory polar cells (Montell et al., 2012) (figure 11).
Pathological collective invasion is available thanks to genetically engineered mice models or mice injected with tumoral which are used to monitor collective invasion of cancer cell *in vivo* (Alexander et al., 2013; Cheung et al., 2013, 2016; Giampieri et al., 2009).

2.3.2 Leader/follower polarization

Polarized Rac1 and Cdc42 activation promotes leader cell fate

The first work to demonstrate that high level of Rac1 is sufficient to induce leader cell formation was conducted in the collectively migrating border cells of Drosophila (figure 12). Using a photoactivatable form of Rac1 that can be transiently activated by illumination, (Wang et al., 2010) were able to redirect the whole border cell migration by promoting Rac1 activity in only one cell of the moving group. Interestingly, preventing leader cell formation by activating dominant negative form of Rac1 in the protruding leader induced formation of multiple protruding leader cells. This suggested that Rac1 activation was necessary to polarize the whole group of border cell, 1) by inducing leader cell protrusion and 2) by instructing the followers not to become leaders.

The requirement of Rac1 polarization to form leader cell has been further confirmed in *in vitro models* of epithelial and astrocytes cells or *in vivo* model anterovisceral (AVE). Rac1activation is required in epithelial leader cells and was shown to be induced by PI3K

a

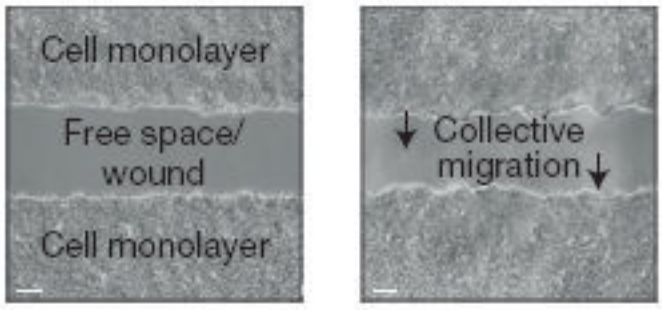

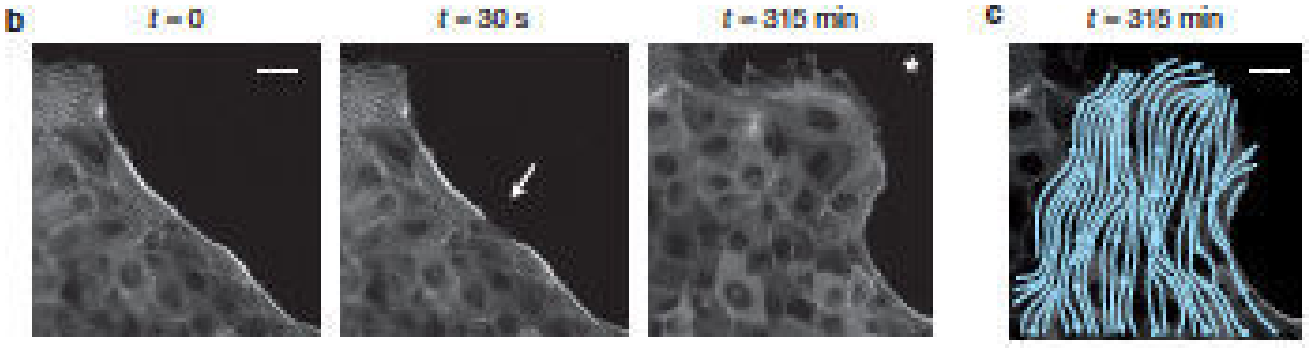

Figure 15.

(a) 2D monolayer collective migration of epithelial cells
The contractile acto-myosin cable controls the initiation of new leader cells.
(b) GFP–actin stained epithelial cells.The ablation of the cable triggers the appearance of a new leader cell, demonstrating its 'confinement' function in preventing the nset of new leaders.
The arrow shows the point of laser ablation, and the asterisk is next to the new leader cell that starts to develop at this ablation point on the cable. Adapted from Reffay, 2014

signaling (Yamaguchi et al., 2015). Besides its activity, the polarization of its activity similarly was demonstrated to be as important to induce leader/follower polarization. In collectively migrating astrocytes as well as in AVE model, spatially restricted activation of Rac1 at the front edge of leaders was necessary to induce directed and efficient cell protrusion for collective migration. Such spatial resolution was achieved by polarized relocalization of Scrib, beta-Pix and Cdc42 at the front edge, which led to activation of Cdc42 at the front edge of the cell (figure 14). Recently, the Merlin protein was also implicated in Rac1 activity polarization. In 2D collectively migrating monolayer of epithelial cells, Merlin decreases Rac1 activation through the Rac1 specific GAP RICH at the rear of leader cells and follower cells to promote lamellipodia formation at the front (Das et al., 2015).

Acto-myosin cable tension restricts leader cell formation

Studies led in 2D collective migration towards free space (wound healing assays) of epithelial cells have revealed a major role of acto-myosin network generated forces in the formation of leader cells (Omelchenko et al., 2003; Reffay et al., 2014; Riahi et al., 2015) (figure 15). In these assays, formation of leader cells is restricted by a pluricellular acto-myosin cable that runs across the edge and align the epithelial cells facing the free space. Photoablation of the cable demonstrated it was under tension and anchored to the substrate thereby exerting traction forces opposite to free space which confined leader cells (Reffay et al., 2014). Few leader cells form at sites of weaker tension where disassembly of the acto-myosin cable can be observed (Omelchenko et al., 2003; Riahi et al., 2015). In support to this, leader cells were spontaneously forming at sites of acto-myosin cable ablation (Reffay et al., 2014). These leader cells harbor straight actin bundles directed toward the free space to form broad lamellipodia, in which microtubules are able to grow (Omelchenko et al., 2003). The traction forces, opposite to the free space, are created by the advancing lamellipodia and are transmitted to the rest of the cells through the junctions and the acto-myosin cable that lines the free edge to promotes forward movement of the monolayer. Myosin II inhibition by the ROCK proteins inhibitor Y27632 or expression of RhoA (T19N) led to the generation of multiple protruding cells with lamellipodia indicating that RhoA/ROCK signaling controlled the acto-myosin cable formation and the leader cell density at leading edge of collectively migrating monolayers (Omelchenko et al., 2003). While RhoA/ROCK controls the traction

forces of the leader cells, it was shown that generation of lamellipodia was dependent on Rac1 activity (Reffay et al., 2014; Yamaguchi et al., 2015). Interestingly, it was demonstrated that the acto-myosin tension was controlling the Notch-Dll4 signalling pathway in the determination of leader cells. In fact, Dll4 expression was induced in cells at the weaker site of the acto-myosin cable's tension. The cells expressing high levels of Dll4 would be leaders and would instruct the follower state to cells that were expressing Notch1 at the rear of monolayer (Riahi et al., 2015). This work provided a mechanostransduction pathway dependent on the acto-myosin cable.

Leader formation in 2D clusters of SCC (squamous carcinoma cells) was also shown to be restricted by supracellular peripheral acto-myosin network. When DDR (Discoidin domain receptor family) was depleted in these models, the peripheral acto-myosin network was lost and led to formation of multiple leader cells (Hidalgo-Carcedo et al., 2011).

Similary, in Drosophila border cells collective migration, it was shown that the late rotation movement of the border cells is no longer protrusion driven but instead relies on high levels of cortical acto-myosin network, suggesting that the actomyosin contractility restricts protrusive leader formation (Combedazou et al., 2017) . In the same model, cortical actin that is bound to moesin was shown to be required to prevent ectopic leader cell formation from multiple cell of the moving group. Here again, the findings are in agreement with the role of a peripheral actin network that restricts leader cell formation (Ramel et al., 2013).

In conclusion acto-myosin generates traction forces under the control of RhoA/ROCK signaling pathway. This regulates leader density at the edge of collectively migrating cells therefore participating in the leader/follower polarization of collectively invading cells.

Anisotropic interaction with the ECM determines leader cell fate

Leader cells display anisotropic contacts with at least one edge that contacts the matrix, which implies engagement of integrins. The attachment to the substrate allows leaders cells to generate traction forces required to drive collective migration of the group. Using different models of collective locomotion, various studies have demonstrated the role of integrins in the leader cell identity. The first work to propose integrins activation as determinants of leader fate used primary melanoma tumors from patients (Hegerfeldt et al., 2002). The authors observed in an *ex vivo* experiment that these tumor were undergoing a polarized front/rear

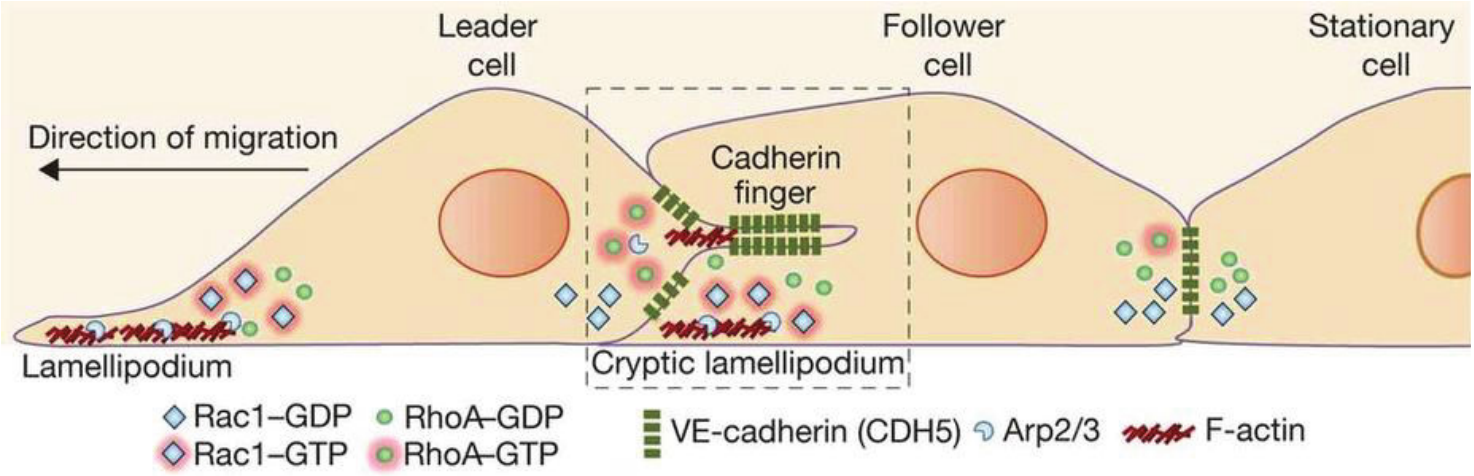

Figure 16. Contribution of follower cell in leader cell formation through establishment of cryptic lamellipodium. Through cell-cell junctions, follower cells are able to induce a region called the cryptic lamellipodium, inducing mechanical forces and establishing leader cell state. Rac1 polarized activation is mandatory for this organelle formation, as well as it is in leader cells to guide movement. Cryptic lamellipodium illustrate the contribution of follower cells in collective migration.

collective invasion in collagen-I invasion assay. The leader cells at the front, were expressing high levels of integrins, which were necessary for efficient collective invasion. Following studies have demonstrated the requirement of integrins activation for leader cell formation in 2D collective migration of epithelial cells and their role in promoting Rac1 activity in the leader cell (Yamaguchi et al., 2015). 2D collective migration of astrocytes have provided more in detail the signaling activated downstream of integrin activation at the front edge of leader cells, which triggers polarization of leader, subsequently leading to polarized activation of Cdc42 and Rac1.

Furthermore, as they pave the way ahead of followers, cancer leader cells also harbor MMPs whereas followers do not. This allows them to modify the ECM to allow the cohort passage (Nabeshima et al., 2000; Wolf et al., 2007).

Leader/follower interaction regulates leader cell formation

For long time follower cells were considered as passive passengers of the collective movement driven by leader cells. However, (Farooqui and Fenteany, 2005) work proved an active contribution of the follower by first reporting the existence of cryptic lamellipodia, formed by followers cells several rows behind the leading edge, that extended underneath adjacent front cells. The formation of these cryptic lamellipodia depends on polarized activation of Rac1 like in leader cells (Das et al., 2015; Plutoni et al., 2016a). The force generated by these organelles is coordinated at a supracellular level to insure the efficient collective movement of the group of cell. The investigation of the role of followers in the collective migration of endothelial cells have revealed the existence of E-cadherin fingers, which E-cadherin rich protusions emitted by a follower. These E-cadherin fingers are polarized and are engulfed by the cell in front of the one emitting the structure. They serve as guidance cue to direct collective invasion (Hayer et al., 2016) (figure 16).

This supracellular coordination relies on cell-cell junctions. They insure the coordinated movement of the migrating cells in 2D. Therefore followers actively contribute to collective migration by generating mechanical forces. The impact of followers on the collective movement is in all cases mediated by cell-cell junctions, which transmit mechanical cues from followers to leaders. Study conducted in mesoderm of Xenopus demonstrated that cadherin mediated pulling forces were sufficient to promote cell protrusion at the opposite site of where the force was exerted. Therefore tension forces exerted on leader cells by followers

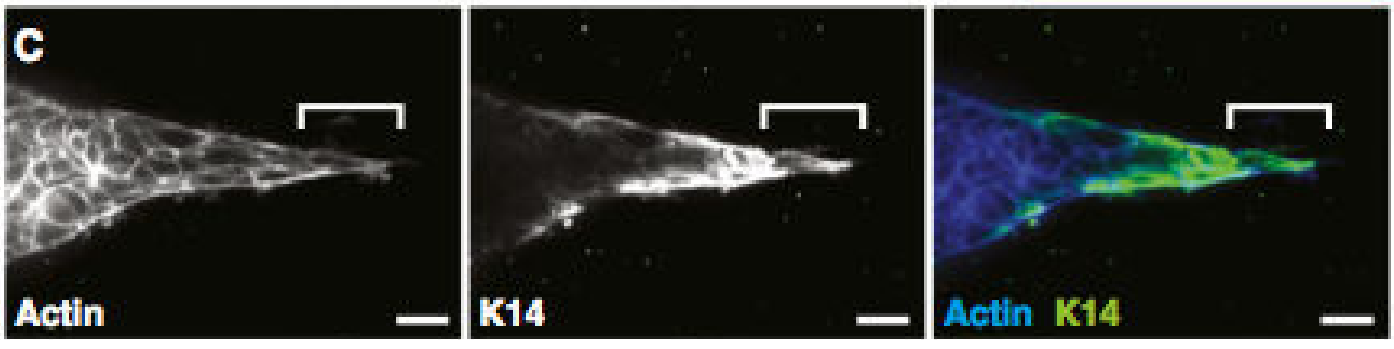

Figure 17.

Immunostaining of the invasive front of primary breast tumor cells invading collagen-I matrix
The leader cells are genetically predefined and express K14

Adapted from Cheung, 2013

contribute to leader cell polarization (Weber et al., 2012). In the same way, border cell's leader cell determination was dependent on E-cadherin cell-cell junction between the follower cells. (Cai et al., 2014) demonstrated that transmission of tensile forces through E-cadherin was restricting leader cell formation while instructing follower cells.

In a different manner, follower cells were shown to contribute to collective movement by actively establishing of a gradient of chemotactic molecules. Sdf1 is the chemotractant that have Cxcr4 and Cxcr7 as receptors. In collectively invading primordium lateral line of the Zebrafish, while leader cells express only Cxcr4, the followers express the Cxcr4 and Cxcr7 receptor. Cxcr7 at the rear of the moving cohort interacts and internalizes sdf1, acting as a molecular sink. This leads to the establishment of Sdf1 gradient, with higher levels at the front, where Sdf1 interacts with Cxcr4 receptor of leader cells. The high activation of Cxcr4 is in leader cells of the lateral line of Zebrafish is sufficient to promote the movement of the whole group (Donà et al., 2013).

Leader cells can be genetically predefined cells

Early work conducted in the collective migration lateral line of Zebrafish, showed that the leader/follower polarization could be a stable state predetermined by a polarized expression of a specific gene program (Aman and Piotrowski, 2008). While all of the cells of the lateral line express the chemokine receptor cxcr4b, the cxcrb7 receptor expression is restricted to the follower cells, under the control of Wnt/beta –catenin activity. Elegant mosaic work proved that activation of Cxcr4b at the front of the lateral line was necessary and sufficient to promote protruding leaders that drove the movement of the lateral line (Haas and Gilmour, 2006).

This predefined state of leader cells was further found in the collective invasion of cancer cells. In models of breast cancer collective invasion, leader cells were found to express specific genes to contribute to their invasive ability (Westcott et al., 2015). Similarly In a lung cancer NSCLC model of collective invasion, isolation of leader cells has proved to be distinct from non invasive followers (Konen et al., 2017). Leader cells were expressing a VEGF dependent signaling pathway that reminds the tip-stalk collaboration of collective invasion that drives vasculogenesis (Konen et al., 2017).

Interestingly, it was shown that leader cells of luminal breast cancer cells were expressing a specialized gene expression program of basal myoepithelial cells. Ewald et al, demonstrated in *in vivo* model of luminal breast cancer and using organoids model in 3D *ex vivo* invasion assay, that expression of K14 and p63, marker of basal myoepithelial cells, was acquired and required to form leader cells and required to induce leader cells (Cheung et al., 2013) (figure 17).

Gaggioli and colleagues have shown that leader cell specification can go as far as being insured by heterologous cell type (Gaggioli et al., 2007). They have shown that fibroblast were able to lead collective invasion of squamous carcinoma (SCC). They remodeled the ECM through RhoA/ROCK/myosin dependent contractility and integrin alpha 3 and 5 to generate the tracks that were used by SCC cells to invade the ECM. Contractility of the acto-myosin network of fibroblast and tumor cell is dependent on GP130-IL6ST ligand signaling through JAK-STAT. JAK is a kinase. A positive feedback loop is induced by acto-myosin contractility which is able to induce activation of STAT (Sanz-Moreno et al., 2011).

Chemotactisme contributes to leader cell fate

Chemokine gradient can contribute to leader cell formation. In different models, it was shown that cells that are the closest to the source of chemokines would be promoted to leader cell state. For example, high level activation of PVR (platelet derived growth factor and vascular endothelial growth factor related receptors) and EGFR (epidermal growth factors receptors) determines the leader cell in Border cells of Drosophila (Duchek et al., 2001).

2.3.3 Cell-cell junctions in collective invasion

Cell-cell junctions stabilization insure efficient collective locomotion

Cell-cell junctions are at the center of collective invasion since they insure the physical cohesion of the group. Their stability relies on the cell-cell junction molecules and on the

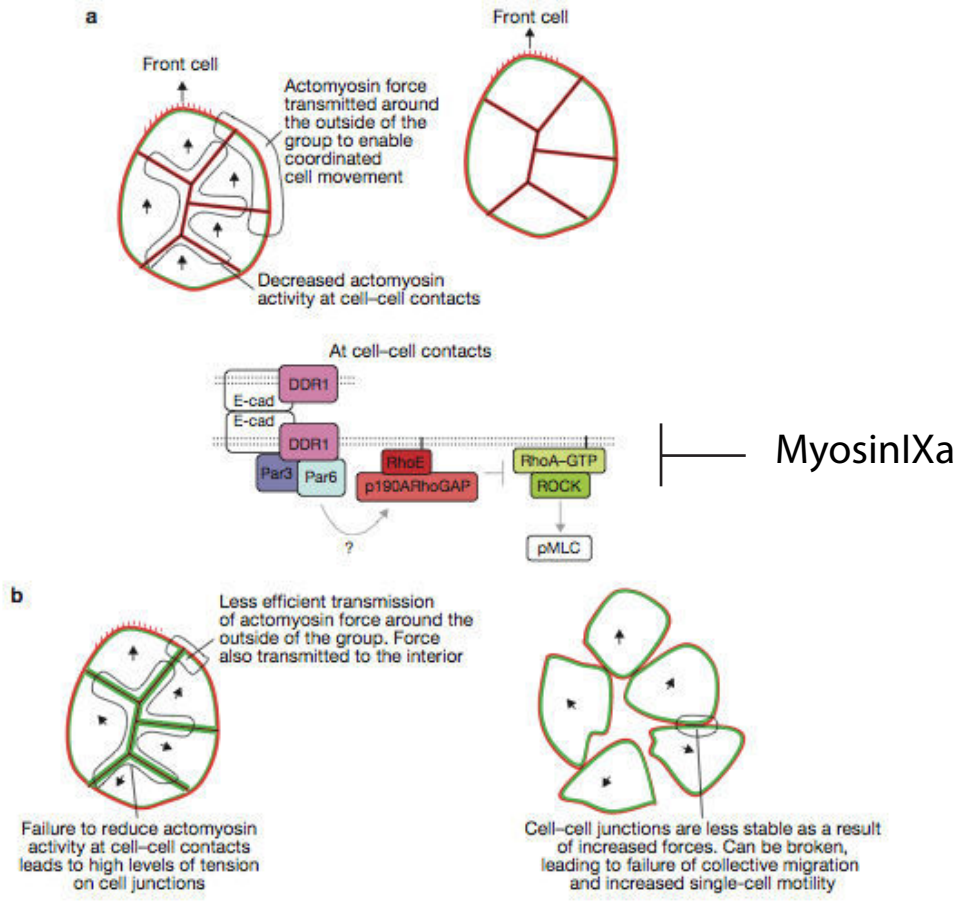

Figure 18.
Junctional acto-myosin must be kept low to allow cohesivness and collective migration

Adapted from Hidalgo-Carcedo, 2012

dynamics of cytoskeleton to which they are attached. Loss of junctional proteins or deregulation of the acto-myosin network contractility can induce cell scattering (figure 18).
Work conducted in 2D collective migration has shown that increasing myosin contractility at cell-cell junction was inducing cell scattering. This was the result of RhoA-GAP MyosinIX downregulation (Omelchenko et al., 2014), by p190Rho-GAP downregulation (Hidalgo-Carcedo et al., 2011) which resulted in high level of RhoA and ROCK. The scattering of cells or absence of cell-cell junction formation is due to tension stress regulation at cell-cell contacts. The effect of acto-myosin contractility on cell-cell adhesion integrity can be explained by the mechanism of formation of the contact, which requires collision of lamellipodium (figure 18).
In border cells the E-cadherin junction between polar cells and border cells are necessary to maintain the cohesion of the border cells.

Cell-cell junctions insure mechanocoupling of the invading group

Besides maintaining group cohesion, cell-cell junctions insure force transmission necessary to coordinate the collective locomotion.
A mechanotransduction pathway involving pulling forces at cell-cell junction uses Merlin to be a molecular transducer that allows supracellular mechanical cooperation. This work came after the first stress force mapping in collectively migrating monolayer which revealed that intercellular shear stress was limited to allow supracellular coordination (Tambe et al., 2011). The downregulation of cell-cell adhesion was increasing intercellular shear stress and inducing loss of supracellular mechanical cooperation.
In 2D cluster of SCC, DDR1 depletion leads to uncoordinated collective behaviour. This was due to elevated actomyosin at cell-cell junction induced by activated ROCK1 downstream of RhoA activation. This activation resulted from inhibition of RhoE-RhoGAP signaling through Par3-Par6 complex whose activity is normally regulated by DDR. This work highlights the signaling hub besides the ones above, the signaling hub present at cell-cell junctions and which insures coordination of the cytoskeleton.

The nature of junctional proteins modulates the adhesion stability and the permeability to cell movement. It was demonstrated that E-, N-, M-, P- and R- cadherin provide different abilities to a collectively migrating group of cell and regulate differently the mechanics of the

moving group(Plutoni et al., 2016b; Weber et al., 2012). A recent work using mice myoblast cells monolayer in the 2D collective migration showed that ectopic expression of E-, R- end P- had distinct effect on the collective migration of myoblast C2C12 cells. In this model overexpressing P-cadherin but not E-cadherin or R-cadherin increased efficiency of collective cell migration through increase of velocity, directionality and persistence.

A tension sensor was used to forces at cell-cell junction in migrating border cells (Cai et al., 2014). The tension generated downstream of PVF and RTK receptor is initiated by protruding cells at the front and gradiently transmitted to rear follower cells where forces are the lowest to promote directional and persistent collective migration of the cluster.

2.3.4 Synchronization of the cytoskeleton

The cytoskeleton dynamic requirement polymerization of actin and generation of contraction through acto-myosin network are the same as in individual cells. However collectively invading cells coordinate these dynamics over many cells in the moving group. Supracellular coordination is mediated by cell-cell junctions, there is also an important part that is operated by the acto-myosin cytoskeleton which is the main integrator of the mechanical and physical forces in invasion.

This acto-myosin coordination was demonstrated to be regulated by DDR, Rac1, and Rab11(Cai et al., 2014; Hidalgo-Carcedo et al., 2011; Ramel et al., 2013).

2.4 Cancer cell invasion determinants

Cancer cell invasion is a plastic adaptive process characterized by modulation of F-actin dynamics, interaction with the ECM and its remodeling that responds to chemical and physical cues. Variations in these features determines the invasion strategy adopted by the cell (Friedl and Alexander, 2011; Sanz-Moreno and Marshall, 2010).

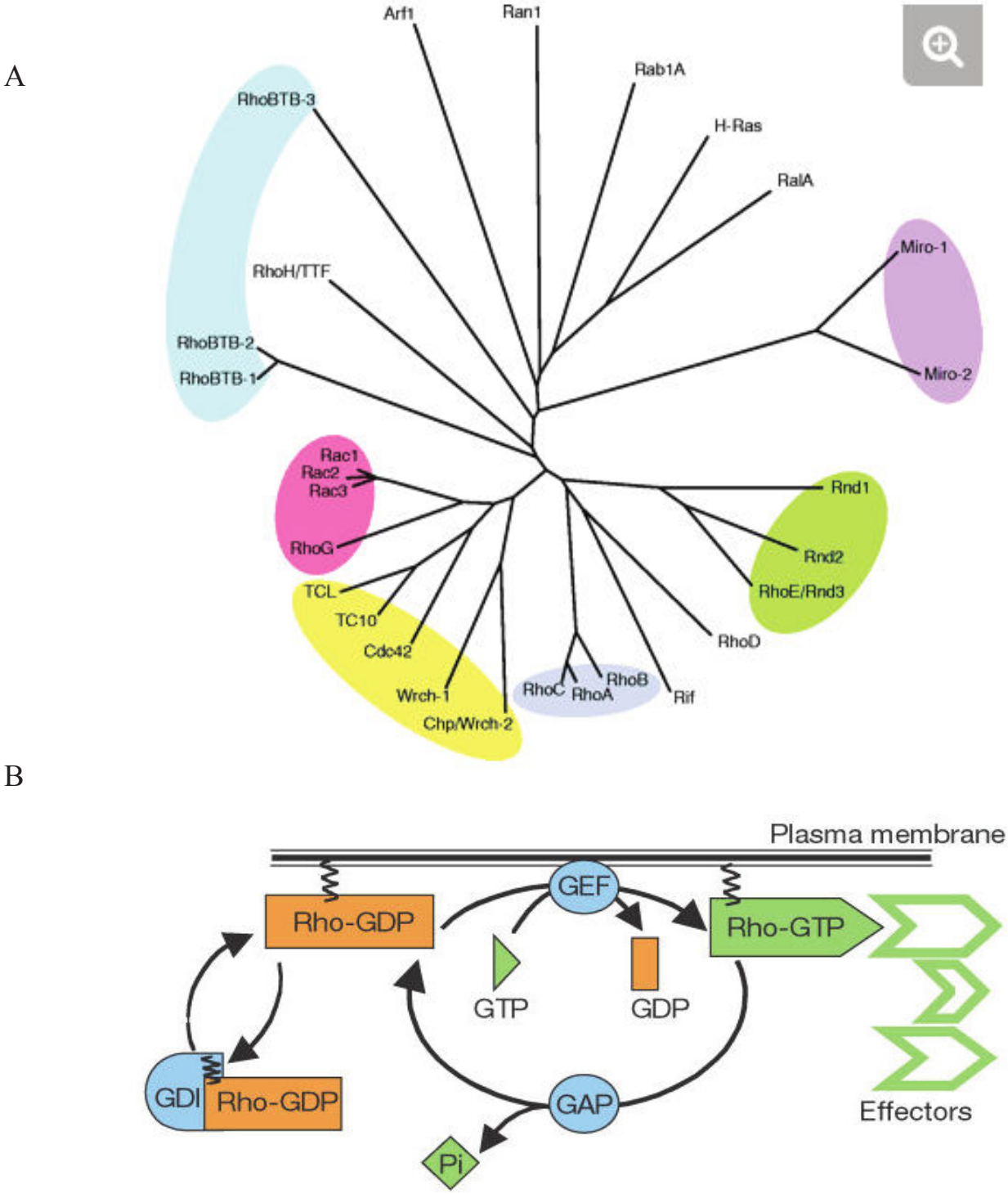

Figure 19. Rho GTPases familly
(A) Phylogenetic tree of the Rho-family GTPases and representatives of other Ras-superfamily GTPases. A phylogenetic analysis of the amino acid sequences of the Rho domains of the 22 Rho-family members made with ClustalW, together with functional data (see text) shows that the family can be roughly divided into six major branches: RhoA-related, Rac-related, Cdc42-related, Rnd proteins, RhoBTB proteins and Miro proteins. Adapted from Wennerberg and Der, 2004.
(B) Rho GTPase cycle between an active (GTP-bound) and an inactive (GDP-bound) conformation. In the active state, they interact with their effectors. The cycle is highly regulated by three classes of proteins: guanine nucleotide exchange factors (GEFs) catalyze nucleotide exchange and mediate activation of Rho GTPases; GTPase-activating proteins (GAPs) stimulate GTP hydrolysis, leading to inactivation of Rho GTPases; and guanine nucleotide exchange inhibitors (GDIs) extract the inactive GTPase from membranes. Adopted from Etienne-Manneville and Hall, 2002.

2.4.1 Extracellular matrix: support and barrier of invasion

The extracellular matrix encountered by invading cells has different compositions depending on the invaded tissue (Willis et al., 2013). In the mesenchymal mode of invasion, it provides the cancer cells with a substrate for adhesion and subsequent traction but also opposes a physical barrier to their movement, which they overcome by engaging a proteolytic or mechanical ECM-remodeling program (Clark and Vignjevic, 2015; Wolf and Friedl, 2011).
Cells invading in an amoeboid way, do not rely on adhesion to the matrix and overcome the barrier imposed by the ECM by modifying their shape in order to navigate through the matrix.
Neoplastic cells invade two major extracellular matrix subtypes: (i) the basement membrane, that lines all the epithelium, and (ii) the interstitium, the connective tissue in organs (Rowe and Weiss, 2008; Wolf and Friedl, 2011). Laminin and Collagen IV are the main components of the basement membrane (Rowe and Weiss, 2009), whereas connective tissue is mainly composed of Collagen-I.
The geometry, the topology and the stiffness impact cell invasion mode which adapts to the microenvironmental constrains (Charras and Sahai, 2014; Clark and Vignjevic, 2015).

Cells are able to sense the stiffness of the ECM by engagement of integrins and proteases can degrade the matrix thereby releasing the cell confinement, relaxing the ECM and generating tracks to facilitate cell invasion (Friedl and Wolf, 2008). These proteases include matrix metalloproteinase (MMPs), ADAMs, cathepsins, urokinase plasminogen activator (uPA) (Mason and Joyce, 2011).

2.4.2 Guiding cues: polarizing and guiding invasion

The microenvironment is full of signaling cues which are gradiently distributed and who will guide the cell through the invasion route. This guiding cues can be either molecules**,** namely cytokines or chemokines or mechanical parameters of the ECM, termed haptotactisme or durotaxisme.
These guiding cues are integrated by receptors or the integrin, whose activation triggers signaling pathways that will polarize the cell in a front-rear manner.

3 Small RhoGTPases signaling pathways

3.1 The RhoGTPase signaling pathway

Small RhoGTPases are members of the Ras superfamily. RhoGTPases are small molecules with a molecular weight between 20 kDa and 30 kDa. They display 30 to 50% of sequence homology with RasGTPase family (Madaule and Axel, 1985; Wennerberg and Der, 2004). Mammalian cells count 24 RhoGTPases encoded by 22 genes. They are divided into six 6 sub-families. Among them RhoA, Rac1 and Cdc42 are the most well studied (figure 19).

Most RhoGTPases are switch proteins, which bind guanines nucleotides to cycle between an active state and an inactive state: a GTP-bound active conformation and a GDP-bound inactive conformation. In their active form they can interact with downstream effectors molecules to regulate several specific signaling pathways and processes. Their cycling between the two states is regulated by three classes of proteins: the activators guanine nucleotide exchange factors (GEF), the inactivators GTPase activating proteins (GAP) and the guanine nucleotide dissociation inhibitors (GDI). GEFs catalyze the exchange between GDP and GTP, GAPs accelerate the intrinsic hydrolytic activity of small Rho GTPases converting GTP into GDP (Etienne-Manneville and Hall, 2002) and GDIs sequester the GDP-bound inactive small RhoGTPases in the cytoplasm preventing their translocation to membranes and activation by GEFs (Hodge and Ridley, 2016).

“Atypical” small RhoGTPases which comprise RhoE/Rnd family do not use the cycling mechanism and do not require GEFs and GAPs. Instead, they are constitutively GTP-bound, because they either possess high intrinsic nucleotide exchange activity or have substitutions in their GTPase domain that prevent GTPase activity (Wennerberg et al., 2003).

At the structural level, small RhoGTPases share the same domain organization with the core G domain, a hallmark of small RhoGTPases, which mediates the guanosine binding. The switch I and switch II regions sense the binding of GDP or a GTP molecule and change their conformation accordingly. The C-terminal CAAX-box to which a lipid anchor is attached allows GTPase binding to membranes (Wennerberg and Der, 2004).

Even if mammalian Small RhoGTPases are only 24, they participate in a wide range of cellular processes. A single RhoGTPases' activity can regulate a wide range signaling pathways (Etienne-Manneville and Hall, 2002; Ridley, 2015). The specificity of their activity relies on a finely tuned spatio-temporal regulation that is achieved thanks to post translational modifications not only at the level of the small RhoGTPases themselves, but also at the level of their regulators (GEFs, GAPs and GDIs) and effectors. Localization into proteique complexes regulates their interaction with specific GEFs and GAPs and effectors. In addition, also protein stability regulation plays an important role in the control of small RhoGTPases activity (Hodge and Ridley, 2016).

The three prototypical members of the small Rho-GTPase family are Ras-related C3 botulinum toxin substrate (Rac1), Ras homolog family member (RhoA) and cell division cycle 42 (Cdc42). All these three small GTPases have been extensively linked to cell migration mainly through their role in cytoskeleton dynamic regulation (Ridley, 2015).

3.2 RhoGTPases effectors

Rho effector protein are proteins that interact preferentially with the GTP-bound form of Rho GTPases. A large number of Rho effectors (more than 90 in humans) have been identified including kinases, phosphatases, lipases, adaptors and scaffolds. Particular GTPases interact with specific effector proteins. Effector proteins are therefore activated by different RhoGTPase family members bound to GTP. The switch I and switch II regions of RhoGTPases are responsible for that specific binding. Indeed, the switch I region shows significant amino acid substitution between the different RhoGTPases, and therefore contributes to the specific RhoGTPase-effector interaction. Moreover, upon GTP binding, RhoGTPases undergo a conformationnal change in the switch I and switch II regions, which is specific of active RhoGTPases and promotes effector proteins binding (Bishop and Hall, 2000; Ihara et al., 1998).

Rho effectors interact with RhoGTPases through their Rho-binding domain (RBD). Conserved RBDs are present in some Rho effectors, and structural studies have shown how selective Rho-GTPase binding occurs (Bishop and Hall, 2000; Zhao and Manser, 2005).

Several Cdc42 and Rac effectors contain a conserved CRIB motif (Cdc42 and Rac interactive binding), including PAK (p21-activated kinase), ACK (activated Cdc42-associated kinase) and WASP (Wiskott-Aldrich syndrome protein). The CRIB motif is a short sequence of 15

A

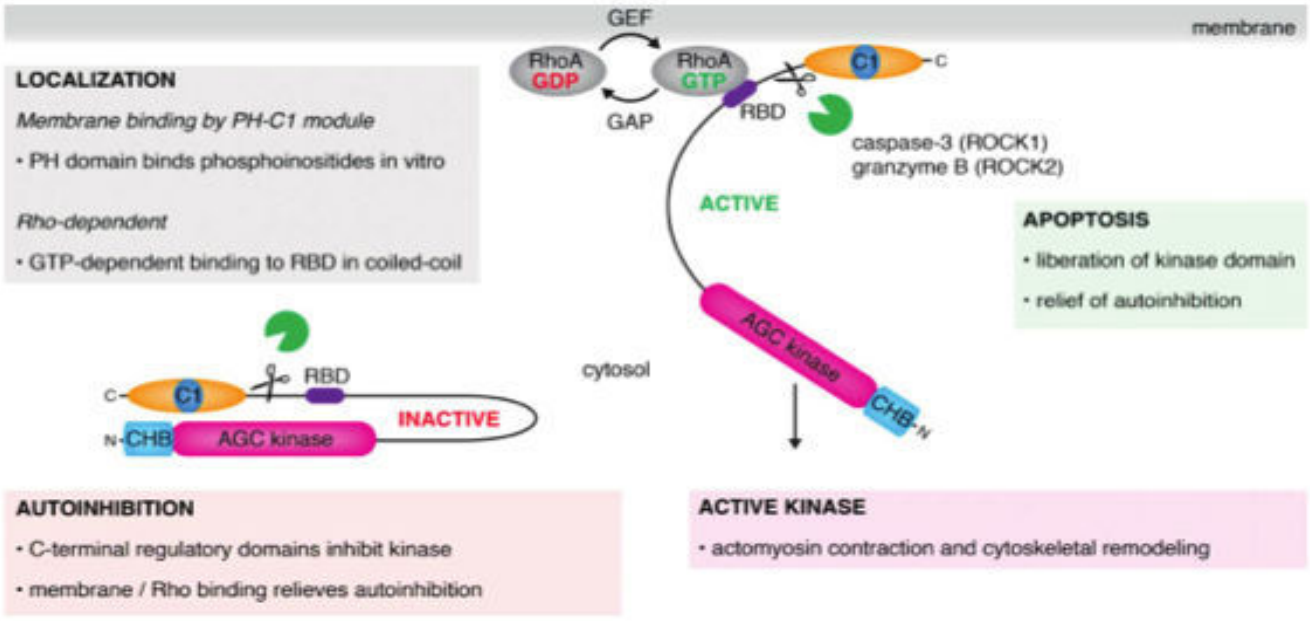

B

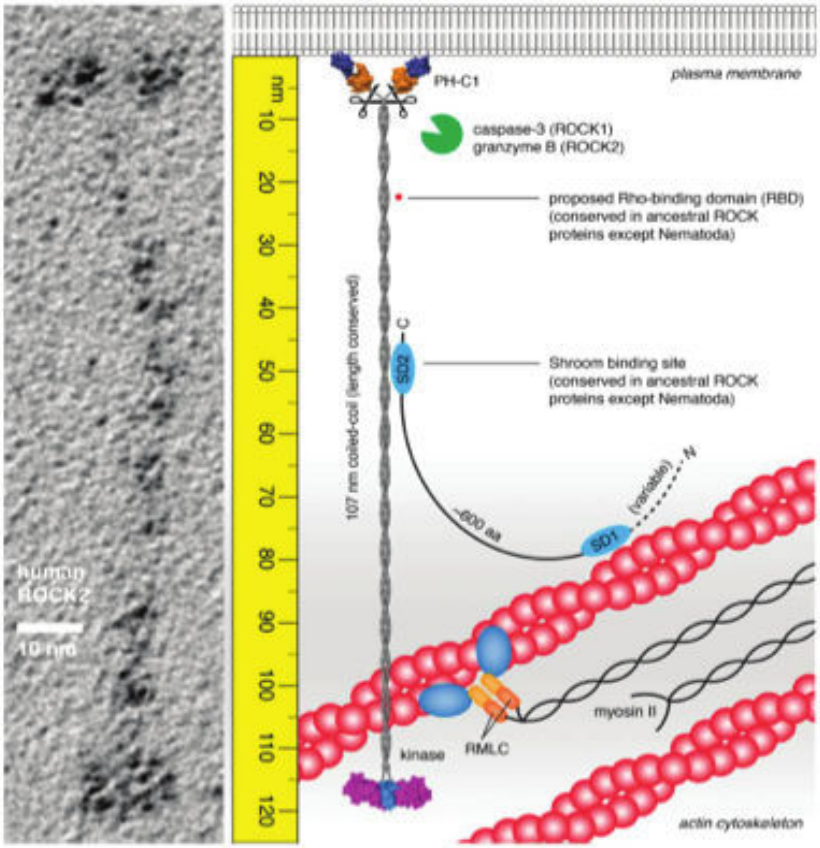

Figure 20. Two models for ROCK kinases activation.

A-MODEL 1 : RhoA-GTP binding unfolds the protein

B-MODEL 2 : Position of the kinase domain relative to its substrate regulates ROCKs activity

Adapted from Truebenstein et al. 2015

amino acids found within a larger RBD, which is typically about 50 amino acids in length. Conserved residues in the CRIB motif interact with the Switch I region of the RhoGTPase. Residues within the RBD but outside the CRIB motif make extensive contacts with the switch regions and also non-switch regions of the RhoGTPase. These contacts involve non-conserved residues, which conditionnes the selectivity of RhoGTPases for specific effector proteins, even amongst those containing CRIB domains.

The RhoA effectors PRK (PKC-related kinase, also called PKN, protein kinase novel) and ROCK (Rho coiled-coil kinase) show a completely different mode of GTPase interaction. Their coiled-coil repeat, which do not share any sequence similarity, contain the RBD and mediate their interaction with RhoA-GTP's switch I and switch II domains as well as non-switch regions(Bishop and Hall, 2000).

3.2.1 RhoA effector : ROCK

ROCK (Rho associated coiled-coil containing kinase) family of proteins, consists of two isozymes ROCK1 (also known as p160 ROCK, ROK beta or Rho-kinase beta) and ROCK2 (also known as Rho-kinase alpha and ROK alpha), which are major RhoA-GTP effectors (Matsui et al., 1996). They belong to the large family of AGC serine/threonine kinases proteins and are closely related to the Rho-activated kinase members of this family: citron Rho-interacting kinase (CRIK), myotonin protein kinase (DMPK) and myotonic dystrophy kinase-related CDC42-binding kinase MRCK (Pearce et al., 2010).

ROCK proteins expression

Historically, ROCK proteins were isolated from humans and rat brain extracts as RhoA interactors (Ishizaki et al., 1996; Leung et al., 1995; Matsui et al., 1996). Their expression is found in vertebrates and invertebrates. In humans, they are encoded on chromosome 18 and chromosome 2 respectively. The tissue distribution of both proteins has been determined by Tissue-specific Gene expression analysis and found ubiquitous expression in 30 human tissues apart for the cervix, tongue and thymus where ROCK2 expression could not be detected (Liu et al., 2008).

ROCK proteins structure

ROCK1 and ROCK2 are approximately 160 kDA proteins of respectively 1354 aminoacids and 1388 aminoacids and they present an overall homology of 64% (Nakagawa et al., 1996). They possess an amino-terminal (N-ter) serine/threonine kinase surrounded by N-ter and carboxyl-terminal (C-ter) extension segments which are necessary for the catalytic activity and dimerization of the protein (Jacobs et al., 2006; Yamaguchi et al., 2006). The kinase is followed by a coiled-coil organized region, which contains the Rho-binding domain (RB). At the carboxy-terminal, the proteins harbor a pleckstrin homology (PH) domain, which contains a cystein rich region. While they display a 92% homology of their kinase domain, ROCK1 and ROCK2 homology in the coil-coiled region and the PH domain drops to 55% and 66% respectively. These regions are proposed to regulate the kinase activity toward specific targets. While the coiled-coil domain may help protein dimerization (Chen et al., 2002a), the PH domain is responsible for ROCK localization at the plasma membrane and the C-ter RB-PH region is thought to interact with kinase domain and promote an inactive auto-inhibited conformation of the proteins (Amano et al., 1999; Chen et al., 2002a) (figure20).

ROCK proteins localization

ROCK kinases localization is thought to contribute to the specificity towards its substrate (Yoneda et al., 2005) and as a matter of fact ROCKs were found in many subcellular compartments. Using immunofluorescence, early studies have found both ROCKs to be distributed in the cytoplasm and to be relocalized to the plasma membrane upon RhoA-GTP activation. (Leung et al., 1995; Matsui et al., 1996). Besides their RhoA-GTP dependent plasma membrane localization, it was also reported that ROCK1 and ROCK2 are able to localize to the plasma membrane thanks to their PH domain (Yoneda et al., 2005) and to the activity of their effectors shrooms (Nishimura and Takeichi, 2008) and Myosin-II (Priya et al., 2015, 2017). In fibroblasts, ROCK2 was found to localize at cellular ruffles and in the nucleus, whereas ROCK1 was mainly cytoplasmic and decorated stress-fibers (Yoneda et al., 2005). Indeed, the localization of ROCK was confirmed by Co-sedimentation experiments where ROCK1 was found in the same fraction of stress fibers of fibroblasts. This localization at stress fibers was assumed to be mediated by the PH domain of ROCK1 that is able to interact with Myosin-II (Kawabata et al., 2004). ROCK2 was reported to localize in the

nucleus (Tanaka et al., 2006) and at cell-cell contacts to regulate adducin interaction with F-actin (Kimura et al., 1998). ROCK2 ability to interact with vimentin or the centrosome was reported (Sin et al., 1998).

In conclusion, ROCK1 and ROCK2 harbor distinct localization, depending on cell types and on cellular process, reflecting the specificity of each isoform and the variety of functions insured by ROCK activity.

Activation of ROCK kinases

Structural analysis have revealed that ROCK proteins act as a homodimer in which the kinase domains interact in head to head homodimer manner, whereas the C-terminal RB and PH domains remain monomeric (Couzens et al., 2009; Truebestein et al., 2015; Yamaguchi et al., 2006).

Although ROCK proteins possess a basal kinase activity, their activity is promoted by RhoA-GTP, considered its main activator. This occurs by binding of the small RhoGTPase to the RB domain of the protein leading to a conformational change initiating interactions of serine/threonine kinases with substrates (Ishizaki et al., 1997; Leung et al., 1996; Matsui et al., 1996). ROCK activity can also be modulated through interaction of C-terminal PH domain with lipid mediators and with the plasma membrane (Chen et al., 2002b; Feng et al., 1999) and through proteolytic cleavage of the C-ter region of ROCK by Caspases or Granzymes (Coleman et al., 2001; Sebbagh et al., 2001, 2005). Truncation of the C-ter regulatory domains of ROCKs results in a constitutively active form of ROCK termed CAT. According to the model 1, the activation is achieved by preventing the auto-inhibited conformation whereas according to the model 2, it is achieved by loss of its specific localization, which conditions its access to spatially restricted substrates.

Although the CAT mutant is an accepted experimental tool to study ROCK functions, it is important to keep in mind that the enzyme loses its specific localization in the cell and therefore might phosphorylate proteins that are usually not targeted by ROCK (Amano et al., 1996; Croft et al., 2004).

Two model for ROCK activity regulation have been proposed (figure 20) :

Model 1: RhoA-GTP activates ROCK kinases

The first mode of regulation of ROCK has been established for more than 20 years and proposes that ROCKs adopts an auto-inhibited conformation, in which the C-ter domains (RBD and PH) interact with the kinase domain thereby preventing access of substrates to the catalytic site. Binding of activated RhoA-GTP to the RB domain induces switch to an activated conformation by releasing the kinase and allowing its interaction with the substrate. This model of activation is supported by multiple observations. 1) RhoA-GTP increases ROCKs activity *in vitro* and *in vivo* (Ishizaki et al., 1996, 1997; Matsui et al., 1996); 2) antibodies targeting the RBD of ROCK which mimic binding of RhoA-GTP also increase ROCK activity (Chen et al., 2002a); 3) the truncated mutant of ROCK (CAT) containing only the catalytic domain harbors increased kinase activity compared to full length protein (Amano et al., 1997). This active form of ROCK is also found *in vivo*, in fact it was shown that ROCK1 and ROCK2 are cleaved by the caspase-3 and the granzyme B respectively to induce constitutive activation of the proteins in apoptotic cells (Coleman et al., 2001; Sebbagh et al., 2001, 2005). ROCK2 was also reported to be cleaved by caspase-2 which induced its activation in endothelial cells. 4) The truncated ROCK mutant (RB-PH) containing only the C-ter domains of ROCK interacts with and inhibits the activity of the ROCK mutant CAT (Amano et al., 1999).

Model 2: Constitutively active ROCKs are regulated by positioning of their kinases relative to their substrates

The recently proposed second model of ROCK activity regulation claims that ROCK activity is regulated by the length and the bending of the central coiled-coil domain (Truebestein et al., 2015). Although the study was conducted on ROCK2 isoform, the resulting model of regulation is proposed for both isoform in agreement with their domain structure homology. Analysis of ROCK structure by electron microscopy revealed that ROCK exists in a constitutively extended unfolded conformation, excluding the auto-inhibited conformation proposed in the first model. In line with this and in agreement with previous observations, authors found that ROCK kinase activation does not require RhoA-GTP binding, which only increases by 2-fold ROCK basal activation (Amano et al., 1996; Truebestein et al., 2015). Authors demonstrated that truncation of the 107 nm long coiled-coil

region is sufficient to inhibit ROCK dependent stress fiber formation in NIH3T3 fibroblasts, proving the importance of positioning of the kinase domain at the extremity of the coil-coiled domain in regulation of ROCKs activity. The new model therefore proposes that ROCK activity is regulated by spatial positioning of its kinase relative to its substrate (Truebestein et al., 2015, 2016). This positioning is mediated by the coiled-coil domain, which has a conserved length, and whose bending by interactors (the authors proposed the ROCK effector Shroom) modulates the localization of the kinase domain hanging in the cytoplasm.

Inhibition of ROCK kinases

To the contrary to RhoA, RhoB and RhoC which activate ROCKs by interacting with their RBD at C-ter (Ishizaki et al., 1997; Leung et al., 1995; Matsui et al., 1996), RhoE/Rnd3 interacts with the N-terminal domain of ROCK1 to inhibit its kinase activity (Guasch et al., 1998; Hidalgo-Carcedo et al., 2011; Nobes et al., 1998; Riento et al., 2003); PDK1 competes with RhoE/Rnd3 for the same binding domain to prevent the negative regulation of ROCK1 by RhoE/Rnd3 (Pinner and Sahai, 2008). Rad and Gem interact with ROCK1 in the coiled-coil region, on a site that is distinct from the RBD to inhibit its activity (Ward et al., 2002) All these studies indicate additional regulatory mechanisms of ROCK kinase catalytic activity and highlight the particular important of the N-ter anc C-ter extended domain of the kinase domain (Jacobs et al., 2006; Yamaguchi et al., 2006).

Because ROCK activation is associated with different diseases such as cardiovascular diseases, neurodegeneratives diseases, research of efficient pharmacological molecules has made available multiple ROCK inhibitors (Hahmann and Schroeter, 2010). Different ROCK inhibitors are available to study ROCKs function. Fasudil, Y27632 and H1152 are the most used. They are small molecules, which target ROCKs kinase domain and prevent its activation in an ATP competitive manner irrespective of the isoform. Y27632 has been first identified in the context of cell muscle contraction, while H1152 was identified in a screen of isoquinoline compounds and displays higher potency toward the kinases (Sasaki et al., 2002; Uehata et al., 1997). Fasudil is an approved drug for vasospasm treatment. Recently, two inhibitors specific to ROCKs, irrespective of the isoform and with *in vivo* compatible pharmacokinetics have been identified CCT12925 and AT13148 (Sadok et al., 2015).

ROCK kinases substrates

ROCK1 and ROCK2 show high homology in their kinase domain, and their consensus phosphorylation sequence is R/KXS/T or R/KXXS/T (X is any amino acid). However ROCK1 null mice and ROCK2 null mice are both lethal, suggesting that ROCK1 and ROCK2 kinases regulate essential distinct functions that cannot be compensated by one another. The functions they regulate depend on the targeted substrates.

In 1996, the Kaibuchi lab identified ROCK2 kinase first two targets: Non-muscle Myosin II (NMMII) and the Phosphatase protein1 (PP1) revealing its central role in the acto-myosin cytoskeleton regulation (Amano et al., 1996; Matsui et al., 1996). More than 20 years later, they developed a new technology, the kinase interacting substrate screening (KISS), which allowed them to identified 140 protein candidates substrates of both ROCK s (Amano et al., 2015). Showing the reliability of this method, already known ROCK targets, which were discovered over the years, were also found.

In the regulation of the acto-myosin complexe

Both ROCK kinases phosphorylate the regulatory light chain of Myosin-II on Thr18 and Ser19 (Amano et al., 1996; Emmert et al., 2004). The phosphorylation leads to a conformational change of the Myosin heads and promotes their interaction with actin filaments. This leads to the ATP-dependent activation of Myosin-II which allows it movement along actin filaments and induces the F-actin contractility. Therefore ROCK phosphorylation of MLC increases acto-myosin network formation and contractility in the cell.

ROCKs phosphorylates the myosin phosphatase target subunit 1 (MYPT1) (or myosin binding subunit (MBS)/ Protein Phosphatase 1 Regulatory Subunit 12A (PPP1R12A)) on two inhibitory sites Thr853 and Thr696 (Feng et al., 1999; Ichikawa et al., 1996; Kawano et al., 1999). MYPT1 is a regulatory subunit of protein phosphatase 1 gamma (PP1gamma) also known as the myosin phosphatase, which also encompasses a small subunit M20. PP1 gamma is a member of a class of the protein phosphatase 1 (PP1) multimeric serine/threonine phosphatases, which is composed of a catalytic subunit (PP1c) and a regulatory subunit. The catalytic subunit complexes with various regulatory subunits which determine PP1's substrate specificity (Cohen, 2002). MYPT1 interacts with and targets PP1c gamma to Myosin-II,

which dephosphorylates MLC on Thr18 and Ser19 and inactivates myosin. ROCK inhibitory phosphorylation of MYPT1 promotes its dissociation from myosin and inhibits MLC dephosphorylation. This leads to a net increase of MLC phosphorylation and thereby an increase of Myosin ATPase activity (Amano et al., 1996; Kawano et al., 1999).

In the regulation of F-actin dynamic

ROCKs phosphorylates and activates LIM kinases 1 and 2 on Thr508 and Thr505 respectively (Maekawa et al., 1999a; Ohashi et al., 2000). Activated LIM kinases phosphorylate and inhibit the actin severing protein cofilin and the actin depolymerizing factor (ADF) resulting in the loss of their capacity to depolymerize actin filaments. Therefore, phosphorylation of LIM kinases by ROCK induces an increase of actin filament stability in the cell.
ROCK1 was reported to phosphorylate the G-actin binding protein profilin and prevent its association to G-actin in the context of the Huntigton disease (Shao et al., 2008).

ROCK is capable of phosphorylating adducin, an actin filament binding protein (Kimura et al., 1998)(Fukata et al., 1999). Phosphorylation of alpha adducing promotes its binding to F-actin and spectrin and induces a specific organization of F-actin in ruffling membrane of migrating cells.

Ezrin, radixin, moesin (ERM) are closely related proteins, which connect the plasma membrane and the actin cytoskeleton. They are phosphorylated by ROCK at Thr567, Thr564, and Thr558, respectively (Matsui et al., 1998) which promotes their cross-linking activity.

Actin binding proteins EEF1, MARCKs and Calponin phosphorylation by ROCK prevents their bindng to F-actin (Izawa et al., 2000; Kaneko et al., 2000; Nagumo et al., 2001).
ROCK1 has been reported to phosphorylate and activate the sodium- hydrogen exchanger NHE1 (Tominaga et al., 1998) thereby promoting stress fiber formation.

In the RhoGTPase signaling pathway

ROCK kinases phosphorylate P190RhoGAP, a GAP for RhoA. Phosphorylation of P190RhoGAP on Ser1150 decreased its activity by preventing binding of RhoGTPase Rnd

which is thought to enhance its activity. Therefore ROCK induces a sustained activation of RhoA GTP by preventing GTP hydrolysis by P190RhoGAP (Mori et al., 2009).

ROCKs phosphorylate FilGAP, a GAP for Rac1, and promotes GTPase activity thereby downregulating Rac1 activation (Ohta et al., 2006). It was also reported that ROCKs phosphorylate Rac1 GEF Tiam1-Tiam2/STEF and prevented Rac1 activation (Takefuji et al., 2007). Therefore, ROCKs mediates a cross-talk between RhoA and Rac1 and is a regulator of the RhoA-Rac1 activation balance (Sanz-Moreno et al., 2008).

Intermediate filament and microtubule dynamic

Vimentin, the glial fibrillary acidic protein (GFAP) and the neurofilaent L protein (NF-L) were found to be ROCK2 substrates (Goto et al., 1998; Kosako et al., 1997, 1999). These are intermediate-filament proteins and their phosphorylation leads to filament disassembly.

ROCKs phosphorylate TAU/MAP2 and CRMP2 and inhibits their microtubule polymerizing activity (Amano et al., 2003)(Arimura et al., 2000).

Cell polarity

The Par3 is part of the polarity complex Par3/Par6/aPKC/Cdc42. ROCK has been reported to phosphorylate Par3 on thr833, promoting its dissociation from the polarity complex (Nakayama et al., 2008). Recently, Scrib polarity protein was identified in a screen and confirmed to be a target of ROCK kinases. In MDCK cells, ROCKs phosphorylate Scrib at Ser1378 and Ser1508 and promotes its binding with Shroom2 thereby forming a ROCK-Shroom-Scrib complex that regulates actin cortical tension (Amano et al., 2015).

ROCK was shown to phosphorylate PTEN, a phosphatase that targets PIP3 to form PIP2 lipids. Li et al in 2005 have elegantly demonstrated that ROCK phosphorylated PTEN to induce polarization of migrating neutrophils.

Given its various effectors, ROCKs activity contributes to many cellular function (Julian and Olson, 2014). ROCK has been most often implicated in the regulation of cell motility, downstream of RhoA.

ROCKs in cancer

Many studies are focused on how the Rho/ROCK pathway is associated with cancer progression. Increased Rho/ROCK activity and/or gene expression have been demonstrated in various types of cancers (Wei et al., 2016) and in experimental *in vivo* models (Croft et al., 2004; Itoh et al., 1999). However, contradicting evidences from *in vitro* studies and data from patients demonstrate the contrary(Lomakin et al., 2015; Sanz-Moreno et al., 2008). In particular, cancer patients were found positive for mutations in the coiled-coil domain of ROCK2, which suggest a possible downregulation of ROCK2 activity (Sari et al., 2013).

3.2.2 RhoA, Rac1 and Cdc42 effectors in cellular functions

The three-prototypical members of the small Rho-GTPase family are Ras-related C3 botulinum toxin substrate (Rac1), Ras homolog family member (RhoA) and cell division cycle 42 (Cdc42). All these three small GTPases have been extensively linked to cell migration (Ridley, 2015).

RhoA, Rac1 and Cdc42 are at the center of cell motility as they orchestrate the F-actin and the microtubule dynamics cytoskeleton dynamics, regulate cell-matrix adhesion and cell-cell adhesion (Etienne-Manneville, 2013; Etienne-Manneville and Hall, 2002). The first role into their cellular function was reported by A. Hall lab in 1992. In their studies, investigators injected activated mutants of RhoA, RAC1 and Cdc42 into fibroblasts. They observed 1) in the case of RhoA injection, formation of stress fibers, that are contractile acto-myosin filaments linked to the extracellular substrates through adhesion , 2) in the case of RAC1, polymerization of actin and formation of membrane ruffling composed of meshed work actin, lamellipodia (Ridley et al., 1992), and 3) in the case of Cdc42, it induced the formation of distinct F-actin, microspike finger-like structures, that are filopodias (Nobes and Hall, 1995). These observations were the first to establish RhoA, RAC1 and Cdc42 as regulators of actin dynamics. Extensive studies followed and allowed the identification of several distinct signaling pathways regulated downstream of the three small RhoGTPase. As actin dynamics,

protrusion and contraction are at the basis of cell motility, small RhoGTPases and dependent signaling pathways were expectedly found to regulate cell invasion.

RhoA, Rac1 and Cdc42 effectors in the F-actin dynamic

Cdc42 promotes actin polymerization through its effector the formin mDia by binding to it and realeasing its autoinhibited conformation. Cdc42 also activates Wiskott-Aldrich Syndrome family of proteins including WASP, N-WASP through direct binding to their CRIB motif within the GTPase binding domain (Rohatgi et al., 1999). The interaction releases an autoinhibited, closed conformation and allows binding of the Arp2/3 complex to the VCA (verprolin homology, cofilin homology, and acidic region) motif and its subsequent activation.

The Arp2/3 complex is composed of seven subunits (Arp2, Arp3, p34, p16, p20, p21 and p40). The Arp2/3 complex is intrinsically inactive and is activated by Nucleation Promoting Factors (NPFs), such as the WASP/Scar family including (N-WASP, WAVE, Scar). These NPFs are activated by Rho GTPases. Rac1 activates Arp2/3 by binding to the SCAR/Wave Regulatory Complex (WRC) components Sra1 and WAVE1 and releases its autoinhibitory coformation by unmasking the VCA motif (verprolin homology, cofilin homology, and acidic region) in WAVE1 which binds and activates the Arp2/3 complex and promotes actin polymerization (Chen et al., 2010; Eden et al., 2002; Miki et al., 1998). WAVE proteins do not have a GTPase binding domain and their activation requires binding of Rac1 to the adapter molecule IRSp53, followed by binding of this complex to the WAVE protein (Miki et al., 1998)· Rac-dependent signaling can also recruit and activate Arpin (for Arp inhibitor) that binds to Arp2/3 but is unable to activate it, and therefore acts as a competitive inhibitor of the Arp2/3 complex (Dang et al., 2013). Arp2/3 binds to the lateral side of a preformed actin ("mother" filament) and nucleates the polymerization of a new "daughter" filament, which results in branched actin network.

ADF/cofilin phosphorylation by Lim kinases inhibits its activity. Lim Kinases are phosphorylated by Rac1 effector protein PAK and RhoA effector proteins ROCK. To destabilize and disassemble F-actin, ADF/cofilins to the side of F-actin and promote severing and depolymerization (Pollard and Borisy, 2003; Revenu et al., 2004).

RhoA provides the trigger for the assembly of contractile acto-myosin filaments

(Ridley and Hall, 1992). RhoA activates ROCK (Rho-associated kinase) which promotes Myosin-II activation by 1) phosphorylation of the myosin light chain (MLC) and 2) inactivation of myosin light chain phosphatas (Amano et al., 1996; Watanabe et al., 1999). In addition, RhoA promotes the polymerization of actin into linear filaments through a direct interaction with its target the formin mDia (an FH (formin homology) domain-containing protein) (Maekawa et al., 1999b; Watanabe et al., 1997). Another target of ROCK is Lim kinase 2, whose phosphorylation by ROCK promotes F-actin stability by inhibiting the activity of the actin severing protein cofilin (Maekawa et al., 1999b; Sumi et al., 2001). This is thought to promote the stability of the acto-myosin network.

RhoA, Rac1 and Cdc42 in the cell-ECM adhesion

Integrins are cell transmembranar receptors which adhere to the ECM with their extracellular domain while their intracellular tail can associate to the cytoskeleton or to signaling proteins such as FAK and SRC. Integrins therefore insure mechanocoupling of the cell cytoskeleton to the ECM, thus playing a central role as mechanotransducers. They are at the center of a signaling hub called Focal Adhesion complexes. Their activation can come from intracellular signaling (inside-out) or extracellular signaling (out-side in) (Campbell and Humphries, 2011). Rho-family GTPases play a key role in integrating intracellular signals downstream of focal adhesions that is needed for the change in cell shape and, eventually, the mode of migration in a given environment. RhoA and its effector ROCK regulate cell adhesion by enhancing acto-myosin contractility (Amano et al., 1997). Conversely cytoskeleton tension also acts on the Focal adhesion to promote their maturation. The Rac/Cdc42-activated PAK family of kinases play key roles in promoting integrin-based adhesion turnover (Lawson and Burridge, 2014) .

RhoA, Rac1 and Cdc42 in the cell-cell adhesion

To assemble adherens junction 1) cells come in contact through exploratory lamellipodial protrusions, when a protrusion contacts a neighboring cell, cadherins and catenins form small clusters at the nascent cell–cell contact, the cell–cell contact and AJs then expand and mature. RhoGTPases regulate cell-cell adhesion, initiation, assembly and stabilization, through regulation of actin dynamics at the site (Yamada and Nelson, 2007)**.** Extensive work on adherens junctions led by A. Yap lab, has demonstrated the important role of RhoA and ROCK1 in the stabilization of cell-cell junction (Priya et al., 2015, 2017). High RhoA and ROCK activity destabilize cell-cell junction through increased ato-myosin contractility

(Hidalgo-Carcedo et al., 2011; Omelchenko and Hall, 2012).

3.3 Guanine nucleotide exchange factors (GEFs)

So far around 80 GEFs have been identified in mammalian cells. These proteins catalyze the exchange of GDP into GTP to promote RhoGTPase activation (Goicoechea et al., 2014; Rossman et al., 2005).

3.3.1 GEFs families: the Dbl homologs (DH) and the dedicated to cytokinesis (DOCKs)

There are two families of GEF proteins: the most abundant is the Dbl-homolgy (DH) domain containing family, characterized by its catalytic DH domain associated to a PH domain to form the DH-PH tandem, and the family DOCK (dedicated to cytokinesis) which contains two conserved domains: the DOCK homology region 1 (DHR1) and its catalytic domain DHR2. The substrates of DOCK family proteins appear to be Rac1 and Cdc42 only (Côté and Vuori, 2002; Meller et al., 2005)(Goicoechea et al., 2014; Rossman et al., 2005).

The DH domains interact extensively with the switch regions of RhoGTPases. Conserved residues that occur within the interface between DH domains and GTPases are likely candidates for determining specific coupling. The DH and PH domains cooperate in the small RhoGTPase activation, as DH-PH domain show greater activity than the DH domain alone. Besides, the PH domain interacts with membrane phospholipids and it is thought to localize the GEF to membranes (He et al., 2013) (Figure 22). Outside of the DH-PH region, GEFs possess a variety of sequence motifs and domains that can connect GEFs to various subcellular sites or signaling pathways and participate to functional specificity. (He et al., 2013; Miller et al., 2014; Rossman et al., 2005).

As for the GEF of the Dbl family, DOCK GEFs present different domains outside of their catalytic DHR2 domain which allow them to interact with other proteins such as the proline rich SH3 (Gadea and Blangy, 2014; Rossman et al., 2005)

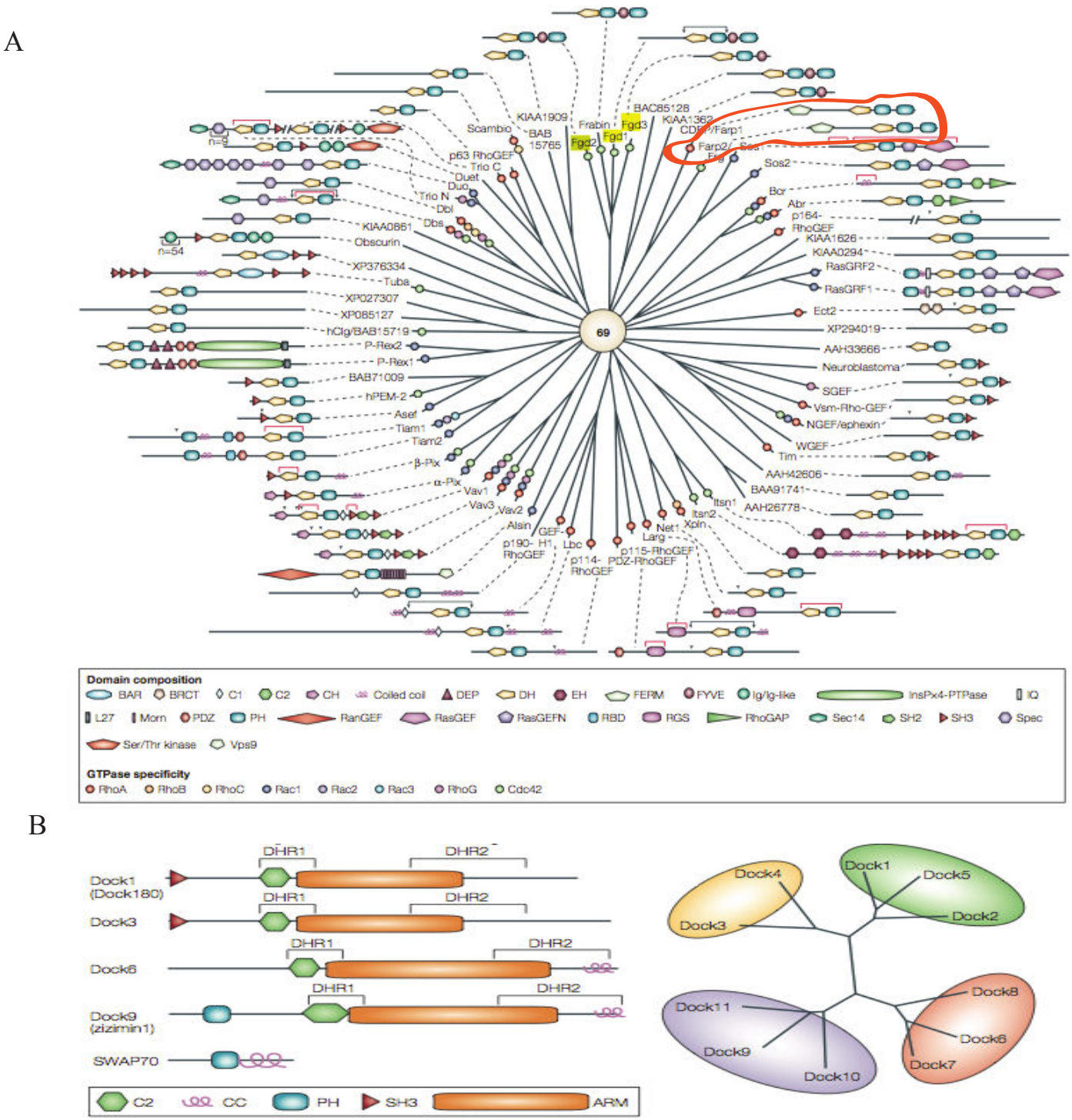

Figure 21. Two GEF families : the DH and the DOCK

(A) The Dbl homology (DH) domains of the 69 unique Dbl proteins in humans have been aligned to produce this phylogenetic tree. Dispersed around the tree branches are illustrations showing the domain composition and domain organization for each member. Black arrowheads above a guanine nucleotide-exchange factor (GEF) indicate truncations that are known to activate either the exchange activity or a related cellular function of the corresponding GEF. Black arrowheads with brackets delineate similarly active fragments. Red brackets indicate regions of Dbl proteins with known three-dimensional structures. The coloured spheres placed on the tree branches designate the reported Rho GTPase specificity of the corresponding Dbl-family member. Note that the specificity summary is not complete for all of the 22 known human Rho GTPases, as the analyses for most Dbl-family proteins has been restricted primarily to RhoA, Rac1 and Cdc42. Furthermore, some Rho GTPases — for example, Rnd3/RhoE and TTF/RhoH — might be constitutively activated and not regulated by GEF activity. Adapted from Rossman and Sondek, 2005

(B) DOCK family GEFs

Adapted from Rossman 2005

3.3.2 Regulation of GEFs activity

By Phosphorylation

RhoGEFs can be regulated by phosphorylation which induces conformational changes in the catalytic domain or promotes GEF binding to scaffolding proteins, resulting usually in activation of the GEF, GDP–GTP exchange and Rho GTPase activation (Hodge and Ridley, 2016). One of the best examples for this type of regulation is Vav GEFs phosphorylation. Non-phosphorylated Vav proteins are inactive due to an auto-inhibited conformation mediated by extensive intramolecular interactions between the N-terminal domain, and the catalytic DH-PH core. (Bustelo, 2014; Yu et al., 2010).Vav GEF is activated by tyrosine phosphorylation, which induces conformational changes of the protein.. In some cases, phosphorylation inhibits GEF activity. For example, Dock6 GEF was shown to be inhibited by phosphorylation *in vitro* and *in vivo*. (Miyamoto et al., 2013). Differently, TIAM1 was shown to be sent for degradation in response to its phosphorylation by Src (Woodcock et al., 2009),

By multi-proteique complex localization

In response to extracellular stimuli, many GEFs interact with specific proteins, including targets of small Rho GTPases, which help to coordinate small Rho GTPase signalling at specific sites in cells. The complexing of DOCK3 to the scaffold protein NEDD9 was shown to promote Rac1 activation in the migration of melanoma (Sanz-Moreno et al., 2008). A well-known example is a complex containing the RAC/CDC42-specific GEF β-PIX with the RAC/CDC42 target PAK, which regulates turnover of integrin-containing focal adhesions (Radu et al., 2014). Among the activating complexes we found the polarity Par complex. It was shown that Tiam1 interaction with Par3 promoted localized Rac1 activation (Nakayama et al., 2008; Nishimura et al., 2005).

By N-terminal truncation

Many GEFs contain an internal inhibitory domain. For several GEFs including Dbl, Vav, Asef, and Ect2, the removal of N-terminal sequences leads to constitutive activation when the protein is expressed in cells (Katzav et al., 1991; Kawasaki et al., 2000; Miki et al., 1993).

3.3.3 The DH GEFs, FARP1 and FARP2

FARP proteins history

FARP1 was the first of the two FARP homologs protein to be discovered and was named CDEP (Chondrocyte Derived Ezrin-like Protein) according to the biological system of cartilage cell differentiation, the chondrocytes, that allowed its first cDNA cloning (Koyano et al., 1997). In this first study, the investigators found that FARP1 expression was induced in response to parathryroid hormone and cAMP during differentiation of chondrocytes that are bone cells.

FARP2 protein was discovered 5 years later by two labs at the same time using a BLAST search of proteins containing the consensus DH domain of Dbl GEFs. The first lab, which named it the FERM including RhoGEF (FIR) was looking for GEF proteins involved in the regulation of neuron development upstream of RhoGTPases (Kubo et al., 2002). The second lab, which searched for the mediator of Src activity to RhoGTP in the endothelin-

GPCR dependent cell motility, named it FRG for FGD1-related Cdc42 GEF (Miyamoto et al., 2003). Only two years later were the two proteins reconciled under the name of FARP2 (Toyofuku et al., 2005).

FARPs structure and expression

FARP proteins (FERM, ArGhef, and Pleckstrin homology domains containing protein) are members of the large family of Dbl GEF proteins. They exist as two homologous proteins FARP1 (or CDEP) and FARP2 (FIR, FRG) that are expressed from two distinct genes, farp1 on the chromosome 13 and farp2 on the chromosome 2 (Figure 22).

FARP1 and FARP2 proteins which are respectively 1045 and 1055 aa long, share 60% of sequence homology and the same domains structure: At their N-terminal extremity, FARP possess a 4.1 band, ezrin, radixin, moesin homology domain (FERM domain), which is able to interact with transmembrane proteins such as CD44. Following is the tandem «Dbl homolog" (DH) – pleckstrin homolog (PH) domain that is characteristic of Dbl family of GEFs. Finally, at the C-terminal end they display a second PH domain (PH2).

FARP1 is highly expressed in human fetal brain and spleen, mildly expressed in the heart, liver and intestine whereas in adults it is expressed in kidney, testis and lung and low

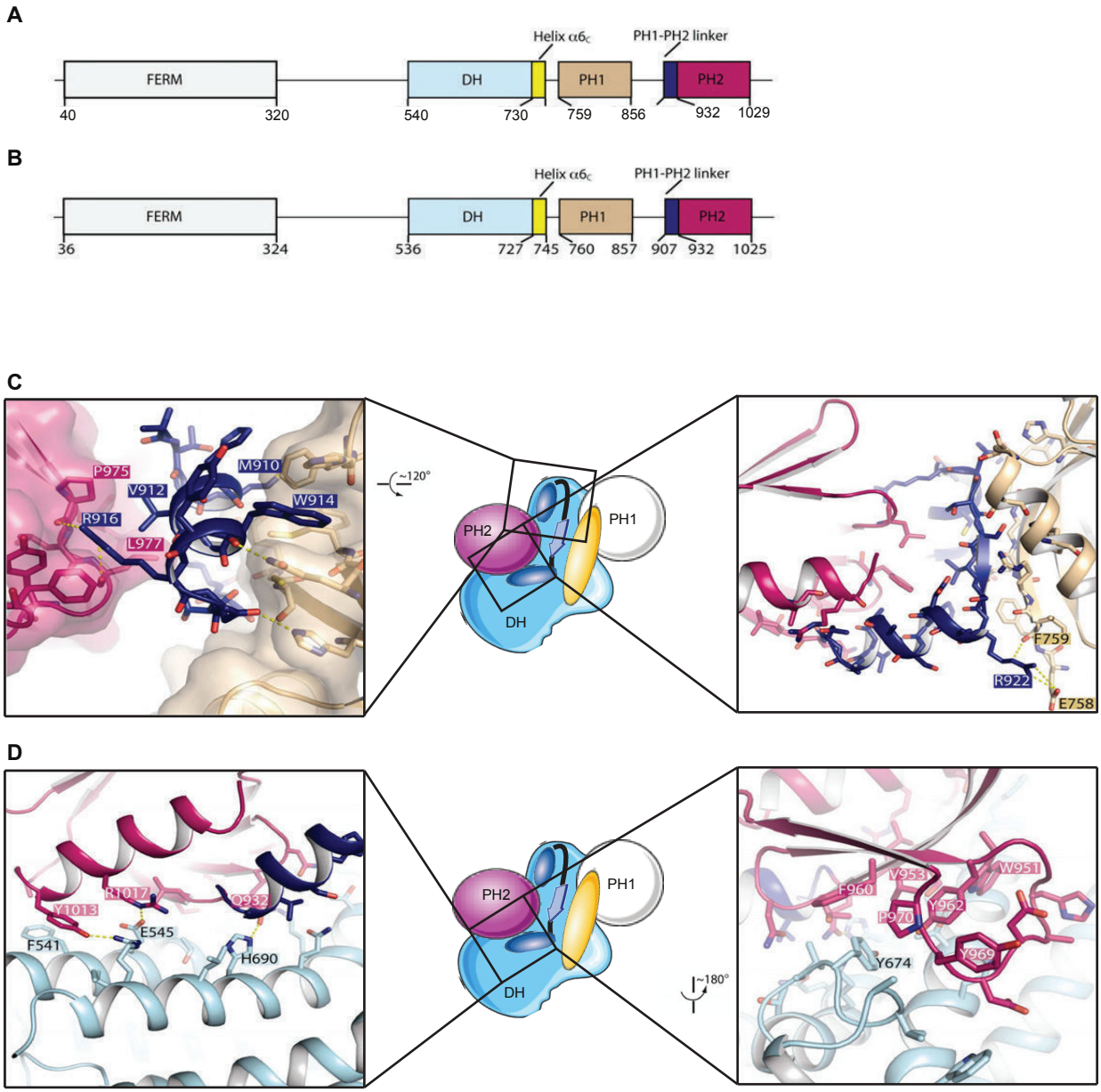

Figure 22. Structure of FARP-1 and FARP-2

(A-B) Schematic representation of FARP-1 and -2 proteins. At their N-terminal extremity, FARP possess a 4.1 band; ezrin, radixin, moesin homology domain (FERM domain),which is able to interact
with transmembrane proteins. Following is the tandem «Dbl homolog» (DH) - pleckstrin homolog (PH) domain which is characteristic of Dbl family of GEFs.Finally, at the C-terminal end they display
a second PH domain (PH2).
(C) Structure of the PH1-PH2 linker and its inbteraction with PH1 and PH2, (D) Interface between PH2 and the DH domain (He et al., 2013).

levels are detected in the brain, heart, liver intestine and muscle (Koyano et al., 1997). FARP2 is highly expressed in the brain and testis and at low levels in the heart and the kidney (Kubo et al., 2002).

FARPs function

FARP1 and FARP2 GEF activity towards a specific RhoGTP (i.e RhoA, RAC1 or Cdc42) is not yet clearly established due to conflicting results.

FARP1, a GEF for RhoA, RAC1 and Cdc42?

The first lab to describe FARP1 in the chondrocyte differentiation process, later described it to be a GEF towards RhoA, using an *in vitro* GDP dissociation approach in Sf9 insect cells (Koyano et al., 2001). However, other studies in the neuronal metabolism, found FARP1 to interact with Rac1 and by *in vitro* pull-down assays conducted on HEK cells lysate demonstrated it to be a GEF for Rac1 (Cheadle and Biederer, 2012). Further, its established role in the regulation of filopodial structures, which rely on the Cdc42 F-actin polymerizing activity and its recently established role in the Cdc42 dependent endothelium permeability presents FARP1 as a GEF for Cdc42 (Amado-Azevedo et al., 2017; Cheadle and Biederer, 2012, 2014; Murata et al., 2006).

Taken together, these results suggest that FARP1 GEF activity towards a specific small RhoGTPases is context dependent and further studies should aim at better understanding FARP1 specificity.

FARP2, a GEF for RAC1 and Cdc42?

FARP2 GEF activity has been more extensively investigated than its homolog FARP1. The first study to investigate its activity claimed FARP2 to be a GEF for Rac1 relying on Rac1-GTP pull down conducted on HEK lysates (Kubo et al., 2002).

Three following studies either using the same pull down *in vitro* approach or the FRET approach have confirmed the specificity towards Rac1 (He et al., 2013; Toyofuku et al., 2005)(Takegahara et al., 2010). However, few studies have instead reported FARP2 to activate Cdc42 activity. The Takai lab, using *in vitro* approach, FRET and functional assays

of actin polymerization at cell-cell junction, demonstrated that FARP2 was promoting Cdc42 activity (Fukuhara et al., 2004; Fukuyama et al., 2005).

In line with the Takai lab reports, *in vitro* pull-down assays using the catalytic domain of FARP2 proved specificity towards Cdc42 (Miyamoto et al., 2003). Finally, a structural study of FARP2 predicted Cdc42 to be its substrate. However, *in vitro* biochemistry experiments conducted in the same study proved FARP2 to regulate Rac1 activity but not Cdc42 (He et al., 2013).

Hence, all these studies keep ambiguous the substrate specificity of FARP2 GEF or may suggest that GEF activity depends on the cell type and the process they regulate.

FARPs localization and activity regulation

Structural analysis predicted that FARP2 could adopt an auto-inhibited conformation in which the two PH domains of the protein hindered the DH catalytic domain of the protein. In addition the Leu730 and Leu733 motif would crowd the catalytic domain by acting like pseudosubstrates (He et al., 2013). Therefore, FARP2 mutant constructs were designed in which the second PH was depleted and the L730 was mutated to Q730. This resulted in an increased basal activity of FARP2 *in vitro.* (Figure 21)

FARP proteins structure suggests a potential localization at the plasma membrane: First, the protein contains a FERM domain, which is found in the ERM proteins. The FERM domain allows ERM to interact with the plasma membrane integral protein CD44 or scaffolding proteins beneath the membrane to insure their function as cross-linkers of the cytoskeleton and the plasma membrane. Second, FARP proteins encompass two PH domains that are known to interact with phospholipids of the plasma membrane.

In neuronal cells, FARP1 was shown to interact with the transmembranar proteins SynCAM1 (Cheadle and Biederer, 2012), PlexinA1 and PlexinA4 through its FERM domain for its functional activation (Cheadle and Biederer, 2012; Zhuang et al., 2009). Similarly, FARP2 interacts with Plexin A1 through its FERM domain which induce its GEF activity (Toyofuku et al., 2005).

Studies conducted in Takai lab demonstrated that FARP2 was recruited at cell-cell junctions by nectins where phosphorylation by Src kinase induced activation of its GEF activity (Fukuhara et al., 2004; Fukuyama et al., 2005). Likewise Src was shown to phosphorylate and activate FARP2 downstream of endothelin receptor GPCR in single migrating cells

(Miyamoto et al., 2003). The phosphorylation site was not determined, but the PH2 domain was experimentally excluded as potential substrate.

FARP proteins have been studied in various but too few contexts limiting my ability to provide a general mechanism of regulation of their activity. Therefore the mechanisms described here may be only contextual.

FARPs in cellular processes

FARP1 and FARP2 regulate neuronal development

Early studies of FARP1 and FARP2 put in light its abundant expression in the neuronal system (Koyano et al., 1997; Kubo et al., 2002). Therefore following studies focused on their contribution to neuronal development and morphology. Neurites dynamics depend on F-actin network regulation. Semaphorin-Plexin signalling pathways are admitted as major regulators of neurite outgrowth or growth cone collapse through RhoGTPase signalling.
FARP1 and FARP2 seem to play distinct roles in neurites dynamics (Mlechkovich et al., 2014). In chicken neurons development, FARP2 was revealed to interact with PlexinA1 to mediate axon retraction whereas FARP1 interaction with PlexinA4 promoted neurites outgrowth (Toyofuku et al., 2005; Zhuang et al., 2009). In the same line, FARP1 promotes dendritic arborization in mammalian neurons, which relies on RAC1 activation (Cheadle and Biederer, 2012, 2014). Interestingly FARP2 promotes growth cones formation whereas it induces neurite shrinking (Kubo et al., 2002).

FARP1 regulates cell motility

Miyamoto et al., have demonstrated the contribution of FARP2 to the migration of HEK cells. Using a Boyden chamber invasion assay, they demonstrated that the binding of Endothelin A (ETA) to its receptor inhibited cell migration. Activated downstream of the ETA receptor, Src kinase phosphorylates FARP2. This phosphorylation was necessary for FARP2 to activate Cdc42 and the downstream jun kinase which inhibited migration. Src recombinant protein was shown to phosphorylate all the domains of FARP2 apart from the second PH domain.

Interestingly, it seemed that the FERM domain of FARP2 had a negative effect on the whole described signaling pathway.
Hence this work is the only one to involve FARP2 in the regulation of cell motility that is dependent on its phosphorylation by Src and GEF activity towards Cdc42.

FARP2 regulates Cell-cell adhesion maturation

FARP2 contribution to cell-cell junction has been extensively studied by the Takaï lab (Fukuhara et al., 2004; Fukuyama et al., 2005). To establish stable adherent cell-cell junction, early contacts are made by transmembranar protein, the Nectins. They engage homophilic contacts between neighbor cells, which induces Cdc42 activation, leading to filopodia formation and promoting closer contact. Eventually, RAC1 is also activated to promote lamellipodia formation and zipping of the junction (Yamada and Nelson, 2007). The Takai lab designed an experimental setting capable of reproducing the early phase of cell-cell junction establishment: epithelial cell overexpressing nectin proteins were put in contact with coverslips or beads coated with the extracellular domain of nectin thereby reproducing the cell-cell contact. Using their experimental setting, they were able to show that FARP2 (namely: FRG), downstream of nectins and after phosphorylation by Src, induced a Cdc42 dependent actin accumulation at the cell-cell contact to promote cell-cell adhesion establishment (Fukuhara et al., 2004). The authors also found Rac1 activation to be necessary for this process. However, *in vitro* pull down assays revealed that FARP2 was only a potent GEF for Cdc42 (Fukuyama et al., 2005). Vav2 was finally identified to be the GEF responsible for Rac1 activation, downstream of Cdc42 activation (Kawakatsu et al., 2005).

Hence this work describes a role of FARP2 at cell-cell junction, dependent on its activation by Src-mediated phosphorylation and on its GEF activity towards Cdc42, which leads to Rac1activation.

FARP1 and FARP2 regulate Bone metabolism

FARP1 expression is induced in response to parathryroid hormone and cAMP during differentiation of chondrocytes which require cell cytoskeleton reorganization (Koyano et al., 2001; Woods et al., 2007).

FARP2 regulates podosomes formation in osteoclast, which are actin rich proteolytic organelles of the cell (Takegahara et al., 2010) . In this study, authors demonstrated by FRET that FARP2 effect on F-actin reorganization relied on its activation of Rac1 and on Beta-3 integrin.

Altogether, studies of FARP proteins have revealed a role in the regulation of small RhoGTPases dependent F-actin dynamics. Considering small RhoGTPases and F-actin dynamics central role in cell invasion, FARP1 and FARP2 present themselves as potential regulators of collective invasion.

3.4 GTPases activating proteins (GAPs)

Members of the RhoGAP family contain a conserved 150-residue RhoGAP domain, which mediates binding to activate GTP bound Rho proteins and stimulates their intrinsic GTP hydrolysis activity. Approximately 70 members of the RhoGAP family exist in humans (Etienne-Manneville and Hall, 2002). As for the GEFs, these proteins can be regulated by phosphorylation. This is the case of FilGAP, a RhoA GAP which is phosphorylated and activated by ROCK kinases proteins (Ohta et al., 2006).
All Rho GAPs share the same mechanism of action. They use a highly conserved arginine residue (commonly referred to as the arginine finger) to intrude between switch-I and II of the small GTPases, thus catalyzing the GTP to GDP exchange. One glutamine residue on the small RhoGTPases (Q61 in Cdc42 and Rac1Q63 in RhoA) is extremely important to allow GAP catalytic activity. Mutation of this glutamine to nonpolar amino acids (most commonly Q to L mutation) results in constitutively GTP-loaded (i.e. active) GTPases. In addition, the cavity into which the arginine finger intrudes is narrow and it is delimited by several conserved glycine residues. Mutation of glycine to any other residue results in blocking GAP access and therefore in a constitutively active small Rho GTPase.

3.5 Rho-GDP dissociation inhibitors (RhoGDI)

RhoGDI function as negative regulators of Rho GTPases by sequestering them in the cytoplasm and preventing their activation. The RhoGDI protein family comprises three

members — RhoGDI1, RhoGDI2 and RhoGDI3, with context dependent expression and, probably, preferential binding toward specific small Rho GTPases. (Garcia-Mata et al., 2011)

3.6 RhoGTPases in cancer

Until recently, it was believed that RhoGTPases were rarely mutated in human tumors. However, thanks to next generation sequencing direct mutations of RhoGTPases in human cancers have been identified (Porter et al., 2016). While Rac1 is mutated in a subset of melanomas, breast tumors and head and neck tumors (Alan and Lundquist, 2013), RhoA is mutated in gastric cancer and angioimmunoblastic T cell lymphoma (Cancer Genome Atlas Research Network, 2014).

Contrary to the activating mutation G12V found in Ras oncogenes, Rac1 is mutated at P29S whereas different recurrent mutation have been identified for RhoA such as R5Q, G17E and Y42C. The P29S mutation induces a fast cyling of the Rac1 between GDP and GTP loaded. It therefore acts as a gain of function mutation and is a driver mutation in melanoma.

Although these mutations can be important for tumor development, in most cases, RhoGTPases are most often found to be upregulated or to have their activity increased by changes in the expression or activity of their GAPs, GEFs and/or GDIs.

PhD aims

My work aimed at identifying the molecular and cellular processes driving colorectal carcinoma (CRC) invasion, which arises from the colon and rectal epithelium and displays a glandular architecture with the apical pole facing the lumen. These structure invade in a collective mode, with a leader/follower polarization. Because of its central role in the regulation of cell motility, we postulated that Rho-GTPases dependent signaling pathways could control the collective invasion of CRC.

The main aims of my PhD project were:

#1 To identify the effector of the RhoGTPases signaling pathway triggering and regulating CRC collective invasion.

#2 To determine its contribution to the Leader/Follower polarity formation

#3 To identify the signaling pathway downstream of the RhoGTPase effector

Additional aims were:

#1 To study the inverted apico-basolateral polarity of new CRC metastatic intermediates called TSIP (Tumor with inverted polarity) from patients.

#2 To investigate the contribution of the RhoGTPases signaling pathway to the invasion of TSIP.

#3 To study the Kif17 dependent RhoA-GTPase regulation at cell-cell junctions of epithelial cells.

CHAPTER 2: RESULTS

KIF17 regulates RhoA-dependent actin remodeling at epithelial cell-cell adhesion

Foreword

This first part of my results chapter originates from a published work to which I contributed and that was conducted by Geri Kreitzer lab

The study investigated the role of the microtubule motor protein Kif17 in the regulation of epithelial architecture. Kreitzer lab found Kif17 to localize at cell-cell junctions, raising the question of its role at this site.

My aim was to 1) to understand how Kif17 was regulating junctional F-actin remodeling, 2) to determine RhoA-GTPase's contribution to it and 3) to determine how it impacted E-cadherin accumulation at cell-cell junction.

To adress these questions, I used MDCK epithelial cells in 2D or in 3D matrices and modulated Kif17 expression using shRNA and evaluated its impact 1) on MDCK cysts morphogenesis and E-cadherin localization by immunofluorescence 2) on RhoA-GTPase activity by pull-down experiments.

© 2016. Published by The Company of Biologists Ltd | Journal of Cell Science (2016) 129, 957-970 doi:10.1242/jcs.173674

RESEARCH ARTICLE

KIF17 regulates RhoA-dependent actin remodeling at epithelial cell–cell adhesions

Bipul R. Acharya[1,*,¶], Cedric Espenel[1,‡,¶], Fotine Libanje[2,¶], Joel Raingeaud[2], Jessica Morgan[1,§], Fanny Jaulin[2,] and Geri Kreitzer[1,**]**

ABSTRACT

The kinesin KIF17 localizes at microtubule plus-ends where it contributes to regulation of microtubule stabilization and epithelial polarization. We now show that KIF17 localizes at cell–cell adhesions and that KIF17 depletion inhibits accumulation of actin at the apical pole of cells grown in 3D organotypic cultures and alters the distribution of actin and E-cadherin in cells cultured in 2D on solid supports. Overexpression of full-length KIF17 constructs or truncation mutants containing the N-terminal motor domain resulted in accumulation of newly incorporated GFP–actin into junctional actin foci, cleared E-cadherin from cytoplasmic vesicles and stabilized cell–cell adhesions to challenge with calcium depletion. Expression of these KIF17 constructs also increased cellular levels of active RhoA, whereas active RhoA was diminished in KIF17-depleted cells. Inhibition of RhoA or its effector ROCK, or expression of LIMK1 kinase-dead or activated cofilin^{S3A} inhibited KIF17-induced junctional actin accumulation. Interestingly, KIF17 activity toward actin depends on the motor domain but is independent of microtubule binding. Together, these data show that KIF17 can modify RhoA–GTPase signaling to influence junctional actin and the stability of the apical junctional complex of epithelial cells.

KEY WORDS: Rho–GTPases, Actin, Cell–cell adhesion, Kinesin

INTRODUCTION

Epithelia play key roles in tissue homeostasis by establishing transport systems for vectorial secretion and absorption and by forming a physical barrier between the internal milieu and the outside environment. Adherens junctions and tight junctions, formed by trans-cellular interactions of transmembrane adhesion proteins linked to the cytoskeleton, are essential for epithelial morphogenesis and function. Known collectively as the apical junctional complex (AJC), adherens junctions couple adjacent cells physically whereas tight junctions set boundaries between apical and basolateral membranes and control paracellular permeability (Guillot and Lecuit, 2013). Components of the AJC are delivered to the membrane by transport along microtubules (Chen et al., 2003; Ivanov et al., 2006; Mary et al., 2002; Nekrasova et al., 2011; Portereiko et al., 2004; Yanagisawa et al., 2004) and are anchored at adhesive sites by their association with actin and microtubule adaptors. As cell–cell adhesions mature, signaling molecules that also associate with the AJC induce changes in actin and microtubule arrays by modifying polymer dynamics and stability (Brieher and Yap, 2013; Chausovsky et al., 2000; Mège et al., 2006; Ratheesh et al., 2012). Thus, the cytoskeleton affects AJC formation and maturation, and signaling at the AJC reciprocally affects actin and microtubules; together, these processes direct morphogenetic responses to numerous cues (Brieher and Yap, 2013; Mack and Georgiou, 2014). Although many of the components involved in remodeling of AJCs and the cytoskeleton are known, the mechanisms employed to coordinate these events are still incompletely defined.

Rho family GTPases and their effectors comprise a major class of signaling molecules at the AJC (Citi et al., 2014; Fukata and Kaibuchi, 2001) and many are regulated by cell–cell adhesion. Signaling by Cdc42, Rac1 and RhoA regulates AJC formation, maturation and remodeling. They also regulate actin and microtubule arrays (Samarin and Nusrat, 2009; Wojnacki et al., 2014). Rac1 and Cdc42 regulate Arp2/3 (also known as Actr2/3) to affect branched actin filament formation (Kraemer et al., 2007; Otani et al., 2006) and RhoA regulates formins in the generation of actin cables (Carramusa et al., 2007; Kher et al., 2014; Kobielak et al., 2004). RhoA signaling, through its effector Rho-associated protein kinase (ROCK, of which there are two isoforms ROCK1 and ROCK2), also exerts indirect effects on branched actin formation by inactivating the actin-severing protein cofilin. In addition, RhoA activation of formin leads to microtubule capture and stabilization in migrating fibroblasts (Bartolini et al., 2008; Cook et al., 1998; Palazzo et al., 2001) and plays a role in regulating microtubule stability in epithelial cells (Nakaya et al., 2008). Combined, these functions allow Rho–GTPases to orchestrate the remodeling of cytoskeletal arrays and cell–cell junctions that accompanies epithelial polarization.

Rho–GTPases are regulated upstream and downstream of the AJC by guanine-nucleotide exchange factors (GEFs) and GTPase-activating proteins (GAPs) that control spatiotemporal activation of Rho effectors (Quiros and Nusrat, 2014). How Rho–GTPase effectors and regulators are targeted to discrete sites for selective activation is still a topic of intense study. Dynamic microtubule plus-ends can interact with proteins at the cortex and can deliver proteins associated with the microtubule plus-end that regulate cytoskeletal and junctional organization, leading to the concentration of E-cadherin at cell–cell contacts (Ligon and Holzbaur, 2007; Ligon et al., 2001; Stehbens et al., 2006). Microtubule capture and stabilization at the cortex may also provide specialized tracks for targeted delivery of cytoplasmic and membrane proteins important for junction maturation and remodeling (Waterman-Storer et al., 2000). As such, delivery of

[1]Department of Cell and Developmental Biology, Weill Cornell Medical College of Cornell University, New York, NY, USA. [2]Gustave Roussy Institute, UMR-8126, 114 rue Edouard Vaillant, Villejuif 94805, France.
*Present address: University of Queensland, Building 80, Brisbane, Australia.
‡Present address: Stanford University, 443 Via Ortega, Stanford, CA, USA. §Present address: University of California, Santa Cruz, Graduate Program in Chemistry and Biochemistry, Santa Cruz, CA, USA.
¶These authors contributed equally to this work

**Authors for correspondence (gek2006@med.cornell.edu; fanny.jaulin@gustaveroussy.fr)

Received 29 April 2015; Accepted 31 December 2015

Journal of Cell Science (2016) 129, 957-970 doi:10.1242/jcs.173674

Rho–GTPase effectors and regulators by microtubule motors can be envisioned as playing a role in regulation of localized signaling cascades at the AJC.

KIF17 is a multifunctional, homodimeric microtubule motor with roles in vesicular transport (Chu et al., 2006; Jenkins et al., 2006; Setou et al., 2000), transport of RNA granules (Chennathukuzhi et al., 2003; Kotaja et al., 2006; Saade et al., 2007; Takano et al., 2007), regulation of transcriptional activators (Kotaja et al., 2005; Macho et al., 2002), and in building sensory cilia (Dishinger et al., 2010; Fan et al., 2011; Insinna et al., 2008; Jenkins et al., 2006; Ou et al., 2005; Pan et al., 2006; Snow et al., 2004). In epithelial cells, KIF17 colocalizes and interacts with components of the microtubule plus-end cortical capture machinery, promoting microtubule stabilization and cell polarization (Acharya et al., 2013; Espenel et al., 2013; Jaulin and Kreitzer, 2010). This can influence cell architecture, but it is not yet known if microtubule modification is the only means by which KIF17 contributes to epithelial polarization. In this study, we provide evidence that KIF17 activates a RhoA signaling pathway at cell–cell contacts that influences both cortical actin and cell–cell junctions. This, in concert with its effects on microtubule stabilization, may serve to integrate cytoskeletal remodeling with maturation and stabilization of the AJC. A role for KIF17 in local RhoA activation also provides an additional potential mechanism by which this kinesin-2 motor exerts effects on epithelial polarization.

RESULTS

KIF17 contributes to actin organization in epithelial cells

We showed previously that KIF17 localizes to microtubule plus-ends with EB1 (also known as MAPRE1) and contributes to microtubule stabilization and polarization of epithelial cells (Jaulin and Kreitzer, 2010). In our analysis of KIF17 distribution in MDCK and Caco-2 epithelial cells, we also identified a pool of KIF17 localized at sites of cell–cell contact that is lost after KIF17 depletion by shRNA (Fig. 1A; Fig. S1A) (Jaulin and Kreitzer, 2010). KIF17 colocalized with E-cadherin and actin at these cell–cell junctions (Fig. 1A), and with α-actinin, a junctional actin-binding protein (Fig. 1B).

In 3D organotypic MDCK cultures, 85±2.6% (mean±s.e.m.; n=322) of cysts that form have a single layer of cells surrounding a

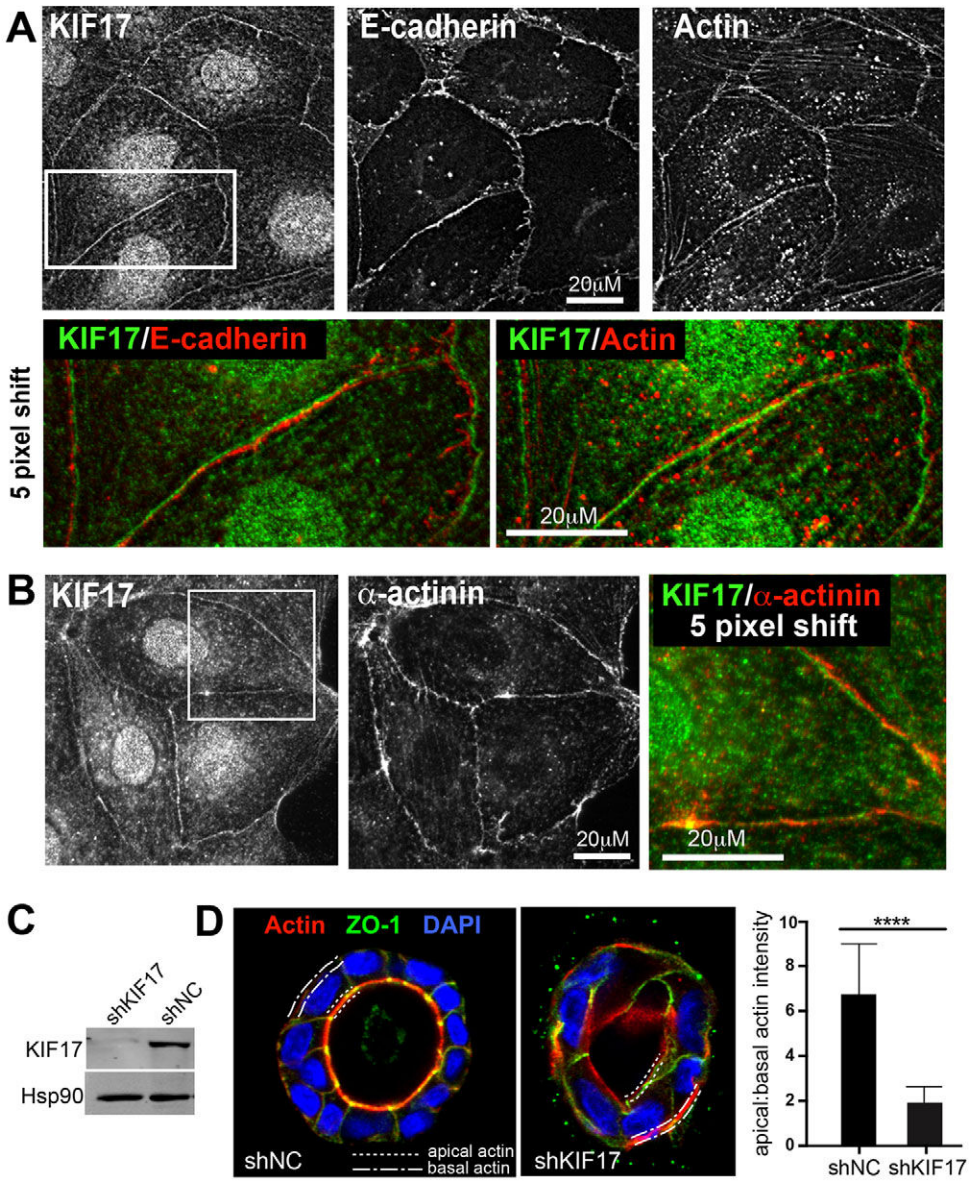

Fig. 1. KIF17 localizes at cell–cell junctions and contributes to actin remodeling during epithelial morphogenesis. (A) Colocalization of KIF17 with actin and E-cadherin at cell–cell contacts in MDCK cells. Color overlay shows an enlarged view of the boxed region of KIF17 and E-cadherin or β-actin images; the KIF17 image was shifted by five pixels to highlight corresponding staining patterns. (B) Colocalization of KIF17 and α-actinin at cell–cell junctions. Color overlay shows an enlarged view of the boxed region; the KIF17 image was shifted by five pixels. (C) Immunoblot showing KIF17 in MDCK cells transduced with control (shNC) or KIF17-targeting (shKIF17) shRNAs. Hsp90 was used as a loading control. (D) Localization of actin (phalloidin), ZO-1 and nuclei (DAPI) in shNC and shKIF17 MDCK cysts grown in Matrigel for seven days. Dotted and dashed lines highlight apical and basal membranes, respectively. Graph shows the ratio of apical to basal actin fluorescence intensity determined by line-scan analysis. n=38 and 48 cells for shNC and shKIF17, respectively. Error bars are s.e.m., significance was determined with a two-tailed, unpaired student's t-test, ****P<0.0001.

Journal of Cell Science (2016) 129, 957-970 doi:10.1242/jcs.173674

central lumen, and actin is enriched at the apical pole of individual cells (Fig. 1C,D; shNC, short hairpin negative control). KIF17 depletion increased the percentage of cysts with either no lumens or multiple lumens as described previously (Jaulin and Kreitzer, 2010), and reduced the percentage of cysts with one lumen to 38±5.4% (n=332). We used line-scan analysis of individual cells in cysts with a single lumen to measure enrichment of actin at the apical pole (dotted line) relative to the basal pole (dashed line) in control (shNC) and KIF17-depleted cells (shKIF17, Fig. 1D). In shNC, the apical/basal actin ratio is 6.74, but only 1.93 in shKIF17, demonstrating that apical actin enrichment is compromised by KIF17 depletion. Thus, KIF17 colocalizes with and contributes to organizing the distribution of actin in epithelial cells.

KIF17 localization at cell–cell contacts is mediated by its N-terminal motor domain

To examine how KIF17 could affect actin organization, we prepared and analyzed the localization of GFP-tagged KIF17 full-length and C-terminal truncation mutants in MDCK cells (Fig. 2A). Proteins were expressed acutely by intranuclear cDNA injection and their localization was analyzed 3 h after injection. Full-length KIF17 appeared primarily as diffuse cytoplasmic fluorescence but a population of the protein localized as discrete puncta, a large proportion of which accumulated at microtubule plus-ends in protruding regions of the cells (Fig. 2A, GFP–KIF17-FL) and as described previously (Jaulin and Kreitzer, 2010). The soluble pool of KIF17-FL represents kinesin in a compact, auto-inhibited conformation (Espenel et al., 2013; Hammond et al., 2010); this auto-inhibited conformation is disrupted by a single point mutation in the hinge region between KIF17 coiled-coil domains (G754E), and when expressed in epithelial cells GFP–KIF17-FL^{G754E} localizes robustly at microtubule plus-ends and in cell protrusions (Espenel et al., 2013; Jaulin and Kreitzer, 2010). Protein expressed from a construct in which the tail and last coiled-coil are deleted, GFP–K490, localized at microtubule plus-ends in cell protrusions (Fig. 2A; Fig. S1B), but was also detected at cell–cell contacts in 24.3% of expressing cells (Fig. 2A,C). Proteins synthesized from two shorter constructs, GFP–K370 (encoding motor and neck) and

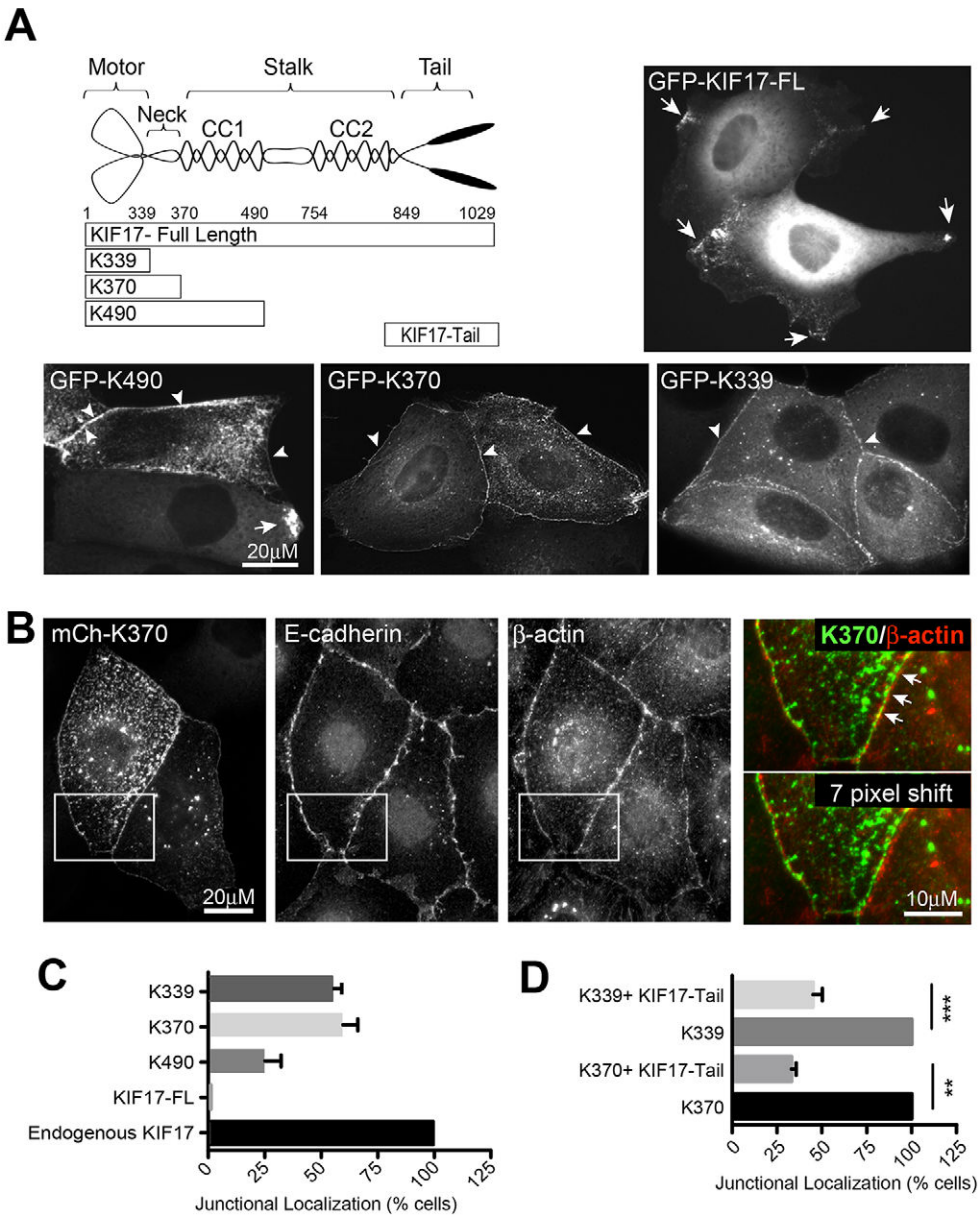

Fig. 2. Localization of expressed, GFP-tagged KIF17 constructs. (A) Diagram showing KIF17 constructs used for these studies. Images show localization of KIF17-FL, K339, K370 and K490 in MDCK cells 3 h after cDNA injection. Arrows indicate localization on microtubules in cell protrusions. Arrowheads indicate localization at cell–cell contacts. (B) Colocalization of GFP–K370 with immunostained E-cadherin and β-actin in MDCK cells. Color overlays show an enlargement of GFP–K370 and β-actin in the boxed region. In the lower overlay, the image of K370 was shifted by seven pixels. (C) Quantification of the junctional localization of endogenous KIF17 and expressed KIF17 constructs 3 h after cDNA injection. Values were calculated as percentage of total cells expressing each construct. Results are from 3–6 independent experiments (endogenous KIF17, n=90 cells; GFP–KIF17-FL, n=60; GFP–K490, n=295; GFP–K370, n=664; GFP–K339, n=794). (D) Quantification of the percentage cells with junctional GFP–K370 or GFP–K339 in the absence and presence of co-expressed mCh–KIF17-Tail. Data are normalized to 100% in control conditions (K370, n=162; K370+ KIF17-Tail, n=121; K339, n=230; K339+ KIF17-Tail, n=324 cells). Results are from ≥2 independent experiments. Error bars are error margins with 95% confidence interval. Significance was determined using a two-tailed unpaired student's t-test, $^{**}P$<0.01; $^{***}P$<0.001.

Journal of Cell Science (2016) 129, 957-970 doi:10.1242/jcs.173674

GFP–K339 (encoding motor alone) can be detected along microtubules when cells are permeabilized briefly before fixation to release soluble protein (not shown) (Jaulin and Kreitzer, 2010) and when expressed at low levels (Fig. S1C). They also localize at the centrosome with γ-tubulin (Fig. S1D). Moreover, K370 and K339 localized prominently at cell–cell contacts in 59.7% and 54.7%, respectively, of the injected cells (Fig. 2A–C). The junctional localization of K339 and K370 is also observed in other epithelial cell types such as MCF10A and Caco-2, is independent of the tag identity (GFP, mCherry, myc, HA), and is seen with both N- and C-terminal fusion constructs (Fig. S1E and not shown) (Jaulin and Kreitzer, 2010). Together, this analysis reveals that the motor domain is sufficient to target KIF17 to cell–cell contacts and that deletion of the C-terminus favors this subcellular localization. Like endogenous KIF17, K370 and K339 colocalized with actin, E-cadherin and α-actinin at cell–cell contacts (Fig. 2B and not shown). We preferentially use K370 going forward since it behaves as a dimer *in vitro*. K339 behaves as a monomer *in vitro* (Acharya et al., 2013), but had nearly identical impact in all experiments where it was tested relative to K370.

Auto-inhibitory interactions of the KIF17 N-terminal motor and C-terminal tail domains regulate KIF17 activity (Espenel et al., 2013; Hammond et al., 2010; Jaulin and Kreitzer, 2010). *In vitro*, the KIF17 tail can bind directly to the KIF17 motor and reduces its microtubule-stimulated ATPase activity (Acharya et al., 2013); as such, it may influence K370 and K339 localization at the cortex. To test this directly, we co-expressed GFP–K339 or GFP–K370 with mCh–KIF17-Tail (Fig. 2A) and analyzed their localizations 3 h after cDNA injection. Co-expression of KIF17-Tail reduced the number of cells with junctional K339 and K370 to 45% and 33%, respectively, of cells expressing these motor domains alone (Fig. 2D). This effect of KIF17-Tail on localization of K339 and K370 could result from either competition with proteins that anchor KIF17 at cell–cell contacts, or by inhibition of the motor domain ATPase activity, which would prevent movement along microtubules (Acharya et al., 2013).

KIF17 motor domain enhances incorporation of actin at cell–cell contacts independently of microtubule binding

The colocalization of KIF17 motor domains with junctional actin, and the effects of KIF17 depletion on actin distribution in cells cultured in 3D prompted us to examine if expression of K370 affects actin organization. We expressed mCh–K370 or mCh–empty vector control (mCh–EV) for 4 h after cDNA injection and analyzed the distribution of actin by immunofluorescence microscopy. In K370-expressing cells, we observed a subtle but consistent enrichment of actin in discrete foci at cell–cell contacts. This enrichment was best detected by applying a Sobel edge detection filter to images (Fig. S2A). These actin foci were not detected by phalloidin labeling, probably because phalloidin strongly labels stress fibers and bundled actin. This can mask signal from non-bundled and branched filaments, which are detected very well with actin antibodies (Lessard, 1988; Nagasaki et al., 1994).

To further examine the change in junctional actin induced by K370, we monitored incorporation of newly synthesized, fluorescently-tagged actin probes (GFP–actin or mCh–LifeAct) into actin filaments by time-lapse fluorescence microscopy. We co-injected cells with GFP–actin and mCh–K370 or mCh–EV cDNAs. One hour after injection, cells were transferred to the microscope and images of GFP–actin were acquired at 10-min intervals for 4 h at 37°C. Newly synthesized GFP–actin (Fig. 3A) and mCh–LifeAct (Fig. S2B) accumulated in discrete foci along cell–cell contacts in control and K370-expressing cells. However, co-expression of K370 accelerated the rate at which these new filaments became apparent (Movie 1, Fig. S3) and increased the number of cells displaying these junctional actin filaments. Furthermore, K370 colocalized with GFP–actin or mCh–LifeAct in these junctional foci (Fig. 3A; Fig. S2B). In the time course of these experiments, fluorescently tagged actin incorporated into more resolvable foci at cell–cell contacts than mCh–LifeAct. For this reason, we used GFP–actin or mCh–actin in experiments going forward to determine how KIF17 can impact junctional actin organization.

We quantified junctional accumulation of GFP–actin from images of cells by drawing polylines along cell–cell contacts of microinjected cells. These regions of interest (ROIs) were further processed and segmented to identify actin foci within these ROIs (Fig. 3C). We then measured the percentage of each ROI that was segmented as a readout of the junctional region covered by GFP–actin foci (% segmented area/total area measured, Fig. 3D) for control and experimental data. This analysis revealed a 4.9- and 5.5-fold increase in junctional GFP–actin foci in cells expressing mCh–K339 or mCh–K370, respectively, as compared with controls expressing mCh–EV. By contrast, junctional GFP–actin foci were not increased in cells expressing the heterodimeric kinesin-2 motor KIF3A (mCh–KIF3A-M, Fig. 3B,D) as compared with controls, demonstrating a selective effect of K370 or K339 on junctional actin accumulation in MDCK cells. The effects of expressing KIF17 constructs on actin in 3D cultured cells could not be determined as they induced substantial changes in cell shape over extended times needed for cysts to develop.

We next tested if the effects of KIF17 on cortical actin accumulation are microtubule dependent. We pre-incubated cells with 33 µM nocodazole to break down microtubules prior to injecting GFP–actin and K370 cDNAs. After an additional 4 h with continuous nocodazole exposure, cells were fixed and analyzed for accumulated GFP–actin at the cell periphery. In the absence of microtubules, K370 localized at cell–cell contacts and the accumulation of junctional GFP–actin was not significantly changed by comparison with untreated controls (Fig. 4A,C). Despite not reaching statistical significance, there was a trend toward increased junctional actin foci in nocodazole-treated cells. This could reflect release of RhoGEF family protein GEF-H1 (also known as ARHGEF2) from microtubules and activation of RhoA, which affects actin organization in many cell types (Krendel et al., 2002; Ren et al., 1998). Microtubule stabilization with 10 µM Taxol also had no significant effect on junctional actin accumulation induced by K370 expression (not shown). Junctional GFP–actin foci also increased 4.8-fold in cells expressing a K370 mutant defective in microtubule binding (Fig. 4B, K370$^{R288/294A}$) (Acharya et al., 2013), as compared with empty vector control. Thus, the effects of K370 on cortical actin accumulation are independent of microtubules and microtubule binding.

Effects of KIF17 on junctional actin are mediated by activation of Rho signaling to ROCK and its downstream effectors LIMK1 and cofilin

Purified K370 and K339 did not interact directly with actin *in vitro* (not shown), suggesting KIF17 exerts its effects on junctional actin by modifying the localization or activity of actin regulatory factors. RhoA is involved in regulating both cortical actin dynamics and cortical microtubule capture and stabilization. To determine if RhoA signaling contributes to the effects of KIF17 on junctional actin, we co-injected MDCK cells with mCh–actin, GFP–K370 and

Journal of Cell Science (2016) 129, 957-970 doi:10.1242/jcs.173674

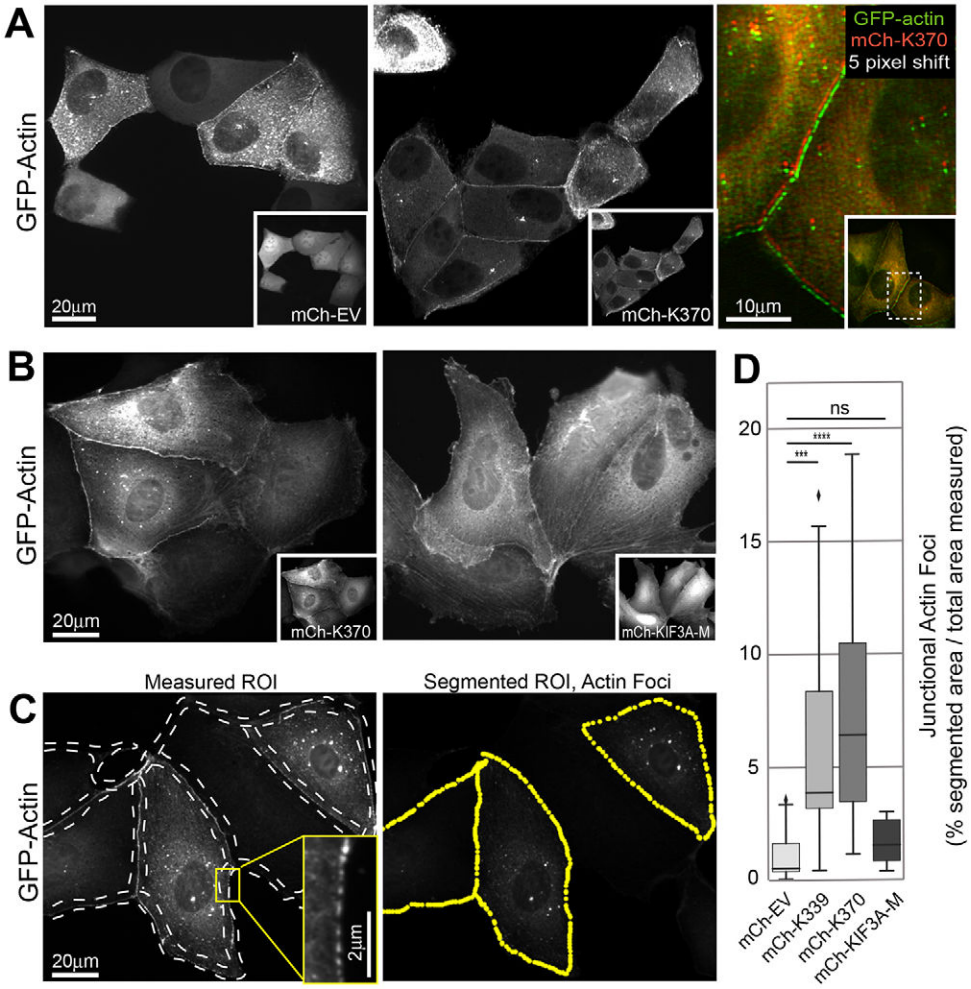

Fig. 3. K370 expression stimulates accumulation of junctional actin. (A) Localization of GFP–actin 4 h after co-injection with mCherry control, empty vector (mCh–EV) or mCh–K370 cDNAs. Insets in grayscale images show mCherry expression. Color overlay shows magnified region of the boxed area of cells shown in inset. mCh–K370 image was shifted by five pixels. (B) Localization of GFP–actin 4 h after co-injection with mCh–K370 or mCh–KIF3A-motor domain (mCh–KIF3A-M). Insets show mCherry expression. (C,D) Analysis of junctional actin accumulation. (C) Sample images of GFP–actin 4 h after cDNA injection. Dashed lines on the left panel highlight regions of interest (ROIs) at cell–cell contact zones within which segmentation was applied to identify junctional actin foci. The right panel shows the segmented image. Yellow puncta highlight the segmented regions within the selected ROI analyzed. Inset shows a magnified view of discrete junctional GFP–actin foci that are identified by segmentation. (D) Box-whisker plots showing quantification of junctional actin foci identified by segmentation as percentage of total ROI selected for measurement in each condition. Plots show minimum, 25th quartile, median, 75th quartile, and maximum values. Diamond symbols indicate outliers. Results are from images of injected cells in ≥3 independent experiments. Significance was determined using a two-tailed Mann–Whitney U test. ns, not significant; ***P<0.001; ****P<0.0001.

either the Rho inhibitor *Clostridium botulinum* toxin C3 (myc–C3), the GDP-bound, inactive mutant RhoA^{N19} (myc–RhoA^{N19}), or a control myc-empty vector (myc–EV). Rho inhibition by expression of myc–C3 or myc–RhoA^{N19} reduced the abundance of junctional GFP–actin foci 58.8-fold and 6.2-fold, respectively, relative to controls expressing K370, and was also reduced relative to controls expressing myc–EV, by 4 h after cDNA injection (Fig. 5A,C). We could not determine if constitutively activated RhoA (RhoA^{V14}) increased accumulation of junctional GFP–actin foci because expression of this construct led to rapid disruption of cell–cell junctions (not shown).

These data suggest KIF17 modifies junctional actin through RhoA signaling. To test if KIF17 activates RhoA, we determined the levels of active GTP–RhoA in cells expressing the different KIF17 constructs. We transfected MDCK cells with myc–EV, myc–K370, myc–KIF17-FL or the conformationally extended, constitutively active mutant myc–KIF17^{G754E} (Espenel et al., 2013; Jaulin and Kreitzer, 2010). Cell lysates were prepared 24 h after transfection and levels of active and total RhoA were determined by pull-down with the Rho-binding domain of Rhotekin fused to 6xHis (His–RBD). Expression of all KIF17 constructs resulted in an increase in Rho activity, with a significant response in cells expressing K370 (Fig. 5D); thus the KIF17 motor domain is sufficient to activate RhoA in epithelial cells. Conversely, active RhoA was reduced to 53% and 24% of control levels in MDCK cells depleted of KIF17 using two independent shRNAs targeting KIF17 (Fig. 5E).

RhoA interacts with its effectors ROCK and diaphanous-related formins to regulate actin dynamics and distribution. As such, we tested if Rho signaling to ROCK or formin contributes to the effects of KIF17 on junctional actin. First, we treated cells with the ROCK inhibitor, Y27632 (10 μM) for 4 h immediately following injection of GFP–actin and mCh–K370 cDNAs. Similar to effects of expressing C3 or dominant-negative RhoA^{N19}, accumulation of junctional actin foci induced by GFP–K370 expression was reduced 5.9-fold in cells treated with Y27632 (Fig. 5B,C). By contrast, abundance of junctional actin foci was not affected in cells treated with the formin inhibitor SMIFH2 (50 μM; Fig. 5B,C). Thus, K370 expression affects junctional actin accumulation through Rho signaling to ROCK.

ROCK activates LIMK1/2 and inhibits myosin light chain phosphatase, which modulate actin organization by phosphorylating cofilin and inhibiting dephosphorylation of myosin light chain, respectively. This results in inactivation of cofilin-mediated actin severing and activation of myosin-II-mediated actin contraction (Riento and Ridley, 2003). We tested the effects of activating cofilin or inhibiting myosin-II on KIF17-mediated accumulation of junctional actin. Co-expression of GFP–K370 and mCh–actin with either a kinase-dead LIMK1 construct (HA–LIMK1^{KD}) that cannot phosphorylate and inactivate cofilin (Arber et al., 1998; Yang et al., 1998), or a constitutively active cofilin mutant (FLAG–cofilin^{S3A}; Moriyama et al., 1996) reduced the median segmented membrane area covered by actin foci to 0.85% (8.3-fold decrease) and 1.66% (4.2-fold decrease),

Journal of Cell Science (2016) 129, 957-970 doi:10.1242/jcs.173674

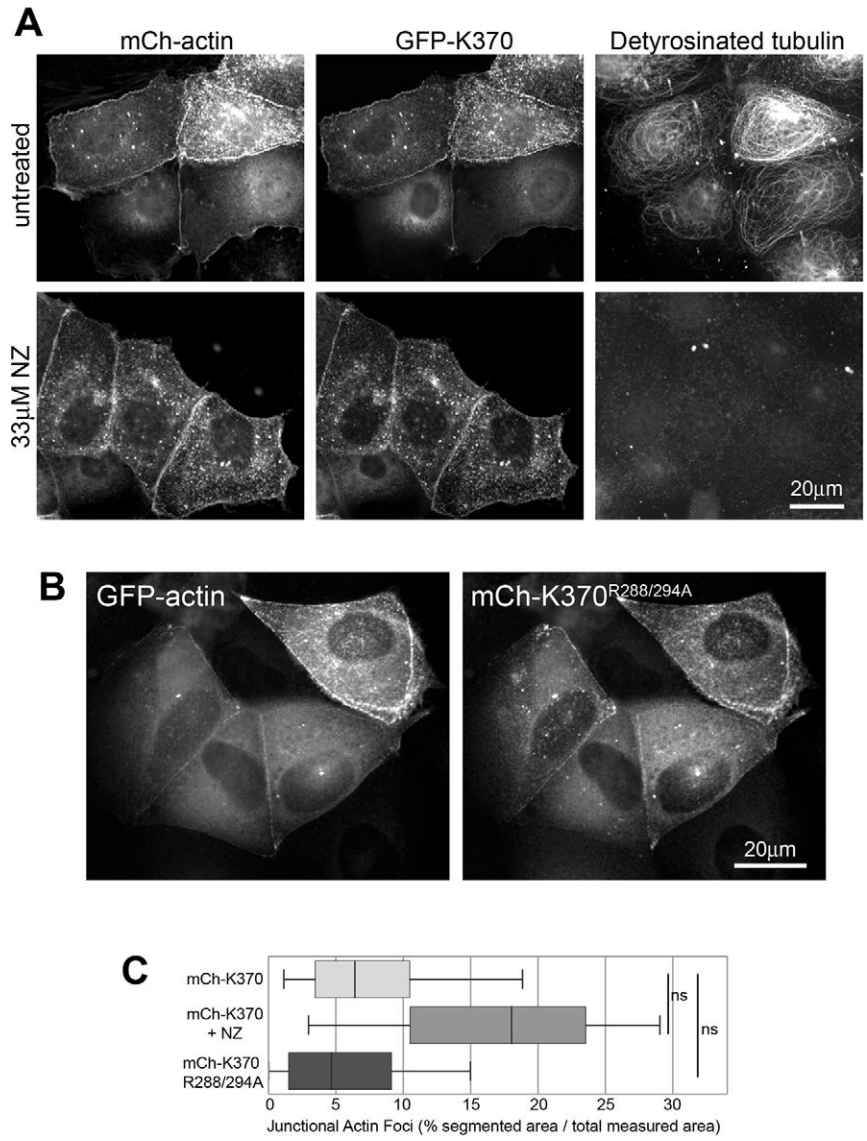

Fig. 4. Junctional actin accumulation induced by K370 is independent of microtubules. (A) Localization of mCh–actin, GFP–K370 and stable (detyrosinated) microtubules in untreated and nocodazole-treated (33 μM) cells. After injection, cells were maintained in nocodazole for 4 h at 37°C before fixation. (B) Localization of GFP–actin and the microtubule-binding mutant mCh–K370$^{G288/294A}$ 4 h after cDNA injection. (C) Box-whisker plots showing quantification of junctional actin foci identified by segmentation as percentage of total ROI selected for measurement in each experimental condition. Results are derived from images of injected cells in ≥2 independent experiments. Significance was determined using a two-tailed Mann–Whitney U test. ns, not significant.

respectively, relative to 6.84% in controls expressing only K370. In these experiments however, we noted significant heterogeneity in the intensity and density of junctional actin foci across individual cells. This reflected a high variability in the expression levels of LIMK1^{KD} or cofilin^{S3A} in cells triply injected with K370 and mCh–actin cDNAs. As such, we also performed a binary phenotype analysis with these samples to determine the percentage of K370-expressing cells with resolvable mCh–actin foci at cell–cell contacts, regardless of fluorescence intensity or density of foci. In this binary analysis, the number of LIMK1^{KD}- or cofilin^{S3A}-expressing cells with resolvable junctional actin foci was reduced to 50.3% and 60.1% of controls expressing only K370 (Fig. 6A,C). By contrast, we measured no significant effect on either the percent membrane area covered by mCh–actin foci or the fraction of cells with resolvable junctional actin foci in K370-expressing cells treated with the myosin light chain kinase inhibitor ML-7 as compared with untreated controls (Fig. 6C).

We reasoned that if KIF17 inhibits actin severing by cofilin, then inhibiting branched actin polymerization mediated by Arp2/3, the major actin-nucleator at cell–cell junctions (Verma et al., 2012), should reduce K370-mediated accumulation of junctional GFP–actin foci. We incubated cells co-injected with GFP–actin and mCh–K370 cDNAs with 100 μM CK666, a selective Arp2/3 inhibitor (Nolen et al., 2009) for 4 h prior to fixation, and analyzed junctional GFP–actin foci. CK666 treatment reduced the median membrane area covered by GFP–actin foci 17-fold to 0.40% and the percentage of cells with junctional actin foci to 47% of untreated controls (Fig. 6A,C). CK666 similarly reduced K370 localized at cell–cell contacts (Fig. 6A), suggesting there is positive feedback between KIF17 junctional localization and enhanced accumulation of junctional actin foci. Inhibition of K370-induced accumulation of junctional GFP–actin foci by CK666 is consistent with studies showing that GFP–actin is incorporated preferentially into branched actin filaments by Arp2/3 (Chen et al., 2012). From these experiments, we conclude that K370 induces accumulation of junctional actin by activating RhoA signaling, leading to inhibition of cofilin-severing activity toward branched actin at cell–cell junctions.

KIF17 tail domain inhibits effects of K370 on cortical actin accumulation

The KIF17 C-terminal tail binds to the KIF17 motor domain directly and reduces the localization of K370 at cell–cell contacts (Fig. 2D). As such, it may also influence the effect of K370 on

Journal of Cell Science (2016) 129, 957-970 doi:10.1242/jcs.173674

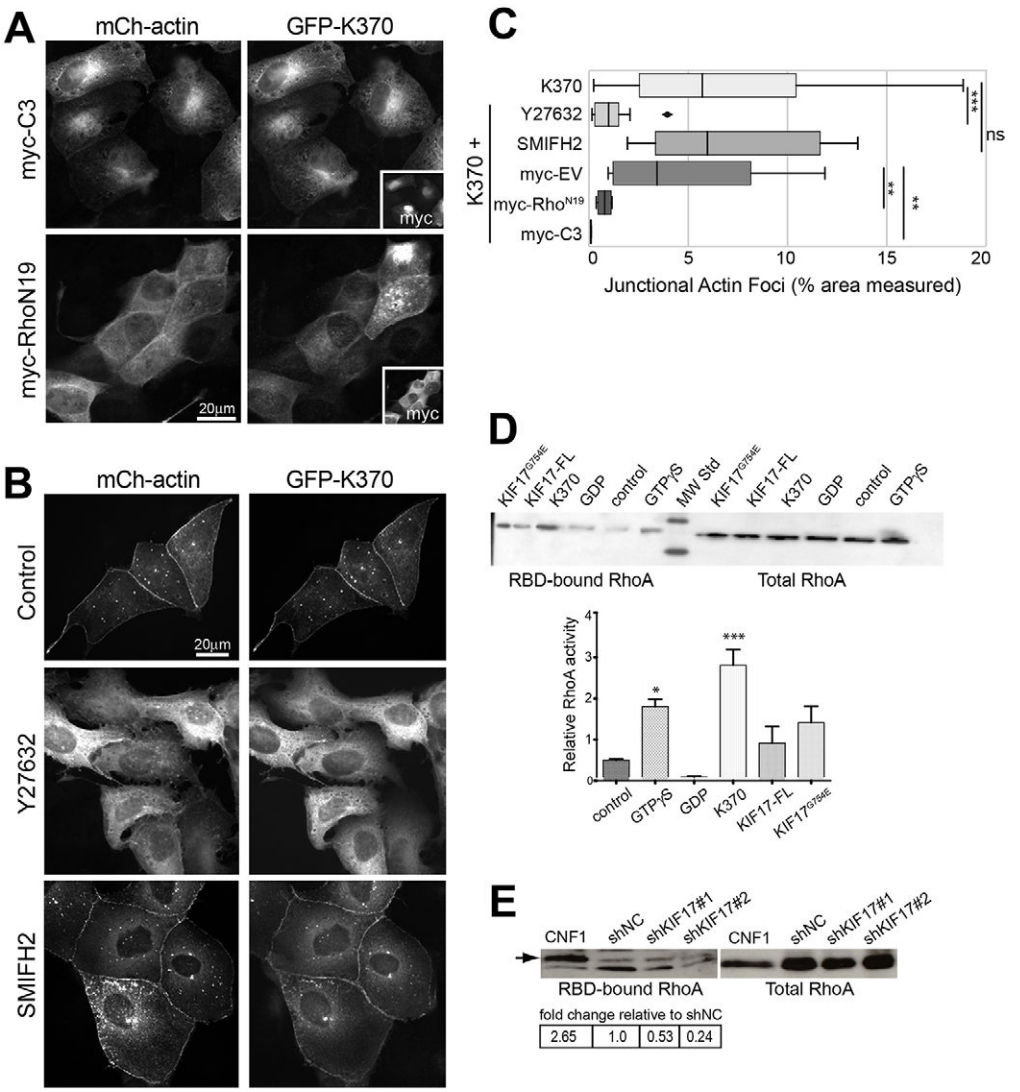

Fig. 5. RhoA signaling regulates junctional actin accumulation mediated by K370. (A) MDCK cells expressing mCh–actin, GFP–K370 and either myc–C3 or myc–RhoA^{N19} and fixed 4 h after cDNA injection. Insets show myc-immunostaining to detect expressed C3 and RhoA^{N19}. (B) Localization of mCh–actin and GFP–K370 in untreated MDCK cells and in cells treated with Y27632 (10 μM) or SMIFH2 (50 μM). Inhibitors were added immediately after cDNA injection and cells were fixed after 4 h. (C) Box-whisker plots showing quantification of junctional actin foci identified by segmentation as a percentage of the total ROI selected for measurement in each experimental condition. Results are from images of injected cells in 2–4 independent experiments. Significance was determined using a two-tailed Mann–Whitney U test. (D) Immunoblots showing pull-down of GTP-bound RhoA with the Rho-binding domain of Rhotekin (RBD) and total RhoA in cells expressing the indicated constructs. Graph shows relative abundance of active GTP–RhoA in each condition. Error bars are s.e.m. Statistical significance was determined using one-way Anova and Bonferroni's multiple comparison test. (E) Immunoblots showing pull-down of GTP-bound RhoA in cells treated with the Rho–GTPase activator CNF1 (0.55 μg/ml for 90 min) or transduced with shNC, shKIF17#1 or shKIF17#2. Table shows relative abundance of GTP–RhoA pulled down under each condition. ns, not significant; *P<0.05; **P<0.01; ***P<0.001.

accumulation of junctional actin. Indeed, co-expression of mCh–KIF17-Tail with myc–K370 and GFP–actin reduced the median segmented membrane area covered by actin foci 1.9-fold (to 2.61%) relative to controls expressing mCh–EV, K370 and actin (4.82%). Co-expression of KIF17-Tail also reduced the percentage of cells with resolvable junctional actin foci to 30% of controls (Fig. 6B,C). This result suggests that KIF17-Tail inhibits the effects of K370 by preventing its junctional localization (Fig. 2D), or possibly, by competing with another factor that could modify actin dynamics. These data are also consistent with the more robust effects of the tail-less K370 over KIF17-FL on RhoA activation (Fig. 5D).

KIF17 is involved in regulating the distribution of E-cadherin and adhesion strength in response to calcium depletion

Actin associates with and anchors AJC components at the plasma membrane during formation, maturation and maintenance of cell–cell adhesions. When adhesions are remodeled, due to either experimental manipulation or in response to physiological cues, transmembrane components of the AJC such as E-cadherin are endocytosed, loosening junctions. Since KIF17 colocalizes with both actin and E-cadherin (Fig. 1A), we hypothesized that, by regulating junctional actin, KIF17 could affect AJC protein localization and junction stability or remodeling. To test this, we first expressed KIF17 constructs in MDCK cells and analyzed the distribution of E-cadherin by immunostaining cells fixed 4 h after cDNA microinjection. In uninjected cells, E-cadherin localized primarily at cell–cell contacts but was also seen in cytoplasmic vesicles. These vesicles likely represent a combination of E-cadherin transport intermediates in the biosynthetic, endocytic or recycling pathways. In cells expressing K370 or K339, we observed a reduction in the number of cytoplasmic vesicles containing E-cadherin (Fig. 7A and not shown). We quantified the number of cytoplasmic E-cadherin vesicles in individual cells and measured a 3.9-fold decrease in the median number of intracellular E-cadherin puncta in cells expressing KIF17 constructs as compared with uninjected controls (Fig. 7C). By contrast, we measured a 2.53-fold increase in the median number of cytoplasmic E-cadherin puncta in KIF17-depleted cells (shKIF17) as compared with shNC controls (Fig. 7B,C). We did not detect a difference in the levels of E-cadherin or actin by immunoblot in KIF17-depleted cells (Fig. 7D) suggesting that KIF17 acts on E-cadherin by modifying its subcellular distribution.

In a fluorescence pulse-chase assay to monitor biosynthetic trafficking of newly synthesized membrane proteins (Kreitzer et al., 2000), we did not measure any change in the kinetics of GFP–E-cadherin export from the Golgi or its delivery to the plasma

Journal of Cell Science (2016) 129, 957-970 doi:10.1242/jcs.173674

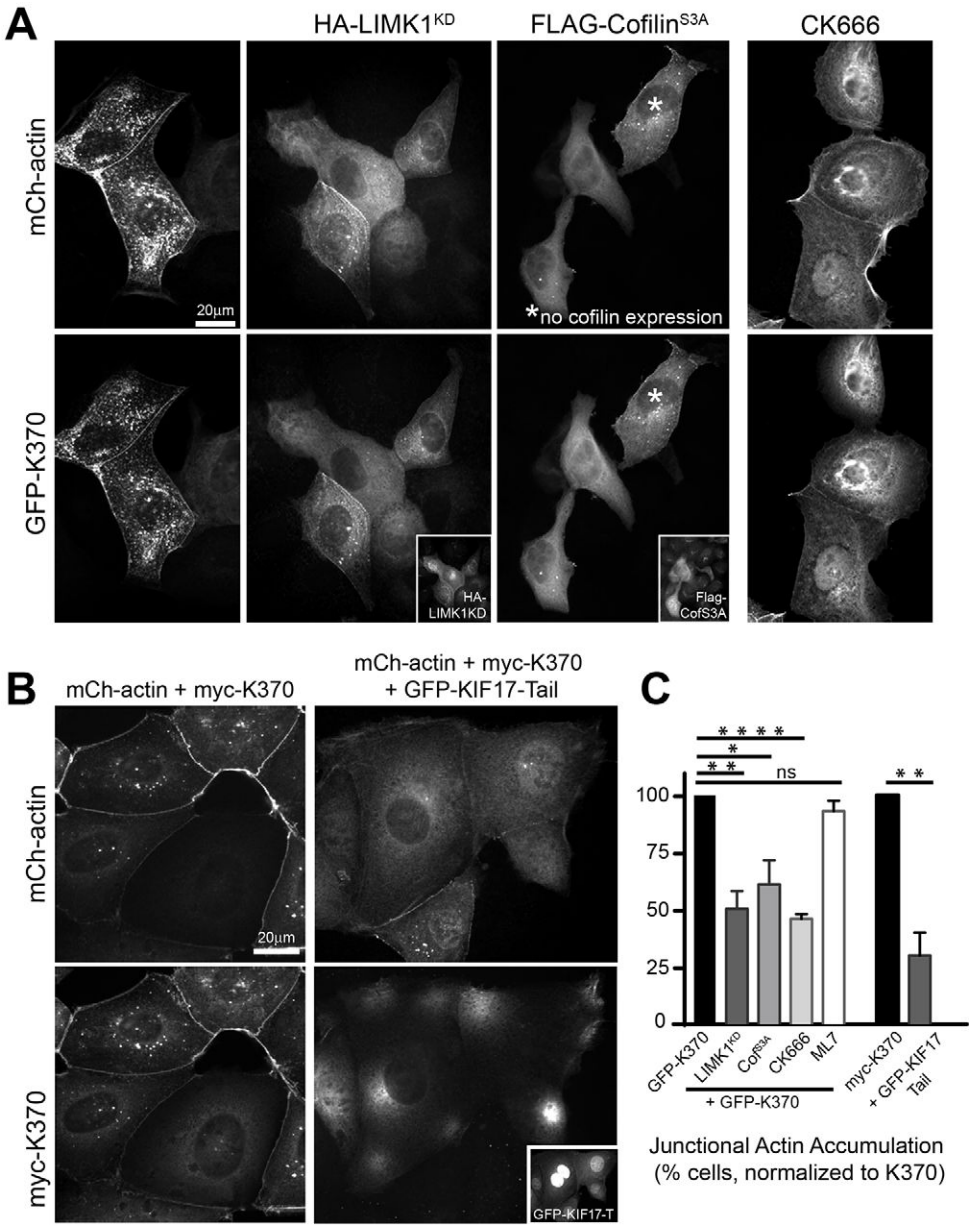

Fig. 6. K370 promotes junctional actin accumulation by inhibiting LIMK and/or cofilin-dependent actin severing. (A) Localization of mCh–actin and GFP–K370 in MDCK cells co-expressing HA–LIMK1 kinase-dead (LIMK1^{KD}) or FLAG–cofilin^{S3A} 4 h after cDNA injection. Insets show HA and FLAG immunostaining to detect expressed LIMK1^{KD} and cofilin^{S3A}. (B) Localization of mCh–actin and myc–K370 in cells co-expressing GFP–EV control or GFP–KIF17-Tail 4 h after cDNA injection. Inset shows GFP–KIF17-Tail in injected cells. GFP–EV was detected in living cells before fixation but was frequently lost during processing for immunofluorescence analysis; thus it is not shown here. (C) Graph showing percentage cells with accumulated junctional actin foci for each experimental condition indicated normalized to GFP–K370 or myc–K370 controls. Cells were injected with K370 and mCh–actin cDNAs alone or in combination with HA–LIMK1^{KD} (*n*=194), Flag–cofilin^{S3A} (*n*=160) or GFP–KIF17-Tail (*n*=60). CK666 (100 μM, *n*=92) and ML7 (10 μM, *n*=186) were added to cells immediately following cDNA injection until fixation 4 h later. Error bars are error margins with 95% confidence interval. Significance was determined using a two-tailed unpaired student's *t*-test. ns, not significant, **P*<0.05; ***P*<0.01; *****P*<0.0001.

membrane when we co-expressed either K339 or KIF17-Tail as compared with cells expressing only GFP–E-cadherin (not shown) (Jaulin et al., 2007). This suggests clearance of E-cadherin puncta in K370-expressing cells and increased abundance of E-cadherin puncta in KIF17-depleted cells result from changes in E-cadherin endocytosis or recycling. To determine if KIF17 affects E-cadherin distribution selectively, or if it also affects the internalization of membrane proteins not associated with the AJC, we loaded transferrin receptors (TfR) with Cy3–transferrin (Cy3–Tf; 25 μg/ml) and monitored TfR endocytosis. Cells were incubated with Cy3–Tf on ice for 60 min and then warmed to 37°C for 30 min and fixed for image acquisition. In these experiments, we detected no difference in TfR internalization in cells expressing GFP–K370 as compared with GFP–EV controls (Fig. S4A), showing that KIF17 does not broadly inhibit endocytosis of plasma membrane proteins.

We next determined if the effects of KIF17 perturbation on E-cadherin distribution and accumulation of junctional actin foci induced by KIF17 perturbations reflect changes in cellular function by analyzing the strength of cell–cell adhesions when challenged by calcium depletion. We expressed K370 or the control KIF3A-M (Jaulin et al., 2007) and incubated cells in media containing 1.5 mM EDTA, beginning 4 h after cDNA injection. Cells were imaged by time-lapse microscopy for 90 min following addition of EDTA. By 60 min, most of the uninjected or KIF3A-M-expressing cells detached from neighbors and had rounded up from the coverslip. Conversely, the majority of cells expressing K370 or K339 remained adhered to each other and did not exhibit significant rounding (Fig. 8A; Fig. S4B). Furthermore, E-cadherin, as well as ZO-1 and γ-catenin, were retained at cell–cell contacts in K370- or K339-expressing cells treated with EDTA (Fig. S4C). Thus, expression of K370 or K339 inhibits internalization of AJC components, attenuating cellular responses to triggers that reduce adhesiveness of cell–cell contacts. Considered together, these data support a model in which KIF17 contributes to regulation of cell–cell junction remodeling by activating RhoA signaling to reduce cofilin-mediated severing of junctional actin (Fig. 8B). We speculate that by shifting the balance between actin polymerization

Journal of Cell Science (2016) 129, 957-970 doi:10.1242/jcs.173674

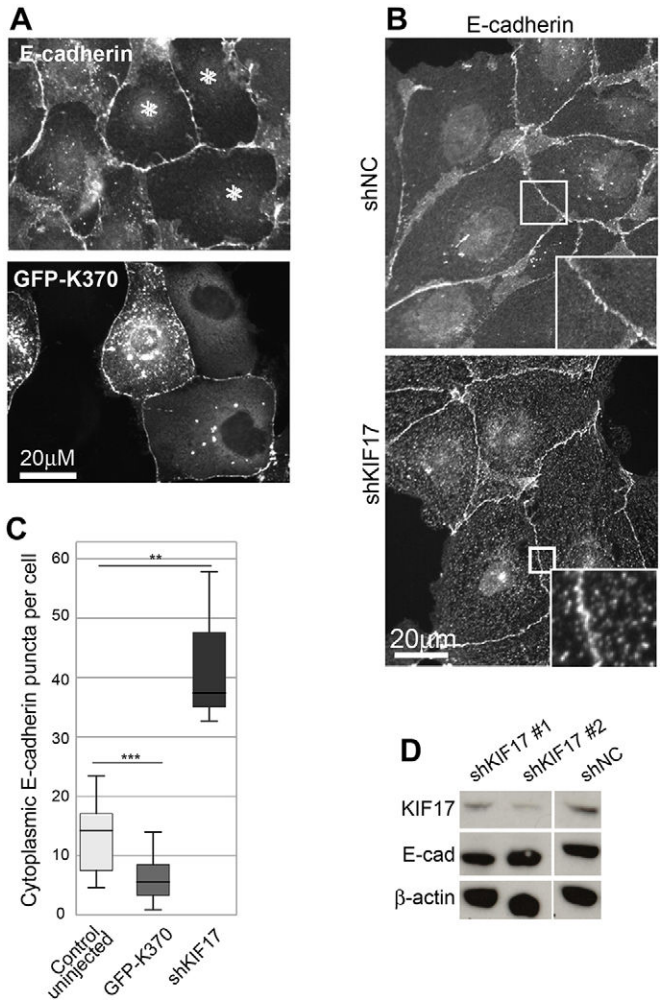

Fig. 7. KIF17 regulates the distribution of E-cadherin. (A) Localization of E-cadherin in MDCK cells expressing GFP–K370 or GFP–KIF17-FL and fixed 4 h after cDNA injection. Asterisks mark injected cells. (B) Localization of E-cadherin in cells transduced with shNC or shKIF17. Boxed regions are magnified in insets. (C) Box-whisker plots showing quantification of cytoplasmic E-cadherin puncta in uninjected controls and in cells expressing GFP–K370 and in KIF17-depleted cells (shKIF17). Results are from images of injected cells in 2–4 independent experiments. Significance was determined using a two-tailed Mann–Whitney U test. $^{**}P<0.01$; $^{***}P<0.001$.
(D) Immunoblots showing KIF17, E-cadherin and β-actin in MDCK cells transduced with shNC, shKIF17#1 or shKIF17#2.

and severing, KIF17 reduces the internalization of AJC proteins and thereby increases the strength of cell–cell adhesions.

DISCUSSION

The data presented here provide evidence that KIF17 contributes to regulation of branched actin stability at cell–cell contacts, stabilization of E-cadherin at the plasma membrane, and to intercellular adhesion strength. Remarkably, these functions are dependent on the kinesin motor domain but independent of microtubules. In concert with EB1 and APC, components of the microtubule plus-end capture machinery, KIF17 also promotes microtubule stabilization in epithelial cells and is sufficient to stabilize microtubules *in vitro* (Acharya et al., 2013; Espenel et al., 2013; Jaulin and Kreitzer, 2010). Considering that KIF17 depletion also compromises apical actin recruitment and lumen formation in 3D culture (Fig. 1) (Jaulin and Kreitzer, 2010), our findings suggest KIF17 plays a central role in coordinating actin and microtubule remodeling with formation and remodeling of cell–cell junctions to promote morphogenesis and epithelial polarization.

During expansion of primordial cell–cell contacts, distinct arrays of branched and unbranched actin associate with E-cadherin as spot junctions are remodeled into mature, junctional complexes at the apicolateral membrane domain of polarized cells. Experiments monitoring actin incorporation by FRAP showed that 80–90% of filaments are very dynamic (Yamada et al., 2005; Kovacs et al., 2011) and are generated by Arp2/3-dependent branched actin nucleation (Kovacs et al., 2002; Otani et al., 2006; Tang and Brieher, 2012). This is consistent with our data in MDCK cells showing that the accumulation of GFP–actin at cell–cell contacts is attenuated by inhibiting Arp2/3. Although circumferential, formin-dependent unbranched actin arrays contribute to maturation of adherens junctions, they do not appear to be regulated by KIF17, and are likely utilized downstream of the initial establishment of cell–cell junctions. Formation and organization of branched actin and actin cables are regulated by a combination of actin nucleation, elongation and severing activities coordinated by junction-associated Rho–GTPases, their regulators and effectors; these concentrate E-cadherin at AJCs during polarization and modulate junction assembly and maintenance (Citi et al., 2014; Mack and Georgiou, 2014). As such, the effects of KIF17 on cortical actin and intercellular junctions can be attributed, at least in part, to activation of RhoA signaling as levels of active RhoA are increased by expression of KIF17 constructs and reduced by KIF17 knockdown. Although Rho has no reported role in regulating nucleation of branched actin filaments, signaling to its effector ROCK activates LIMK1, which then phosphorylates and inhibits cofilin-mediated severing of branched actin. This would be expected to shift the balance between actin polymerization and depolymerization at cell–cell contacts. In support of a role for KIF17 in this pathway, we found that pharmacological inhibitors of ROCK, or expression of either kinase-dead LIMK1 or a cofilin phospho-mimic, inhibited the effect of KIF17 expression on accumulation of junctional actin.

KIF17 may have additional functions in regulating establishment and remodeling of the AJC. Microtubule capture and cortical stabilization by KIF17 (Jaulin and Kreitzer, 2010) could generate specialized tracks comprising post-translationally modified, stable microtubules, for targeted delivery of cytoplasmic and membrane proteins important for junction formation and remodeling (Waterman-Storer et al., 2000). However, neither microtubule depolymerization nor expression of a K370 mutant that cannot bind microtubules ($K370^{R288/294A}$) impinges on the ability of K370 to induce accumulation of junctional actin foci. Based on this, we believe that the effects of KIF17 on junctional actin are independent of its effects on microtubules.

In contacting, but not yet polarized cells, microtubules are organized primarily in radial arrays emanating from the MTOC, with a subset of plus-ends localizing in close proximity to the developing AJC. Kinesin-mediated transport on microtubules is used to both deliver and retrieve cadherin and other adhesion components to and from the plasma membrane (Chen et al., 2003; Ivanov et al., 2006; Krylyshkina et al., 2002; Mary et al., 2002; Nekrasova et al., 2011; Portereiko et al., 2004; Yanagisawa et al., 2004). Dynamic microtubule plus-ends, where KIF17 localizes with EB1 and APC (Jaulin and Kreitzer, 2010), can interact with proteins at the cortex and deposit microtubule plus-end-associated proteins that regulate cytoskeletal and junctional organization, such as APC, leading to the concentration of E-cadherin at cell–cell contacts (Ligon and Holzbaur, 2007; Ligon et al., 2001; Stehbens et al.,

Journal of Cell Science (2016) 129, 957-970 doi:10.1242/jcs.173674

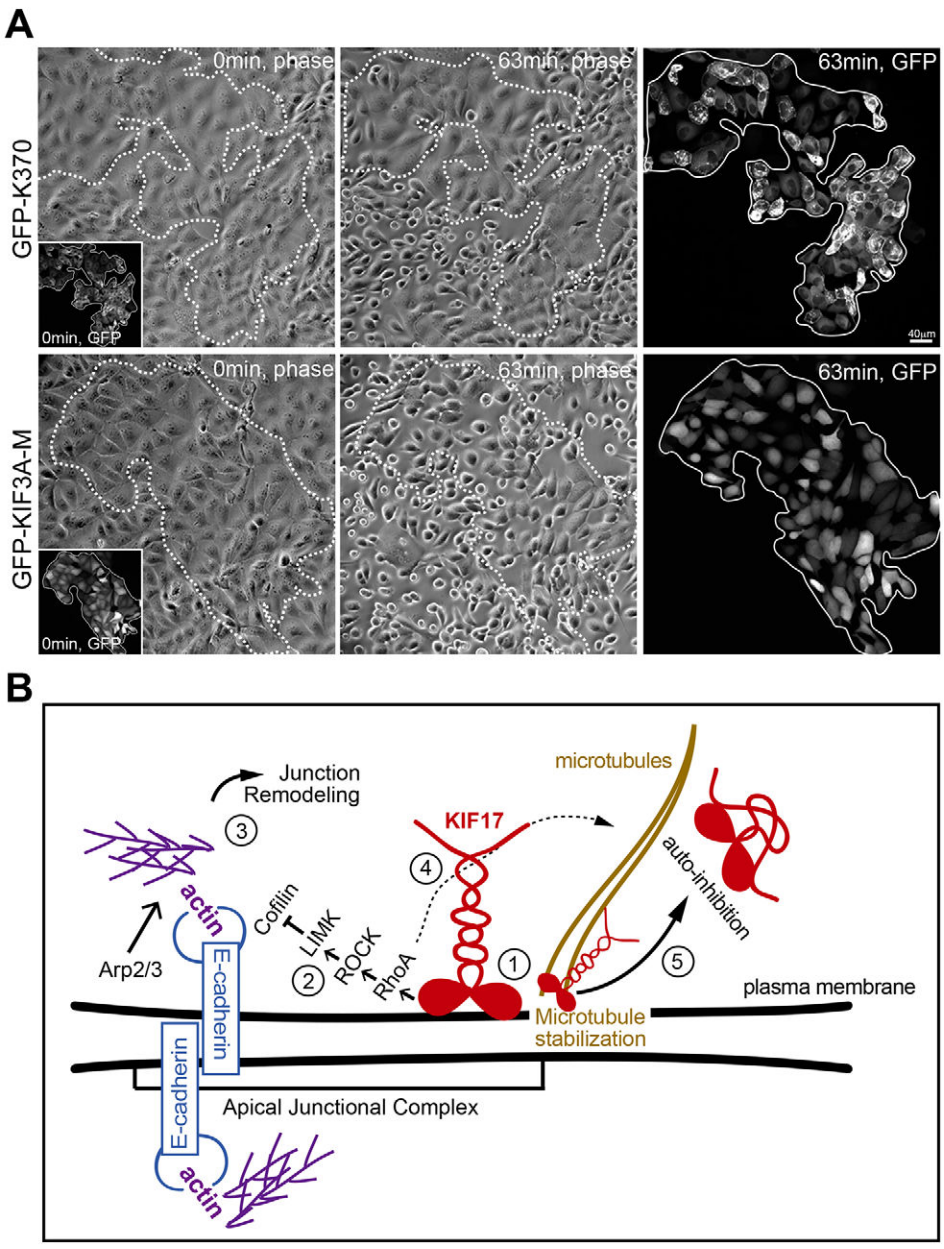

Fig. 8. K370 strengthens cell–cell adhesions to challenge with calcium chelators. (A) Phase-contrast and fluorescence images showing first and last frames from a time-lapse recording of MDCK cells incubated with 1.5 mM EDTA. EDTA was added 4 h after cDNA injection and cells were imaged at 1-min intervals. Upper panels show cells expressing GFP–K370. Lower panels show cells expressing GFP–KIF3A-M. Insets show GFP fluorescence of expressed constructs at the start of the recordings. Outlined regions on phase-contrast images show the area encompassed by GFP–KIF-expressing cells. Fluorescent images on the far right show GFP–KIFs at the last frame of the time-lapse. (B) Model for KIF17 function at the AJC of epithelial cells: (1) KIF17 associates with the AJC, where it colocalizes with E-cadherin and junctional actin. (2) The KIF17 motor domain is sufficient for junctional localization and triggers activation of a RhoA signaling pathway leading to inhibition of cofilin. (3) Decreased cofilin severing activity allows for the accumulation of junctional actin, alters E-cadherin trafficking and impairs junction dissociation in response to calcium depletion. (4) KIF17 also regulates microtubule stabilization (Jaulin and Kreitzer, 2010), likely downstream of RhoA signaling. (5) KIF17 functions at the AJC and on microtubules are inhibited by intramolecular interactions between the motor and tail domains.

2006). We show here that KIF17 overexpression clears E-cadherin-containing vesicles from the cytoplasm, and conversely, that KIF17 depletion results in an increase in cytoplasmic E-cadherin. As there is no evidence implicating KIF17 in biosynthetic trafficking of E-cadherin, we speculate that by modifying cortical actin through RhoA signaling, KIF17 stabilizes E-cadherin in the plasma membrane and affects junction stability by enhancing anchorage of AJC proteins to the underlying cortical cytoskeleton. This would be expected to attenuate endocytosis of E-cadherin and AJC components both at steady-state, and in response to signals that induce junction remodeling and is consistent with our data showing that internalization of E-cadherin induced by calcium depletion is blocked by expression of K370 and K339 motor domain constructs.

We do not yet fully understand how KIF17 and K370 activate RhoA signaling to promote junctional actin accumulation and stabilization of cell–cell adhesions. KIF17 may activate RhoGEFs, or inhibit RhoGAPs (also known as ARHGAPs), to maintain high levels of active RhoA, either on microtubule plus-ends or at the cortex when it contacts the plasma membrane. In one possible scenario, the KIF17 motor could interact with a RhoGEF and deliver it to the cortex, where it would be activated when off-loaded from microtubules (Enomoto, 1996). Candidates for activating RhoA signaling for microtubule stabilization and/or remodeling of the AJC include GEF-H1, p115-RhoGEF and ECT2. The KIF17 motor domain does interact with several cytoplasmic proteins (our unpublished data and Jaulin and Kreitzer, 2010), thus, it is reasonable to suspect additional protein interactions could occur in this domain. Microtubule capture, stabilization, and the subsequent accumulation of post-translationally modified microtubules by KIF17 could also trigger a change in the captured microtubule that induces local GEF release from the lattice of that microtubule. Indeed, inactive GEF-H1 localizes preferentially on dynamic, unmodified microtubules and is not seen on stable, acetylated or detyrosinated microtubules (Nagae et al., 2013; Yoshimura and Miki, 2011). Because KIF17 is activated by PKC (Espenel et al., 2013), which contributes to RhoA-dependent microtubule stabilization in

Journal of Cell Science (2016) 129, 957-970 doi:10.1242/jcs.173674

fibroblasts (Wen et al., 2004), we also envision a model wherein feedback signaling could amplify microtubule capture in response to initial Rho activation events at cell–cell contacts (Fig. 8B).

The effects of full-length KIF17 on junctional actin and RhoA activation are less robust than that of the motor domain alone, suggesting the KIF17 tail domain is a negative regulator of these KIF17 activities. In support of this, we showed previously that KIF17 tail interacts directly with the motor domain, decreasing its ATPase activity (Acharya et al., 2013; Espenel et al., 2013), and we show here that KIF17 tail expression abrogates accumulation of junctional actin induced by expression of K370. Our localization studies suggest that the KIF17 tail competes with a factor(s) that anchors KIF17 at cell–cell junctions, in line with our previous demonstration that the KIF17 tail domain competes with EB1 for binding to the KIF17 head (Acharya et al., 2013). Alternatively, the KIF17 tail could interfere with the motor-dependent activation of RhoA signaling by carrying a cargo that acts as a negative regulator of RhoA. A precedent for regulation of a RhoGEF and a RhoGAP by a single kinesin has been reported, although the mechanism of action may differ somewhat from that of KIF17. MKLP1 (KIF23, kinesin-6 family), a component of the centralspindlin complex, affects microtubule and actin arrays, formation of adherens junctions, and polarization of foregut epithelia in *Caenorhabditis elegans* through an interaction with CYK4−RhoGAP (Portereiko et al., 2004). CYK4−RhoGAP induces a conformational change in MKLP1 leading to activation of RhoA (Saade et al., 2007; Yamamoto et al., 2006). MKLP1, as part of the centralspindlin complex, also binds and recruits the RhoGEF ECT2 to cell–cell junctions, and inhibits junctional localization of p190 RhoGAP in MCF-7 cells, leading to activation of RhoA (Ratheesh et al., 2012). These data support the idea that a kinesin can influence the activities of both RhoGEFs and RhoGAPs at cell–cell junctions, fine-tuning local RhoA signaling.

Mounting evidence shows an interdependence between signaling events at the cortex of mammalian cells with cytoskeletal dynamics and organization that lead to cell polarization (Gundersen, 2002a,b; Siegrist and Doe, 2007). An emerging theme is that protein delivery to and retrieval from the cortex can influence cytoskeletal dynamics and organization. Remodeling of actin and microtubule arrays is mediated by an overlapping set of effectors that respond to cortical stimuli (Bartolini et al., 2008; Gundersen et al., 2004; Mikhailov and Gundersen, 1998; Tatebe et al., 2008; Watanabe et al., 2004). Both focal adhesions and the AJC are sites of microtubule plus-ends targeting and where cytoskeletal dynamics may be regulated locally (Chausovsky et al., 2000; Efimov et al., 2008; Ezratty et al., 2005; Waterman-Storer et al., 2000). These cortical adhesions are also sites of active membrane recycling and kinesin-dependent delivery and retrieval of transmembrane and membrane–cytoskeleton linkers (Chen et al., 2003; Ivanov et al., 2006; Krylyshkina et al., 2002). The effects of KIF17 on RhoA activity, actin and microtubule arrays, and on stability of the AJC lend support to the idea that KIF17 plays an important role in coordinating formation of nascent cell–cell adhesions with remodeling of actin and microtubules to initiate morphological polarization of epithelial cells.

MATERIALS AND METHODS

Cell culture and treatments

Madin–Darby canine kidney (MDCK) cells were cultured in DMEM (4.5 g/l glucose) with 5% FBS, 20 mM HEPES, pH 7.2, and were tested for mycoplasma contamination prior to initiating these studies. MCF10A cells were purchased from ATCC (CRL-10317). MDCK cells were seeded on sterilized coverslips and used at ∼80% confluence 2–3 days after plating. For 3D cultures, cells were infected with lentiviral shRNAs and allowed to grow for 2–4 days. Cells were then trypsinized and suspended in complete medium containing 2% Matrigel™ (BD Biosciences) and layered onto Matrigel at 10^4 cells/well in 8-well chamber slides (Lab-Tek) as described (O'Brien et al., 2006). Cysts were fixed after 7 days in culture in 4% PFA for 30 min and permeabilized with 0.5% Triton X-100 for 15 min before immunostaining.

Microtubules were depolymerized completely by incubating cells on an ice-slurry in bicarbonate-free, complete media supplemented with 33 µM nocodazole (Sigma) for 30 min followed by incubation at 37°C for an additional 30 min prior to microinjection. Cells were maintained in 33 µM nocodazole during microinjections and subsequently transferred back into bicarbonate-containing complete media with 33 µM nocodazole. Cells were fixed 4 h after cDNA injection and processed for immunofluorescence analysis and imaging. Inhibitors of Arp2/3 (CK666, 100 µM), ROCK (Y27632, 10 µM), myosin light chain kinase (ML-7, 10 µM) and formins (SMIFH2, 50 µM) (Sigma), were added to cells immediately following cDNA injections.

Immunofluorescence staining and immunoblot analysis

Cells were fixed in −20°C methanol for 1–2 min or in 2% paraformaldehyde for 5 min at room temperature followed by permeabilization in either PBS-CM (PBS with 100 µM $CaCl_2$, 1 mM $MgCl_2$) with 0.1% Triton X-100 for 2 min or in −20°C methanol (for immunolabeling of endogenous actin). KIF17 was detected with a rabbit polyclonal antibody at 1:100 dilution described and characterized previously (Jaulin and Kreitzer, 2010). Endogenous actin was detected by indirect immunofluorescence with mouse anti-β-actin ascites fluid diluted 1:200 (clone AC-74, Sigma). Other antibodies: rat anti-E-cadherin (1:200; DECMA, Sigma), mouse anti-α-actinin (1:200; clone BM75.2, Sigma) mouse-anti-myc tag (1:200; 9B11, Sigma), mouse anti-FLAG M2 tag (1:100; F3165, Sigma), mouse anti-HA tag (1:100 dilution; MMS-101P, Covance), rabbit-anti-detyrosinated tubulin [1:400; SG, provided by Gregg Gundersen, Columbia University, USA (Gundersen et al., 1984)]. Fluorescently conjugated secondary antibodies raised in donkey and cross-adsorbed against related species were from Jackson Immunoresearch. Antibodies for immunoblots are: rabbit anti-KIF17 (1:1000; K3638, Sigma), mouse anti-E-cadherin (1:500; 610181, BD Biosciences) and mouse anti-β-actin (1:5,000; clone AC-74, A5316, Sigma).

Expression constructs

KIF17 constructs used for this study were amplified by PCR from human A549 or Caco2 cells and cloned into Gateway expression vectors (Invitrogen) as recommended by the manufacturer and as described previously (Jaulin and Kreitzer, 2010; Acharya et al., 2013). Myc–C3, GFP–RhoA WT, myc–$RhoA^{V14}$, and myc–$RhoA^{N19}$ were generous gifts from Dr Alan Hall (Memorial Sloan Kettering Cancer Center, NY, USA). HA-$LIMK1^{KD}$ and FLAG-$cofilin^{S3A}$ (Salvarezza et al., 2009) were provided by Enrique Rodriguez-Boulan (Weill Cornell Medical College, NY, USA).

Protein expression

Exogenous proteins were expressed by intranuclear injection of cDNAs, either individually or together (10–50 µg/ml for each plasmid), in HKCl (10 mM HEPEs, 140 mM KCl, pH 7.4) using a Narishige micromanipulator with back-loaded capillary glass needles. Protein expressed from injected cDNAs could be detected after incubation at 37°C for 60–90 min. Cells were fixed at indicated times after injection and processed for direct fluorescence or indirect immunofluorescence microscopy.

Protein knock-down

pGIPZ lentiviral shRNAs targeting KIF17 and pLKO.1 lentiviral control plasmid (Open Biosystems) were prepared and introduced by viral transduction as described previously (Jaulin and Kreitzer, 2010).

Fixed cell imaging and analysis

Fixed cell images were acquired on either a Nikon E400 Eclipse or a Nikon TiE using a 40× (NA 1.0) plan-apochromat oil immersion objective and collected with digital charge-coupled device cameras (ORCA II-ER, 6.45 µm pixels, 1 MHz for 14-bit images, Hamamatsu Photonics; or Neo

sCMOS, 6.45 µm pixels, 200 MHz for 16-bit images, Andor Technology). 14–16-bit images were scaled linearly to illustrate features of interest as indicated in the Results and converted to 8-bit copies for figure assembly. Devices were controlled by either MetaMorph (Molecular Devices, Inc.) or Elements (Nikon Instruments). Post-acquisition analysis and processing were performed using MetaMorph. Images of 3D cysts were acquired with a Zeiss LSM510 scanning confocal microscope (Rockefeller University Bioimaging Resource Center).

Time-lapse imaging

After microinjection, cells were transferred to recording medium (Hanks' balanced salt solution with 20 mM HEPES, 1% FBS, 4.5 g/l glucose, essential and non-essential amino acids) and incubated at 37°C in a thermal-controlled chamber (Harvard Apparatus) on a TE-2000U (Nikon). Time-lapse images were acquired using a 20× (NA 0.5) plan-fluor, phase contrast, dry objective and collected with a Neo sCMOS camera (6.45 µm pixels, 200 MHz for 16-bit images, Andor Technology). 14–16-bit images were scaled to illustrate features of interest and converted to 8-bit copies for figure assembly. Devices were controlled with Elements software (Nikon Instruments). Post-acquisition analysis and processing were performed with MetaMorph.

Quantitative image analysis

Image processing and analysis was performed using Python scripts using scikit-image (van der Walt et al., 2014) and OpenCV (Bradski, 2000) packages, as well as Fiji software (Schindelin et al., 2012). All source codes developed are open source and freely available at https://github.com/cespenel/image_processing.

Analysis of junctional actin foci

We developed an image segmentation method called, 'membrane_accumulation'. Briefly, a polyline with a thickness of 4 pixels (~700 nm) was drawn following the membrane at sites of cell–cell contact. These polylines were used as regions of interest (ROIs), averaging ~2200 pixels^2/cell, inside which the following processing was performed. Images were smoothed using a median blur filter of 5 and then images were convolved with a 3×3 Laplacian kernel with values from −1 to 8. Images were further smoothed using a median blur. For segmentation of actin foci, we use a marker-controlled watershed with two seed points (or markers), one given by an Otsu threshold and a second by 30% of the value given by the Otsu method. From these thresholded images, we measured the percentage of the ROI that was segmented.

Analysis of cytoplasmic E-cadherin puncta

Two methods were developed. The first, 'blobs per cell', was used for analysis of KIF17-depleted cells wherein the number of cells was calculated automatically based on the number of DAPI-stained nuclei. The second, 'blobs_per_cell_click', was used for analysis of cells expressing microinjected KIF17 constructs wherein we extracted the number of blobs (puncta) in injected cells and uninjected cells. We then created a mask on the injected cells images, and applied this mask to the corresponding images of E-cadherin. We then determined the number of puncta in the masked (injected cells) and non-masked (uninjected cells) areas. All images were first convolved with a 3×3 Laplacian kernel with values from −1 to 8 and then a Gaussian filter with a sigma value of 3 was applied. Blobs/puncta were identified using the difference of Gaussians approach above a defined Otsu threshold.

Graphs and statistical analysis of junctional actin foci and E-cadherin puncta

Boxplots were generated using the 2D python-plotting library Matplotlib (Hunter, 2007) and show minima, 25% quartile, median, 75th quartile, and maxima. Statistical tests were performed using a two-tailed Mann–Whitney U test (Python library SciPy, scipy.stats.mannwhitneyu). Statistical significance is defined as: ns, not significant (P>0.05); *P<0.05; **P<0.01; ***P<0.001 and ****P<0.0001.

Statistics for binary analysis

Statistical significance was determined by two-tailed unpaired Student's t-test unless noted otherwise in the figure legends. Data are presented as mean±s.e.m. for quantitative values and error margins for percentages (95% level of confidence). Sample size (n) and P-values are specified in the text or figure legends. Data were collected from at least three independent experiments.

Rho–GTP binding assay

Rhotekin-RBD was purchased from Cytoskeleton (Denver, CO) and RhoA–GTP binding was performed as recommended by the manufacturer. Briefly, MDCK were transfected with indicated constructs. After 24 h, cells were washed in PBS and lysed in 25 mM HEPES pH 7.5, 150 mM NaCl, 1% NP-40 (Igepal CA-630), 10 mM $MgCl_2$, 1 mM EDTA and 10% glycerol, 10 µg/ml leupeptin, 10 µg/ml pepstatin, and 10 µg/ml aprotinin. For assays in KIF17-depleted cells, cells were also treated with RhoA activator, cytotoxic necrotizing factor 1 (CNF1, 55 µg/ml) as a positive control. Lysates were clarified by centrifugation at 13,000 ***g*** at 4°C for 1 min. Clarified lysates (200 µg) were divided in two; one to detect total RhoA, and one for use in pull-downs. 100 µg of lysate was incubated with Rhotekin–RBD protein beads (50 µg) at 4°C for 90 min. The beads were collected by centrifugation, washed thoroughly and resuspended in 2× Laemmeli buffer. Input samples and collected beads were analyzed by western blot using a RhoA-specific antibody. Densitometry was performed using ImageJ (NIH). The amount of RBD-bound RhoA was normalized to total RhoA in cell lysates for comparison of Rho activity (level of GTP-bound Rho) across samples.

Acknowledgements

We thank Alan Hall (Memorial Sloan Kettering Cancer Center, NY, USA) and Enrique Rodriguez-Boulan (Weill Cornell Medical College, NY, USA) for providing plasmids.

Competing interests

The authors declare no competing or financial interests.

Author contributions

B.R.A., C.E., F.L., J.R., J.M., F.J. and G.K. performed experiments. C.E. developed algorithms for quantitative image analysis. F.J. and G.K. conceived the project and wrote the manuscript.

Funding

This work was supported by grants from the National Institutes of Health [R01GM087575] and the Irma T. Hirschl Trust to G.K., and from the Centre national de la recherche scientifique (ATIP-AVENIR program) and the Gustave Roussy Foundation to F.J. Deposited in PMC for release after 12 months.

Supplementary information

Supplementary information available online at
http://jcs.biologists.org/lookup/suppl/doi:10.1242/jcs.173674/-/DC1

References

Acharya, B. R., Espenel, C. and Kreitzer, G. (2013). Direct regulation of microtubule dynamics by KIF17 motor and tail domains. *J. Biol. Chem.* **288**, 32302-32313.

Arber, S., Barbayannis, F. A., Hanser, H., Schneider, C., Stanyon, C. A., Bernard, O. and Caroni, P. (1998). Regulation of actin dynamics through phosphorylation of cofilin by LIM-kinase. *Nature* **393**, 805-809.

Bartolini, F., Moseley, J. B., Schmoranzer, J., Cassimeris, L., Goode, B. L. and Gundersen, G. G. (2008). The formin mDia2 stabilizes microtubules independently of its actin nucleation activity. *J. Cell Biol.* **181**, 523-536.

Bradski, G. (2000). The OpenCV library. *Dr Dobb's J.* **25**, 120-125.

Brieher, W. M. and Yap, A. S. (2013). Cadherin junctions and their cytoskeleton(s). *Curr. Opin. Cell Biol.* **25**, 39-46.

Carramusa, L., Ballestrem, C., Zilberman, Y. and Bershadsky, A. D. (2007). Mammalian diaphanous-related formin Dia1 controls the organization of E-cadherin-mediated cell-cell junctions. *J. Cell Sci.* **120**, 3870-3882.

Chausovsky, A., Bershadsky, A. D. and Borisy, G. G. (2000). Cadherin-mediated regulation of microtubule dynamics. *Nat. Cell Biol.* **2**, 797-804.

Chen, X., Kojima, S., Borisy, G. G. and Green, K. J. (2003). p120 catenin associates with kinesin and facilitates the transport of cadherin-catenin complexes to intercellular junctions. *J. Cell Biol.* **163**, 547-557.

Chen, Q., Nag, S. and Pollard, T. D. (2012). Formins filter modified actin subunits during processive elongation. *J. Struct. Biol.* **177**, 32-39.
Chennathukuzhi, V., Morales, C. R., El-Alfy, M. and Hecht, N. B. (2003). The kinesin KIF17b and RNA-binding protein TB-RBP transport specific cAMP-responsive element modulator-regulated mRNAs in male germ cells. *Proc. Natl. Acad. Sci. USA* **100**, 15566-15571.
Chu, P.-J., Rivera, J. F. and Arnold, D. B. (2006). A role for Kif17 in transport of Kv4.2. *J. Biol. Chem.* **281**, 365-373.
Citi, S., Guerrera, D., Spadaro, D. and Shah, J. (2014). Epithelial junctions and Rho family GTPases: the zonular signalosome. *Small GTPases* **5**, e973760.
Cook, T. A., Nagasaki, T. and Gundersen, G. G. (1998). Rho guanosine triphosphatase mediates the selective stabilization of microtubules induced by lysophosphatidic acid. *J. Cell Biol.* **141**, 175-185.
Dishinger, J. F., Kee, H. L., Jenkins, P. M., Fan, S., Hurd, T. W., Hammond, J. W., Truong, Y. N.-T., Margolis, B., Martens, J. R. and Verhey, K. J. (2010). Ciliary entry of the kinesin-2 motor KIF17 is regulated by importin-beta2 and RanGTP. *Nat. Cell Biol.* **12**, 703-710.
Efimov, A., Schiefermeier, N., Grigoriev, I., Ohi, R., Brown, M. C., Turner, C. E., Small, J. V. and Kaverina, I. (2008). Paxillin-dependent stimulation of microtubule catastrophes at focal adhesion sites. *J. Cell Sci.* **121**, 196-204.
Enomoto, T. (1996). Microtubule disruption induces the formation of actin stress fibers and focal adhesions in cultured cells: possible involvement of the rho signal cascade. *Cell Struct. Funct.* **21**, 317-326.
Espenel, C., Acharya, B. R. and Kreitzer, G. (2013). A biosensor of local kinesin activity reveals roles of PKC and EB1 in KIF17 activation. *J. Cell Biol.* **203**, 445-455.
Ezratty, E. J., Partridge, M. A. and Gundersen, G. G. (2005). Microtubule-induced focal adhesion disassembly is mediated by dynamin and focal adhesion kinase. *Nat. Cell Biol.* **7**, 581-590.
Fan, S., Whiteman, E. L., Hurd, T. W., McIntyre, J. C., Dishinger, J. F., Liu, C. J., Martens, J. R., Verhey, K. J., Sajjan, U. and Margolis, B. (2011). Induction of Ran GTP drives ciliogenesis. *Mol. Biol. Cell* **22**, 4539-4548.
Fukata, M. and Kaibuchi, K. (2001). Rho-family GTPases in cadherin-mediated cell–cell adhesion. *Nat. Rev. Mol. Cell Biol.* **2**, 887-897.
Guillot, C. and Lecuit, T. (2013). Mechanics of epithelial tissue homeostasis and morphogenesis. *Science* **340**, 1185-1189.
Gundersen, G. G. (2002a). Evolutionary conservation of microtubule-capture mechanisms. *Nat. Rev. Mol. Cell Biol.* **3**, 296-304.
Gundersen, G. G. (2002b). Microtubule capture: IQGAP and CLIP-170 expand the repertoire. *Curr. Biol.* **12**, R645-R647.
Gundersen, G. G., Kalnoski, M. H. and Bulinski, J. C. (1984). Distinct populations of microtubules: tyrosinated and nontyrosinated alpha tubulin are distributed differently in vivo. *Cell* **38**, 779-789.
Gundersen, G. G., Gomes, E. R. and Wen, Y. (2004). Cortical control of microtubule stability and polarization. *Curr. Opin. Cell Biol.* **16**, 106-112.
Hammond, J. W., Blasius, T. L., Soppina, V., Cai, D. and Verhey, K. J. (2010). Autoinhibition of the kinesin-2 motor KIF17 via dual intramolecular mechanisms. *J. Cell Biol.* **189**, 1013-1025.
Hunter, J. D. (2007). Matplotlib: a 2D graphics environment. *Comput. Sci. Eng.* **9**, 90-95.
Insinna, C., Pathak, N., Perkins, B., Drummond, I. and Besharse, J. C. (2008). The homodimeric kinesin, Kif17, is essential for vertebrate photoreceptor sensory outer segment development. *Dev. Biol.* **316**, 160-170.
Ivanov, A. I., McCall, I. C., Babbin, B., Samarin, S. N., Nusrat, A. and Parkos, C. A. (2006). Microtubules regulate disassembly of epithelial apical junctions. *BMC Cell Biol.* **7**, 12.
Jaulin, F. and Kreitzer, G. (2010). KIF17 stabilizes microtubules and contributes to epithelial morphogenesis by acting at MT plus ends with EB1 and APC. *J. Cell Biol.* **190**, 443-460.
Jaulin, F., Xue, X., Rodriguez-Boulan, E. and Kreitzer, G. (2007). Polarization-dependent selective transport to the apical membrane by KIF5B in MDCK cells. *Dev. Cell* **13**, 511-522.
Jenkins, P. M., Hurd, T. W., Zhang, L., McEwen, D. P., Brown, R. L., Margolis, B., Verhey, K. J. and Martens, J. R. (2006). Ciliary targeting of olfactory CNG channels requires the CNGB1b subunit and the kinesin-2 motor protein, KIF17. *Curr. Biol.* **16**, 1211-1216.
Kher, S. S., Struckhoff, A. P., Alberts, A. S. and Worthylake, R. A. (2014). A novel role for p115RhoGEF in regulation of epithelial plasticity. *PLoS ONE* **9**, e85409.
Kobielak, A., Pasolli, H. A. and Fuchs, E. (2004). Mammalian formin-1 participates in adherens junctions and polymerization of linear actin cables. *Nat. Cell Biol.* **6**, 21-30.
Kotaja, N., Macho, B. and Sassone-Corsi, P. (2005). Microtubule-independent and protein kinase A-mediated function of kinesin KIF17b controls the intracellular transport of activator of CREM in testis (ACT). *J. Biol. Chem.* **280**, 31739-31745.
Kotaja, N., Lin, H., Parvinen, M. and Sassone-Corsi, P. (2006). Interplay of PIWI/Argonaute protein MIWI and kinesin KIF17b in chromatoid bodies of male germ cells. *J. Cell Sci.* **119**, 2819-2825.
Kovacs, E. M., Goodwin, M., Ali, R. G., Paterson, A. D. and Yap, A. S. (2002). Cadherin-directed actin assembly: E-cadherin physically associates with the Arp2/3 complex to direct actin assembly in nascent adhesive contacts. *Curr. Biol.* **12**, 379-382.
Kovacs, E. M., Verma, S., Ali, R. G., Ratheesh, A., Hamilton, N. A., Akhmanova, A. and Yap, A. S. (2011). N-WASP regulates the epithelial junctional actin cytoskeleton through a non-canonical post-nucleation pathway. *Nat. Cell Biol.* **13**, 934-943.
Kraemer, A., Goodwin, M., Verma, S., Yap, A. S. and Ali, R. G. (2007). Rac is a dominant regulator of cadherin-directed actin assembly that is activated by adhesive ligation independently of Tiam1. *Am. J. Physiol. Cell Physiol.* **292**, C1061-C1069.
Kreitzer, G., Marmorstein, A., Okamoto, P., Vallee, R. and Rodriguez-Boulan, E. (2000). Kinesin and dynamin are required for post-Golgi transport of a plasma-membrane protein. *Nat. Cell Biol.* **2**, 125-127.
Krendel, M., Zenke, F. T. and Bokoch, G. M. (2002). Nucleotide exchange factor GEF-H1 mediates cross-talk between microtubules and the actin cytoskeleton. *Nat. Cell Biol.* **4**, 294-301.
Krylyshkina, O., Kaverina, I., Kranewitter, W., Steffen, W., Alonso, M. C., Cross, R. A. and Small, J. V. (2002). Modulation of substrate adhesion dynamics via microtubule targeting requires kinesin-1. *J. Cell Biol.* **156**, 349-360.
Lessard, J. L. (1988). Two monoclonal antibodies to actin: one muscle selective and one generally reactive. *Cell Motil. Cytoskeleton* **10**, 349-362.
Ligon, L. A. and Holzbaur, E. L. F. (2007). Microtubules tethered at epithelial cell junctions by dynein facilitate efficient junction assembly. *Traffic* **8**, 808-819.
Ligon, L. A., Karki, S., Tokito, M. and Holzbaur, E. L. F. (2001). Dynein binds to beta-catenin and may tether microtubules at adherens junctions. *Nat. Cell Biol.* **3**, 913-917.
Macho, B., Brancorsini, S., Fimia, G. M., Setou, M., Hirokawa, N. and Sassone-Corsi, P. (2002). CREM-dependent transcription in male germ cells controlled by a kinesin. *Science* **298**, 2388-2390.
Mack, N. A. and Georgiou, M. (2014). The interdependence of the Rho GTPases and apicobasal cell polarity. *Small GTPases* **5**, e973768.
Mary, S., Charrasse, S., Meriane, M., Comunale, F., Travo, P., Blangy, A. and Gauthier-Rouvière, C. (2002). Biogenesis of N-cadherin-dependent cell-cell contacts in living fibroblasts is a microtubule-dependent kinesin-driven mechanism. *Mol. Biol. Cell* **13**, 285-301.
Mège, R.-M., Gavard, J. and Lambert, M. (2006). Regulation of cell–cell junctions by the cytoskeleton. *Curr. Opin. Cell Biol.* **18**, 541-548.
Mikhailov, A. and Gundersen, G. G. (1998). Relationship between microtubule dynamics and lamellipodium formation revealed by direct imaging of microtubules in cells treated with nocodazole or taxol. *Cell Motil. Cytoskeleton* **41**, 325-340.
Moriyama, K., Iida, K. and Yahara, I. (1996). Phosphorylation of Ser-3 of cofilin regulates its essential function on actin. *Genes Cells* **1**, 73-86.
Nagae, S., Meng, W. and Takeichi, M. (2013). Non-centrosomal microtubules regulate F-actin organization through the suppression of GEF-H1 activity. *Genes Cells* **18**, 387-396.
Nagasaki, T., Liao, G. and Gundersen, G. G. (1994). Isolated plasma membranes induce the loss of oriented detyrosinated microtubules and other contact inhibition-like responses in migrating NRK cells. *J. Cell Sci.* **107**, 3413-3423.
Nakaya, Y., Sukowati, E. W., Wu, Y. and Sheng, G. (2008). RhoA and microtubule dynamics control cell–basement membrane interaction in EMT during gastrulation. *Nat. Cell Biol.* **10**, 765-775.
Nekrasova, O. E., Amargo, E. V., Smith, W. O., Chen, J., Kreitzer, G. E. and Green, K. J. (2011). Desmosomal cadherins utilize distinct kinesins for assembly into desmosomes. *J. Cell Biol.* **195**, 1185-1203.
Nolen, B. J., Tomasevic, N., Russell, A., Pierce, D. W., Jia, Z., McCormick, C. D., Hartman, J., Sakowicz, R. and Pollard, T. D. (2009). Characterization of two classes of small molecule inhibitors of Arp2/3 complex. *Nature* **460**, 1031-1034.
O'Brien, L. E., Yu, W., Tang, K., Jou, T.-S., Zegers, M. M. P. and Mostov, K. E. (2006). Morphological and biochemical analysis of Rac1 in three-dimensional epithelial cell cultures. *Methods Enzymol.* **406**, 676-691.
Otani, T., Ichii, T., Aono, S. and Takeichi, M. (2006). Cdc42 GEF Tuba regulates the junctional configuration of simple epithelial cells. *J. Cell Biol.* **175**, 135-146.
Ou, G., Blacque, O. E., Snow, J. J., Leroux, M. R. and Scholey, J. M. (2005). Functional coordination of intraflagellar transport motors. *Nature* **436**, 583-587.
Palazzo, A. F., Cook, T. A., Alberts, A. S. and Gundersen, G. G. (2001). mDia mediates Rho-regulated formation and orientation of stable microtubules. *Nat. Cell Biol.* **3**, 723-729.
Pan, X., Ou, G., Civelekoglu-Scholey, G., Blacque, O. E., Endres, N. F., Tao, L., Mogilner, A., Leroux, M. R., Vale, R. D. and Scholey, J. M. (2006). Mechanism of transport of IFT particles in C. elegans cilia by the concerted action of kinesin-II and OSM-3 motors. *J. Cell Biol.* **174**, 1035-1045.
Portereiko, M. F., Saam, J. and Mango, S. E. (2004). ZEN-4/MKLP1 is required to polarize the foregut epithelium. *Curr. Biol.* **14**, 932-941.
Quiros, M. and Nusrat, A. (2014). RhoGTPases, actomyosin signaling and regulation of the Epithelial Apical Junctional Complex. *Semin. Cell Dev. Biol.* **36**, 194-203.
Ratheesh, A., Gomez, G. A., Priya, R., Verma, S., Kovacs, E. M., Jiang, K., Brown, N. H., Akhmanova, A., Stehbens, S. J. and Yap, A. S. (2012). Centralspindlin and alpha-catenin regulate Rho signalling at the epithelial zonula adherens. *Nat. Cell Biol.* **14**, 818-828.

Ren, Y., Li, R., Zheng, Y. and Busch, H. (1998). Cloning and characterization of GEF-H1, a microtubule-associated guanine nucleotide exchange factor for Rac and Rho GTPases. *J. Biol. Chem.* **273**, 34954-34960.
Riento, K. and Ridley, A. J. (2003). Rocks: multifunctional kinases in cell behaviour. *Nat. Rev. Mol. Cell Biol.* **4**, 446-456.
Saade, M., Irla, M., Govin, J., Victorero, G., Samson, M. and Nguyen, C. (2007). Dynamic distribution of Spatial during mouse spermatogenesis and its interaction with the kinesin KIF17b. *Exp. Cell Res.* **313**, 614-626.
Salvarezza, S. B., Deborde, S., Schreiner, R., Campagne, F., Kessels, M. M., Qualmann, B., Caceres, A., Kreitzer, G. and Rodriguez-Boulan, E. (2009). LIM kinase 1 and cofilin regulate actin filament population required for dynamin-dependent apical carrier fission from the trans-Golgi network. *Mol. Biol. Cell* **20**, 438-451.
Samarin, S. and Nusrat, A. (2009). Regulation of epithelial apical junctional complex by Rho family GTPases. *Front. Biosci.* **14**, 1129-1142.
Schindelin, J., Arganda-Carreras, I., Frise, E., Kaynig, V., Longair, M., Pietzsch, T., Preibisch, S., Rueden, C., Saalfeld, S., Schmid, B. et al. (2012). Fiji: an open-source platform for biological-image analysis. *Nat. Methods* **9**, 676-682.
Setou, M., Nakagawa, T., Seog, D. H. and Hirokawa, N. (2000). Kinesin superfamily motor protein KIF17 and mLin-10 in NMDA receptor-containing vesicle transport. *Science* **288**, 1796-1802.
Siegrist, S. E. and Doe, C. Q. (2007). Microtubule-induced cortical cell polarity. *Genes Dev.* **21**, 483-496.
Snow, J. J., Ou, G., Gunnarson, A. L., Walker, M. R. S., Zhou, H. M., Brust-Mascher, I. and Scholey, J. M. (2004). Two anterograde intraflagellar transport motors cooperate to build sensory cilia on C. elegans neurons. *Nat. Cell Biol.* **6**, 1109-1113.
Stehbens, S. J., Paterson, A. D., Crampton, M. S., Shewan, A. M., Ferguson, C., Akhmanova, A., Parton, R. G. and Yap, A. S. (2006). Dynamic microtubules regulate the local concentration of E-cadherin at cell-cell contacts. *J. Cell Sci.* **119**, 1801-1811.
Takano, K., Miki, T., Katahira, J. and Yoneda, Y. (2007). NXF2 is involved in cytoplasmic mRNA dynamics through interactions with motor proteins. *Nucleic Acids Res.* **35**, 2513-2521.
Tang, V. W. and Brieher, W. M. (2012). alpha-Actinin-4/FSGS1 is required for Arp2/3-dependent actin assembly at the adherens junction. *J. Cell Biol.* **196**, 115-130.
Tatebe, H., Nakano, K., Maximo, R. and Shiozaki, K. (2008). Pom1 DYRK regulates localization of the Rga4 GAP to ensure bipolar activation of Cdc42 in fission yeast. *Curr. Biol.* **18**, 322-330.
van der Walt, S., Schönberger, J. L., Nunez-Iglesias, J., Boulogne, F., Warner, J. D., Yager, N., Gouillart, E. and Yu, T. (2014). scikit-image: image processing in Python. *PeerJ.* **2**, e453.
Verma, S., Han, S. P., Michael, M., Gomez, G. A., Yang, Z., Teasdale, R. D., Ratheesh, A., Kovacs, E. M., Ali, R. G. and Yap, A. S. (2012). A WAVE2-Arp2/3 actin nucleator apparatus supports junctional tension at the epithelial zonula adherens. *Mol. Biol. Cell* **23**, 4601-4610.
Watanabe, T., Wang, S., Noritake, J., Sato, K., Fukata, M., Takefuji, M., Nakagawa, M., Izumi, N., Akiyama, T. and Kaibuchi, K. (2004). Interaction with IQGAP1 links APC to Rac1, Cdc42, and actin filaments during cell polarization and migration. *Dev. Cell* **7**, 871-883.
Waterman-Storer, C. M., Salmon, W. C. and Salmon, E. D. (2000). Feedback interactions between cell-cell adherens junctions and cytoskeletal dynamics in newt lung epithelial cells. *Mol. Biol. Cell* **11**, 2471-2483.
Wen, Y., Eng, C. H., Schmoranzer, J., Cabrera-Poch, N., Morris, E. J. S., Chen, M., Wallar, B. J., Alberts, A. S. and Gundersen, G. G. (2004). EB1 and APC bind to mDia to stabilize microtubules downstream of Rho and promote cell migration. *Nat. Cell Biol.* **6**, 820-830.
Wojnacki, J., Quassollo, G., Marzolo, M.-P. and Cáceres, A. (2014). Rho GTPases at the crossroad of signaling networks in mammals: impact of Rho-GTPases on microtubule organization and dynamics. *Small GTPases* **5**, e28430.
Yamada, S., Pokutta, S., Drees, F., Weis, W. I. and Nelson, W. J. (2005). Deconstructing the cadherin-catenin-actin complex. *Cell* **123**, 889-901.
Yamamoto, H., Imai, K., Kamegaya, E., Takamatsu, Y., Irago, M., Hagino, Y., Kasai, S., Shimada, K., Yamamoto, T., Sora, I. et al. (2006). Repeated methamphetamine administration alters expression of the NMDA receptor channel epsilon2 subunit and kinesins in the mouse brain. *Ann. N. Y. Acad. Sci.* **1074**, 97-103.
Yanagisawa, M., Kaverina, I. N., Wang, A., Fujita, Y., Reynolds, A. B. and Anastasiadis, P. Z. (2004). A novel interaction between kinesin and p120 modulates p120 localization and function. *J. Biol. Chem.* **279**, 9512-9521.
Yang, N., Higuchi, O., Ohashi, K., Nagata, K., Wada, A., Kangawa, K., Nishida, E. and Mizuno, K. (1998). Cofilin phosphorylation by LIM-kinase 1 and its role in Rac-mediated actin reorganization. *Nature* **393**, 809-812.
Yoshimura, Y. and Miki, H. (2011). Dynamic regulation of GEF-H1 localization at microtubules by Par1b/MARK2. *Biochem. Biophys. Res. Commun.* **408**, 322-328.

ROCK inhibition triggers the collective invasion of colorectal carcinomas through the Guanine Exchange factor FARP2

Foreword

This second part of my results chapter constitutes my main PhD work, which is ready for submission and future publication.

The aim of this work was to determine the contribution of Rho-GTPases dependent signaling pathways to the collective invasion of CRC. To conduct this work, I used 3D organotypic models of non-invasive CRC generated from cell lines or from patient-derived xenografts (PDX) : Caco-2 cyst and organoids repectively. We performed invasion assays in collagen matrices. To identify candidates to the regulation of CRC invasion, we performed two siRNA screens targeting Rho-GTPases effectors and exchange factors (GEFs).

ROCK2 inhibition triggers the collective invasion of colorectal carcinomas through the Guanine Nucleotide Exchange Factor FARP2

Libanje Fotine[1], Raingeaud Joel[1], Ap Thomas Zoé[1], Zajac Olivier[1,*], Veiga Joel[2,#], Diane Goéré[3], Hall Alan[2], Soazec Jean-Yves[4], Dartigues Peggy[4], and Jaulin Fanny[1]

[1] INSERM U-981, Gustave Roussy, Villejuif, F-94805, France

[2] Cell Biology Program, Memorial Sloan-Kettering Cancer Center, New York, NY 10065

[3] Digestive Cancer Unit, Gustave Roussy, Villejuif, F-94805, France

[4]Pathology Department, Gustave Roussy, Villejuif, F-94805, France

[*] Current address: Department of Translational Research, Curie Institute, Paris, F-75005, France

[#] Current Address: Imagine Institute, Paris, F-75015, France

Correspondence should be addressed to FJ, fanny.jaulin@gustaveroussy.fr

The authors have declared that no conflict of interest exists

Final character count: 84600

Abstract

The metastatic progression of cancer is a multi-step process initiated by invasion of the peritumoral stroma. In this study, we aimed at identifying the molecular and cellular mechanisms underlying colorectal carcinoma (CRC) invasion. Our analysis of fixed and live human primary cancer specimens revealed that CRCs retain their epithelial glandular architecture while undergoing collective invasion. To investigate the signaling pathways regulating CRC collective invasion, we used microscopy-based analyses on 3D organotypic models, Caco-2 cysts and organoids generated from Patient Derived Xenografts. We performed two siRNA screens targeting Rho-GTPases effectors and guanine nucleotide exchange factors (GEFs) to identify the essential players in CRC invasion. The first screen revealed that ROCK2 inhibition triggers the initial leader/follower polarization of the CRC cell cohorts, inducing collective invasion under chemokine gradient. We further demonstrate that ROCK2 inhibition induces Rac1 activation. Seeking for the GEF mediating this effect, we carried a second screen and identified FARP2 as the Rac1 GEF necessary for CRC collective invasion. However, FARP2 overexpression alone is not sufficient to trigger leader cell formation whereas the concomitant inhibition of Myosin-II induces collective invasion through leader formation.. Thus, we show that the ROCK/Rac1 balance controls the early step of CRC collective invasion and identified FARP2 as a new regulator of this crosstalk. In these highly polarized CRC glands, ROCK activity suppresses collective invasion, contrasting with its pro-invasive function in other models of cancers. The contribution of ROCK to metastatic spread likely depends on tumour types and invasion mode, it is therefore important to question the benefit of therapeutic strategies aiming at delivering ROCK inhibitors to cancer patients.

INTRODUCTION

With 90% of cancer patients succumbing from their metastases, there is a pressing need to understand the mechanisms of cancer cell dissemination (Ferlay et al., 2015). The acquisition of invasive properties triggers the transition from *in situ* to invasive tumours, and is therefore a crucial step in the metastatic progression of cancers.

Cancer cell invasion has long been considered as a single cell process (Valastyan and Weinberg, 2011). These single cells originate from leukemia or loosely organized tissues such as sarcomas, as well as from highly cohesive carcinomas that have undergone an epithelial-to-mesenchymal transition (EMT) (Friedl and Alexander, 2011; Nieto et al., 2016). Mechanistically, there are two modes of single cell invasion relying on distinct requirement for adhesion, proteolysis of the extracellular matrice (ECM) and F-actin dynamic (Friedl, 2004; Wolf et al., 2003). As central regulators of the cytoskeleton, the small GTPases of the Rho family play important functions in all mode of cell migration (Ridley, 2015). The mesenchymal mode of invasion is a traction-based locomotion relying on integrin/ECM interaction and Rac1-dependent polymerization of branched actin at the protrusive leading edge. At the rear, RhoA/ROCK/Myosin signaling is necessary for the cell retraction but do not directly contribute to the forward force generation (Ridley et al., 2003). In contrast, cell undergoing amoeboid migration use propulsive forces to squeeze between the fibers of 3D environments. The locomotion relies on the friction forces generated by myosin contractility and F-actin retrograde flow while integrin adhesion and ECM proteolysis are negligible (Liu et al., 2015; Orgaz et al., 2014; Paluch and Raz, 2013). As an adaptive response to their environment and/or the balance between endogenous RhoA and Rac1 activities, single cell can switch between mesenchymal and amoeboid invasion (Liu et al., 2015; Sahai and Marshall, 2003; Sanz-Moreno et al., 2008; Wolf et al., 2003). Guanine Nucleotide Exchange Factors (GEFs) and GTPase activating proteins (GAPs) control the spatiotemporal activation

of Rho-GTPases and as such are crucial to migration and plasticity. In melanoma cell lines, DOCK3 and ARHGAP22 control the antagonistic activation of ROCK and Rac1 and therefore govern invasion mode (Sanz-Moreno et al., 2008). The identity of the proteins balancing the activation of Rac1 and RhoA varies with cell types, and among the hundreds of genes encoding GAPs and GEFs, many of them have been shown to participate in invasion (Even-Ram et al., 2007; Ohta et al., 2006; Tsuji et al., 2002).

Cohesive cancer cell clusters can also invade 3D environments. The first observation of collective invasion was made from primary tumour explants over 20 years ago (Friedl et al., 1995). Since then, this process has been confirmed by intravital microscopy in mice xenografts and corroborated by pathologists (Alexander et al., 2008; Friedl, 2004; Giampieri et al., 2009; Prall et al., 2009). Yet, the cellular and molecular mechanisms underlying the collective invasion of neoplastic tissues have been poorly investigated and most of our knowledge is based on the collective migration driving the embryonic development of model organisms. In the multicellular unit, the front-rear polarization of the cohort translates into distinct cells, the leaders and the followers, cooperating to tract the collective (Haas and Gilmour, 2006; Wang et al., 2010). The leaders, protrusive cells at the front, respond to extracellular guiding cues and adhere to the matrix to generate traction forces. They are either defined by their closest position relative to the chemokine gradient (such as in drosophila border cells or mammalian vascular sprouting (Duchek et al., 2001) or by the expression of a transcriptional program pre-existing to the migration process such as in the migration of the Zebrafish lateral line (Aman and Piotrowski, 2008; Haas and Gilmour, 2006). The leader cell fate is also predetermined in the migrating cohort of breast and lung cancer cells (Cheung et al., 2013; Konen et al., 2017; Westcott et al., 2015). In border cells, the activation of Rac1 is sufficient to generate leaders and, through E-cadherin dependent mechanotransduction, to drive the movement of the cluster (Cai et al., 2014; Wang et al., 2010). These results have

been confirmed in mouse embryo where Rac1 activation downstream of the GEF β-Pix controls the collective migration of antero-visceral endoderm cells (Migeotte et al., 2010; Omelchenko et al., 2014). However, most studies tracking Rho-GTPases activation within collectives comes from the migration of cell monolayers *in vitro* on stiff 2D substrates. In addition to β-Pix, the GEFs Tiam-1 and DOCK180 were shown to polarize and restrict Rac1 and Cdc42 activation to the leading edge of wounded monolayers (Bianco et al., 2007; Ellenbroek et al., 2012; Osmani et al., 2006, 2010; Yamaguchi et al., 2015). As in single cells, RhoA activity antagonizes Rac1 and should be down-regulated to allow the formation of protrusive leaders (Omelchenko et al., 2014; Reffay et al., 2014). The level of RhoA-GTP must also be tightly controlled at cell-cell contact between followers, through the GAP Myosin IXA or the GEFs ECT2 and ARHGEF18 in order to relax the junctions while maintaining de the communication and the cohesion of the group during the migration (Omelchenko and Hall, 2012; Zaritsky et al., 2017).

Rac1 and RhoA have an essential role in the regulation of collective locomotion. However, the regulatory elements controlling their activation during the collective invasion of neoplastic cells into 3D environments remain poorly characterized. In this study, we investigated how Rho-GTPases effectors and their activators, the GEFs, regulate the collective invasion of colorectal carcinoma (CRC), the second leading cause of cancer-related death.

RESULTATS

Colorectal carcinomas undergo collective invasion

To determine the mode of invasion contributing to CRC dissemination, we analyzed 10 Formalin-Fixed Parafin Embeded (FFPE) surgical specimens of human primary tumours that have invaded the submucosa (tumour stages pT1 and pT2, see Fig. 1Ai for a representative

example). These invasive CRCs were immunostained using antibodies against E-cadherin (E-cadh) and vimentin (Vim). Both markers were expressed in all the specimens. E-cadherin localized at cell-cell contact of normal and transformed epithelial cell sheets (Fig. 1A). This staining highlighted the epithelial organization of the neoplastic tissue, including the invasive front, with cohesive cancer cells surrounding a small luminal space (Fig. 1Ai arrowheads, 1Aii and 1Aiii). Between the neoplastic glands, the stromal cells display a robust vimentin (Vim(+)) staining. Although we do not exclude that some Vim(+) cells could be CRC cells that have completely lost E-cadherin expression and localize among the normal stromal cells, most of the tumour is organized as a cohesive tissue with E-cadherin-based junctions. The glandular architecture of the tumour suggested that CRC cells may have maintained their apico-basolateral polarity in the course of invasion. In support to this, immunostaining revealed the polarized localization of the apical marker villin at the plasma membrane facing the luminal cavity of normal and transformed epithelial glands (Fig. 1B, arrowheads). The cell-cell adhesion molecule EpCam is excluded from the apical membrane and rather localize at the basolateral compartment in contact with adjacent cancer cells and stromal cells (Fig. 1B). Therefore, the staining of fixed human cancer specimens shows that most of the invasive tumour cells maintain their cohesion and epithelial identity, preferentially organizing in glandular structures in the peritumoral stroma.

To investigate whether CRC undergo collective invasion, we used videomicroscopy to monitor live tumour specimens from metastatic patients. We collected peritoneal effusions from CRC patients with peritoneal metastases during cytoreductive surgery (Elias et al., 2009). Tumour cell clusters were pull-downed by centrifugation as previously described, immediately embedded into collagen-I gels and monitored for up to 6 days (Zajac et al, Nature Cell Biology, in Press). Timelapse imaging revealed that tumour cell clusters expressing the CRC markers EpCam and CK20 were highly invasive. These clusters

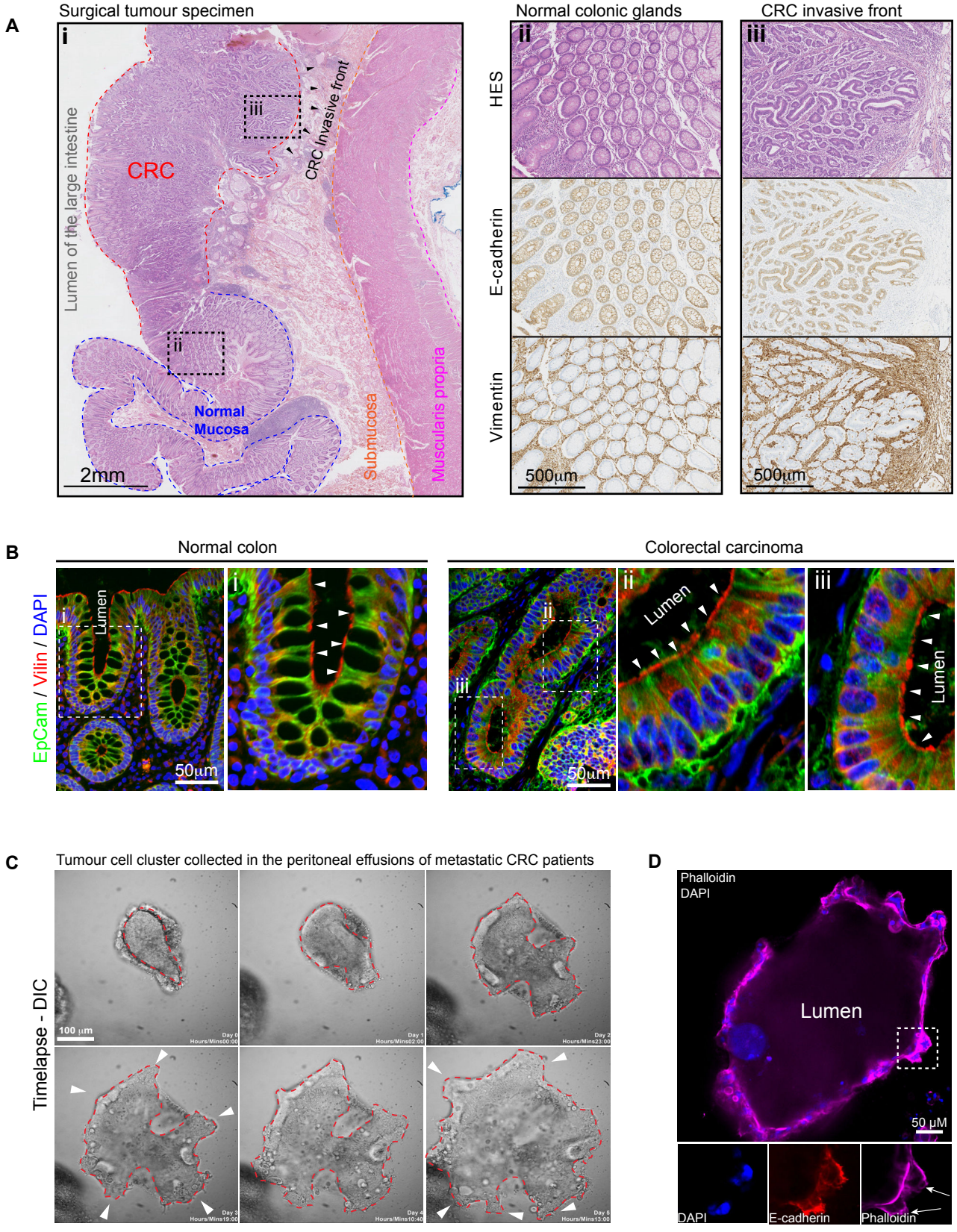

Figure 1. Colorectal carcinomas (CRC) undergo collective invasion

A) Representative specimen of colorectal (CRC) primary tumor stained with i) haematoxylin/eosin/saffron (HES), or antibodies against E-cadherin or Vimentin. i) The blue, orange and pink dotted lines highlight the normal mucosa, the submucosa and the muscularis propria. Red dotted line highlights the colorectal carcinoma (CRC). Black arrowheads indicate the direction of invasion. Boxed regions ii and iii show high magnification of (ii) normal colonic (ii) glands and the CRC invasive front (iii). Scale bar: 2 mm and 500 µm. (B) Representative images of histological sections of normal colon and primary CRC tumor stained for EpCam and Villin. Boxed regions i, ii and iii are high magnifications of the luminal cavity of normal colonic gland (i) and colorectal carcinoma glands (ii and iii). White arrows point to the apical pole enriched in villin. Scale bars: 50 µm. (C) Time lapse sequences of tumor specimen collected from peritoneal effusion of metastatic CRC patients and embedded into collagen-I gels. The red dotted line highlights the tumor cluster's periphery. White arrows point to the invasive pole. Time is displayed as day and hh:mm. Scale bars: 100 µm. (D) Patient primary tumor specimen stained for F-actin (Phalloidin), E-cadherin and nuclei (DAPI) after 6 days of culture in collagen-I. Boxed region shows high magnification of a protruding invasive pole, white arrows point to actin rich protrusions. Scale bar: 50 µm

displayed the hallmarks of collective invasion, i.e. cell-cell contacts and protruding leader cells driving the invasive front (arrows). We did not observe the detachment of single cells (Fig 1C, Video1, Supp. Fig 1A and not shown). Immunostaining after fixation revealed two patterns of collective invasion: solid tumour cell masses (Supp. Fig. 1A) and hollow cysts harboring a layer of neoplastic cells surrounding a central lumen (Fig. 1D).

Together, the results we obtained from the analyses of fixed and live human primary cancer specimens revealed that CRCs use collective invasion during their metastatic dissemination. As neoplastic cells maintain their apico-basolateral polarity, their collective invasion occurs in the form of invasive glands.

To investigate the mechanisms regulating the transition from *in situ* to collectively invasive CRCs, we first sought an *in vitro* model system. We grew the CRC line Caco-2 in tridimensional (3D) gel made of extracellular matrices (ECM). Immunostaining for the apical marker prominin-1 and actin revealed that Caco-2 organized as cysts formed by a polarized monolayer surrounding a single central lumen, as seen in patients' specimens. Moreover, Caco-2 cysts harbor a smooth periphery due to the absence of protruding cell, demonstrating they do not possess spontaneous invasive properties (Fig.2A, left panel). As such, Caco-2 grown in 3D matrices represent a pertinent organotypic model of non-invasive CRC neoplastic glands for gain-of-function studies.

ROCK inhibition triggers collective invasion from CRC organotypic models

In order to identify the signaling pathways regulating CRC collective invasion we performed a siRNA-based screen in Caco-2 cysts. Since RhoGTPases are central to all modes of cell motility, we hypothesized they would also regulate CRC collective invasion. We transfected Caco-2 using a siRNA library targeting the 98 known human effectors of RhoGTPases.

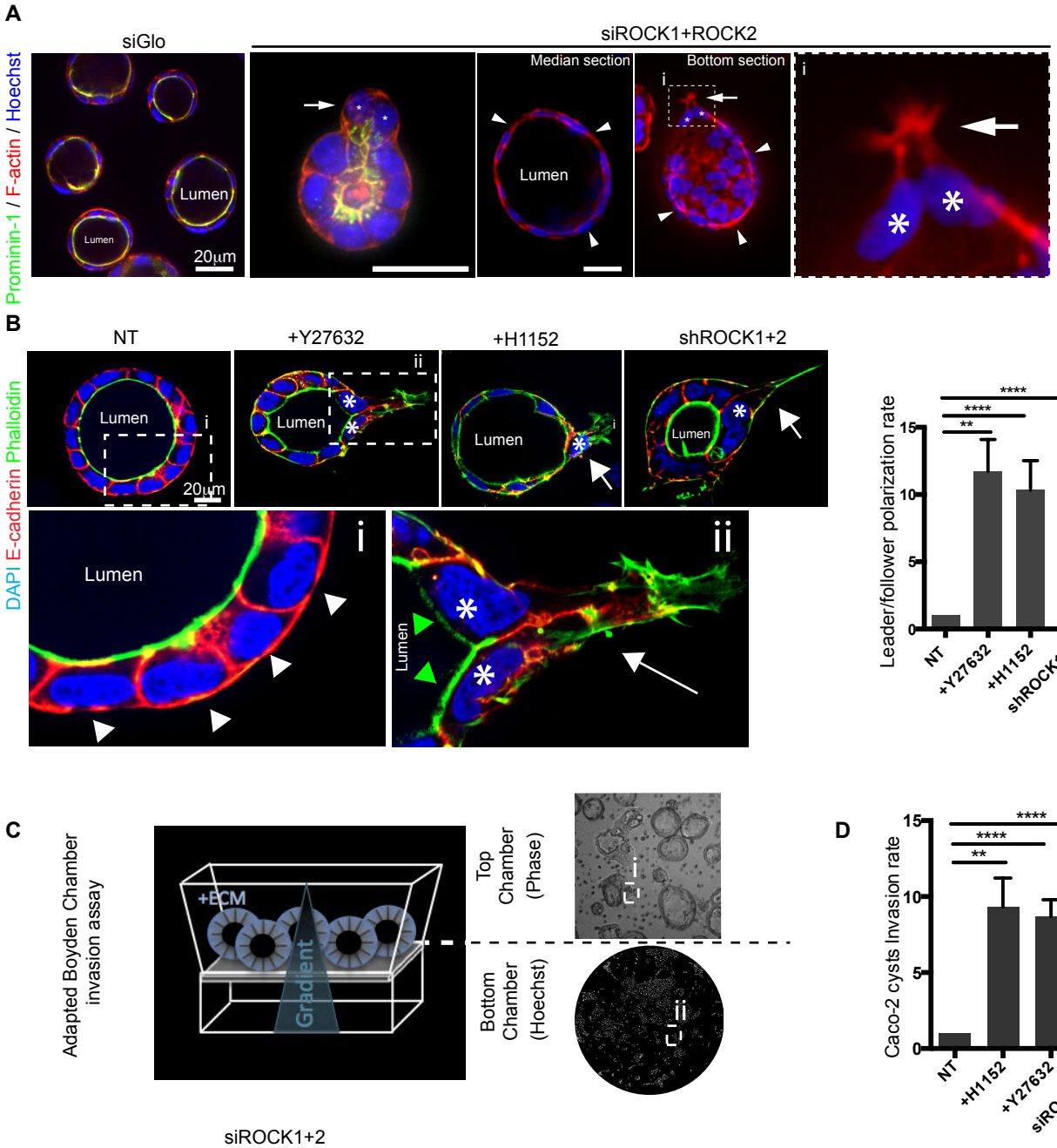

Figure 2: ROCK inhibition induces the collective invasion of CRC model Caco-2 cysts

(A) Representative images of Caco-2 cysts transfected with control siRNA (siGlo) or siRNAs targeting ROCK1 and ROCK2, fixed and stained for prominin-1, F-actin (Phalloidin) and Nuclei (Hoechst). Confocal Z-sections of cysts are displayed. Arrowheads show non-protruding cells. Arrows point to protruding cells. White stars mark nuclei that are off-centered relative to the cyst's monolayer of cells. Scale bars: 20 µm. (B) Left panel, representative confocal images of Caco-2 cysts treated with ROCK inhibitors Y27632 and H1152, non-treated (NT) or transduced with shRNA ROCK1 and shRNA ROCK2 (shROCK1+2). The cysts were fixed 2 days after invasion and stained for E-cadherin, F-actin (Phalloidin) and nuclei (DAPI). Boxed regions i and ii are displayed at high magnification. White arrowheads point to non-protruding cells, green arrowheads point to the apical pole, arrows point to protruding cells and white stars show off-centered nucleus. Right panel, The percentage of leader/follower polarized cysts was normalized to control condition and represented on a bar graph as a result of three independent experiments and the error bar represents the Standard Error of the Mean (Means ± SEM). P values were calculated using unpaired t-test (****p<0.0001, ***p<0.001, **p<0.01). (C) Left panel, schematic representation of the 3D Boyden chamber invasion assay. The Caco-2 were grown as cysts in 3D matrigel on the top chamber of the Boyden for 3 days, then the serum gradient was induced. 2 days after, the nuclei of the cells that have reached the bottom side of the membrane were stained with Hoechst and quantified by automated acquisition and segmentation. Right panel, DIC image of the membrane facing the top chamber reveals the cysts and the immunofluorescence image of the membrane facing the bottom chamber stained with Hoechst reveals the cells that have invaded. (D) The number of cells that have invaded from the top to the bottom chamber of the Boyden chamber were quantified by automated segmentation in non-treated (NT), in ROCK inhibited conditions (Y27632, H1152) or in cells transfected with siRNA against ROCK1 and ROCK2 (siROCK1+2). The number of cells that have invaded were normalized to control conditions and reported as the average invasion rate from at least three independent experiments (Means ± SEM). P values were calculated using unpaired t-test (****p<0.0001, ***p<0.001, **p<0.01). (E) i and ii are higher magnification of boxed region of (C) the top(i) and the bottom(ii) side of the Boyden chamber membrane were stained for F-actin, E-cadherin, ZO-1, Ezrin and Hoechst. Arrows point to the protrusive cells of an invasive cyst and the white stars show the nuclei that engage in the protrusion. Scale bars: 40 µm

Accounting for functional redundancy between homologs, we co-depleted the closest pair of RhoGTPases effectors (Supp Table1). We verified that the co-transfection of two siRNAs do not alter the depletion of each protein (data not shown). This screen yielded only one hit: Caco-2 cysts co-depleted for ROCK1 and ROCK2 displayed a supracellular polarization: a subset of protruding cells, usually two neighbors, get off-centered but remained attached to the cyst (Fig. 2A, middle panel, arrows). The nuclei were engaged into the protrusion, loosing the alignment with the monolayer (Fig. 2A, stars). In a validation round, Z-stacks acquisition of Caco-2 cysts transfected with siROCKs further demonstrated that the bulging cells formed actin-rich protrusions toward the ECM gel (Fig.2A right panel, arrow) while the rest of the cohort do not protrude (Fig.2A right panel, arrowheads). This supra-cellular polarization of Caco-2 cysts is reminiscent of the leader/follower organization associated with the front-rear polarity of invasive collectives (Haas and Gilmour, 2006). To confirm this result and exclude an off-target effect of the siRNAs, we used alternative reagents. First, we transduced Caco-2 cysts using shRNAs against ROCK1 and ROCK2. This induced a 11,7±2,4 fold increase in the number of cysts with protruding cells, demonstrating that the phenotype was specific to ROCK depletion (Fig. 2B). We then used pharmacological inhibitors Y27632 and H1152 to determine whether ROCK kinase activity was sufficient to control this phenotype. Treatment with Y27632 and H1152 respectively increased by 11,7±2,4 fold and 10,3±2,2 fold the number of protruding cysts as compared to untreated controls (Fig. 2B). Using live imaging, we confirmed that the “leader/follower” polarization of Caco-2 cysts treated with ROCK inhibitors Y27632 and H1152 resulted from the neoformation of protrusions (Supp Fig. 1B). E-cadherin staining confirmed that all cells of the cohort remained cohesive and that the luminal cavity is conserved (Fig.2B). Hence inhibiting ROCK kinase activity is sufficient to induce the formation of Caco-2 cysts harboring the features of collective invasion.

To determine whether the “leader/follower” polarization of protruding Caco-2 cysts efficiently translate into invasion, we adapted the Boyden chamber to 3D organotypic cultures. The membrane was coated with matrigel and Caco-2 cells were grown as cysts in 3D gels in the top chamber. To allow chemotactism, a serum gradient was established from the bottom chamber (Fig. 2C). In this new assay, we evaluated the ability of Caco-2 cells to invade from the top to the bottom chamber of the transwell. The number of cells that have invaded was analyzed by automated segmentation and quantification 3 days after induction of the serum gradient**.** As expected for a non-invasive CRC model, very few cells reach the bottom chamber in control condition. In contrast, treatment with Y27632 and H1152 or transfection of siROCK1 and siROCK2 increased by 9,3±1,9, 8,7±1,1 and 8,5±2,7 fold respectively the number of cells reaching the bottom chamber **(**Fig. 2D). Immunostaining of the top and bottom side of the membrane using antibodies against E-cadherin, ZO-1 and Ezrin demonstrate that Caco-2 cells remain cohesive in both compartments and we did not notice the presence of individual cells (Fig. 2E). In support to this, we did not detect any change in the expression level of epithelial (E-cadherin and Keratins) and mesenchymal (N-cadherin and Vimentin) markers, showing that the acquisition of the invasive phenotype occurs independently of the activation of an EMT program (Sup. Fig. 1C). Thus, ROCK inhibition triggers collective invasion from Caco-2 cysts.

To confirm that ROCK has a broad function in the control of CRC invasion we turned to organoids, a more physiological model of CRC. We used organoids made from CRC patient derived xenograft (PDX). We selected PDX that do not display spontaneous invasion profile. When embedded into collagen-I gels the organoids form glandular structures characterized by cohesive cells (highlighted by E-cadherin staining) and apico-basolateral polarity (highlighted by the central lumen, Fig. 3A) as previously described (Sato and Clevers, 2013). Treatment with ROCK inhibitors Y27632 and H1152 triggered the appearance of protrusive cells and

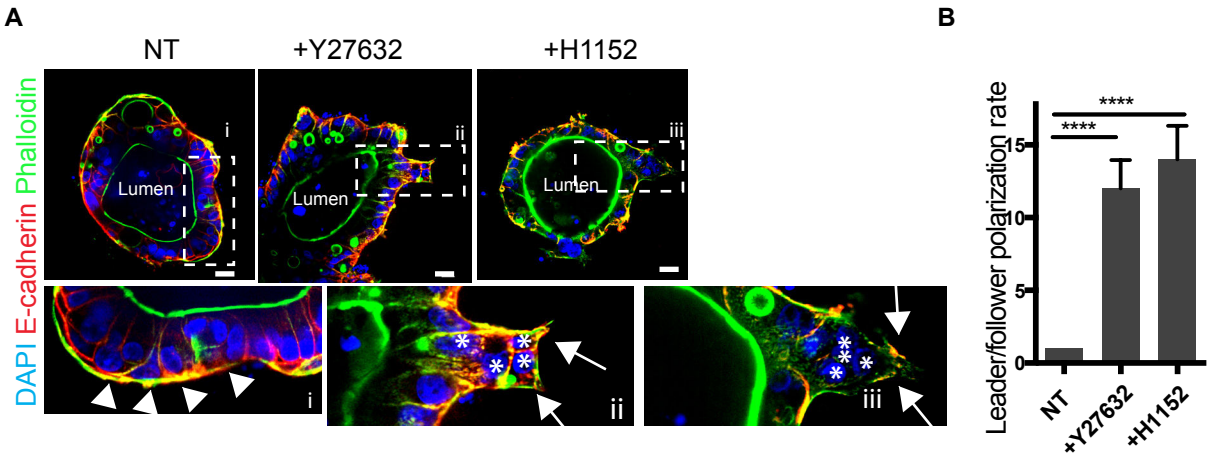

Figure 3: ROCK inhibition promotes the collective invasion of CRC tumoroids
(A) Representative images of tumoroids formed from patient derived xenografts (PDX) that have undergone 3-day invasion assay, in non-treated (NT) or ROCK inhibitors treated-conditions (+Y27632) and (+H1152) and were stained for E-cadherin, F-actin (Phalloidin) and nuclei (DAPI). i, ii, and iii are higher magnification of boxed regions of NT, +Y27632, and +H1152 tumoroids respectively. Arrowheads point to non-protruding cells. Arrows point to protruding cells. White stars show nuclei that engage in protrusions. Scale bars: 20µm. (B) Over 50 tumoroids were counted per condition, tumoroids displaying protrusive cells remaining attached to the tumoroid were considered as leader/Follower polarized. The bar graph represents the average polarization rate normalized to control conditions resulting from three independent experiments (Means ± SEM). P values were calculated using unpaired t-test (****p<0.0001). Scale bars: 20 µm

increased by 12±2 fold and 14±2,3 fold respectively the number of invading organoids (Fig. 3B).

Altogether our results demonstrate that the inhibition of ROCK activity triggers the supra-cellular polarization of CRC models into leader and follower cells and induces their collective invasion.

ROCK2 inhibition is sufficient to induce collective invasion

To differentiate the respective contribution of ROCK1 and ROCK2, we transduced Caco-2 cysts using shRNA targeting either ROCK1 or ROCK2 and assessed for invasion (Fig. 4A). Caco-2 cysts depleted for ROCK1 did not significantly invade when compared to controls. In contrast, depletion of ROCK2 increased the number of invasive cysts by 10,6±2,8 fold, comparable to the co-depletion of both kinases and the treatment with Y27632 (Fig. 4B). To investigate the role of ROCK2 kinase activity in collective invasion, we generated dominant negative mutants (DN), ROCK2DN#1 and ROCK2DN#2, as previously described by the Kaïbuchi lab (Amano et al., 1999)**(**Fig. 4C**)**. They correspond to the carboxy-terminal region of ROCK2 which includes the Rho binding (RB) and the Plekstrin homology (PH) domains. The ROCK2DN#2 harbor a point mutation in the RB domain to prevent interaction with RhoA-GTP. Both constructs are predicted to bind ROCK2 catalytic domain, thereby competing with its substrates. To confirm that, in our Caco-2 cells, the DN constructs interact with ROCK2, but not ROCK1, we tested their ability to interact with endogenous ROCK proteins. Caco-2 cells were transfected with GFP-tagged ROCK2 DN constructs and protein complexes were immunoprecipitated using GFP trap® beads. Western blot revealed that GFP-ROCK2DNs interact with endogenous ROCK2, but not ROCK1 (Fig. 4D). When stably expressed in Caco-2 cells, ROCK2DN#1 perturbed Caco-2 cysts morphogenesis, a phenotype likely due to the titration of RhoA-GTP (Supp. Fig. 2A). In support to this, mutation of the

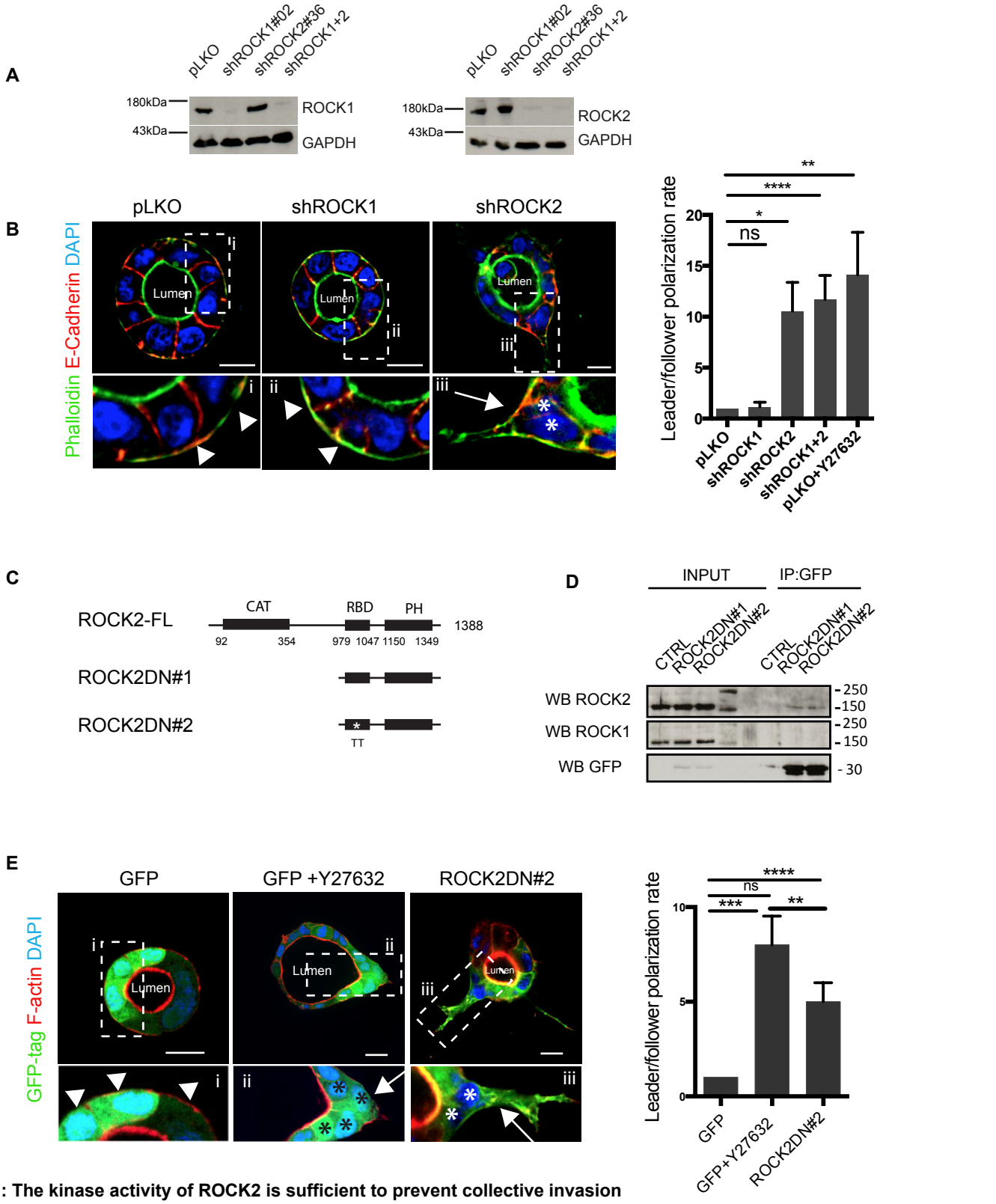

Figure 4 : The kinase activity of ROCK2 is sufficient to prevent collective invasion

A) Representative immunoblot analysis of Caco-2 cells transduced with an empty vector (pLKO) shROCK1 (shROCK1#02) or shROCK2 (shROCK2#36) or both (shROCK1+2), with an anti-ROCK1 and anti-ROCK2 antibodies. GAPDH was used as a loading control. Representative of three independent experiments. (B) Left panel Caco-2 cysts expressing an empty vector (pLKO) or shRNA ROCK1 (shROCK1#02) or shRNA ROCK2 (shROCK2#36) or both (shROCK1+2) after 2 days of invasion were fixed and stained for E-cadherin, F-actin (Phalloidin) and nuclei (DAPI). i,ii, and iii are higher magnifications of boxed regions. Arrowheads point to non-protruding cells. Arrows point to protruding cells. White stars show nucleus that engage in protrusions. Right panel leader/Follower polarization was quantified and plotted as rate normalized to pLKO condition on a bar graph (Means ± SEM of at least 3 independent experiments) (unpaired t-test, ***p<0.001, **p<0.01, *p<0.05 n.s : non significant). Scale bars: 20µm. (C) Schematic representation of ROCK2 full length (ROCK2-FL) and the ROCK2 dominant negative constructs ROCK2DN#1 and ROCK2DN#2. (D) Representative immunoprecipitation of endogenous ROCK1 and ROCK2 using GFP trap beads in Caco-2 cells transfected with GFP-ROCK2DN#1 or ROCK2DN#2. Immunoblot analysis was performed with anti-ROCK1, anti-ROCK2 and anti-GFP antibodies. Representative of three independent experiments. (E) Left panel Caco-2 cysts stably expressing GFP alone or GFP-ROCK2DN#2, were submitted to 2 days long invasion assay, were fixed and stained for F-actin (Phalloidin) and nuclei (DAPI). i,ii, and iii are higher magnifications of boxed regions. Arrowheads point to non-protruding cells. Arrows point to protruding cells. White and black stars show nuclei that engage in protrusions Right panel, leader/follower polarization was quantified and plotted as rate normalized to GFP condition on a bar graph. (Means ± SEM of at least 3 independent experiments) (unpaired t-test, ****p<0.0001, ***p<0.001, **p<0.01 n.s: non significant). Scale bars: 20 µm

RB domain in ROCK2DN#2 allowed the formation of normal cysts with a single central lumen (Supp Fig. 2A). We therefore only used the stable cell line expressing ROCK2DN#2 in our invasion assay. Caco-2 cysts expressing ROCK2DN#2 had an invasion rate 5±1 fold higher than the empty vector (Fig.4E). The invasion rate induced by ROCK2DN#2 construct is lower than shROCK2 or ROCK inhibitors (compare Fig. 4B and Fig 4E). We attribute this difference to the low level of expression of the construct in the cell line, which may not titer all endogenous activated ROCK2.

Taken together our results demonstrate that the specific inhibition of ROCK2 kinase activity is sufficient to induce collective invasion of Caco-2 cysts.

ROCK2 inhibition promotes leader cell formation

ROCK2 inhibition triggers the supracellular polarization of Caco-2 cyst resulting in the appearance of protrusive leader cells and non-protrusive followers. We reasoned that ROCK2 inhibition could either directly induce the formation of leaders or followers, or alternatively, unleash cysts containing cells with a preexisting leader/follower fate. To examine this, we generated mosaic cysts to inhibit ROCK2 activity in a small subset of cells (Fig. 5A). Mature Caco-2 cysts were transduced using a suboptimal concentration of lentiviral particles encoding GFP-ROCK2DNs in order to only target 1 or 2 cells per cyst. The acute mosaic expression of ROCK2DN#2 was sufficient to increase the invasion rate by 5,5+/-2,5, similar to the treatment by Y27632 (Fig. 5B,C). This demonstrated that the inhibition of ROCK2 activity in one or two cells per cysts is sufficient to stimulate collective invasion. We then measured whether ROCK2DNs expressing cells become leader of follower cells. In control cysts treated with Y27632, 34,6±5,5 % of cells expressing GFP became leader cells. In contrast, 79,9±3,9% of cells expressing ROCK2DN#2 were protrusive leaders (Fig. 5D).

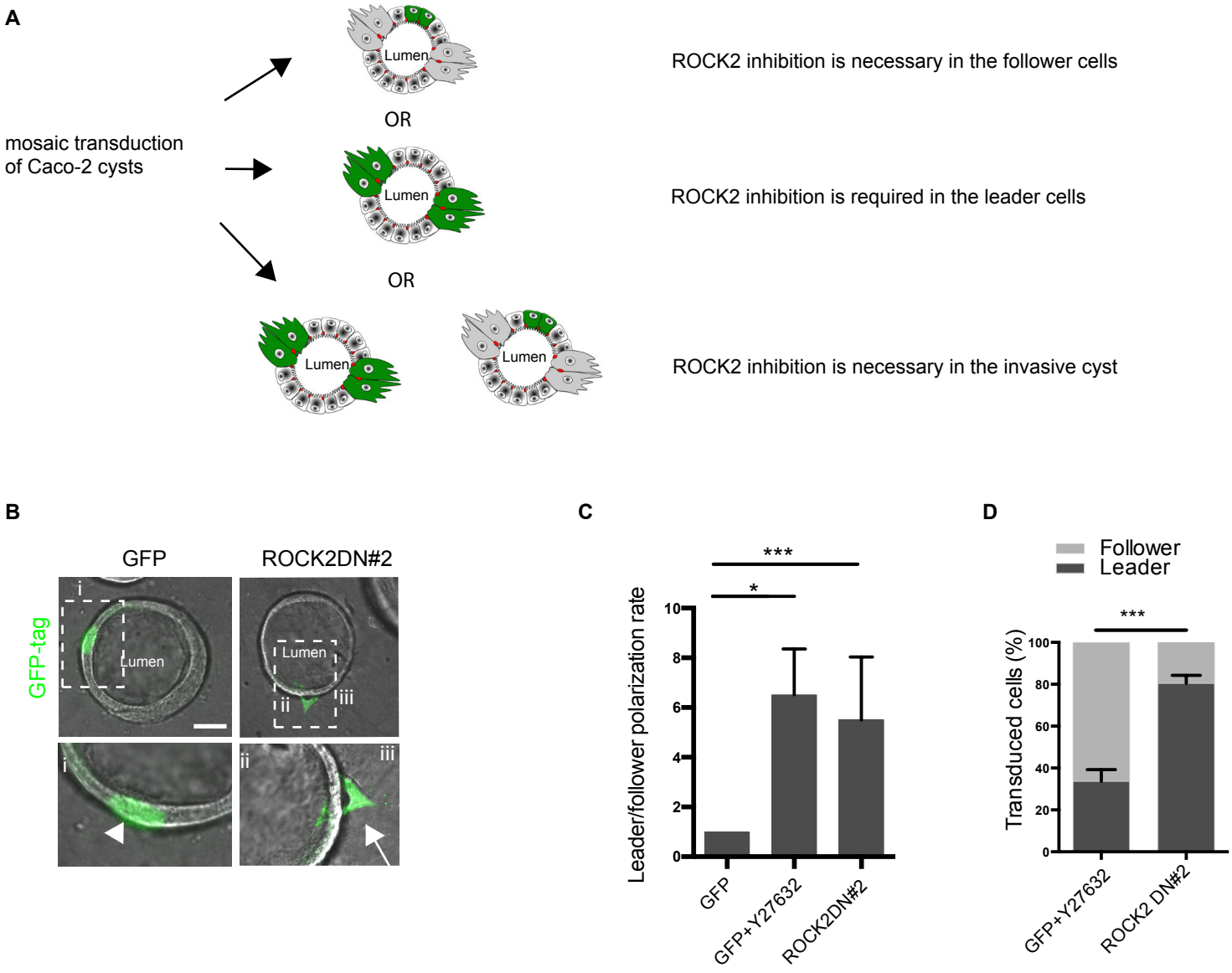

Figure 5: ROCK2 inhibition promotes leader cell formation
(A) Schematic representation of Caco-2 cysts mozaicly transduced with ROCK2DN#2, and the potential phenotypes occuring after 2 days of invasion. (B) Acquisition of fixed Caco-2 cysts mozaicly transduced with GFP alone or GFP-ROCK2DN#1 or GFP-ROCK2DN#2 following 2 days of invasion. i,ii, and iii are higher magnifications of boxed regions. Arrowheads point to non-protruding cells. Arrows point to protruding cells. (C) Quantification of Caco-2 cysts leader/follower polarization presented in panel B) as a bar graph representing leader/follower polarization rate (Means ± SEM of at least 3 independent experiments) (unpaired t-test, ***p<0.001, **p<0.01). Scale bars: 20µm. (D) Quantification of the fate of the GFP positive cells, leader or follower, in polarized cysts mozaicly transduced with the GFP-alone and treated with Y27632 (GFP+Y27632) or GFP-ROCK2D-N#2 transduced (Means ± SEM of at least 3 independent experiments) (unpaired t-test, ***p<0.001).

These results demonstrate that the inhibition of ROCK2 promotes the formation of leader cells, which triggers collective invasion.

Caco-2 cysts invasion relies on FARP2 a GEF for Cdc42 and RAC1

We then aimed at identifying the effectors of ROCK2 involved in Caco-2 cysts collective invasion. In other model systems, the small GTPases Rac1 controls F-actin polymerization in leader cells and gets activated downstream of ROCK inhibition (Salhia et al., 2005; Sanz-Moreno et al., 2008) (Wang et al., 2010; Yamaguchi et al., 2015). We therefore reasoned that Rac1 could participate in leader cell formation downstream of ROCK inhibition. To verify this hypothesis, we first used the CRIB domain of PAK to pull-down GTP-bound Rac1 in cell treated with the ROCK inhibitors. Western blot analyses revealed a robust increase in the level of Rac1-GTP 12 hours after the treatment by Y27632 (Fig. 6A). Next, we verified that Rac1 activation was necessary for Caco-2 collective invasion. The cysts were co-treated with Y27632 or H1152 and the Rac inhibitor NSC23766 during our organotypic invasion assay. The treatment with NSC23766 decreased by 3,3±0,9 and 3,7±0,4 fold the invasion rate as compared to cysts treated with Y27632 or H1152 alone, respectively(Fig. 6B). To identify the GEF mediating the activation of Rac1 downstream of ROCK inhibition, we performed a siRNA-based screen. We aimed at identifying the siRNAs that would prevent collective invasion induced by ROCK inhibition. For this, we transfected Caco-2 cells using a siRNA library targeting all known GEFs of the human genome. To prevent any functional redundancy we grouped the siRNA targeting the two closest homologs (Sup.Table 2). We used our automated quantification method to assess for invasion in the 3D Boyden chamber assay (Fig. 2C). This screen yielded 3 hits decreasing invasion rate by 3 fold or more (Fig. 6C). Two of the hits, targeting GEFs for RhoA and RhoG, were not confirmed in the validation round. The third hit, combining siRNA against FARP1 and FARP2, GEFs for Rac1

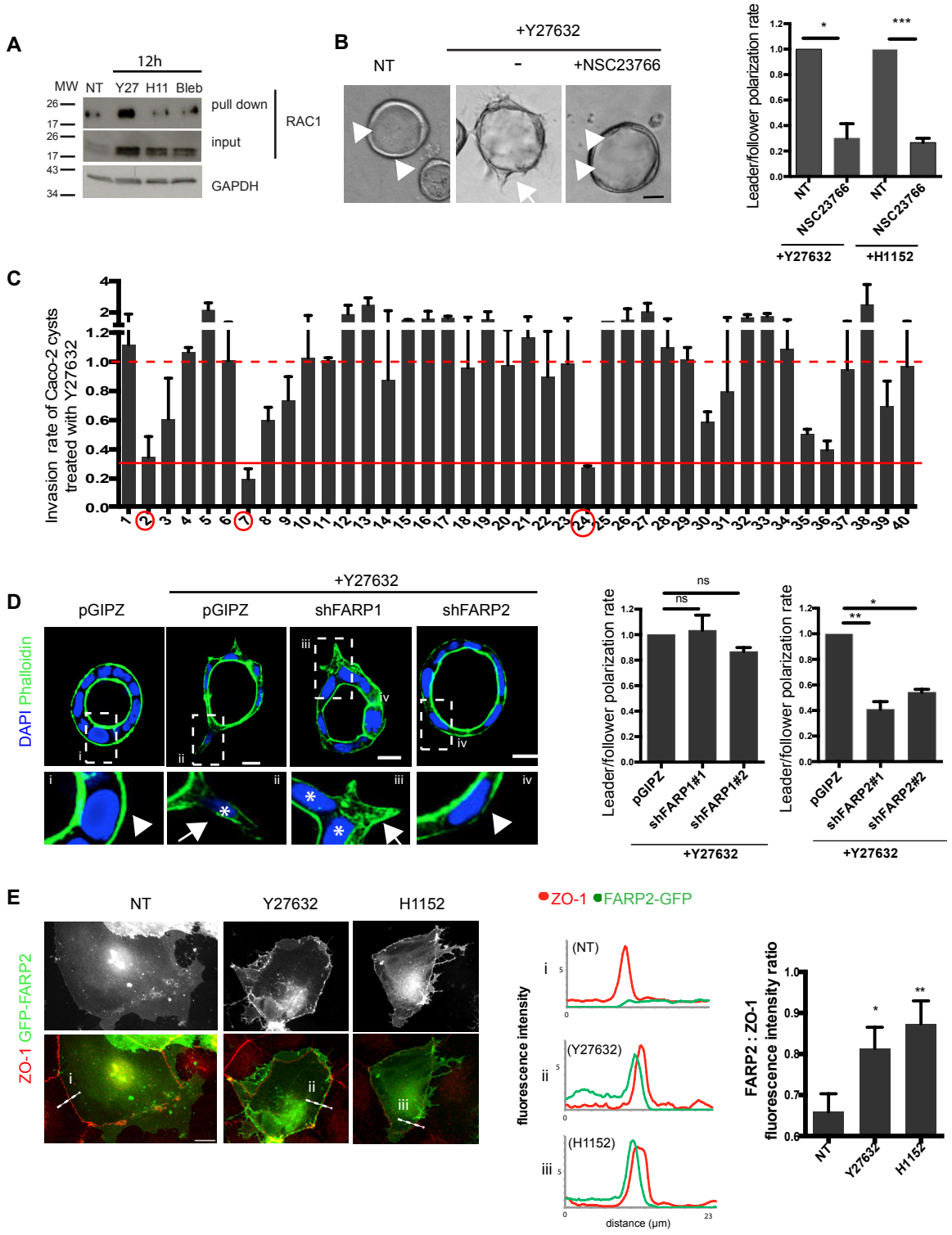

Figure 6: Caco-2 cysts collective invasion relies on the Guanine nucleotide Exchange Factor FARP2
(A) Representative pull-down of RAC1-GTP by PAK-Crib, in Caco-2 cell treated with ROCK inhibitor Y27632 or H1152 or with the Myosin-II inhibitor Blebbistatin for the indicated time. Immunoblot analyses were performed with anti-RAC1 and anti-GAPDH antibody. The experiment was repeated 3 times. (B) Left panel, DIC acquisition of fixed Caco-2 cysts treated with ROCK inhibitors alone (Y27632 or H1152), or in combination with RAC1 inhibitor NSC23766. Arrowheads point to non-protruding cells. Arrows point to protruding cells. Right panel, leader/follower polarization of the Caco-2 cysts was quantified and plotted on a bar graph representing the Leader/Follower polarization rate. (Means ± SEM of at least 3 independent experiments) (unpaired t-test, ***p<0.001, *p<0.05). Scale bar 20 µm. (C) SiRNA screen was performed in Caco-2 cysts treated with ROCK inhibitor Y27632: Caco-2 cysts transfected with control siRNA (40) or pairs of siRNA targeting homologous GEF of RhoGTPases (2:ARHGEF18+RNEF, 7: SGEF+ARHGEF16, 24: FARP1+FARP2) were treated with Y27632 and subjected to 2 days long invasion assay. Bar graph presenting the invasion rate normalized to the median invasion rate. The red dotted line highlights the median invasion rate, the red full line highlights the threshold of 3 fold decrease of invasion rate induced by positive hits (circled in red) of the screen. (D) Left panel, Caco-2 cysts stably expressing empty vector (pGIPZ) or 2 distinct shRNA FARP1 (shFARP#1 and shFARP#2) or shRNA FARP2 (shFARP2#1 and shFARP2#2) were treated with ROCK inhibitor Y27632 and allowed to invade for 2 days, fixed and stained for F-actin (Phalloidin). i, ii, iii and iv are higher magnification of boxed regions. Arrowheads point to non-protruding cells. Arrows point to protruding cells. White stars show nuclei that engage in protrusions. Right panel, Leader/Follower polarization of the Caco-2 cysts was quantified and plotted in a bar graph representing the leader/follower polarization rate. (Means ± SEM of at least 3 independent experiments)(unpaired t-test, ns: non significant, **p<0.01, *p<0.05). Scale bars: 20µm. (E) Left panel, Representative acquisition of 2D Caco-2 cells overexpressing GFP-FARP2 cells stained with ZO-1, in non-treated (NT) and 2 h ROCK inhibitor treated (Y27632, H1152) conditions. i, ii and iii, are representative linescans. Middle panel, fluorescence intensity of ZO-1 staining and GFP-FARP2 along the linescans i, ii, iii in non-treated, oe in Y27632 or H1152 treated conditions, normalized to GFP-FARP2 maximum intensity in NT conditions. Right panel, bar graphs presenting the average ratio of GFP-FARP2 and ZO-1 staining maximum fluorescence intensity measured with linescans crossing cell-cell junctions. (Unpaired t-test **p<0.01, *p<0.05). Scale bars: 20µm

and Cdc42, decreased by 3,8± 0,1fold the rate of invasion induced by Y27632 (Fig. 6C, Pair#24)(He et al., 2013). To confirm these results and determine whether both FARP homologs participate in collective invasion, we independently depleted FARP1 or FARP2 using specific shRNAs in our Caco-2 cysts organotypic invasion assay (Supp. Fig. 3A). We verified that depleting these proteins did not perturb Caco-2 cystogenesis (Supp. Fig. 3B**).** Silencing FARP2 using two independent hairpins reduced by 1,85±0,1 to 2,4±0,3 fold the invasion triggered by ROCK inhibition while FARP1 depletion had no significant effect (Fig. 6D). Then, we asked how ROCK was regulating FARP2 activity in Caco-2 cells. We investigated whether FARP2 could be a substrate of ROCK2. We could not co-immunoprecipitate overexpressed ROCK2 and FARP2 constructs or detect by western blot any band-shift suggestive of FARP2 phosphorylation (Data not shown). In support to this, FARP2 is not part of the ROCK substrate candidates identified by proteomic analyses (Amano et al., 2015). Alternatively, ROCK2 could indirectly regulate FARP2 by controlling its localization. To test this hypothesis, we examined the subcellular localization of the proteins by immunofluorescence. Both endogenous ROCK2 and FARP2 associate with the plasma membrane of Caco-2 cells and are enriched at cell-cell contacts (Supp. Fig. 3C). To evaluate whether ROCK activity could affect FARP2 localization, we expressed GFP-FARP2-FL protein in 2D Caco-2 cells and treated with Y27632 or H1152. We co-stained with ZO-1 to visualize cell-cell contacts. The treatment with both ROCK inhibitors promoted GFP-FARP2 recruitment at cell-cell contacts (Fig. 6E). This could be measured by linescan (Fig. 6E, left panel and middle panel). In addition, we used ZO-1 as a marker of cell-cell junction and calculated the average ratio of GFP-FARP2 and ZO-1 staining maximum fluorescence intensity (Fig.6E, right panel). While it was 0,66 ± 0,04 in non-treated condition, Y27632 and H1152 treatment induced an increase of the GFP-FARP2/ZO-1 ratio to 0,81 ± 0,05 and 0,87 ± 0,06 respectively.

Altogether, these results support that the GEF FARP2 is a downstream effector of ROCK2 necessary for the collective invasion of Caco-2 cysts. ROCK2 does not directly phosphorylate FARP2, however it controls its localization at the plasma membrane

FARP2 activation and Myosin-II inhibition cooperate to induce collective invasion downstream of ROCK2 inhibition

We next examined whether FARP2 was sufficient to induce collective invasion from Caco-2 cysts. We overexpressed the full length FARP2 protein (FARP2-FL) and assessed for invasion. The invasion rate of cysts overexpressing the FARP2-FL constructs was not significantly different than the invasion of cysts expressing GFP alone (Fig. 7A). Since FARP2-FL may be folded in an inactive conformation, we turned to activated mutants harboring point mutations on residues 730 and 733 (FARP2-Mut), a truncation of the PH2 domain (FARP2-del) or both (FARP2-del/Mut, Fig. 7B)(He et al., 2013). The invasion rate of the cysts expressing any of the FARP2 mutants was not significantly different from cysts overexpressing FARP2-FL or GFP alone (Fig. 7A). Hence, FARP2 activation was not sufficient to induce collective invasion from Caco-2 cysts. We hypothesized that Myosin-II may contribute to collective invasion. To address this, we first inhibited the motor activity of Myosin-II by treating Caco-2 cysts with blebbistatin. Some cells formed long and thin F-actin rich-elongations and we did not detect any engagement of their nucleus toward this structure. This phenotype was very different from the broad protrusions produced by leader cells under ROCK inhibition (Fig. 7C). We then used siRNAs to assess whether other function of Myosin-II, such as its F-actin cross-linking role (Vicente-Manzanares et al., 2009), could participate in collective invasion (Supp. Fig. 4A). The depletion of Myosin-IIA, but not Myosin-IIB, reproduced the phenotype induced by Blebbistatin but failed to induce leader cell formation (Fig. 7C). We finally checked whether myosin-II and FARP2 could cooperate

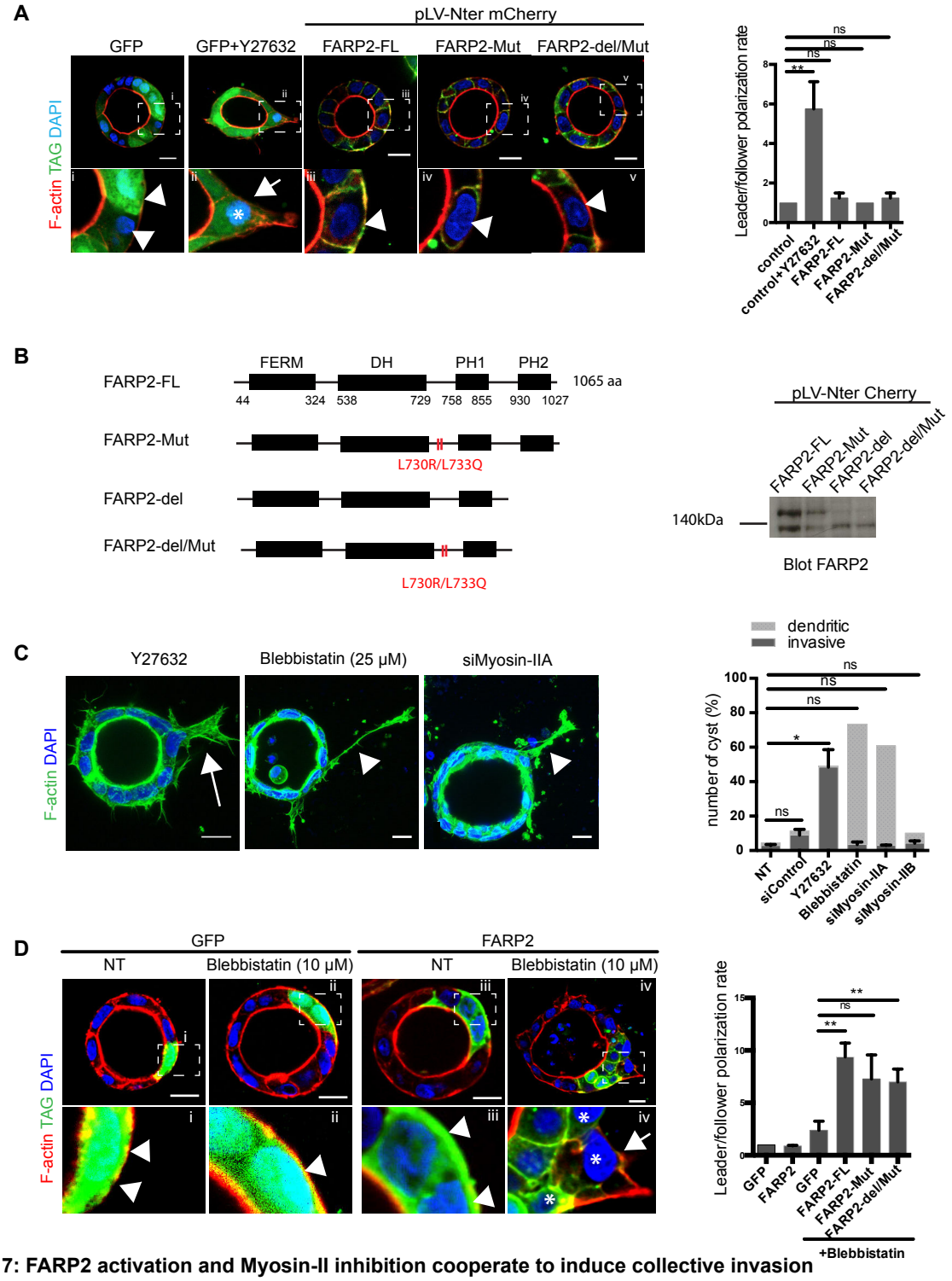

Figure 7: FARP2 activation and Myosin-II inhibition cooperate to induce collective invasion

(A) Left panel, Caco-2 cysts stably expressing empty vector (GFP) treated or not with ROCK inhibitor Y27632, or stably expressing Cherry-FARP2-full length (FARP2-FL), FARP2-730/733 mutant (FARP2-Mut) or FARP2 del PH 730/733 (FARP2-del/Mut) were allowed to invade for 2 days and were fixed and stained for F-actin. i, ii, iii, iv and v are higher magnification of boxed regions. Arrowheads point to non-protruding cells. Arrows point to protruding cells. White stars show nucleus that engages in protrusion. Right panel, leader/follower polarization of the Caco-2 cysts was quantified and plotted on a bar graph representing the leader/follower polarization rate (Means ± SEM of at least 3 independent experiments)(t-test,**p<0,01, n.s: non significant). (B), Left panel, Schematic representation of FARP2 constructs. Right panel, Immunoblot analysis of Caco-2 cell transduced with FARP2 constructs: Cherry-FARP2-full length (FARP2-FL), FARP2-L730R/L733Q mutant (FARP2-Mut) or FARP2 del PH /L730Q/L733R (FARP2-del/Mut) with an anti-FARP2 antibody. (C) Left panel, Caco-2 cysts were treated with ROCK inhibitor Y27632 or Myosin-II inhibitor Blebbistatin or transfected with siRNA targeting Myosin-IIA or Myosin-IIB (siMyosin-IIA or siMyosin-IIB) and allowed to invade for 2 days. They were fixed and stained for F-actin (Phalloidin) and nuclei (DAPI). Representative Y27632 induced « invasive » phenotype and Blebbistatin induced « dendritic »phenotype are displayed. Arrowheads point to “dendritic” protrusions. Arrows point to protruding cells. Right panel, The “invasive” phenotype and “dendritic” phenotype of Caco-2 treated with ROCK inhibitor Y27632 or Myosin-II inhibitor Blebbistatin or expressing Myosin-IIA or Myosin-IIB siRNA were quantified and plotted in a bar graph. (Means ± SEM of at least 3 independent experiments)(unpaired t-test,*p<0,05, n.s: non significant). (D) Left panel, Caco-2 cysts transduced after morphogenesis was completed, with empty vector or Cherry-FARP2-full length (FARP2-FL), FARP2-730/733 mutant (FARP2-Mut) or FARP2 del PH/730/733 (FARP2-del/Mut), were treated or not with Myosin-II inhibitor Blebbistatin and allowed to invade for 2 days. They were fixed and stained for F-actin. i, ii, iii and iv are higher magnification of boxed regions. Arrowheads point to non-protruding cells. Arrows point to protruding cells. White stars show nucleus that engage in protrusions. Right panel, Leader/Follower polarization of the Caco-2 cysts was quantified and plotted on a bar graph representing the rate invasion (Means ± SEM of more than 3 independent experiments)(t-test,**p<0,01, n.s: non significant). Scale bars: 20 µm

downstream of ROCK to control collective invasion. We performed a dose-response experiment to identify the concentration of blebbistatin that did not induce the "dendritic" phenotype (Supp. Fig. 4B). We further combined this concentration of blebbistatin with the expression of FARP2 constructs and quantified Caco-2 cysts invasion. Expressing FARP2-FL or the activated mutant of FARP2delmut in combination with 10mM of blebbistatin increased invasion by 7±1,3 and 6±1 fold respectively (Fig. 7D). This demonstrates that FARP2 can induce the formation of leader cells solely when the acto-myosin cytoskeleton is relaxed.

Altogether these results demonstrate that FARP2 activation and Myosin-II inhibition cooperate downstream of ROCK2 to induce the collective invasion of caco-2 cysts.

DISCUSSION

This study revealed that CRCs undergo collective invasion and maintain their epithelial glandular architecture to conquer the successive layers of the digestive wall. We identified ROCK2 as an essential kinase controlling the transition from non-invasive to collectively invasive CRCs models such as cysts and organoids. ROCK2 inhibition triggers the formation of leader cells through a dual mechanism involving the reduction of acto-myosin contractility to unchain the collective and the activation of Rac1 through the GEF FARP2 to generate protrusive forces.

Enabling invasive properties is the first step of the metastatic cascade and a challenge to patient treatment. Here, we show that CRCs invasion can occur collectively and does not automatically require carcinoma cell individualization. In the past decades, most of the biomedical research investigations have focused on the EMT program, seen as the main, if not the sole driver of cancer cell dissemination (Chaffer et al., 2016). This conception has recently been challenged by the demonstration that pancreas and breast cancer metastases

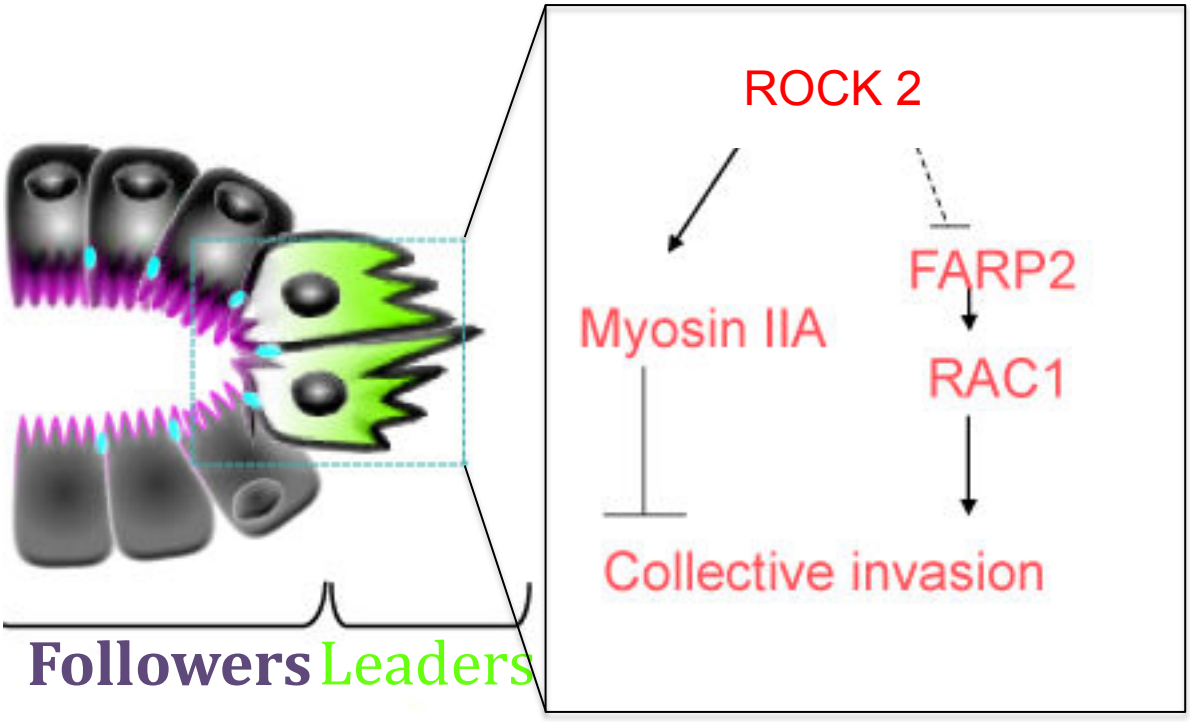

Figure 8 : Model of collective invasion regulation of CRC model by ROCK2 dependent signaling pathway : ROCK2 inhibition triggers collective invasion of CRC models by inducing leader cells formation through Myosin-IIA inhibition in combination with FARP2 GEF/Rac1 activation.

form without activation of the EMT transcription factors in mice (Fischer et al., 2015; Zheng et al., 2015) or that the EMT program is in fact activated into the stromal component of CRCs (Kim and Verhaak, 2015). Inter and intra-tumoral heterogeneity, together with cancer cell plasticity, imply that dissemination strategies can be multiple (Alexander and Friedl Cell 2011) and possibly complementary. Our results are in line with the growing body of evidences supporting the contribution of collective behaviour to carcinoma invasion (Cheung and Ewald, 2016; Friedl et al., 2012). Our analysis of FFPE samples of CRCs invading into the submucosa demonstrate that most of the tumour area remains cohesive, consistent with recent report in breast carcinomas (Khalil et al., 2017). Our time-lapse imaging of live cancer specimens collected from the peritoneal cavity of metastatic patients provides dynamic insights proving that large tumour cells cohorts are highly invasive and collectively conquer their environment, without the contribution of single cells. This collective behaviour has now been reported from several cancer types originating from patients or mice models, at early or late stages of cancer progression (Friedl et al., 1995; Giampieri et al., 2009; Konen et al., 2017). Surprisingly, we found that CRCs primary samples, organoids and cysts retain their epithelial polarity and architecture, invading as glandular structures in vivo into the peritumoral stroma or in collagen-I gel in vitro. This is consistent with the fact that 80% of CRCs are well to moderately-well differentiated tumours (Fleming et al., 2012; Prall et al., 2009). This is a distinctive feature among the collective behaviours reported to date for neoplastic cells. However, during normal development and organogenesis, epithelial cell cohorts organized around central lumens undergo collective migration. There, the lumen enable growth factors concentration or exosome transfer favouring the activation of tyrosine kinase receptors (Durdu et al., 2014; Kwon et al., 2014; Revenu et al., 2014). Whether the luminal cavity of CRC glands provides a selective advantage for tumour dissemination or proliferation is an attracting area of investigation.

We found that inhibition of ROCK triggers the transition from non-invasive cysts or organoids to protrusive cohorts that undergo collective invasion. This is in contradiction with the promoting role of ROCK in cancer progression revealed by the xenograft of several cancer cell lines into mice (Croft et al., 2004; Itoh et al., 1999; Sadok et al., 2015). In addition, in transgenic mice models of skin cancer, expression of an active form of ROCK2 increases proliferation, but not invasion (Samuel et al., 2011). Although we cannot exclude that the anti-invasive function of ROCK2 are restricted to the early step of collective invasion studied in our in vitro experimental system, our results are in agreement with the recent large scale in vivo RNAi screen revealing that loss of Myosin-II triggers the formation of invasive squamous cell carcinomas (Schramek et al., 2014). The discrepancies in the role of ROCK in invasion could be related to several aspects of cancer heterogeneity. First, the crosstalk with specific oncogenes and tumour suppressor, such as KRAS, Smad4 or JAK1, can modify the ROCK expression level and activity (Sahai et al., 2001; Sanz-Moreno et al., 2011; Voorneveld et al., 2014). Second, ROCK may have different actions if the tumour spread as individual cells or collectives. In single cells, increased acto-myosin contractility would promote fast amoeboid invasion, likely accelerating metastases formation (Sahai and Marshall, 2003). In contrast, reducing cortical tension in cell cohorts, at cell-cell junctions or the basal membrane, would be beneficial for collective invasion (Fischer et al., 2009; Giampieri et al., 2009; Hidalgo-Carcedo et al., 2011). Third, the tissue in which the tumour is born may influence ROCK function and elicit different responses to its inhibition. In support to this, interfering with ROCK and myosin II activity has long been known to impede fibroblast movement while more recently it has been shown to promote the migration of single epithelial cells (Lomakin et al., 2015). Finally, but importantly, while the above-mentioned studies use motile cells to study the role of ROCK, we started from non-migratory

Caco-2 cysts or organoids to identify the proteins governing the first step in the invasion process. In this gain of function study, we found that ROCK2 activity constrains the neoplastic glandular structures and that its inhibition unleashes invasion, a function that could not have been identified from spontaneously invasive cells. This is supported by the results obtained by Lomakin et al. showing that myosin and ROCK inhibition trigger the migratory behaviour of non-motile single epithelial cells (Lomakin et al., 2015).

How does ROCK2 control the invasive behaviour of CRC neoplastic glands? Using the acute expression of dominant negative mutants, we targeted ROCK2 inhibition in a restricted number of cells within the cohort. This was sufficient to induce leader cell formation, demonstrating that unlike in breast and lung carcinomas, CRC leaders are not predetermined by a transcriptional program (Cheung et al., 2013; Konen et al., 2017). Nevertheless, the activation of specific gene expression maybe induced downstream of ROCK inhibition by mechanosensing proteins such as YAP/TAZ or Stat3 (Dupont et al., 2011; Sanz-Moreno et al., 2011). We show that ROCK controls two distinct F-actin dynamics, F-actin polymerization through Rac1 and F-actin contractility through myosin-II. Rac1 activation is a common determinant of leader cell formation (Wang et al., 2010; Yamaguchi et al., 2015). Yet, our screen targeting all human GEFs did not identify
bPix, Tiam1 or DOCK180 that have previously been described to activate Rac1 in collective migration (Bianco et al., 2007; Ellenbroek et al., 2012; Osmani et al., 2006). Instead we found that FARP2 activity was necessary for Caco-2 collective invasion induced by ROCK inhibition. Although the ROCK/Rac1 balance is a core mechanism controlling all migratory processes, the GEFs and GAPs governing their spatiotemporal activation vary with cell types and stimuli (Sadok and Marshall, 2014).
βPix and Tiam1 are activated by integrins at the front row of wounded astrocytes monolayers

and DOCK180 responds to growth factors stimulation in drosophila border cells (Bianco et al., 2007; Ellenbroek et al., 2012; Osmani et al., 2006). This contrasts with our Caco-2 model where we do not provide any external stimuli, either mechanical or biochemical, to elicit leaders formation. We found that FARP2 but not FARP1 was necessary for the collective invasion of CRC. Although both FARP1 and FARP2 were shown to regulate the cytoskeleton dynamics in neuronal development,(Cheadle and Biederer, 2012, 2014; Kubo et al., 2002; Mlechkovich et al., 2014; Toyofuku et al., 2005; Zhuang et al., 2009), they act downstream of distinct signaling pathways to control neurite outgrowth or axon collapse, in addition to other cellular processes such as podosome formation or bone metabolism (Koyano et al., 1997, 2001; Takegahara et al., 2010). To date, only FARP2 is described to regulate cell motility in an endothelin dependent manner (Miyamoto et al., 2003).

While the photo-activation of Rac1 is sufficient to drive the collective migration of border cells, FARP2 expression is ineffective at triggering Caco-2 collective invasion. Downstream of ROCK, we found that relaxing acto-myosin contractility is required to unleash collective invasion. This is in agreement with previous reports from 2D cultures, where breaking up the supracellular marginal actin bundle and loosening acto-myosin tension at cell-cell junctions both contribute to collective migration (Hidalgo-Carcedo et al., 2011; Omelchenko and Hall, 2012; Omelchenko et al., 2003; Reffay et al., 2014). More recently, it has been shown in single cells that releasing actin bundles frees actin monomers which increases the soluble pool of G-actin available for the polymerization of branched F-actin in protrusion (Lomakin et al., 2015) which could also participate to the protrusive activity of leader cells within the collective.

Together, our results show that ROCK activity synchronize the cytoskeleton to harness CRC invasive behavior. ROCK inhibitors being already used in the clinic for the treatment of

several cardiovascular conditions, it has been proposed to target ROCK in cancer patients to prevent or reduce invasion and metastasis formation(Croft et al., 2004; Narumiya et al., 2009; Sadok and Marshall, 2014). Yet, it remains essential to elucidate the tumor specific context enabling pro or anti-invasive functions of this kinase in order to propose relevant therapeutic strategies to patients and avoid paradoxical effects.

MATERIAL AND METHODS

Colorectal cancer patients Tumour sphere recovery and invasion assay:

Peritoneal effusions were obtained after informed patient consent, per institutional review board (CPP IDF 10) protocol #NI-2015-06-03, at Gustave Roussy Hospital. The patients received neoadjuvant chemotherapy 2 to 3 weeks before surgery. The peritoneal effusion samples were collected at the onset of Hyperthermic Intraperitoneal Chemotherapy treatment (HIPEC). Immediately after laparotomy, and before cytoreductive surgery, serous fluid was collected by addition and reabsorption of 500 ml of saline solution. The fluids were processed in the laboratory within 2 hours after collection. The freshly isolated samples were transferred to sterile tubes. DMEM containing 4.5 g/l glucose, glutaMAX (Life Technologies, 31966021) and 1% Penicillin-Streptomycin (Life Technologies, 15140-122) was added to a final volume of 10 ml. Differential centrifugations, spin down up to 2000 rpm, were performed at least 4 times. The pelleted tumor clusters were directly used for functional studies.

3D Patient Tumor specimen invasion: Patient tumor specimen embedded in neutralized Rat collagen-I, as for tumoroids invasion assay, were added on top of the pre-coated well at a concentration of 1-2 cluster per microliter. The gel was allowed to polymerize for 45 min at 37°C. Tumors were then cultured in culture medium supplemented with FBS 10 % for up to 6 days.

Patient derived xenograft (PDX) recovery, tumoroids morphogenesis and invasion :

Animal experiments were compliant with French legislation and EU Directive 2010/63. The project was validated by the Ethical Committe (CEEA) n°26 and was then granted French government authorizations under number 517-2015042114005883 and 2734-2015111711418501. Mice were obtained from Charles River, housed and bred at the Gustave Roussy animal core facility (accreditation number E-94-076-11). Animals were humanely euthanized according to endpoints that were validated by the Ethical Commitee and the French government (Ministère de l'Enseignement Supérieur, de la Recherche et de l'Innovation).

Tumoroids morphogenesis: Apico-basolateral polarized tumoroids were formed from the morphogenesis of Patient Derived Xenograft's (PDX) tumor fragments as follows: A human colorectal tumor corresponding to LRB-0010P from the CReMEC tumor collection was maintained in NOD SCID Gamma (NSG from Charles River, France) mice as previously described by Julien et al., 2012. Briefly, small tumor fragments were subcutaneously engrafted on the flank of anesthetized mice (2.5% isoflurane). Tumor growth was measured at least once a week. When the volume reach 1000-1500 mm^3, mice were sacrificed and tumors were used for *ex vivo* experiments and 50 mm^3 fragments engrafted on the flank of new mice. Tumoroids were prepared according to (Ewald et al., 2012). Tumors were minced into small fragments and were incubated for 1h30 at 37°C in a final volume of 5 to 10 ml of DMEM supplemented with 2 mg/ml of collagenase. Digested tumor clusters were pelleted by 4 pulse-centrifugations at 1500 rpm. The tumor fragments, free of single cells, were maintained 3 days in culture medium supplemented with 15 % Matrigel to allow formation of polarized organoids. Then, tumoroids were washed in DMEM, pelleted at 1500 rpm and used for invasion assay.

3D tumoroids invasion assay: The tumoroids were embedded in 2 mg/ ml of neutralized Rat-tail Collagen-I, allowed to polymerize in ice for 1h and were added on top of Collagen-I pre-coated well at a concentration of 1-2 tumoroids per microliter. The gel was allowed to polymerize for 45 min at 37°C. Culture medium supplemented with FBS (10 %) was added to the wells and invasion was allowed to proceed for up to 6 days with or without Y27632 (25 μM) or H1152 (2 μM).

Tumoroids invasion quantification: Invasive tumoroids were defined as the ones with strand of cells invading the collagen matrix and that remained attached to the tumoroid gland, led by few protrusive cells at the front. At least 40 tumoroids were counted per condition.

Cell lines and culture conditions:

Colorectal carcinoma Caco-2 cell lines (ATCC) were grown in complete medium (DMEM/Glutamax supplemented with 10% Fetal Bovine Serum (FBS) and 50 μg/ml Penicillin, 50 μg/ml Streptomycin (P/S). Normal colon fibroblast CCD-18CO (ATCC) were grown in EMEM medium supplemented with 1% non-essential amino acids (NEAA) 10% FBS and 50 μg/ml PS.

To prepare CCD-18-CO condition medium, fresh medium with FBS was added to cells at 70 to 80% of confluence and was harvested after 24h and stored at -20°C until use.

All cells were grown in a humidified atmosphere at a temperature of 37°C and with 5%CO_2.

Small molecules inhibitors:

H1152 (Tocris, 2414), Y27632 (Calbiochem, 688000), Blebbistatin (Calbiochem, 203391), NSC-23766 (Tocris, 2161).

siRNA library and functional screen

The screen targeting ROCK was a morphological screen of Caco-2 cysts.

The screen targeting Rho-GTP GEFs was carried out in the adapted Boyden Chamber assay.

siRNA transfection:

siRNA oligonucleotides (100 nM) were transfected into Caco-2 cells using Dharmafect 1 Transfection Reagent (Dharmacon™, T-2001, 1 :57)diluted in Opti-MEMmedium (Gibco, 31985070). Briefly, Caco-2 cells were plated in culture dish in complete medium, after one day the medium was replaced with complete medium without antibiotics and the siRNA/Dharmafect mix (1:5) was added to the medium. After 6 hours, the transfection medium was replaced with complete medium. The cells were allowed to recover overnight before their use in morphogenesis assay. Depletion of the siRNA targeted protein was verified by Western Blotting after 3 days.

ROCK siRNA were purchased from Dharmacon™ :

ROCK1 ON-Target smart-pool (L-003536-00-0005)

ROCK2 ON-Target smart-pool (L-004610-00-0005)

Lentiviruses transduction:

Single Caco-2 cells were infected at a MOI=1. Lentiviral particles were added to Caco-2 cells in suspension (2.10^5 cells/mL) in complete medium supplemented with protamine (8 µg/mL) and were left to adhere and grow for 3 days. pGIPZ and pLKO transduced Caco-2 cells were trypsinized and selected in puromycine (6 µg/mL) supplemented complete medium.

Caco-2 cysts were transduced with 1.10^4 to 1.10^5 per mL of lentiviral particles to reach a mosaic or acute transduction of the cyst. Briefly, after 3 days of Caco-2 cysts morphogenesis in ibidi chambers, the 2% Matrigel (BD, 354230) supernatant medium was removed and replaced with complete medium supplemented with Cholera Toxin (0.05µg/mL) mixed with

the appropriate amount of lentiviral particles. The ibidi was kept 24 hours at 37°C before fixation or performing the invasion assay.

Virus production: The shFARP1#1 and #2, shFARP2#1 and #2, shROCK1#02, shROCK2#36, ROCK2DN#1, ROCK2DN#2, FARP1, FARP2-FL, FARP2Mut, FARP2delMut lentiviral particles were obtained by transfecting the respective expression lentiviral vectors with the packaging vectors pMD2G (Addgene, 12259) and pCMVdR8.74 (Addgene, 22036) into HEK293T (ATCC) cells with the transfection reagent JetPrime (Polyplus, 114-15, 1:250) diluted in the JetPrime buffer (Polyplus, 712.60). Lentiviruses-containing supernatants were collected on days 2 and 3 following transfection and were concentrated by ultracentrifugation (24500 g, 2h) and then stored at -80 °C.

shRNA sequences: FARP1 and FARP2 targeted shRNA were contained in a pGIPZ expression vector and purchased from Thermofisher :

FARP1#1 (V3LHS_325427): TTAACATAGTCGAGAACCT

FARP1#2 (V3LHS_325430): TGAACAGGAAGAACATGCG

FARP2#1 (V2LHS_95483): TAACTTCTAAATCCTTGAG

FARP2#2 (V3LHS_369923): TGTGTACAGCAACATATCT

ROCK shRNAs were contained in a pLKO.1 expression vector and were purchased from Sigma. shRNA ROCK1 (TRCN0000195202) shRNA ROCK2 (TRCN0000194836)

Lentiviral expression vectors generation by Gateway cloning system:

cDNA expression sequences of FARP2-FL, FARP2-Mut, FARP2-del/Mut, were cloned into lentiviral expression vectors pLV-Nter Cherry and cDNA expression sequences of ROCK2DN#1, RROCK2DN#2 were cloned into lentiviral expression vectors pLV-Nter GFP

using the Gateway recombination cloning system. Briefly, in the BP reaction (attB × attP→ attL × attR), the polymerase chain reaction (PCR) product of FARP1, FARP2-FL, FARP2Mut, FARP2delMut, ROCK2DN#1 and ROCK2DN#2 cDNA expression fragments flanked by the attB sites was inserted into the donor vector pDONR with the attP sites yielding the entry clone containing FARP1, FARP2-FL, FARP2Mut, FARP2delMut, ROCK2DN#1 and ROCK2DN#2. In the LR reaction (attL × attR→attB × attP), the entry clone containing FARP1, FARP2-FL, FARP2Mut or FARP2delMutflanked with the attL sites were then integrated into the destination vector pDESTpLV-Nter Cherry flanked with the attR sites whereas the entry clone containing ROCK2DN#1 or ROCK2DN#2 were integrated into the destination vector pDESTpLV-Nter GFP flanked with the attR sites, yielding the final expression clone which is used for protein expression. The att recombination sites in the donor and the destination vectors contains a *ccdB* gene (control of cell death) and a chloramphenicol-resistance gene, thus this vector can only be propagated in *ccdB* T1 or *ccdB* T2 resistant cells.

Primer designing and Polymerase Chain Reaction Amplification of DNA Fragments

AttB flanked expression cDNA fragments were generated by polymerase chain reaction (PCR) amplification using the Phusion High-fidelity Taq DNA polymerase (NEB, M0530) according to the manufacturer instructions with the following primers sequences, plasmids templates and the specified temperatures of PCR cycles

primer name	template	primer sequence	amplified construct
F1STARTMETF	pCDNA3.1+FARP1 FL nter flag(human)	5' GGGG ACA AGT TTG TAC AAA AAA GCA GGC TTC ATGGGAGAAATAGAGCAGAGG 3'	FARP1-FL (human)
F1ENDSTOPR		5' GGGG AC CAC TTT GTA CAA GAA AGC TGG GTC TCA ATA CAC AAG AGA CTC TTT GTG 3'	
F1ENDR		5' GGG GAC CAC TTT GTA CAA GAA AGC TGG GTC ATA CAC AAG AGA CTC TTT GTG 3'	
F2STARTMETF	pCDNA3.1+FARP2 FL nter flag(mouse)	5' GGGG ACA AGT TTG TAC AAA AAA GCA GGC TTC ATGGGAGAGATAGAAGGAACATAC 3'	FARP2-FL (mouse)
F2ENDSTOPR		5' GGGG AC CAC TTT GTA CAA GAA AGC TGG GTC TCAGAGGTTCTTGTCCAAGCAGGGT 3'	
F2ENDR		5'GGGG AC CAC TTT GTA CAA GAA AGC TGG GTC GAG GTT CTT GTC CAA GCA GGG T 3'	

Entry clones generation by BP clonase reaction

Entry Clones were created using Gateway BP Clonase II Enzyme mix (Thermofisher, 11789020) in a reaction between AttB flanked PCR products and pDONR™ vector. Briefly, *att*B expression cDNA ((40-100 fmol) 1-10 µl) , pDONR™ vector ((supercoiled, 150 ng/µl) 2 µl), 5X BP Clonase™reaction buffer (4 µl), TE Buffer,(pH 8.0 to 16 µl) and BP Clonase™ enzyme (Thermofisher, 11789021 4µL) were mixed and incubated 1h at 25°C. Proteinase K was then added to the reaction product and incubated 10 min at 37°C. DH5 alpha competent E.Coli (Thermofisher, reference) were transformed and the appropriate antibiotic-resistant entry clone expressing colonies was selected and DNA preparation was performed using mini-prep kit (Qiagen, 27104).

Expression clone generation by LR clonase reaction

Expression vectors were generated using Gateway LR Clonase II Enzyme mix (Thermofisher, 11791100) in a reaction between pDONR™ vector and destination vector pLV DEST. Briefly, pDONR-insert (150 ng), pLV DEST plasmid (150 ng), TE buffer (pH8 up to 10 µL), 5X LR Clonase™ reaction buffer (4 µl) and LRII clonase enzyme mix (2 µL) were mixed and incubated 1h at room temperature. DH5 alpha competent E.Coli were transformed and the appropriate antibiotic-resistant entry clone expressing colony was selected and DNA preparation was performed using mini-prep kit (Qiagen, 27104). DH5 alpha competent E.Coli were transformed and the appropriate antibiotic-resistant entry clone expressing colony was selected and DNA preparation was performed using mini-prep kit.

3D Rac-GTP and cdc42-Pull down:

Caco-2 cysts were formed on 22 cm^2 culture dishes: briefly, 22 cm^2 dishes were coated with the Matrigel/Collagen-I (Corning, 354236) mix (110 µl/dish) prepared as described in the

'Caco-2 cyst morphogenesis' section (described bellow) and 1.10^6 cell/mL Caco-2 cell suspension in complete medium supplemented with 2% Matrigel and cholera toxin (0.01µg/mL) was added on top of the coating. After 3 days, Caco-2 cysts were treated with Y27632 (12h, 25 µM) or with H1152 (16h, 2µM). Caco-2 cysts were then incubated 15 min with 2 mg/ml of collagenase (Sigma-Aldrich, C2139) in DMEM. The collagenase activity was blocked with complete medium and the cysts were washed twice with ice cold PBS supplemented with $MgCl_2$ (25 mM). Caco-2 cysts were scraped from dish in ice cold PBS-$MgCl_2$, transferred to tubes and separated from the matrix by pelleting through 3 successive centrifugations of 1 min at 1500 rpm. Retreived Caco-2 cysts were then lysed in buffer (PBS supplemented with 50 mM Tris-HCl pH 7.5, 1% Triton X-100, 25 mM MgCl2, 500 mM NaCl, 40 mM Na pyrophosphate, 1 mM NaVO4, 2 mM phenylmethylsulphonyl fluoride (PMSF), 0.025% deoxycholate, 10 µg ml^{-1} aprotinin, 10 µg ml^{-1} leupeptin). Lysates were clarified by centrifugation, and equal concentrations of lysates were incubated with 20 µL of purified glutathione S-transferase (GST)-CRIB immobilized on glutathione-Sepharose beads (Amersham Pharmacia Biotech, Baied'Urfe, Canada) for 1 hour rocking at 4°C. The beads were washed and incubated with SDS sample buffer (62.5 mM Tris-HCl pH 6.8, 10% glycerol, 0.002% bromophenol blue, 2% SDS, and 5% β-mercaptoethanol) 10 min at 95°C. The sample was submitted to Western Blot analysis with anti-Rac1 (1:500; Cell Signaling, Beverly, MA)

Co-Immunoprecipitation:

Caco-2 cells were transfected with plasmids expressing GFP-ROCK2DN#1 or GFP-ROCK2DN#2 lysed after 48 hours with lysis buffer(PBS supplemented with 50 mM Tris-HCl pH 7.5, 1% Triton X-100, 25 mM MgCl2, 500 mM NaCl, 40 mM Na pyrophosphate, 1 mM NaVO4, 2 mM phenylmethylsulphonyl fluoride (PMSF), 0.025% deoxycholate, 10 µg

ml^{-1}aprotinin, 10 μg ml^{-1}leupeptin). Protein lysates were clarified by centrifugation, and equal concentrations of lysates were incubated with GFP-Trap®beads (fournisseurs, reference). The beads were then washed with lysis buffer and incubated 10 min at 95°C in sample buffer (62.5 mM Tris-HCl (pH 6.8), 10% glycerol, 0.002% bromophenol blue, 2% SDS, and 5% β-mercaptoethanol) before Western blot analysis with anti-ROCK1, anti-ROCK2 and anti-eGFP antibodies.

Western Blot and antibodies:

Appropriately treated cells were lysed with SDS sample buffer (62.5 mM Tris-HCl (pH 6.8), 2% SDS). Lysates were boiled in SDS sample buffer (described above) for 10 min. The samples were subjected to SDS-polyacrylamide gel electrophoresis (PAGE) using precast acrylamide gels (Thermofisher, NP0335BOX) and proteins were transferred to nitrocellulose membranes. Membranes were incubated for 30 min in Blocking Solution (Tris-buffered saline (TBS) containing 0.1% Tween-20, 3% BSA or 5% milk) and further incubated with the appropriate primary antibody diluted in Blocking solution at 4°C overnight. The membranes were then washed three times with TBS-Tween (0.1%) and incubated for 45 min with secondary antibody conjugated to horseradish peroxidase (HRP).Bound antibodies were detected with enhanced chemioluminescence.

The following primary antibodies were used at the indicated dilutions: HSC70 (1:4000, Santa Cruz, sc-59560), GAPDH-HRP (1:10000, Abcam, ab9482), ROCK1 (1:1000, Abcam, ab134181), ROCK2 (1:1000, Santa Cruz, sc-5561), FARP1 (1:100, Santa Cruz, sc-293249), FARP2 (1:50, Santa Cruz sc-390744), GFP (1:1000 Santa Cruz, sc-8334), eGFP (1:1000, Covance), RAC1 (1:500, BD Bioscience, 610650)

Immunofluorescence (IF) and antibodies

Samples were washed twice in PBS supplemented with calcium (0.1 mM) and magnesium (1 mM) (PBS-CM) and fixed in PFA (4%) diluted in PBS-CM for 10 min for coverslip and tissue section, 30 min for Caco-2 cysts and 45 min for tumoroids. Permeabilization was performed in PBS supplemented with 0.1% Triton X-100 during 10 min for coverslip and tissue section, 0.5% Triton X-100 during 30 min for Caco-2 cysts and tumoroids. Samples were washed and incubated with primary antibodies diluted in PBSwith 10% FBS (supplemented with 0.1% Triton X-100 for tumoroids) 1h at room temperature for coverlip, overnight at 4°C for Caco-2 cysts, tissue section and tumoroids. Then samples were washed in PBS (PBS-Tween20 0.05% for Caco-2 cysts and tumoroids) and incubated with secondary antibodies diluted in antibody diluent at least 45 min at room temperature. After washing, the coverslips and tissue section were mounted using Fluoromount-G (Southern Biotech, 0100-01).

The following primary antibodies were used at the indicated dilutions: ROCK1 (1:1000, Abcam, ab134181), ROCK2 (1:1000, Santa Cruz, sc-5561), E-cadherin (1:100, Abcam, ab1416), E-cadherin (1:100, Cell Signaling Technology, 3195S), phospho-ERM (1:100, Cell Signaling Technology, 3149), ezrin (1:100, BD Biosciences, 610603), ZO-1 (1:200, Invitrogen, 40-2300), beta-catenin (1:100, Thermo, MA1-300) alpha-catenin (1:100, Sigma Aldrich, C2081), Alexa Fluor™ Phalloidin 488 (1:200, Thermofischer, A12379).

Quantitative IF images analysis: Metamorph software was used to trace lines crossing the cell-cell contact of fixed Caco-2 cells plated on 2D coverslips overexpressing GFP-FARP2 and stained for ZO-1 junctional protein, for measurement of fluorescence intensity, at least 10 lines of 20 µm were measured around a cell. The ratio of GFP-FARP2:ZO-1 maximum intensities was calculated.

Histology and Immunohistochemistry:

Histology: Colorectal cancer specimens obtained after chirurgical resection were formalin-fixed and paraffin embedded (FFPE). 3 µm sections of FFPE samples were deparaffinised, demasked (pH 8) and rehydrated prior to Hematoxylin Eosin Saffron (HES) immunohistochemistry.

Immunohistochemistry: Sections were immunostained with CK20 specific mouse monoclonal antibody, (clone Ks20.8, Dako, Glostrup, Denmark) and Vimentin (Thermofisher, PA1-16759). Stainings were performed with Ventana BenchMark XT immunostainer (Ventana Medical Systems, Tucson, AZ) utilizing UltraView DABv3 kit (Ventana, 7600-500). The chromogene was 3,3'-diaminobenzidine (DAB) in all the stainings.

Caco-2 cysts morphogenesis: Caco-2 cysts were formed from single Caco-2 cells as follows*:* Matrigel was mixed with Rat-tail Collagen-Ineutralized with NaOH (1M), Hepes (1M) and MEM (10x) (Life Technologies, 21430-02) according to the ratio 0.843:0.025:0.032:0.1 (vol/vol/vol/vol), adjusted to the right concentration with DMEM 1X and allowed to polymerize in ice for 30 min before adding of Matrigel. The final concentration were 4.5 mg/ml for Matrigel, 1.3 mg/ml for Collagen-I. The mix was used to coat the wells of 8-well ibidi chamber (10 µL per well) and let to polymerize for 30 min at room temperature. Caco-2 cells were dissociated into single cells with trypsin-EDTA and resuspended in ice cold DMEM complete medium supplemented with Matrigel (2%), and cholera toxin (0.01µg/ml) (DMEM-MG-CT). The cell suspension was then added on top of the coating (10^5 cells per well) in the ibidi's well. The morphogenesis proceeded for 3 days at 37°C to allow formation of Caco-2 cysts.

Caco-2 cysts invasion assays:

Adapted boyden chamber invasion assay: Caco-2 cyst morphogenesis was allowed to proceed on the top chamber of the Boyden as follows: Matrigel was mixed with ice cold

DMEM 1X to a final concentration of 4.5 mg/ml, was used to coat the top side of the Boyden membrane (4 µl per membrane) and allow to polymerize at 37°C for 10 min. Caco-2 cells were dissociated into single cellsand resuspended in ice cold DMEM-MG-CT. The cell suspension was then added on top of the Boyden chamber and left to form cysts for 3 days at 37°C. Once the cysts were formed, a growth factor gradient between the top and bottom chamber of the Boyden was created by replacing the top's chamber complet medium with DMEM-MG-CT without FBS whereas the bottom chamber was renewed with DMEM-CT supplemented with FBS (10%). Caco-2 cells were allowed to invade through the pores of the Boyden of the membrane for 2 days with or without inhibitorsY27632 (25 µM) and H1152 (2 µM).

Invasion quantification: Invasion was defined as the number of cells that had gone through the pores of the Boyden chambers' separating membrane and were located on the bottom side of the membrane. Quantification was conducted in a segmentation automated way on cell nucleus stained with Hoechst using Metamorph software.

3D Organotypic invasion assay:

After morphogenesis or after transduction, the ibidi containing the Caco-2 cysts was recovered. The complete medium supplemented with 2% Matrigel or the lentiviruses containing complete medium was discarded, while the cysts remained adherent to the Matrigel/Collagen-I coating in the ibidi well. The Collagen-I at a final concentration of 1.3 mg/ml was adding on top of the Caco-2 cysts and allowed to polymerize 15 min at room temperature. Then CCD-18-CO cells conditioned medium supplemented with cholera toxin with or without inhibitors (NSC-23766 (200 µM), Y27632 (25 µM), H1152 (2 µM) and Blebbistatin (10-25µM)) was added in the wells. Caco-2 cysts were allowed to perform invasion for 2 days at 37°C=.

Caco-2 cyst invasion quantification: Collective invasion of the Caco-2 cysts was quantified by eyes assisted by microscopy, and F-actin staining of fixed sample. It was defined as the number of invasive cyst over total counted cysts. Invasive cysts were defined as the ones displaying cells with broad protrusions that remained attached to the rest of non-protruding cells of the cysts thereby breaking symmetry and inducing Leader/follower polarization of the cyst. At least 100 cysts per condition were counted in experiments with or without inhibitor (At least 50 cysts for ROCK2DN or FARP2 constructs induced by lentiviruses transduction of mature cysts).

Microscope assisted quantification, Microscopy acquisition and live imaging: Microscopy assisted eye-quantification of invasion was performed on, and images were acquired using an Olympus Epifluorescence inverted X73 microscope or a SpinningDisk CSU-W1 (Yokogawa) with a ZylasCMOC camera piloted with an Olympus X83. Patients samples behaviors in 3D culture were imaged by DIC time-lapse microscopy, motorized stage, temperature and CO2 controllers.

Statistical Analyses:

All errors indicated in the text are SEM for quantitative values or error margin for percentages. Non-parametric, unpaired t test was performed to determine whether the difference between two groups was significantly different in their mean value using Prism 6.

ACKNOWLEDGMENTS

We thank Fatiha Sangar for cloning the human version of the ROCK2 constructs published by Amano et al. We thank the members of the Jaulin lab and Digestive Cancer Unit for discussion. This work was supported by the French government PhD fellowship and "Fondation pour la recherche medicale" fourth year PhD fellowship to FL, the CNRS INSERM ATIP-AVENIR program and the Gustave Roussy foundation (Natixis, ANR PIA-IHUB) support to FJ.

AUTHOR CONTRIBUTIONS

FL designed, performed, analyzed experiments and wrote the manuscript. Additional experiments were performed by JR (Pulldowns), ZAT (siRNAs Myosin-II), OZ (Organoids) and JV (siRNA screens). PD, JYS and DG provided clinical samples and performed histological analyses. AH supported the siRNA screens. FJ conceived the project, designed the research, supervised the experimental design and wrote the manuscript. All provided intellectual input.

CONFLICT OF INTERESTS

The authors declare no competing financial interests.

REFERENCES

Alexander, S., Koehl, G.E., Hirschberg, M., Geissler, E.K., and Friedl, P. (2008). Dynamic imaging of cancer growth and invasion: a modified skin-fold chamber model. Histochem. Cell Biol. *130*, 1147–1154.

Aman, A., and Piotrowski, T. (2008). Wnt/beta-catenin and Fgf signaling control collective cell migration by restricting chemokine receptor expression. Dev. Cell *15*, 749–761.

Amano, M., Chihara, K., Nakamura, N., Kaneko, T., Matsuura, Y., and Kaibuchi, K. (1999). The COOH Terminus of Rho-kinase Negatively Regulates Rho-kinase Activity. J. Biol. Chem. *274*, 32418–32424.

Amano, M., Hamaguchi, T., Shohag, M.H., Kozawa, K., Kato, K., Zhang, X., Yura, Y.,

Matsuura, Y., Kataoka, C., Nishioka, T., et al. (2015). Kinase-interacting substrate screening is a novel method to identify kinase substrates. J Cell Biol *209*, 895–912.
Bianco, A., Poukkula, M., Cliffe, A., Mathieu, J., Luque, C.M., Fulga, T.A., and Rørth, P. (2007). Two distinct modes of guidance signalling during collective migration of border cells. Nature *448*, 362–365.
Cai, D., Chen, S.-C., Prasad, M., He, L., Wang, X., Choesmel-Cadamuro, V., Sawyer, J.K., Danuser, G., and Montell, D.J. (2014). Mechanical Feedback through E-Cadherin Promotes Direction Sensing during Collective Cell Migration. Cell *157*, 1146–1159.
Chaffer, C.L., Juan, B.P.S., Lim, E., and Weinberg, R.A. (2016). EMT, cell plasticity and metastasis. Cancer Metastasis Rev. *35*, 645–654.
Cheadle, L., and Biederer, T. (2012). The novel synaptogenic protein Farp1 links postsynaptic cytoskeletal dynamics and transsynaptic organization. J. Cell Biol. *199*, 985–1001.
Cheadle, L., and Biederer, T. (2014). Activity-Dependent Regulation of Dendritic Complexity by Semaphorin 3A through Farp1. J. Neurosci. Off. J. Soc. Neurosci. *34*, 7999–8009.
Cheung, K.J., and Ewald, A.J. (2016). A collective route to metastasis: Seeding by tumor cell clusters. Science *352*, 167–169.
Cheung, K.J., Gabrielson, E., Werb, Z., and Ewald, A.J. (2013). Collective invasion in breast cancer requires a conserved basal epithelial program. Cell *155*, 1639–1651.
Croft, D.R., Sahai, E., Mavria, G., Li, S., Tsai, J., Lee, W.M.F., Marshall, C.J., and Olson, M.F. (2004). Conditional ROCK activation in vivo induces tumor cell dissemination and angiogenesis. Cancer Res. *64*, 8994–9001.
Duchek, P., Somogyi, K., Jékely, G., Beccari, S., and Rørth, P. (2001). Guidance of cell migration by the Drosophila PDGF/VEGF receptor. Cell *107*, 17–26.
Dupont, S., Morsut, L., Aragona, M., Enzo, E., Giulitti, S., Cordenonsi, M., Zanconato, F., Le Digabel, J., Forcato, M., Bicciato, S., et al. (2011). Role of YAP/TAZ in mechanotransduction. Nature *474*, 179–183.
Durdu, S., Iskar, M., Revenu, C., Schieber, N., Kunze, A., Bork, P., Schwab, Y., and Gilmour, D. (2014). Luminal signalling links cell communication to tissue architecture during organogenesis. Nature *515*, 120–124.
Elias, D., Lefevre, J.H., Chevalier, J., Brouquet, A., Marchal, F., Classe, J.-M., Ferron, G., Guilloit, J.-M., Meeus, P., Goéré, D., et al. (2009). Complete cytoreductive surgery plus intraperitoneal chemohyperthermia with oxaliplatin for peritoneal carcinomatosis of colorectal origin. J. Clin. Oncol. Off. J. Am. Soc. Clin. Oncol. *27*, 681–685.
Ellenbroek, S.I.J., Iden, S., and Collard, J.G. (2012). The Rac activator Tiam1 is required for polarized protrusional outgrowth of primary astrocytes by affecting the organization of the microtubule network. Small GTPases *3*, 4–14.
Even-Ram, S., Doyle, A.D., Conti, M.A., Matsumoto, K., Adelstein, R.S., and Yamada, K.M. (2007). Myosin IIA regulates cell motility and actomyosin-microtubule crosstalk. Nat. Cell Biol. *9*, 299–309.
Ewald, A.J., Huebner, R.J., Palsdottir, H., Lee, J.K., Perez, M.J., Jorgens, D.M., Tauscher, A.N., Cheung, K.J., Werb, Z., and Auer, M. (2012). Mammary collective cell migration involves transient loss of epithelial features and individual cell migration within the epithelium. J. Cell Sci. *125*, 2638–2654.
Ferlay, J., Soerjomataram, I., Dikshit, R., Eser, S., Mathers, C., Rebelo, M., Parkin, D.M.,

Forman, D., and Bray, F. (2015). Cancer incidence and mortality worldwide: sources, methods and major patterns in GLOBOCAN 2012. Int. J. Cancer J. Int. Cancer *136*, E359–86.
Fischer, K.R., Durrans, A., Lee, S., Sheng, J., Li, F., Wong, S.T.C., Choi, H., El Rayes, T., Ryu, S., Troeger, J., et al. (2015). Epithelial-to-mesenchymal transition is not required for lung metastasis but contributes to chemoresistance. Nature *527*, 472–476.
Fischer, R.S., Gardel, M., Ma, X., Adelstein, R.S., and Waterman, C.M. (2009). Local cortical tension by myosin II guides 3D endothelial cell branching. Curr. Biol. CB *19*, 260–265.
Fleming, M., Ravula, S., Tatishchev, S.F., and Wang, H.L. (2012). Colorectal carcinoma: Pathologic aspects. J. Gastrointest. Oncol. *3*, 153–173.
Friedl, P. (2004). Prespecification and plasticity: shifting mechanisms of cell migration. Curr. Opin. Cell Biol. *16*, 14–23.
Friedl, P., and Alexander, S. (2011). Cancer Invasion and the Microenvironment: Plasticity and Reciprocity. Cell *147*, 992–1009.
Friedl, P., Noble, P.B., Walton, P.A., Laird, D.W., Chauvin, P.J., Tabah, R.J., Black, M., and Zänker, K.S. (1995). Migration of Coordinated Cell Clusters in Mesenchymal and Epithelial Cancer Explants in Vitro. Cancer Res. *55*, 4557–4560.
Friedl, P., Locker, J., Sahai, E., and Segall, J.E. (2012). Classifying collective cancer cell invasion. Nat. Cell Biol. *14*, 777–783.
Giampieri, S., Manning, C., Hooper, S., Jones, L., Hill, C.S., and Sahai, E. (2009). Localized and reversible TGFβ signalling switches breast cancer cells from cohesive to single cell motility. Nat. Cell Biol. *11*, 1287–1296.
Haas, P., and Gilmour, D. (2006). Chemokine signaling mediates self-organizing tissue migration in the zebrafish lateral line. Dev. Cell *10*, 673–680.
He, X., Kuo, Y.-C., Rosche, T.J., and Zhang, X. (2013). Structural Basis for Autoinhibition of the Guanine Nucleotide Exchange Factor FARP2. Structure *21*, 355–364.
Hidalgo-Carcedo, C., Hooper, S., Chaudhry, S.I., Williamson, P., Harrington, K., Leitinger, B., and Sahai, E. (2011). Collective cell migration requires suppression of actomyosin at cell-cell contacts mediated by DDR1 and the cell polarity regulators Par3 and Par6. Nat. Cell Biol. *13*, 49–58.
Itoh, K., Yoshioka, K., Akedo, H., Uehata, M., Ishizaki, T., and Narumiya, S. (1999). An essential part for Rho–associated kinase in the transcellular invasion of tumor cells. Nat. Med. *5*, 221–225.
Julien, S., Merino-Trigo, A., Lacroix, L., Pocard, M., Goéré, D., Mariani, P., Landron, S., Bigot, L., Nemati, F., Dartigues, P., et al. (2012). Characterization of a large panel of patient-derived tumor xenografts representing the clinical heterogeneity of human colorectal cancer. Clin. Cancer Res. Off. J. Am. Assoc. Cancer Res. *18*, 5314–5328.
Khalil, A.A., Ilina, O., Gritsenko, P.G., Bult, P., Span, P.N., and Friedl, P. (2017). Collective invasion in ductal and lobular breast cancer associates with distant metastasis. Clin. Exp. Metastasis 1–9.
Kim, H., and Verhaak, R.G.W. (2015). Transcriptional mimicry by tumor-associated stroma. Nat. Genet. *47*, ng.3255.
Konen, J., Summerbell, E., Dwivedi, B., Galior, K., Hou, Y., Rusnak, L., Chen, A., Saltz, J., Zhou, W., Boise, L.H., et al. (2017). Image-guided genomics of phenotypically heterogeneous populations reveals vascular signalling during symbiotic collective cancer invasion. Nat.

Commun. *8*, 15078.
Koyano, Y., Kawamoto, T., Shen, M., Yan, W., Noshiro, M., Fujii, K., and Kato, Y. (1997). Molecular cloning and characterization of CDEP, a novel human protein containing the ezrin-like domain of the band 4.1 superfamily and the Dbl homology domain of Rho guanine nucleotide exchange factors. Biochem. Biophys. Res. Commun. *241*, 369–375.
Koyano, Y., Kawamoto, T., Kikuchi, A., Shen, M., Kuruta, Y., Tsutsumi, S., Fujimoto, K., Noshiro, M., Fujii, K., and Kato§, Y. (2001). Chondrocyte-derived ezrin-like domain containing protein (CDEP), a rho guanine nucleotide exchange factor, is inducible in chondrocytes by parathyroid hormone and cyclic AMP and has transforming activity in NIH3T3 Cells. Osteoarthritis Cartilage *9*, *Supplement 1*, S64–S68.
Kubo, T., Yamashita, T., Yamaguchi, A., Sumimoto, H., Hosokawa, K., and Tohyama, M. (2002). A novel FERM domain including guanine nucleotide exchange factor is involved in Rac signaling and regulates neurite remodeling. J. Neurosci. Off. J. Soc. Neurosci. *22*, 8504–8513.
Kwon, S.-H., Liu, K.D., and Mostov, K.E. (2014). Intercellular transfer of GPRC5B via exosomes drives HGF-mediated outward growth. Curr. Biol. CB *24*, 199–204.
Liu, Y.-J., Le Berre, M., Lautenschlaeger, F., Maiuri, P., Callan-Jones, A., Heuzé, M., Takaki, T., Voituriez, R., and Piel, M. (2015). Confinement and low adhesion induce fast amoeboid migration of slow mesenchymal cells. Cell *160*, 659–672.
Lomakin, A.J., Lee, K.-C., Han, S.J., Bui, D.A., Davidson, M., Mogilner, A., and Danuser, G. (2015). Competition for actin between two distinct F-actin networks defines a bistable switch for cell polarization. Nat. Cell Biol. *17*, 1435–1445.
Migeotte, I., Omelchenko, T., Hall, A., and Anderson, K.V. (2010). Rac1-Dependent Collective Cell Migration Is Required for Specification of the Anterior-Posterior Body Axis of the Mouse. PLOS Biol. *8*, e1000442.
Miyamoto, Y., Yamauchi, J., and Itoh, H. (2003). Src Kinase Regulates the Activation of a Novel FGD-1-related Cdc42 Guanine Nucleotide Exchange Factor in the Signaling Pathway from the Endothelin A Receptor to JNK. J. Biol. Chem. *278*, 29890–29900.
Mlechkovich, G., Peng, S.-S., Shacham, V., Martinez, E., Gokhman, I., Minis, A., Tran, T.S., and Yaron, A. (2014). Distinct Cytoplasmic Domains in Plexin-A4 Mediate Diverse Responses to Semaphorin 3A in Developing Mammalian Neurons. Sci. Signal. *7*, ra24.
Narumiya, S., Tanji, M., and Ishizaki, T. (2009). Rho signaling, ROCK and mDia1, in transformation, metastasis and invasion. Cancer Metastasis Rev. *28*, 65–76.
Nieto, M.A., Huang, R.Y.-J., Jackson, R.A., and Thiery, J.P. (2016). EMT: 2016. Cell *166*, 21–45.
Ohta, Y., Hartwig, J.H., and Stossel, T.P. (2006). FilGAP, a Rho- and ROCK-regulated GAP for Rac binds filamin A to control actin remodelling. Nat. Cell Biol. *8*, 803–814.
Omelchenko, T., and Hall, A. (2012). Myosin-IXA regulates collective epithelial cell migration by targeting RhoGAP activity to cell-cell junctions. Curr. Biol. CB *22*, 278–288.
Omelchenko, T., Vasiliev, J.M., Gelfand, I.M., Feder, H.H., and Bonder, E.M. (2003). Rho-dependent formation of epithelial "leader" cells during wound healing. Proc. Natl. Acad. Sci. *100*, 10788–10793.
Omelchenko, T., Rabadan, M.A., Hernández-Martínez, R., Grego-Bessa, J., Anderson, K.V., and Hall, A. (2014). β-Pix directs collective migration of anterior visceral endoderm cells in

the early mouse embryo. Genes Dev. *28*, 2764–2777.
Orgaz, J.L., Pandya, P., Dalmeida, R., Karagiannis, P., Sanchez-Laorden, B., Viros, A., Albrengues, J., Nestle, F.O., Ridley, A.J., Gaggioli, C., et al. (2014). Diverse matrix metalloproteinase functions regulate cancer amoeboid migration. Nat. Commun. *5*, 4255.
Osmani, N., Vitale, N., Borg, J.-P., and Etienne-Manneville, S. (2006). Scrib controls Cdc42 localization and activity to promote cell polarization during astrocyte migration. Curr. Biol. CB *16*, 2395–2405.
Osmani, N., Peglion, F., Chavrier, P., and Etienne-Manneville, S. (2010). Cdc42 localization and cell polarity depend on membrane traffic. J. Cell Biol. *191*, 1261–1269.
Paluch, E.K., and Raz, E. (2013). The role and regulation of blebs in cell migration. Curr. Opin. Cell Biol. *25*, 582–590.
Prall, F., Ostwald, C., and Linnebacher, M. (2009). Tubular invasion and the morphogenesis of tumor budding in colorectal carcinoma. Hum. Pathol. *40*, 1510–1512.
Reffay, M., Parrini, M.C., Cochet-Escartin, O., Ladoux, B., Buguin, A., Coscoy, S., Amblard, F., Camonis, J., and Silberzan, P. (2014). Interplay of RhoA and mechanical forces in collective cell migration driven by leader cells. Nat. Cell Biol. *16*, 217–223.
Revenu, C., Streichan, S., Donà, E., Lecaudey, V., Hufnagel, L., and Gilmour, D. (2014). Quantitative cell polarity imaging defines leader-to-follower transitions during collective migration and the key role of microtubule-dependent adherens junction formation. Dev. Camb. Engl. *141*, 1282–1291.
Ridley, A.J. (2015). Rho GTPase signalling in cell migration. Curr. Opin. Cell Biol. *36*, 103–112.
Ridley, A.J., Schwartz, M.A., Burridge, K., Firtel, R.A., Ginsberg, M.H., Borisy, G., Parsons, J.T., and Horwitz, A.R. (2003). Cell Migration: Integrating Signals from Front to Back. Science *302*, 1704–1709.
Sadok, A., and Marshall, C.J. (2014). Rho GTPases: masters of cell migration. Small GTPases *5*, e29710.
Sadok, A., McCarthy, A., Caldwell, J., Collins, I., Garrett, M.D., Yeo, M., Hooper, S., Sahai, E., Kuemper, S., Mardakheh, F.K., et al. (2015). Rho Kinase Inhibitors Block Melanoma Cell Migration and Inhibit Metastasis. Cancer Res. *75*, 2272–2284.
Sahai, E., and Marshall, C.J. (2003). Differing modes of tumour cell invasion have distinct requirements for Rho/ROCK signalling and extracellular proteolysis. Nat. Cell Biol. *5*, 711–719.
Sahai, E., Olson, M.F., and Marshall, C.J. (2001). Cross-talk between Ras and Rho signalling pathways in transformation favours proliferation and increased motility. EMBO J. *20*, 755–766.
Salhia, B., Rutten, F., Nakada, M., Beaudry, C., Berens, M., Kwan, A., and Rutka, J.T. (2005). Inhibition of Rho-kinase affects astrocytoma morphology, motility, and invasion through activation of Rac1. Cancer Res. *65*, 8792–8800.
Samuel, M.S., Lopez, J.I., McGhee, E.J., Croft, D.R., Strachan, D., Timpson, P., Munro, J., Schröder, E., Zhou, J., Brunton, V.G., et al. (2011). Actomyosin-mediated cellular tension drives increased tissue stiffness and β-catenin activation to induce epidermal hyperplasia and tumor growth. Cancer Cell *19*, 776–791.
Sanz-Moreno, V., Gadea, G., Ahn, J., Paterson, H., Marra, P., Pinner, S., Sahai, E., and

Marshall, C.J. (2008). Rac Activation and Inactivation Control Plasticity of Tumor Cell Movement. Cell *135*, 510–523.
Sanz-Moreno, V., Gaggioli, C., Yeo, M., Albrengues, J., Wallberg, F., Viros, A., Hooper, S., Mitter, R., Féral, C.C., Cook, M., et al. (2011). ROCK and JAK1 Signaling Cooperate to Control Actomyosin Contractility in Tumor Cells and Stroma. Cancer Cell *20*, 229–245.
Sato, T., and Clevers, H. (2013). Growing self-organizing mini-guts from a single intestinal stem cell: mechanism and applications. Science *340*, 1190–1194.
Schramek, D., Sendoel, A., Segal, J.P., Beronja, S., Heller, E., Oristian, D., Reva, B., and Fuchs, E. (2014). Direct in vivo RNAi screen unveils myosin IIa as a tumor suppressor of squamous cell carcinomas. Science *343*, 309–313.
Takegahara, N., Kang, S., Nojima, S., Takamatsu, H., Okuno, T., Kikutani, H., Toyofuku, T., and Kumanogoh, A. (2010). Integral roles of a guanine nucleotide exchange factor, FARP2, in osteoclast podosome rearrangements. FASEB J. *24*, 4782–4792.
Toyofuku, T., Yoshida, J., Sugimoto, T., Zhang, H., Kumanogoh, A., Hori, M., and Kikutani, H. (2005). FARP2 triggers signals for Sema3A-mediated axonal repulsion. Nat. Neurosci. *8*, 1712–1719.
Tsuji, T., Ishizaki, T., Okamoto, M., Higashida, C., Kimura, K., Furuyashiki, T., Arakawa, Y., Birge, R.B., Nakamoto, T., Hirai, H., et al. (2002). ROCK and mDia1 antagonize in Rho-dependent Rac activation in Swiss 3T3 fibroblasts. J. Cell Biol. *157*, 819–830.
Valastyan, S., and Weinberg, R.A. (2011). Tumor metastasis: molecular insights and evolving paradigms. Cell *147*, 275–292.
Vicente-Manzanares, M., Ma, X., Adelstein, R.S., and Horwitz, A.R. (2009). Non-muscle myosin II takes centre stage in cell adhesion and migration. Nat. Rev. Mol. Cell Biol. *10*, 778–790.
Voorneveld, P.W., Kodach, L.L., Jacobs, R.J., Liv, N., Zonnevylle, A.C., Hoogenboom, J.P., Biemond, I., Verspaget, H.W., Hommes, D.W., de Rooij, K., et al. (2014). Loss of SMAD4 alters BMP signaling to promote colorectal cancer cell metastasis via activation of Rho and ROCK. Gastroenterology *147*, 196–208.e13.
Wang, X., He, L., Wu, Y.I., Hahn, K.M., and Montell, D.J. (2010). Light-mediated activation reveals a key role for Rac in collective guidance of cell movement in vivo. Nat. Cell Biol. *12*, 591–597.
Westcott, J.M., Prechtl, A.M., Maine, E.A., Dang, T.T., Esparza, M.A., Sun, H., Zhou, Y., Xie, Y., and Pearson, G.W. (2015). An epigenetically distinct breast cancer cell subpopulation promotes collective invasion. J. Clin. Invest. *125*, 1927–1943.
Wolf, K., Mazo, I., Leung, H., Engelke, K., Andrian, U.H. von, Deryugina, E.I., Strongin, A.Y., Bröcker, E.-B., and Friedl, P. (2003). Compensation mechanism in tumor cell migration. J. Cell Biol. *160*, 267–277.
Yamaguchi, N., Mizutani, T., Kawabata, K., and Haga, H. (2015). Leader cells regulate collective cell migration via Rac activation in the downstream signaling of integrin β1 and PI3K. Sci. Rep. *5*, srep07656.
Zaritsky, A., Tseng, Y.-Y., Rabadán, M.A., Krishna, S., Overholtzer, M., Danuser, G., and Hall, A. (2017). Diverse roles of guanine nucleotide exchange factors in regulating collective cell migration. J. Cell Biol. *216*, 1543–1556.
Zheng, X., Carstens, J.L., Kim, J., Scheible, M., Kaye, J., Sugimoto, H., Wu, C.-C., LeBleu,

V.S., and Kalluri, R. (2015). Epithelial-to-mesenchymal transition is dispensable for metastasis but induces chemoresistance in pancreatic cancer. Nature *527*, 525–530.
Zhuang, B., Su, Y.S., and Sockanathan, S. (2009). FARP1 promotes the dendritic growth of spinal motor neuron subtypes through transmembrane Semaphorin6A and PlexinA4 signaling. Neuron *61*, 359–372.

	Name	Accession #	Dharmacon Catalog #		Name	Accession #	Dharmacon Catalog #		Name	Accession #	Dharmacon Catalog #
1	SWAP70	NM_015055	M-010323-00	**27**	ECT2	NM_018098	M-006450-00	**53**	ARHGEF9	XM_377014	M-020314-00
2	SGEF	NM_015595	M-009833-00	**28**	FARP1	NM_005766	M-008519-01	**54**	ARHGEF6	NM_004840	M-010231-00
3	PREX1	NM_020820	M-010063-00	**29**	FARP2	XM_376193	M-009237-01	**55**	ARHGEF7	NM_003899	M-009616-00
4	ARHGEF16	NM_014448	M-010234-00	**30**	ABR	NM_001092	M-008611-00	**56**	RASGRF1	NM_002891	M-009323-00
5	FLJ10521	NM_018125	M-017096-00	**31**	ALS2	NM_020919	M-014168-01	**57**	RASGRF2	NM_006909	M-024516-01
6	FGD6	XM_370702	M-026895-00	**32**	ARHGEF3	NM_019555	M-013243-00	**58**	SOS1	NM_005633	M-005194-01
7	DNMBP	NM_015221	M-026304-00	**33**	ARHGEF4	NM_015320	M-008235-00	**59**	SOS2	NM_006939	M-005195-01
8	MCF2	NM_005369	M-003904-01	**34**	ARHGEF10	NM_014629	M-013460-00	**60**	TIAM1	NM_003253	M-003932-00
9	MCF2L	NM_024979	M-010098-00	**35**	ARHGEF15	NM_173728	M-009731-00	**61**	TIAM2	NM_012454	M-008434-01
10	DOCK4	NM_014705	M-017968-00	**36**	BCR	NM_004327	M-003875-04	**62**	ARHGEF5	NM_005435	M-005093-00
11	DOCK5	NM_024940	M-018931-00	**37**	PLEKHG2	NM_022835	M-023690-00	**63**	TRIO	NM_007118	M-005047-00
12	DOCK6	NM_020812	M-031950-00	**38**	DOCK1	NM_001380	M-011253-00	**64**	VAV1	NM_005428	M-003935-01
13	DOCK7	NM_033407	M-031725-00	**39**	DOCK2	NM_004946	M-019915-00	**65**	VAV2	NM_003371	M-005199-00
14	DOCK8	NM_203447	M-026106-00	**40**	DOCK3	NM_004947	M-012695-00	**66**	VAV3	NM_006113	M-010178-01
15	NGEF	NM_019850	M-009354-00	**41**	FLJ10665	NM_018173	M-020318-00	**67**	FGD5	XM_371619	M-028077-00
16	FGD2	NM_173558	M-008431-00	**42**	NET1	NM_005863	M-003915-01	**68**	PLEKHG1	XM_027307	M-024745-00
17	SPATA13	NM_153023	M-015469-00	**43**	C9ORF100	NM_032818	M-015006-00	**69**	RGNEF	XM_371755	M-024506-01
18	MCF2L2	NM_015078	M-009313-00	**44**	FLJ20148	NM_017700	M-020676-00	**70**	FLJ10357	XM_370737	M-030269-00
19	DEF6	NM_022047	M-017817-00	**45**	ITSN1	NM_003024	M-008365-00	**71**	KIAA1909	NM_052909	M-031878-00
20	FGD4	NM_139241	M-007123-00	**46**	ITSN2	NM_006277	M-009841-00	**72**	FLJ46688	NM_001004330	M-032389-00
21	ARHGEF19	NM_153213	M-008370-01	**47**	ARHGEF12	NM_015313	M-008480-00	**73**	LOC345930	XM_294019	M-024733-00
22	FGD3	NM_033086	M-010371-00	**48**	ARHGEF2	NM_004723	M-009883-01	**74**	DOCK11	NM_144658	M-015696-00
23	DOCK10	XM_371595	M-023079-00	**49**	ARHGEF18	NM_015318	M-009654-00	**75**	FGD1	NM_004463	M-009612-01
24	KIAA0720	NM_020631	M-013873-00	**50**	ARHGEF1	NM_004706	M-009421-00	**76**	KALRN	NM_003947	M-010019-00
25	DOCK9	NM_015296	M-014040-00	**51**	ARHGEF17	NM_014786	M-009751-01	**77**	PLEKHG4	NM_015432	M-022573-00
26	AKAP13	NM_006738	M-008868-01	**52**	ARHGEF11	NM_014784	M-010360-00	**78**	PLEKHG3	NM_015549	M-022051-01

Table 1: List of RhoGTPase effectors, corresponding accession number and siRNA Dharmacon catalog number

Pair	Genes	Pair	Genes
1	ABR + BCR	**21**	DOCK9 + DOCK11
2	ARHGEF18 + RGNEF	**22**	DOCK8 + DOCK10
3	ARHGEF2 + AKAP13	**23**	ECT2 + FLJ10357
4	ARHGEF11 + ARHGEF12	**24**	FARP1 + FARP2
5	ARHGEF1 + ALS2	**25**	FGD6 + FGD5
6	ARHGEF10 + FLJ10521	**26**	FGD3 + FGD1
7	SGEF + ARHGEF16	**27**	FGD2 + FGD4
8	ARHGEF19 + ARHGEF5	**28**	KIAA1909 + PLEKHG4
9	NGEF + ARHGEF15	**29**	KALRN + TRIO
10	ARHGEF14 + ARHGEF9	**30**	MCF2 + MCF2L
11	ARHGEF3 + NET1	**31**	MCF2L2 + PLEKHG1
12	ARHGEF4 + SPATA13	**32**	PLEKHG2 + PLEKHG3
13	ARHGEF6 + ARHGEF7	**33**	KIAA0720 + FLJ10665
14	LOC345930 + C9ORF100	**34**	FLJ46688 + VAV2
15	DEF6 + SWAP70	**35**	RASGRF1 + RASGRF2
16	PREX1 + DOCK2	**36**	SOS1 + SOS2
17	DNMBP + FLJ20148	**37**	TIAM1 + TIAM2
18	DOCK1 + DOCK5	**38**	VAV1 + VAV3
19	DOCK3 + DOCK4	**39**	ITSN1 + ITSN2
20	DOCK6 + DOCK7	**40**	siGlo

Suppl Table 2 : Pairs of homologous Guanine Exchange Factors genes

Supplementary Figure 1

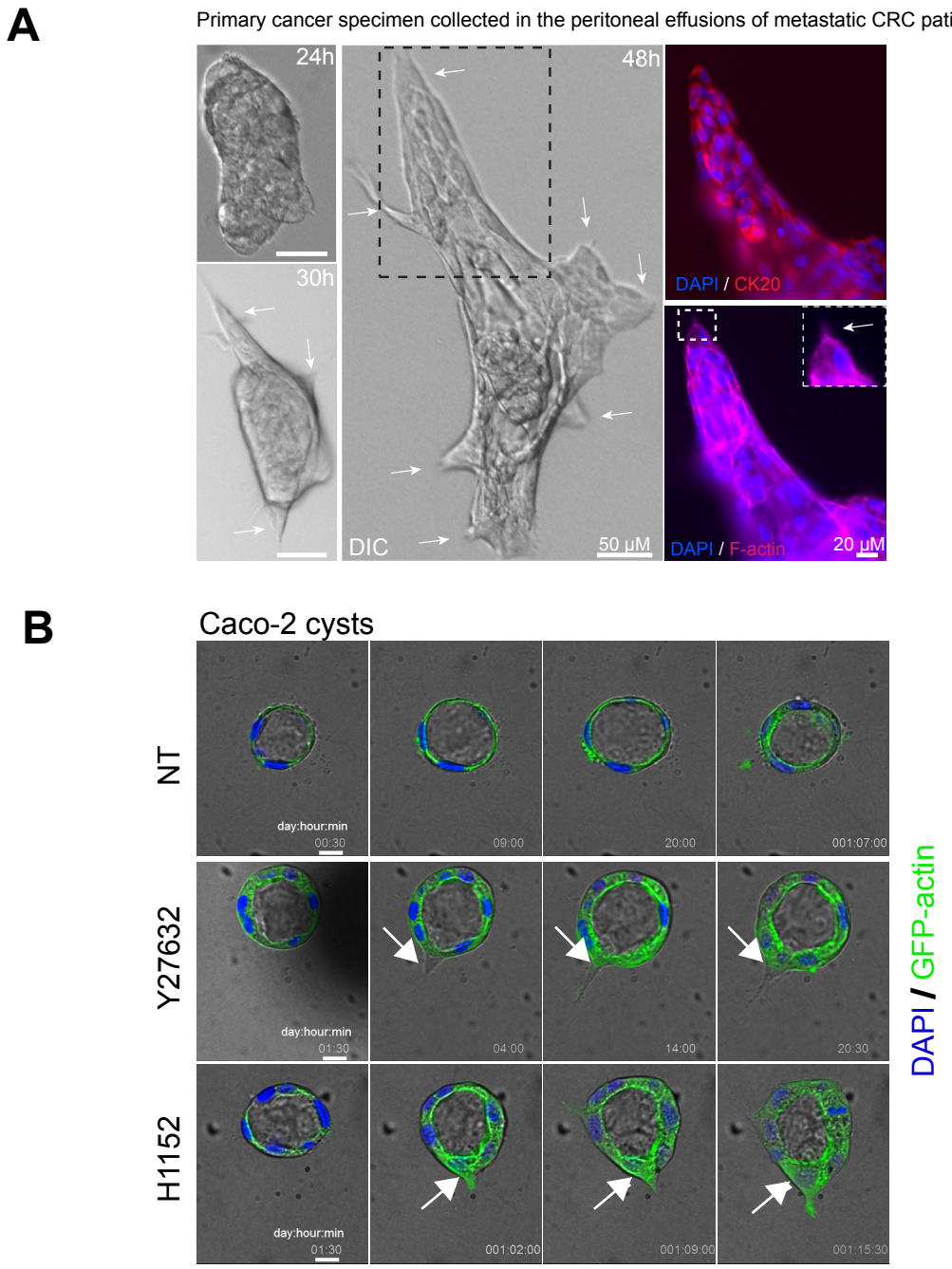

Supplementary Figure 1

(A) Left panel shows time lapse images of collective cell invasion by DIC microscopy from patient tumor specimen collected in the peritoneal effusion of metastatic CRC. White arrows point to the invasive pole. After 48 h of invasion in collagen-I, the sample was fixed and stained for cytokeratin20 (CK20), F-actin (Phalloidin) and nuclei (DAPI). Right panel shows a high magnification of the black boxed region White boxed region is shown at high magnification of a protruding invasive pole and white arrow point to actin rich protrusion.

(B) Time lapse images of Caco-2 cysts stably expressing GFP-actin in control condition or treated with Y27632 or H1152. White arrows point to the actin rich protrusive leader cell. Time is displayed as day and hh:mm.

(C) Immunoblot analysis of E-cadherin, Keratin, N-cadherin and Vimentin expression in Caco-2 cysts grown in control condition or transfected with siRNAs ROCK1 and ROCK2 (siROCK1+2) or treated with Y27632.

Supplementary Figure 2

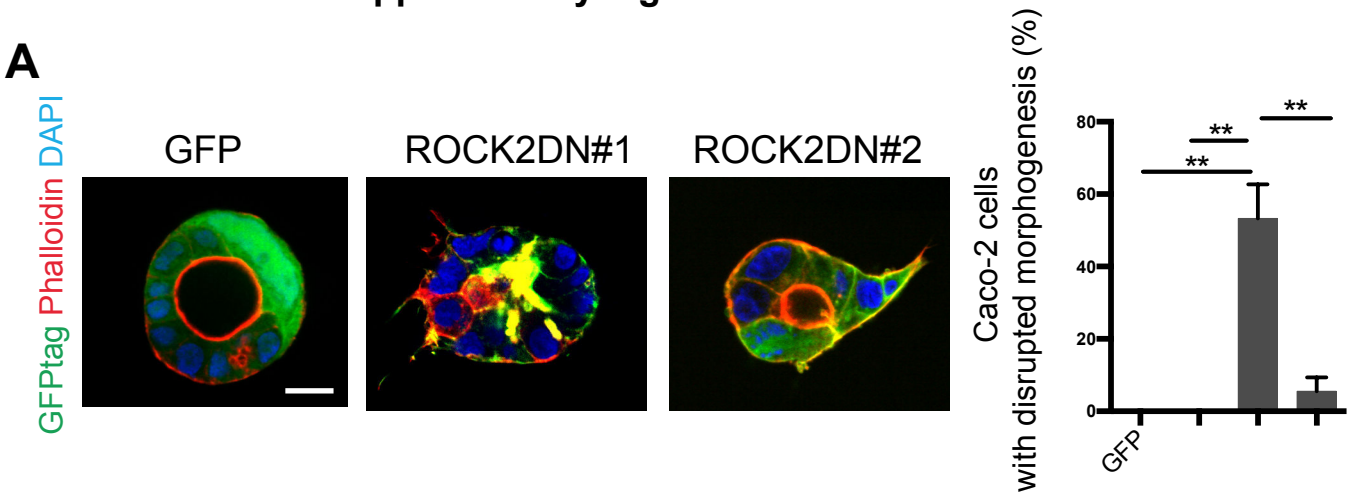

Supplementary figure 2

Left panel Caco-2 cysts stably expressing GFP alone or GFP-ROCK2DN#2, were submitted to 2 days long invasion assay, fixed and stained for F-actin. Right panel, Caco-2 cysts with disrupted morphogenesis (multilumens and non circular) were quantified and reported in bar graph as rate of disrupted morphogenesis (Means ± SEM of more than 3 independent experiments) (unpaired t-test, ****p<0.0001, ***p<0.001, **p<0.01 n.s: non significant). Scale bars: 20 µ m

Supplementary Figure 3

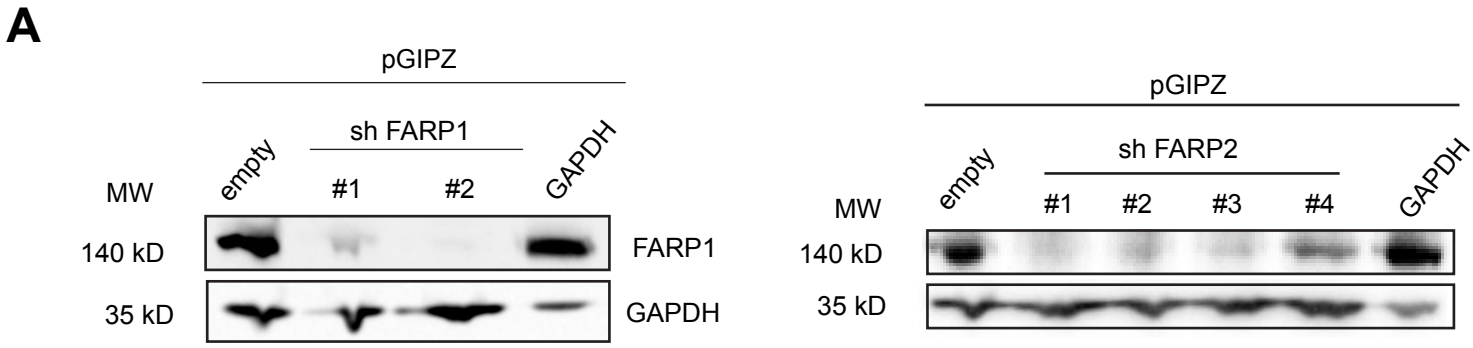

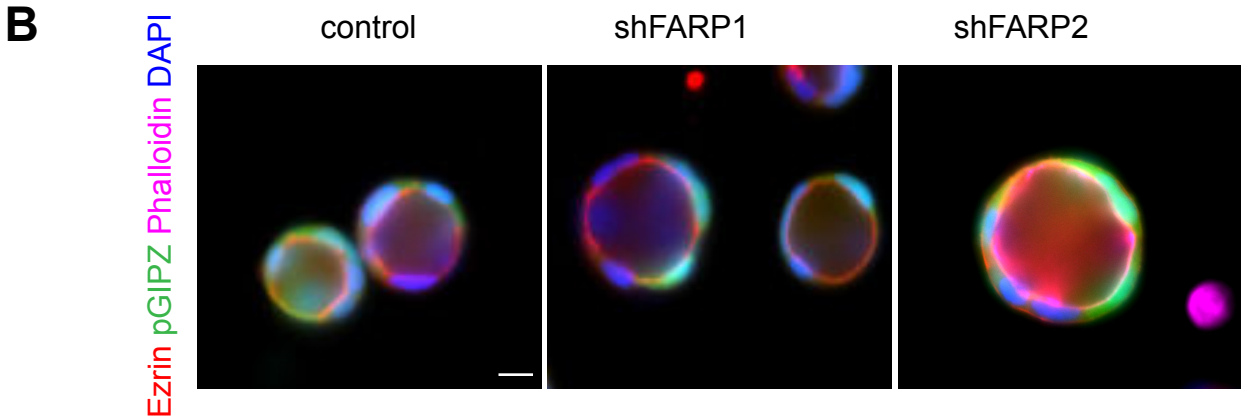

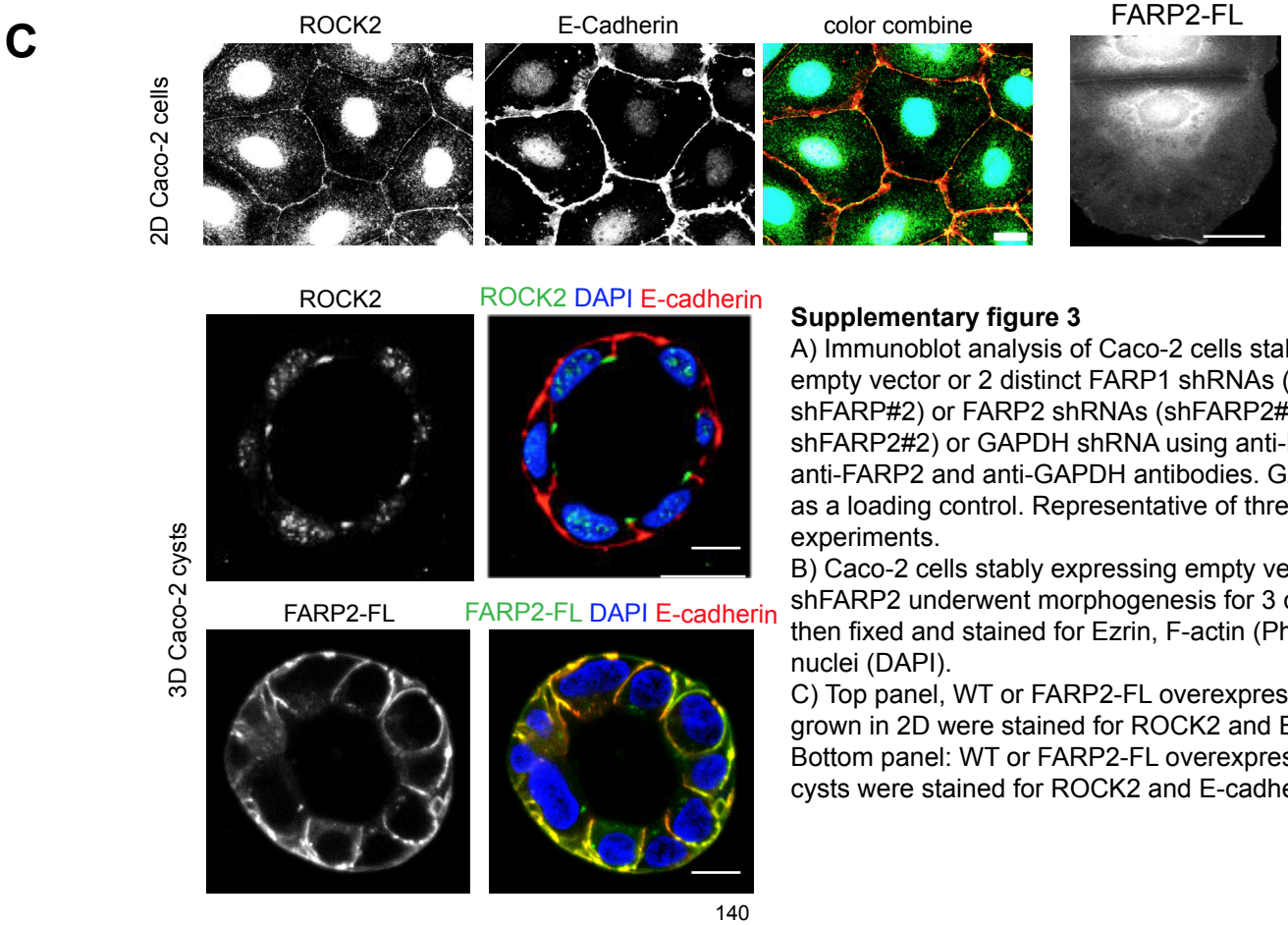

Supplementary figure 3
A) Immunoblot analysis of Caco-2 cells stably expressing empty vector or 2 distinct FARP1 shRNAs (shFARP#1 and shFARP#2) or FARP2 shRNAs (shFARP2#1 and shFARP2#2) or GAPDH shRNA using anti-FARP1, anti-FARP2 and anti-GAPDH antibodies. GAPDH was used as a loading control. Representative of three independent experiments.
B) Caco-2 cells stably expressing empty vector, shFARP1 or shFARP2 underwent morphogenesis for 3 days and were then fixed and stained for Ezrin, F-actin (Phalloidin) and nuclei (DAPI).
C) Top panel, WT or FARP2-FL overexpressing Caco-2 cells grown in 2D were stained for ROCK2 and E-Cadherin. Bottom panel: WT or FARP2-FL overexpressing 3D Caco-2 cysts were stained for ROCK2 and E-cadherin.

Supplementary Figure 4

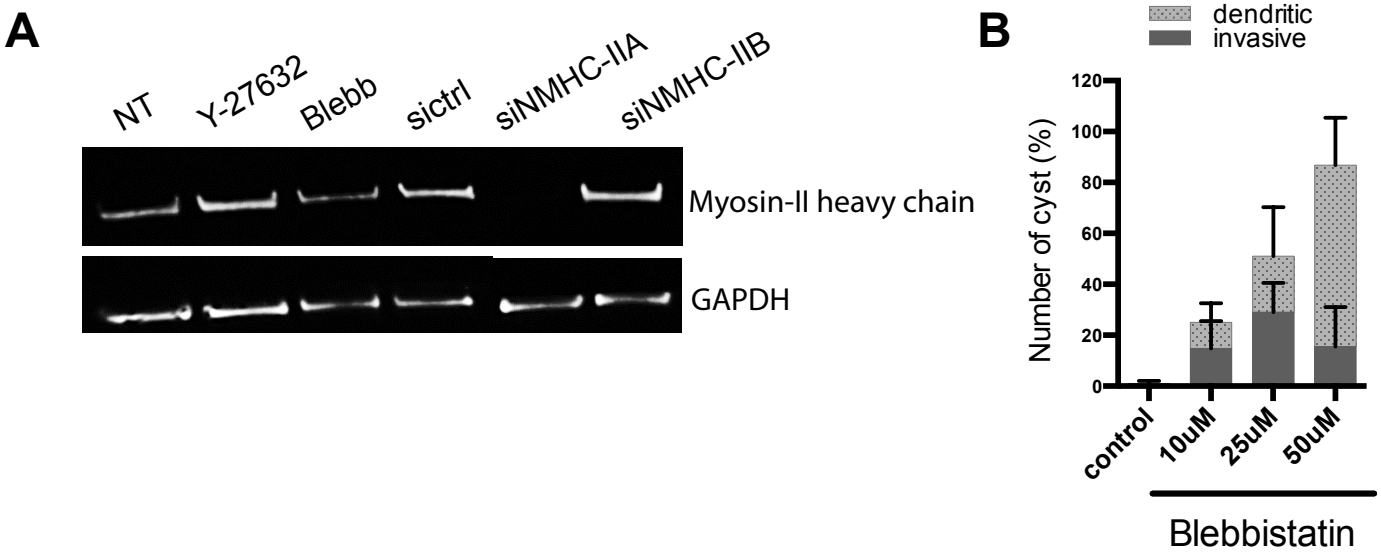

Supplementary figure 4

A) Immunoblot analysis of myosin-II expression in Caco-2 cysts treated with ROCK inhibitor Y27632 or MyosinII inhibitor Blebbistatin, or transfected with siRNA targeting Myosin-IIA or Myosin-IIB (siMyosin-IIA or siMyosin-IIB) GAPDH is used as a loading control. The experiment was repeated three times. B) The invasive phenotype and “dendritic” phenotype of Caco-2 treated with increasing concentrations of Myosin-II inhibitors Blebbistatin was quantified and represented as percentage on a bar graph.

Collective epithelial-based metastatic cascade in colorectal carcinoma patients

Foreword

This third part of my results section is a work conducted in the lab by Olivier Zajac and to which I contributed. Here is the complete manuscript of the paper, which is accepted for publication in Nature Cell Biology.

This study investigated the metastatic dissemination of CRC to the peritoneum in patients. Olivier Zajac et al. identified cluster of cancers cells, with an inverted apico-basolateral polarity axis, which was kept throughout dissemination. These cluster were termed TSIPs.

My aim was 1) to understand how TSIPs inverted polarity came about and 2) to determine whether Rho-GTPases dependent signaling pathways contributed to their invasion.

To address these questions, I used LS174T cell lines clusters with normal apico-basolateral polarity in 3D matrices and evaluated the impact of polarity proteins depletion by shRNA on the orientation of their polarity axis. I then used *in vitro* models of TSIPs generated from cell patient-derived xenografts (PDX) and evaluated the effect of Mysoin-II or ROCK kinases downregulation on their invasive ability.

Tumour Spheres with Inverted Polarity drive the formation of peritoneal metastases in patients with hypermethylated colorectal carcinomas

Olivier Zajac[1,10], Joel Raingeaud[1], Fotine Libanje[1], Celine Lefebvre[1], Dora Sabino[1], Isabelle Martins[2,3], Pétronille Roy[1], Clara Benatar[1], Charlotte Canet-Jourdan[1], Paula Azorin[1], Mélanie Polrot[4], Patrick Gonin[4], Salima Benbarche[5], Sylvie Souquere[6], Gerard Pierron[6], Damien Nowak[1], Ludovic Bigot[1], David Malka[7], Camille Lobry[5], Jean-Yves Scoazec[8], Clarisse Eveno[9], Marc Pocard[9], Jean-Luc Perfettini[2,3], Dominique Elias[7], Peggy Dartigues[8], Diane Goéré[7] and Fanny Jaulin[1]

[1] U-981, Gustave Roussy, Villejuif, F-94805, France

[2] Université Paris Saclay, 114 rue Edouard Vaillant, Villejuif, F-94805, France

[3] U-1030, Gustave Roussy, Villejuif, F-94805, France

[4] Plateforme d'Evaluation Préclinique, AMMICA UMS 3655/ US 23, Gustave Roussy, Villejuif, F-94805, France

[5] UMR-1170, Gustave Roussy, Villejuif, F-94805, France

[6] UMR-9196, Gustave Roussy, Villejuif, F-94805, France

[7] Digestive Cancer Unit, Gustave Roussy, Villejuif, F-94805, France

[8] Pathology Department, Gustave Roussy, Villejuif, F-94805, France

[9] UMR-965 Lariboisière Hospital, Paris, 75475, France

[10] Current address: Department of Translational Research, Institut Curie, Paris, F-75005, France

Correspondence should be addressed to FJ, fanny.jaulin@gustaveroussy.fr

The authors have declared that no conflict of interest exists

ABSTRACT

Metastases account for 90% of cancer-related deaths, it is therefore vital to understand the biology of tumour dissemination. Here, we collected and monitored over 50 patient specimens *ex vivo* to investigate the cell biology of colorectal cancer (CRC) metastatic spread to the peritoneum. This reveals an unpredicted mode of dissemination. Large clusters of cancer epithelial cells displaying a robust outward apical pole, which we termed Tumour Spheres with Inverted Polarity (TSIPs), were observed throughout the process of dissemination. TSIPs form and propagate through the collective apical budding of hypermethylated CRCs downstream of canonical and non-canonical TGFβ signalling. TSIPs maintain their apical-out topology and use acto-myosin contractility to collectively invade 3D extracellular matrices. TSIPs invade paired patients' peritoneum explants, initiate metastases in mice xenograft models and correlate with adverse patient prognosis. Thus, despite their having a robust epithelial architecture, TSIPs appear to drive the metastatic spread of hypermethylated CRCs.

INTRODUCTION

As a critical step in cancer progression, and a challenge to patient treatment, tumour cell dissemination has been the subject of intense investigations. It is commonly assumed that carcinomas progression and dissemination is associated with the loss of epithelial architecture and apico-basolateral polarity [1-3] as an epithelial-to-mesenchymal (EMT) program is activated and undifferentiated single tumour cells escape from the primary tumour [4,5]. To reach secondary sites, these single cells use two distinct mechanisms: a traction-based mesenchymal migration that requires actin-rich protrusions and adhesion to the extracellular matrix (ECM) or a propulsive amoeboid locomotion that relies on the peripheral contractility of the acto-myosin cortex to squeeze between ECM fibres [6-8]. Nevertheless, the metastatic dissemination of carcinomas can occur without activation of the EMT program [9,10] and it has been proposed that collective migration could contribute to cancer spread [6,11,12]. Similar to the collective movements orchestrating embryonic development, leader cells sense and adhere to their environment to exert the dragging forces pulling the rest of the cohort [13,14]. However, the knowledge we have on cancer cell dissemination essentially comes from experimental model systems, *in vitro* and in animals, and the mechanisms underlying the metastatic spread in patients are under-investigated. The respective contribution of tumour cell collectives and individuals remains unclear and whether cancers can use specific strategies to disseminate in the body has never been addressed.

Here, we explored colorectal carcinomas (CRCs) dissemination to the peritoneum (peritoneal carcinomatosis). CRCs, the second leading-cause of cancer related-death, evolve through distinct genetic and epigenetic pathways. The chromosomal instability (CIN) pathway,

initiated by APC loss-of-function, represents the majority of CRCs and is the best characterised [15,16]. However, poor prognosis cancers mainly originate from the CpG Island Methylator Phenotype (CIMP) group of CRCs [17-20]. About 10% of these hypermethylated tumours evolve toward micro-satellite instability (MSI-High), while most of them remain microsatellite stable (MSS) or display an intermediate phenotype (MSI-low) [21-23]. CIMP cancers develop from serrated polyps and progress toward specific histological subtypes of CRCs with dismal outcome (Mucinous, Micropapillary and Cribriform) [24,25]. CRCs metastasise to the liver, the lung and the peritoneum, a serous membrane lining the abdominal organs [26,27]. Tumour cells reach the peritoneal cavity by full-thickness invasion of the digestive wall or via systemic circulation. Then, they attach to the peritoneum and invade through the connective tissue, producing dozens of metastatic nodules substantially worsening patient outcome [28,29]. To date, the molecular and cellular mechanisms underlying CRC metastatic seeding of the peritoneum are unknown.

In this systematic prospective study, we applied cell biology methods to study live tumour specimens collected from peritoneal effusions during the cytoreductive surgery of 56 CRC patients. Our results revealed that collective behaviour predominates in the peritoneal microenvironment, and, unpredictably, cancer cell apico-basolateral polarity is maintained, but inverted, during the metastatic spread.

Tumour Spheres with Inverted Polarity (TSIPs) predominate in peritoneal effusions of patients with CRCs of poor prognosis.

To characterise CRCs dissemination to the peritoneum, we collected and examined *ex vivo* peritoneal effusions from 43 CRC patients with peritoneal metastases undergoing cytoreductive surgery. We identified single tumour cells and clusters (defined as aggregates of 4 or more cells) co-expressing the CRC markers Epithelial Cell Adhesion Molecule (EpCam) and cytokeratin 20 (CK20). Both were negative for vimentin (Sup. Table 1a, Sup. Fig. 1a). When compared to single cells, tumour cell clusters were the most frequent (68%) and, comprising 257±45 cells in average, the most abundant tumour intermediates (by 66 fold, Sup. Table 1a). Conventional cytology analyses confirmed the presence of large dense tumour cell clusters and observation of live samples by phase microscopy enabled us to discriminate between irregular and spherical morphologies, segregating in different patients. Tumour spheres, defined by their round shape and smooth edges, represent 88% of all clusters (Sup. Fig. 1b,c and Sup. Table 1a).

Strikingly, tumour spheres exhibit a robust epithelial organisation. Adherens junction proteins E-cadherin and β-catenin are concentrated at contacts between tumour cells. The basolateral proteins Scribble, β1-integrin and EpCam are found within the spheres on internal membranes. By contrast, apical markers ezrin, villin, aPKC, NHERF1, CD133, and prominent actin bundles are enriched at the periphery of the spheres (Fig.1a,c and Sup. Fig. 1d). This polarised epithelial organisation was confirmed using electron microscopic micrographs, which revealed the presence of densely packed microvilli covered with glycocalyx at the external surface of these spheres, together with tight junctions, adherens junctions and desmosomes at zones of cell-cell contact along the apical-basal axis (Fig. 1b). These experiments, together with staining for ZO-1 and the Golgi apparatus, show that in contrast to normal epithelial tissues, the spheres display an inverted apico-basolateral polarity,

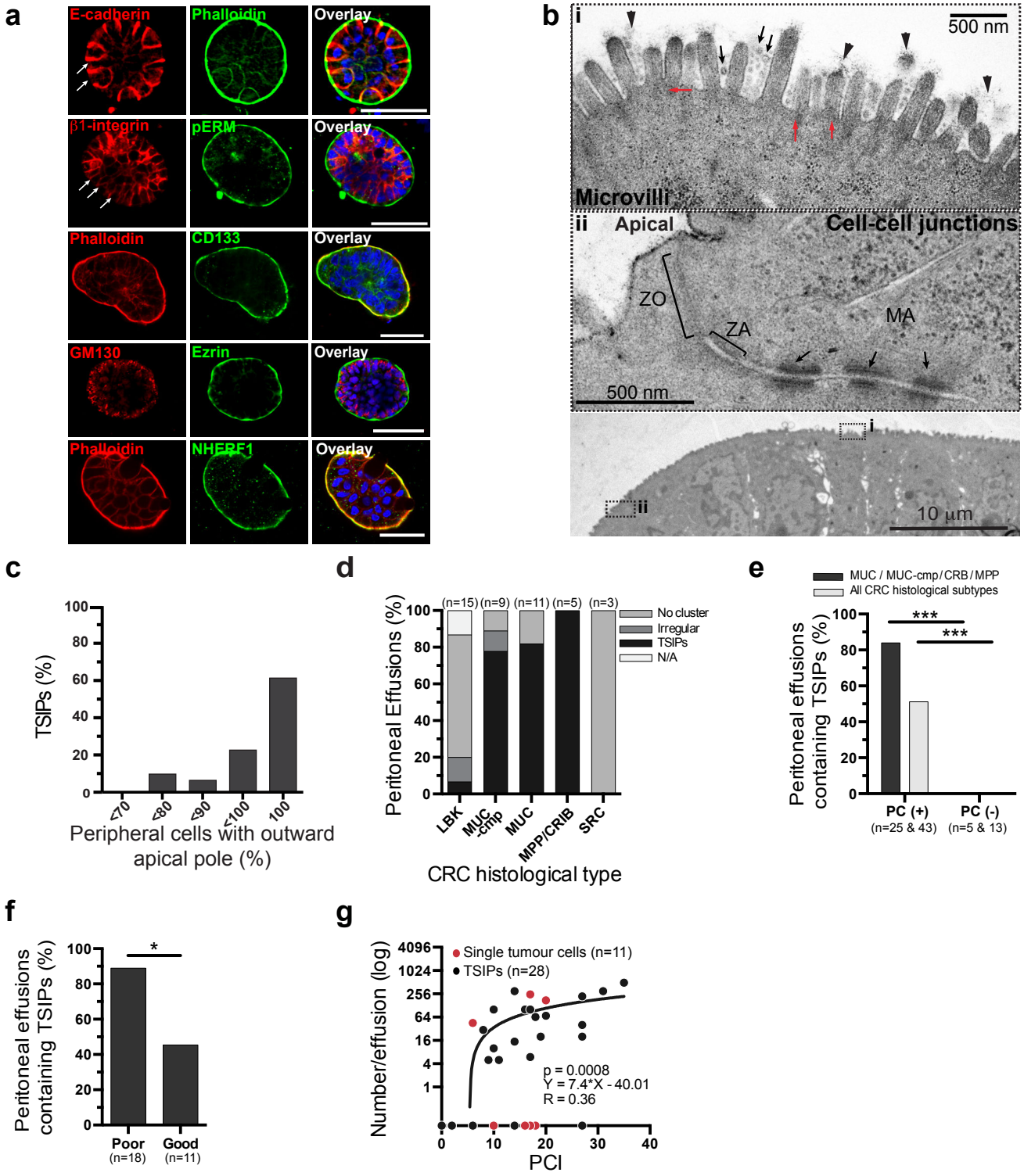

Figure 1. Tumour Spheres with Inverted Polarity (TSIPs) predominate in peritoneal effusions of patients with CRCs of poor prognosis

(a) TSIPs collected from patients' peritoneal effusions were immunostained for E-cadherin, β1-integrin, Ezrin, p-ERM, CD133, NHERF1, GM130, Phalloidin and DAPI (one median section of confocal z-stack is displayed). Arrows point to the absence of basolateral markers at the apical membrane. Representative images from 3 independent patients' samples, 7 for Ezrin and Phalloidin. Scale bars: 50 µm

(b) Electron microscopic micrographs of TSIPs: region (i) shows the peripheral membrane of outer cells decorated with microvilli containing actin-containing core rootlets (red arrows), glycocalyceal bodies (black arrows) and glycocalyx coating (arrowheads), ultrastructural markers of intestinal cells. Region (ii) points to the tripartite junctional complex between adjacent peripheral cells of the TSIP. ZO: zonula occludens; ZA: zonula adhaerens, MA: macula adherens (desmosomes). Similar structures were observed from 10 TSIPs from 2 independent patients.

(c) Quantification of polarity inversion on TSIPs from peritoneal effusions. The graph shows the distribution of the TSIPs depending on the percentage of peripheral cells with outward apical Ezrin relative to total peripheral cell number in one confocal Z-section (30 TSIPs from 6 patients).

(d) Frequency of tumour cell clusters (TSIPs or irregular) stratified by CRC histological subtypes (Lieberkuhnian (LBK), Mucinous (MUC), Mucinous-component, Cribriform/Micropapillary (CRIB/MPP) and Signet Ring Cells (SRC)).

(e) Correlation between TSIPs and patient metastatic status (PC+, patient with peritoneal carcinomatosis and PC-, without) considering all CRCs or only indicated subtypes (***pF=0.0009 and 0.0007 respectively).

(f) Correlation between the frequency (%) of TSIPs positive peritoneal effusions and patients outcome after cytoreductive surgery and HIPEC (MUC, CRIB and MPP CRC subtypes, *pF=0.03).

(g) Linear regression of the number of TSIPs (black dots) or single tumour cells (red dots) for each patient, in a log scale, plotted against the PCI (Peritoneal Cancer Index) (TSIPs>1000 from patients #8 and #12 were excluded). pLR=0,0008 indicates the correlation between the PCI and the number of TSIPs in the confidence interval of 95%.

In all graphs, n represents the number of patients, p-values were determined by two-sided Fisher exact test.

with their apical pole oriented outward (Fig.1a and Sup. Fig. 1e). We named these structures Tumour Spheres with Inverted Polarity (TSIPs). Despite their robust epithelial architecture, TSIPs almost exclusively associated with histological subtypes with an adverse prognosis and increased metastases occurrence, including mucinous (MUC) carcinomas, the second most common form of CRCs (Fig. 1d) [30,31]. To evaluate whether TSIPs could act as malignant tumour intermediates, we analysed peritoneal effusions from 13 patients with advanced CRCs (pT3 or pT4) but without peritoneal metastases (PC-, Sup. Table 1b). These samples were all free from TSIPs, demonstrating that TSIPs are specifically associated with PC as expected if they are a key intermediate in the process of tumour dissemination (Fig. 1e). Moreover, TSIPs were found in 88% of poor prognosis patients (16/18, with a average number of 146 TSIPs/effusion) but only in 45% of good prognosis CRC PC+ patients (5/11, Fig. 1f) [32]. In addition, the number of TSIPs found in effusions taken from PC+ patients correlates with the peritoneal cancer index (PCI): an integrated measure of the extent, number and size of the peritoneal metastatic nodules (Fig. 1g) [33].

Hence, TSIPs are tumour intermediates with a robust epithelial identity and an inverted apico-basolateral polarity that have disseminated to the peritoneal cavity of CRC patients with poor prognosis.

TSIPs form through the collective apical budding of hypermethylated CRCs

We initially reasoned that TSIPs could originate from the adhesion and/or proliferation of disseminated single mesenchymal cells following a mesenchymal-to-epithelial transition (MET)[4]. However, when we analysed gene expression profiles of MUC CRCs and normal samples from two different datasets (Carte d'identité des tumeurs (CIT) and the Cancer Genome Atlas (TCGA)) [17,19] with Gene Set Enrichment Analyses (GSEA) [34], we did not detect any activation of an EMT program in MUC CRCs (Sup. Fig. 2a,b) [35]. As a further test of this

hypothesis, we collected and monitored single cells from peritoneal effusions. To avoid selecting for epithelial states (EpCam(+)), we also used total single cell fractions or only depleted for CD45(+) hematopoietic cells. The single tumour cells did not proliferate or aggregate to form multicellular structures over a period of 9 days, whether grown in suspension or in ECM (Matrigel and collagen-I, Fig. 2a,b). Instead, these cells tended to rapidly die in isolation, while tumour cells remained viable and proliferate within collectives, so that 67.5±7.5% of TSIPs were alive after 9 days (Fig. 2c, mitotic index: 1.064). When TSIPs were dissociated using trypsin, the resulting single cells died almost as rapidly as cells in the single cell fractions (only 2.3±1.9% cells were alive by 9 days, Fig. 2c) suggesting that cell-cell interactions provide important survival signals. Using the mucus-secreting line LS174T [36] and Patient-Derived Xenografts (PDX#1 and PDX#2) [37], we confirmed that MUC CRC single cells died, even in the presence of collagen-I or laminin-rich matrices (Fig. 2d-f). Supplementing Matrigel with Y27632 as previously described [38], allowed single cells from PDX#1 and PDX#2 (11±5% and 6±4% respectively) to subsist, proliferate and generate small colonies, which did not display TSIP features (Fig. 2f). The survival of single cells in suspension could be prolonged by promoting the aggregation of LS174T single cells (Fig. 2g). This depended on E-cadherin engagement, as shown by the effect of a DECMA1 function blocking antibody and calcium chelating agent, while β1-integrin inhibition had no effect (Fig. 2h). Together these results show that MUC CRC single cells are both short-lived and unable to form TSIPs, neither in suspension nor in ECM matrices.

We then investigated whether TSIPs could form in primary tumours. Immunostainings of histological sections of TSIP-producing CRC specimens revealed densely organised tumour cell clusters outlined by villin or ezrin staining, demonstrating that TSIPs exist within patients' primary tumours, as well as lymph nodes and peritoneal metastases, often representing more than half of the cancer area (Fig. 3a,b and Sup. Fig. 3a-c). We investigated

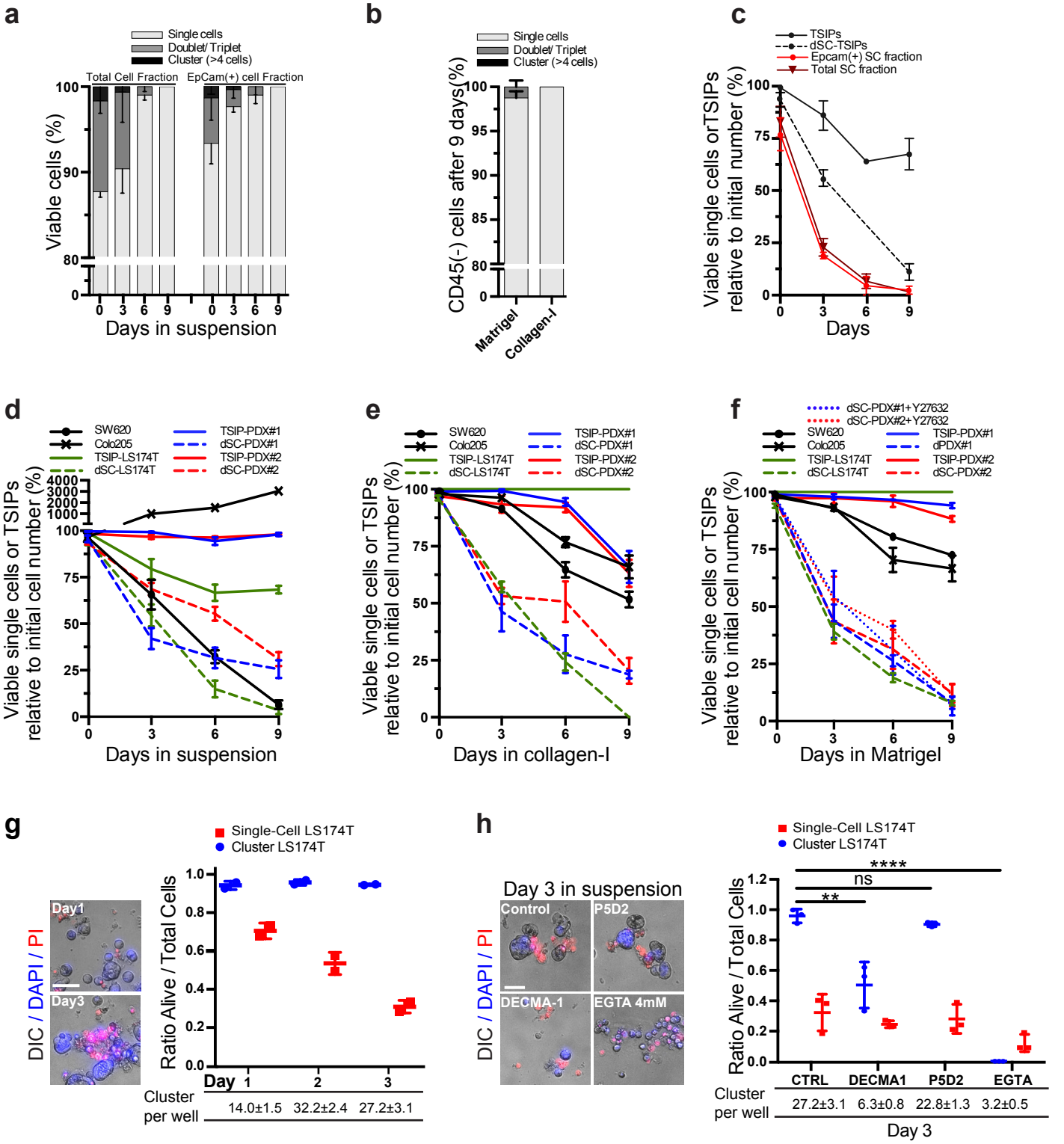

Figure 2. MUC CRC cell survival is sustained by cell-cell interactions

(a) Total single cells fraction and EpCam(+) enriched single cells fraction were isolated from 3 independent patients' peritoneal effusions. Viable single cells, doublets plus triplets, and clusters found in suspension were quantified for up to 9 days.

(b) The CD45(-) single cells fraction from peritoneal effusions were isolated from 3 independent patients and embedded in collagen-I or Matrigel. After 9 days, single cells, doublets plus triplets, and clusters were quantified after CK20 and Vimentin staining.

(c) Line graph representing the percentage of viable TSIPs or single cells (total fraction, EpCam(+), or obtained by the trypsinisation of TSIPs) over 9 days quantified by DIC and trypan blue. The results are from 3 independent patients and expressed as % relative to initial cell or TSIP numbers.

(d-e-f) Line graph showing percentage of viable cells or TSIPs relative to initial number. The adherent cell line SW620 and the non-adherent Colo205 are used as controls. Controls, dissociated single cells (dSC) and TSIPs were seeded (100-250 spheres/cells per mL) in suspension (d), collagen-I (e) or Matrigel (f), with or without Y27632 and cultivated for 9 days.

(g) Graph showing the ratio between living and total cells in clusters and unclustered single cells after promoting the aggregation of LS174T dSC from 2 biologically independent experiments. PI was used to highlight dead cells. Representative pictures of LS174T-clusters formation and viability corresponding to the quantification are shown (DAPI in blue, PI in red).

(h) Graph representing the ratio between living and total LS174T cells in clusters and unclustered single cells in medium, DECMA1 (E-cadherin function blocking antibody, 12 µg/mL), P5D2 antibody (β1-integrin function blocking antibody, 1 µg/mL) or EGTA (4 mM). Representative images of cluster formation and viability are shown. p values were calculated from 3 biologically independent experiments using unpaired two-sided t test (****pTT<0.0001, **pTT=0.0078, ns pTT=0.128).

All graphs represent Mean±SEM from 3 biologically independent experiments or 3 different patients unless otherwise specified.

Scale bars: 50 µm.

whether core polarity proteins could participate in TSIPs formation by altering the apico-basolateral polarity of tumour cell groups. However, silencing ParD3, Scribble or Llgl2 in small clusters of LS174T embedded in 3D matrices did not promote polarity inversion and TSIP formation (Fig. 3c, Sup Fig 4a and 4b).

How then do TSIPs form and propagate? To identify the cellular and molecular events associated with TSIP-based dissemination, we compared the transcriptomic profiles of TSIP-producing (MUC) and non-producing (Lieberkuhnian, LBK) CRCs. Using two independent datasets, we noted that virtually 100% of MUC CRCs associate with the CpG island methylator phenotype (CIMP), rather than chromosome instable cancers (CIN), and express the serrated genes signature (Fig. 3d,e) [17,18,39]. The serrated precursor lesions are defined by their peculiar morphology of serial bulges protruding apically into the lumen of their neoplastic precursor glands [25] (Fig. 3fii, red arrows). Ezrin immunostaining of serrated precursors and MUC primary tumours suggested that TSIPS could be generated by budding as the serrated precursor lesions progress toward MUC CRCs (Fig. 3fiii and Sup. Fig.3biii). To assess whether TSIPs could specifically bud from MUC CRCs, we grew several cell lines in culture. Only the mucus-secreting LS174T was found to bud. Over 7-8 days period, they liberated in suspension 267±25 TSIPs displaying an inverted apico-basolateral polarity (Fig. 3g,h). Strikingly, time-lapse imaging revealed that immobilized patients' TSIPs themselves bud. These buds formed and grew over a period of ~3 days, leading to scission events that liberated new independent and viable TSIPs (Fig. 3i and Supplementary Movie 1).

These experiments support the idea that CIMP MUC CRCs possess an intrinsic and specific mode of propagation through the generation of TSIPs by a morphogenetic event that we named collective apical budding (Fig. 3j). Through this process, tumour cell collectives detach from the primary tumour and revert the topology of their apico-basolateral polarity. TSIPs initially accumulate in the lumen of MUC CRCs glands (Sup. Fig. 3bi). As the cancers

Figure 3

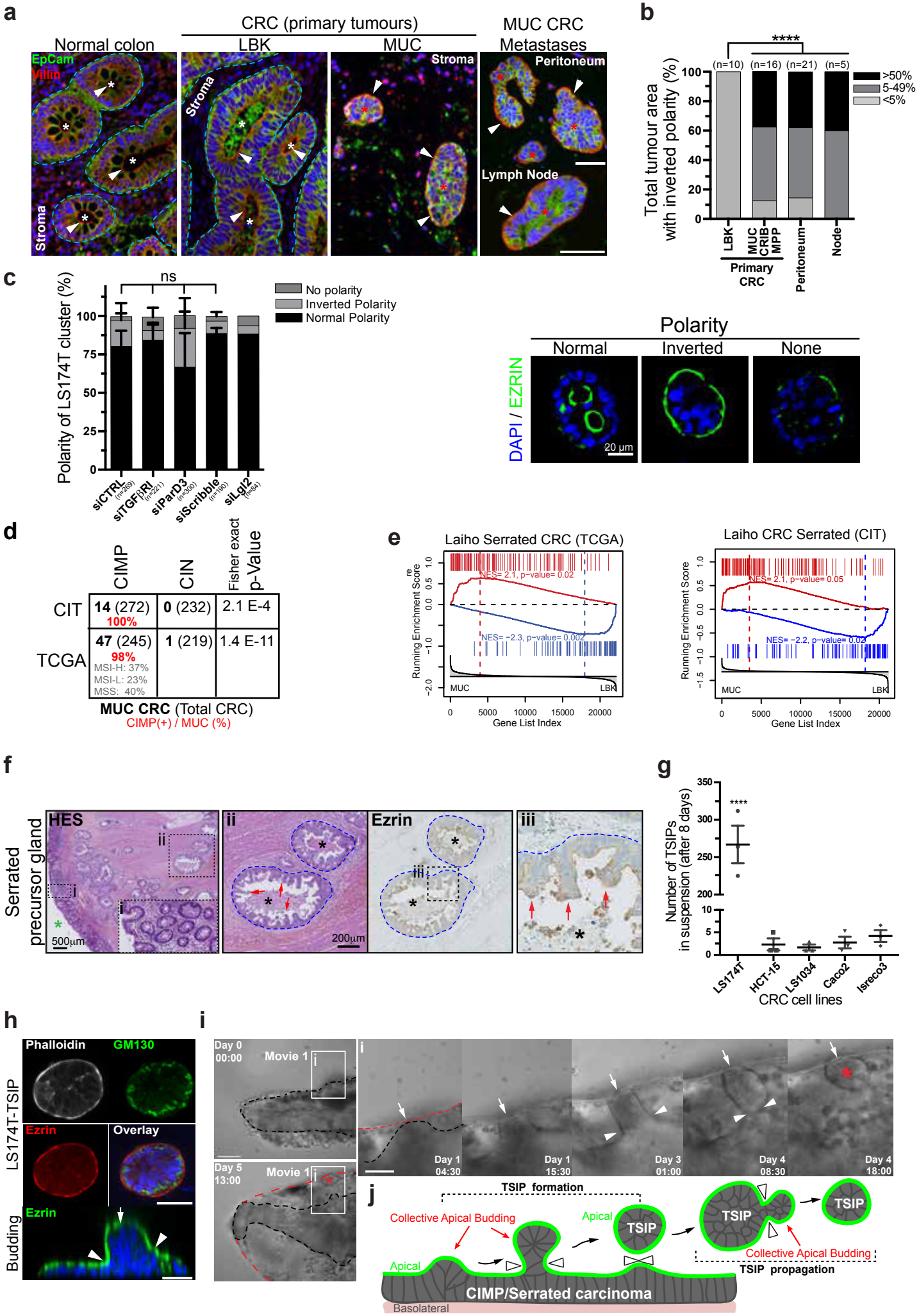
a
CRC (primary tumours)
Normal colon
LBK
MUC
MUC CRC Metastases
EpCam
Villin
Stroma
Peritoneum
Lymph Node
b
****
Total tumour area with inverted polarity (%)
(n=10) (n=16) (n=21) (n=5)
>50%
5-49%
<5%
LBK
MUC CRIB MPP
Primary CRC
Peritoneum
Node
c
ns
Polarity of LS174T cluster (%)
No polarity
Inverted Polarity
Normal Polarity
siCTRL
siTGFβRI
siParD3
siScribble
siLgl2
Polarity
Normal
Inverted
None
DAPI / EZRIN
20 µm
d
CIMP
CIN
Fisher exact p-Value
CIT
14 (272) 100%
0 (232)
2.1 E-4
TCGA
47 (245) 98%
MSI-H: 37%
MSI-L: 23%
MSS: 40%
1 (219)
1.4 E-11
MUC CRC (Total CRC)
CIMP(+) / MUC (%)
e
Laiho Serrated CRC (TCGA)
NES= 2.1, p-value= 0.02
NES= −2.3, p-value= 0.002
Running Enrichment Score
MUC
LBK
Gene List Index
Laiho CRC Serrated (CIT)
NES= 2.1, p-value= 0.05
NES= −2.2, p-value= 0.02
f
Serrated precursor gland
HES
Ezrin
500µm
200µm
g
Number of TSIPs in suspension (after 8 days)
****
LS174T
HCT-15
LS1034
Caco2
Isreco3
CRC cell lines
h
LS174T-TSIP
Budding
Phalloidin
GM130
Ezrin
Overlay
i
Day 0 00:00
Movie 1
Day 5 13:00
Day 1 04:30
Day 1 15:30
Day 3 01:00
Day 4 08:30
Day 4 18:00
j
TSIP formation
Collective Apical Budding
Apical
TSIP
TSIP propagation
CIMP/Serrated carcinoma
Basolateral

Figure 3. TSIPs form by collective apical budding from Serrated/hypermethylated CRCs

(a) Representative images of histological sections of normal colon (n=3 patients), primary tumours (LBK, n=10 and MUC, n=16 patients) and metastases from MUC CRC (peritoneum n=21 and lymph node n=5 from 21 patients) stained for EpCam and Villin. Arrowheads point to apical poles, white stars show luminal cavities and red stars show TSIPs.

(b) Area of LBK and MUC tumour histological sections showing an inverted polarity (represented as % of the total tumour area in the specimen), n represents the number of tumour specimens analyzed. p values were calculated using two-sided Fisher exact test for each MUC tumour location in comparison with LBK (****pF<0.0001).

(c) Bar graph representing the topology of LS174T clusters, control or transfected by the mentioned siRNAs, according to the following phenotypes: normal polarity (inward apical pole), no polarity (diffuse staining) or inverted polarity (outward apical pole) based on Ezrin staining. See immunostaining on the right panel for representative images. The error bars represent error margins from the average of 3 biologically independent experiments (except siLlgl2, n=2). P-values were calculated using two-sided unpaired t-test (all p-values are non significant (ns), p>0.05).

(d) Distribution of MUC CRC samples from TCGA and CIT in the CpG Island Methylator Phenotype (CIMP) and Chromosomal Instable (CIN) tumour groups according to gene expression classification from Guinney et al.16. The p-value was obtained with a one-sided Fisher exact test testing the distribution of the mucinous samples in the CIMP and CIN phenotypes as compared to the rest of the CRC samples. % represents the proportion of MUC CRC with a CIMP signature in each subtype of CRCs. CIMP MUC CRCs from the TCGA dataset include microsatellite instable (MSI-H), microsatellite stable (MSS) and intermediate phenotypes (MSI-Low).

(e) Gene Set Enrichment Analysis (GSEA) of the Laiho gene sets39 in the CRC mucinous (MUC) versus lieberkuhnian (LBK) gene signature from TCGA (left) and CIT (right) datasets (nMUC/CIT=15 nLBK/CIT=188, nMUC/TCGA=61, nLBK/TCGA=389). GSEA was run with the LAIHO-_UP and LAIHO_DN gene sets obtained in the C2 collection of MSigDB and are represented in red and blue respectively. The reference list of genes was sorted using the significance of the test comparing gene expression in MUC and LBK samples from the TCGA and CIT.

(f) Representative images of 3 independent patients' histological sections of serrated precursor lesions. The specimens were stained using Hematoxylin/Eosin/Saffron (HES) and anti-Ezrin antibody. The boxed region (i) shows normal glands, (ii and iii) display high magnification of serrated glands. The green star indicates the luminal cavity of the digestive tube, the black stars the lumen of the glands, the blue dotted line highlights the basal pole of the neoplasic gland, the red arrows point to region of budding toward the lumen.

(g) Quantification of TSIPs released in culture media by 2D culture of adherent CRC cell lines, HCT-15, LS174T, LS1034, Caco-2 and Isreco3, over 3 biologically independent experiments. Dots represent a single experiment, bars represent Means ± SEM. ****pA<0.0001 calculated by one-way ANOVA test.

(h) Representative images of immunofluorescence of LS174T cells from 3 biologically independent experiments. The bottom panel shows the orthogonal view of budding adherent cell stained with Ezrin and DAPI. The white arrow points to the budding region at the apical pole and the arrowheads to the neck region. The top panels display immunostaining using phalloidin, GM130 and Ezrin of a LS174T-TSIP released in suspension.

(i) DIC microscopy time lapse sequences of patient's TSIP undergoing collective apical budding (Boxed region corresponds to Supplementary Movie 1, from one patient). The black dotted line highlights the TSIP periphery; the red dotted line outlines the mucus front. Time is displayed as day and hh:mm. Arrow points to the budding region, arrowheads to the fission region and the red star to the newly formed TSIP. The budding has been observed from two independent recordings.

(j) Schematic representation of cellular mechanism underlying collective apical budding from neoplasic epithelial tissues of the MUC/CIMP type (TSIP formation) or from TSIPs themselves (TSIP propagation). The green line highlights the apical pole and grey line the basolateral one. Red arrows indicate collective apical budding, arrowheads point to the fission region.

Scale Bars: 50 µm unless otherwise indicated.

progress, active budding and increased mucus secretion breach the neoplastic epithelial monolayers, the glandular architecture being progressively lost to the profit of TSIPs (Fig. 3a,b and Sup. Fig. 3biii).

Canonical and non-canonical TGFβ signalling regulates TSIPs production by collective apical budding

To identify the molecular mechanisms underlying TSIPs formation by collective apical budding, we analysed by GSEA the pathways differentially regulated in TSIP producing tumours (MUC CRCs) as compared to non-producing cancers (LBK CRCs). The analysis revealed that TGFβ signalling was down-regulated in MUC CRCs (Fig. 4a). This correlates with the elevated frequency of somatic mutations in genes encoding TGFβ receptors in these tumours relative to LBK CRCs (Fig. 4b). To test the influence of the TGFβ on TSIPs production in LS174T cultures, we first verified that, as previously described [40], transcriptomic slippages correct part of the TGFβR frame-shift mutations, giving rise to low but functional signalling (detected by increased Smad2 phosphorylation upon TGFβ stimulation in Fig. 4c). TGFβ treatment reduced TSIP-LS174T production by 6.3±0.05 fold (while Noggin had no effect, Fig. 4d). Conversely, inhibiting TGFβRI by SB431542 or siRNA, increased TSIP-LS174T production by 3.9±0.4 and 2±0.13 fold respectively (Fig. 4d and Sup. Fig. 4c). None of the treatments altered cell proliferation (Sup. Fig. 4d). To investigate the contribution of downstream players, we first depleted R-Smads proteins. Silencing Smad2, but not Smad3 or Smad4, mimicked the depletion of TGFβRI, increasing TSIP-LS174T formation by 3±0.4 fold (Fig. 4e, Sup. Fig. 4e). This likely reflects specific features of Smad2 among R-Smads [41]. In addition, depleting the non-canonical effector ParD6A by shRNA augmented TSIP-LS174T production up to 2.4±0.3 fold and increased RhoA protein level and myosin-II phosphorylation (Fig. 4e,f and Sup. Fig. 4f). Furthermore,

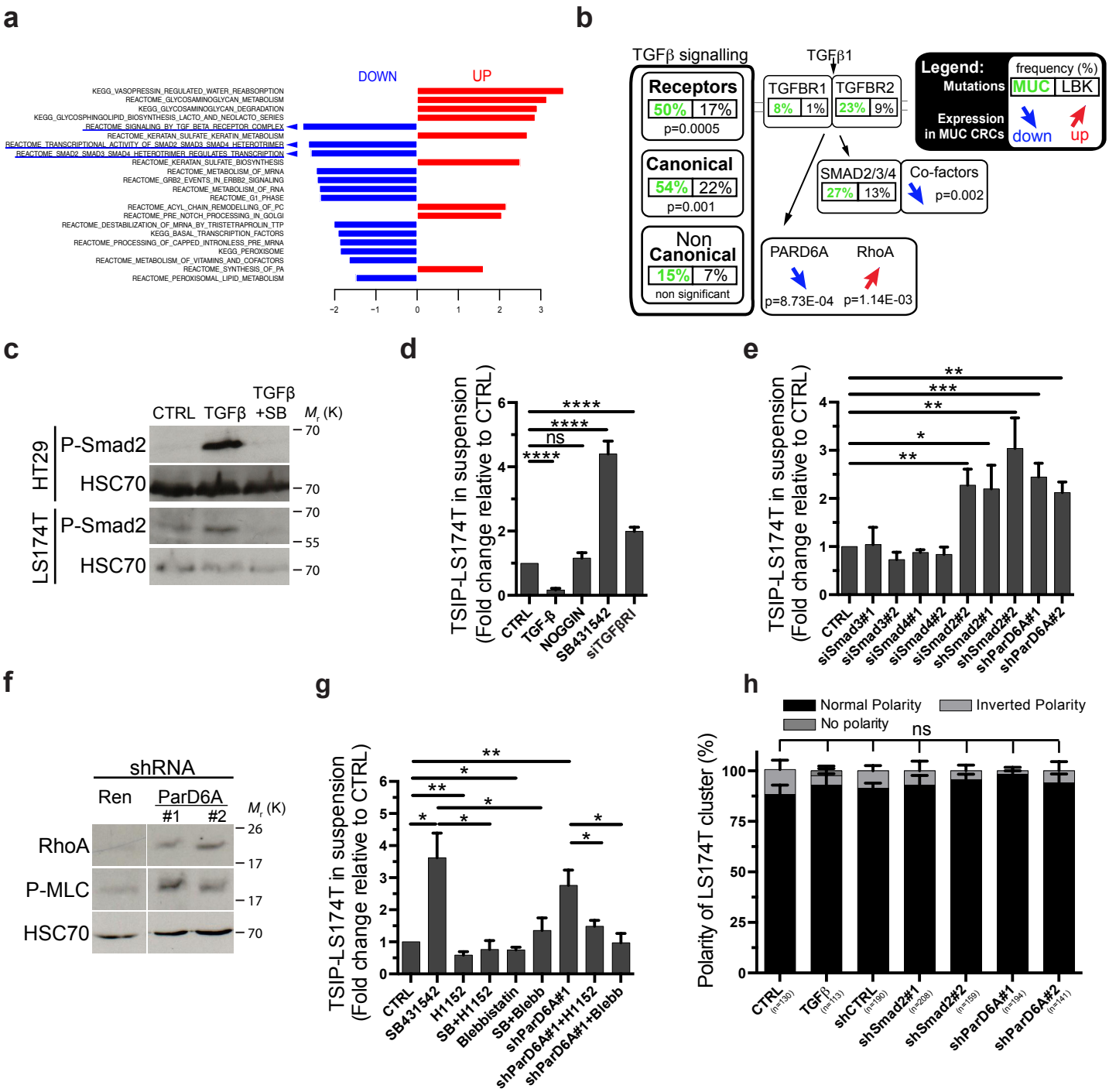

Figure 4. Decreased canonical and non-canonical TGFβ signalling promotes TSIP formation by collective apical budding.

(a) Significantly enriched pathways in MUC vs LBK samples in the CIT and TCGA datasets (nMUC/CIT=15 nLBK/CIT=188, nMUC/TCGA=61, nLBK/TCGA=389). Enrichment was computed with GSEA (FDR < 0.2). Blue and red horizontal bars show the Normalized Enrichment Score of the pathway in the CIT dataset. See Supplementary Table 1 for additional information.

(b) Left part: For each gene or group of genes, the frequency of mutations in Mucinous (left box, n=26) and LBK (n=174, right box) is reported and the p-value of one-sided Fisher Exact test testing for the difference of frequency in the 2 histologies is given just below if pF < 0.05 (non significant: pF=0,136). The blue and red arrows indicate a significant differential expression per gene or per set of genes (GSEA for set of genes and limma voom for individual genes). In the right part, individual genes significantly contributing to the differential expression or mutation in the group of genes are documented. Data were extracted from the TCGA dataset9, the detailed analyses can be found in Supplementary Table 2.

(c) Immunoblot analysis of Smad2 phosphorylation in HT29 and LS174T cell lines, untreated or treated for 1 hour with SB431542 (10 μM) and/or TGFβ (10 ng/ml). HSC70 was used as a loading control. The results were repeated in 3 biologically independent experiments.

(d-e) Bar graphs representing the number of TSIPs produced by LS174T cultures normalized to control conditions (untreated, control siRNA (non-targeting) or shRNA (Renilla)). The number of biologically independent experiments and the p values are as follows: For (d), CTRL (n=7), TGFβ (n=6, pTT<0.0001), Noggin (n=3, pTT=0.25) SB431542 (n=7, pTT<0.0001) and siTFGβRI (n=5, pTT<0.0001). For (e): CTRL (n=6), siSmad2#2 (n=6, pTT=0.007), shSmad2#1 (n=5, pTT=0.0388), shSmad2#2 (n=6, pTT=0.0174), shParD6A#1 (n=6, pTT=0.0014) and shParD6A#2 (n=5, pTT=0.001).

(f) Immunoblot analysis of LS174T cell line infected with lentiviruses encoding shRNA against renilla or ParD6A using RhoA and Phospho-T18/S19-MLC specific antibodies. HSC70 was used as a loading control, representative examples from 3 biologically independent experiments.

(g) Bar graph representing the number of TSIPs produced by LS174T cultures normalized to control conditions (untreated or control shRNA (Renilla)). The number of biologically independent experiments and the p values are as follow: CTRL (n=4), SB431542 (n=4, pTT=0.0137), H1152 (n=8, pTT=0.002), SB+H1152 (n=4, pTT=0.0124), Blebbistatin (n=6, pTT=0.01), SB+Blebb (n=4, P=0.0382), shParD6A#1 (n=4, pTT=0.003), shParD6A#1+H1152 (n=4, pTT=0.048), shParD6A#1+Blebb (n=4, pTT=0.0191).

(h) Bar graph representing the polarity of LS174T clusters, control or transfected by the mentioned siRNAs (see Fig. 3(a) for phenotypes). All p values were non significant (ns, pTT>0.05).

All graphs represent Means±SEM from 3 biologically independent experiments unless otherwise specified. P-values were calculated using two-sided unpaired T-test (****p<0.0001, ***p<0.001, **p<0.01, *p<0.05, ns:p>0.05).

inhibiting ROCK and Myosin-II using pharmacological inhibitors H1152 and blebbistatin, decreased TSIP-LS174T production both in control and shParD6A treated cells (Fig. 4g). In contrast, interfering with the TGFβ pathway does not promote the reversion of polarity in small clusters of LS174T embedded in ECM (Fig. 4h) and silencing Scribble, Lgl2 or ParD3 did not contribute to TSIP production by LS174T budding (Sup. Fig. 4g).

Thus, these results show that the progression from serrated/CIMP precursors lesions to MUC CRCs is associated with low canonical and non-canonical TGFβ signalling, both of which participate in TSIP formation by collective apical budding.

TSIPs collectively invade in their apical-out topology

Since TSIPs are present all along the path of cancer dissemination, from the primary tumour to the peritoneal metastases, and because single cells are unable to survive in isolation and generate TSIPs, we reasoned that TSIPs may spread via a collective mode of invasion [14]. To test this hypothesis, we collected fragments of peritoneum from a non-metastatic region during surgery and incubated them *ex vivo* with paired patient's TSIPs. After 3 days, we stained the tissues for CK20 and Ezrin, revealing that, in 77±19% of cases, TSIPs collectively invaded peritoneal explants and maintain their inverted polarity during this process. We could not detect any instance of single cell invasion (Fig. 5a,b). To further validate these findings, we embedded patients' TSIPs into collagen-I matrices and monitored their behaviours. In all cases, and in line with our previous results (Fig. 2), the single cells that were released through TSIP spontaneous dissociation (5% of cases), or from TSIPs delamination, died and stained positive for cleaved Caspase-3 (Fig. 5c arrowheads, 5d and 5e). This absence of mesenchymal cell invasion contrasts with the *bona fide* EMT observed in irregular clusters isolated from peritoneal effusions (Sup. Fig. 2c). Strikingly, and as observed in patients' peritoneum, most TSIPs maintain their outward apical pole in contact with the ECM, yet, collectively invade

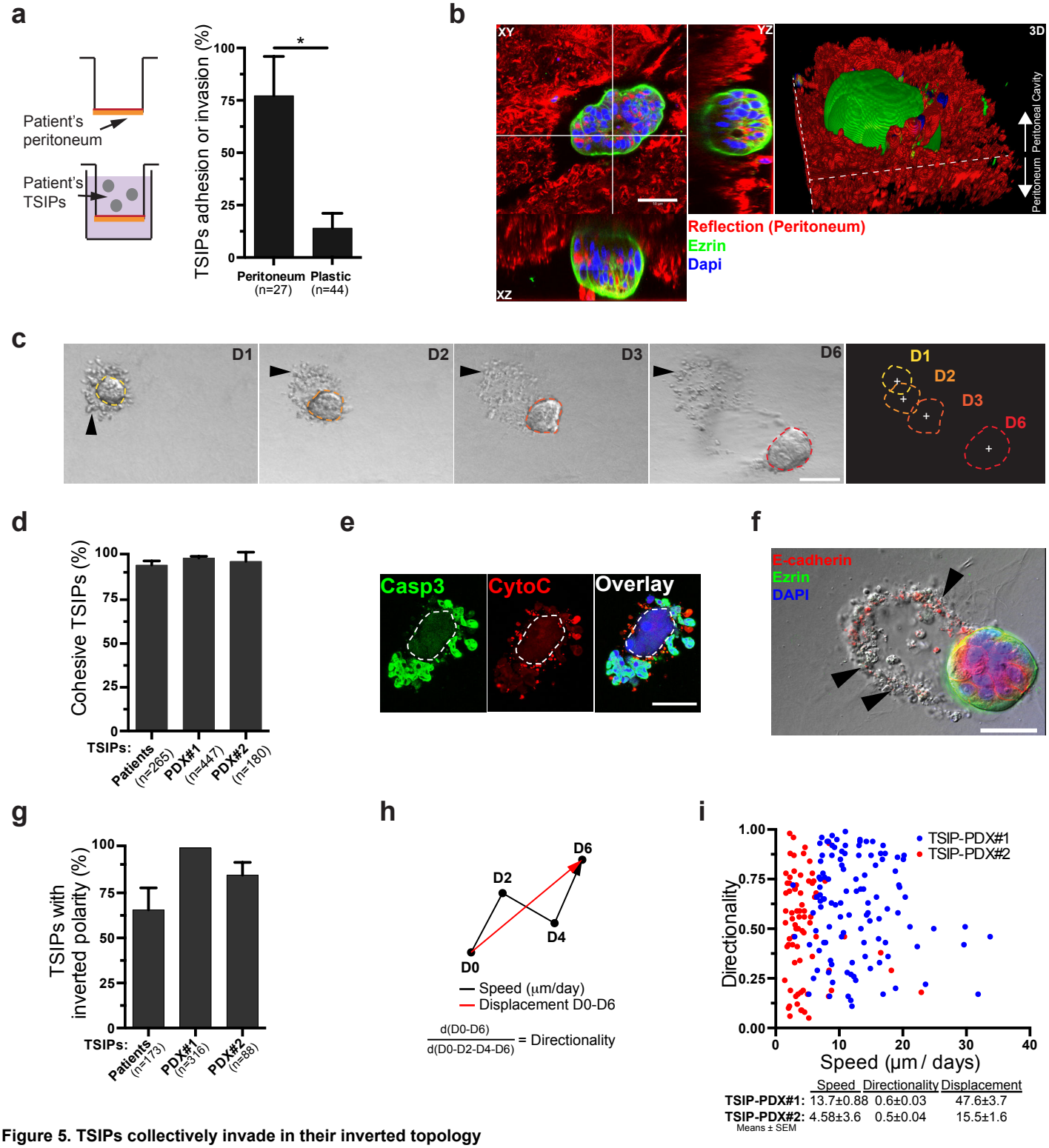

Figure 5. TSIPs collectively invade in their inverted topology

(a) Left: Schematic representation of the peritoneum invasion assay. Right: Associated bar graph shows the quantification of TSIPs adhesion/invasion in paired peritoneum or plastic dish after 3 days in culture from 3 different patients represented as % of initial TSIPs incubated (n represents the number of TSIPs, *pTT=0.0345).

(b) Representative images of TSIP invading matching patient's peritoneum explant from 2 different patients samples, stained for Ezrin (green) and DAPI (blue). The peritoneum is visualized by reflection microscopy (Red). The XY and XZ view represent orthogonal confocal section. The right panel displays a 3D reconstruction.

(c) Time lapse sequences of patient TSIP displacement in collagen-I gel monitored by DIC microscopy over 6 days. Arrowheads point to cell debris. TSIP perimeters and centroids are respectively highlighted by coloured dotted lines and white crosses. TSIPs displacements were observed from 3 independent patients.

(d) Number of cohesive TSIPs from patients, PDX#1 and PDX#2 after 6 days in collagen-I, represented as % of total TSIPs, counted from 7 patients and 3 biologically independent experiments for TSIP-PDX.

(e) Patients' TSIPs were stained for Hoechst-33342, Cytochrome C (CytoC), and cleaved caspase3 (Casp3), repeated for 5 patients. Dotted line represents the TSIP periphery.

(f) Representative image from 3 different patients of TSIPs collected and embedded into collagen-I. After 6 days, TSIPs were stained for Ezrin, E-cadherin and DAPI. Arrowheads show cell corpses and debris.

(g) Bar graph representing the number of TSIPs with inverted polarity after 6 days in collagen-I (as % of cohesive TSIPs). The number of TSIPs analysed (n) is indicated and has been calculated from 7 patients or 3 biologically independent experiments for TSIP-PDX.

(h) Schematic representation of the measurements of TSIPs displacement.

(i) Speed (µm/day) plotted against the directionality for TSIP-PDX#1 (blue – 114 TSIPs) and TSIP-PDX#2 (red – 75 TSIPs). Table shows the Mean±SEM speed, displacement and directionality from 3 biologically independent experiments.

Scale bars 50 µm unless otherwise specified. All graphs represent Mean±SEM from 3 patients or biologically independent experiments unless otherwise specified. P-values were calculated using two-sided unpaired T-test (*p<0.05).

into the 3D gel (Fig. 5c,f,g). We confirmed these results using TSIPs generated from patients' MUC CRCs propagated in immune-deficient mice (PDX#1 and PDX#2, Sup. Fig. 5a,b). Like patients' TSIPs, TSIP-PDX#1 and TSIP-PDX#2 both maintain their outward apical pole and migrate through collagen-I gel with an average centroid displacement of 47.6±3.7 μm and 15.5±1.6 μm over 6 days respectively (Fig. 5d,g,h,i Sup. Fig. 5c and Supplementary Movie 2).

Thus, TSIPs undergo collective invasion in their apical-out topology. They appear to migrate slower than most cancer cell lines [42]. Yet, their speed is in the order of magnitude of collective invasion rates measured *in vivo* and the scale of cancer progression in patients [43,44].

TSIPs collective invasion is driven by the peripheral apical acto-myosin contractility.

To decipher the mechanism underlying TSIPs unique mode of collective invasion, we first examined whether the TGFβ pathway, controlling TSIP formation, could also contribute to TSIPs apico-basolateral polarity orientation in ECM. Stimulating TSIPs with TGFβ strongly reduced the number of TSIPs with inverted polarity to 13.3±3.7%. This could partially be rescued by the expression of shParD6A, but not shSmad2 (Fig. 6a,b). Treating TSIPs with the ROCK inhibitor Y27632 completely abolished TSIP polarity inversion and blebbistatin reduced it to 32.7±16.5%, confirming that non-canonical TGFβ signalling is essential to maintain TSIPs outward apical pole in ECM (Fig. 6a,b). Then, to identify the molecular machinery driving TSIPs invasion, we inhibited the proteins known to control collective migration, such as FAK, Rac1 or integrins and analysed TSIP-PDX#1 displacement and invasion speed over 6 days. None of the treatments affected TSIP-PDX#1 movement, consistent with these basolateral proteins being segregated away from the collagen-I and the absence of protrusion detected by video-microscopy (Fig. 6c Sup. Fig. 5c,d and Supplementary Movie 2). To address the contribution of apical proteins to TSIPs invasion, we

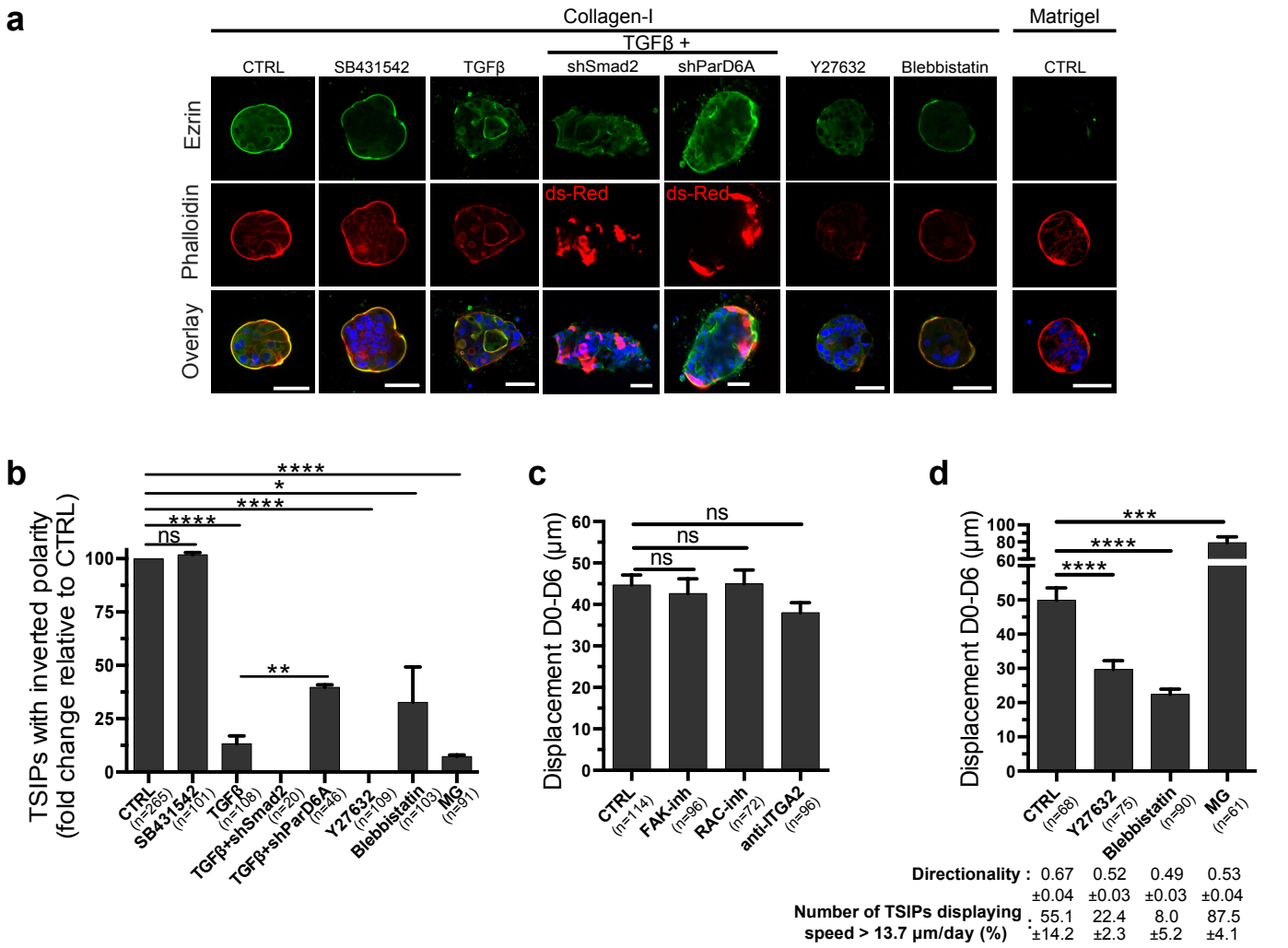

Figure 6. TSIPs collective invasion is driven by Rock and Myosin-II activity downstream of the non-canonical TGFβ signalling

(a) Representative images from 3 biologically independent experiments of TSIP-PDX#1 in collagen-I (or Matrigel) in control conditions or treated with SB431542, TGFβ, Y27632, Blebbistatin or a combination of TGFβ stimulation after transduction with shRNA targeting Smad2 and ParD6A (infected cells expressed Ds-Red). After 3 days, TSIPs were fixed, and stained using anti-Ezrin, phalloidin and DAPI to assess their apico-baso-lateral polarity (the quantification is in Fig. 6b).

(b) Bar graph representing the percentage of TSIPs with inverted polarity after 3 days in collagen-I, normalized to control condition. TSIPs were treated with SB431542, TGFβ, Y27632, Blebbistatin or a combination of TGFβ stimulation after infection with lentiviruses encoding shRNA Smad2 and ParD6A. Alternatively, TSIPs were incubated into 3mg/ml of Matrigel. n represents the number of TSIPs quantified per each condition. SB431542 (pTT=0.1218), TGFβ (pTT<0.0001), TGFβ/shParD6A (pTT=0.0024), Y27632 (pTT<0.0001), Blebbistatin (pTT=0.0152), and MG (pTT<0.0001). TGFβ/shSmad2 experiments were performed only twice.

(c) TSIP-PDX#1 displacement (D0-D6) in collagen-I in control condition or supplemented with inhibitors of FAK (FAK-Inh, PF-573228, pTT=0.63) and Rac (Rac-Inh, NSC23766, pTT=0.95) or integrin alpha-2 function-blocking antibody (anti-ITGA2, pTT=0.058). The total number of TSIPs across the 3 independent experiments is indicated in the graph.

(d) TSIP-PDX#1 displacement (D0-D6) in collagen-I supplemented with the ROCK inhibitor Y27632 (pTT=0.0001), Blebbistatin (pTT=0.0001) or in Matrigel (pTT=0.0004). The total number of TSIPs is indicated in the graph. The associated table shows the directionality (Mean ± SEM) and the percentage of TSIPs with an invasion speed higher than 13.7 µm/day for the above-mentioned conditions.

Scale bars: 50 µm.

All graphs represent Means±SEM from 3 biologically independent experiments unless otherwise specified. p-values were calculated using two-sided unpaired T-test (****p<0.0001, ***p<0.001, *p<0.05, ns: p>0.05).

incubated TSIPs in Matrigel. This induced a long-lasting inhibition of apical membrane polarisation, but preserved the peripheral acto-myosin cortex (Fig. 6a,b) [45]. In these conditions, TSIP-PDX#1 invaded even more efficiently, with an average displacement of 79±7.2 μm (Fig. 6d and Sup. Fig. 5e). We then hypothesized that the increased acto-myosin contractility generated by low non-canonical TGFβ signalling could mediate the force-generation propelling TSIPs in 3D environments, similar to the mechanism reported for single cells undergoing amoeboid migration [8]. In line with this hypothesis, immunostaining revealed that Myosin-II was phosphorylated at the peripheral apical cortex of invading TSIPs (Sup. Fig. 5f). Moreover, inhibiting ROCK and Myosin-II significantly reduced TSIP-PDX#1 average displacement from 49.9±3.6 μm to 29.7±2.5 μm and 22.4±1.5 μm, respectively (Fig. 6d and Sup. Fig. 5e). Inhibiting Myosin-II activity had a greater effect than Y27632 on TSIPs migration but not on apico-basolateral polarisation (Fig. 6a,b). This confirmed that, at TSIPs' apical pole, the contractility of the acto-myosin cortex, and not the membranous proteins, plays a prevalent role in migration.

Thus, TSIPs invade tissues using a unique mode of collective invasion that does not involve the formation of adhesion-based protrusions. Rather, it relies on the high contractility of the apical peripheral acto-myosin cortex resulting from decreased non-canonical TGFβ signalling.

TSIPs are efficient initiators of metastases

To assess whether TSIPs possess tumour-initiating properties, we turned to mice xenograft models. We injected TSIPs (TSIP-PDX#1 and TSIP-PDX#2) expressing the luciferase reporter gene into the peritoneal cavity of immuno-deficient mice. As controls, we injected the equivalent number of single cells (SCs). Bioluminescence monitoring demonstrated that TSIP-PDX#1 and TSIP-PDX#2 efficiently seed peritoneal metastases (TSIP-PDX#1 were 60

times more efficient than TSIP-PDX#2 at colonizing the peritoneum (Fig. 7a,b) and, in addition, gave rise to abundant ascites. In contrast, by 40 days, the tumour burden was respectively 20 fold lower or absent in mice injected with their single cell counterparts (Fig. 7a,b). The presence of metastases was confirmed at sacrifice and measured using a modified Peritoneal Cancer Index assessment[33] (Sup. Fig. 6a). In the ascites, TSIP-PDX#1 propagated surrounded by mostly apoptotic caspase3(+) single tumour cells (Fig.7d, Sup. Fig. 6b,c). Staining using Hematoxylin/Eosin/Saffron (HES) or an antibody specific of human MHC class-I demonstrated the presence of mucinous secondary tumours that have deeply invaded the peritoneum, penetrating several organs (liver, bladder, intestine, Fig. 7d to panels). We investigated the architecture of metastases initiated by TSIPs. They were almost exclusively composed of cohesive epithelial EpCam(+)/Vim(-) tumour cell masses (Fig. 7c-f and Sup. Fig. 6d). In mice injected with TSIP-PDX#1 and TSIP-PDX#2, respectively 1% and 3% of tumour cells were visible as individuals, among which only cells from TSIP-PDX#2 expressed vimentin, alone or in combination with EpCam (Fig. 7e,f and Sup. Fig. 6d). Finally, staining for ezrin and Scribble proved that tumour cell groups all displayed an inverted apico-basolateral polarity, as we observed in MUC CRC patients (Fig. 7d, bottom panels), compare with Fig. 3a and Sup. Fig. 3c). Together, these data demonstrate that TSIPs are efficient initiators of peritoneal metastases and that EMT and MUC CRC single tumour cells do not make a significant contribution to this process.

DISCUSSION

In sum, by investigating specimens from metastatic CRC patients we have identified a new collective and epithelial mode of cancer dissemination, based upon collective budding, growth and invasion processes. Remarkably, throughout the process of dissemination, the TSIPs that constitute the malignant metastatic intermediates linking primary tumours to

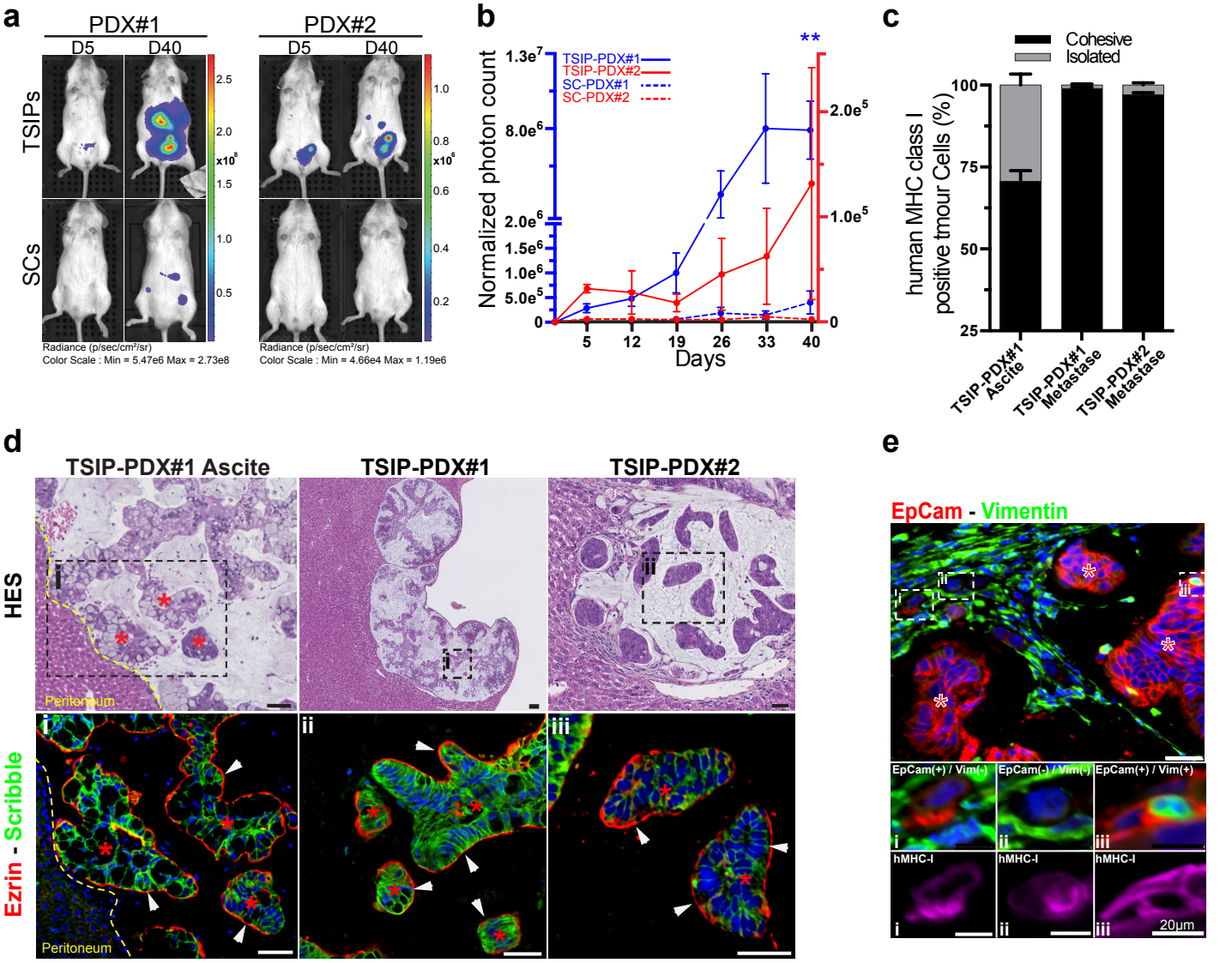

Figure 7. TSIPs are efficient initiators of metastases

(a) Representative bioluminescence images collected from 5 mice per group, 5 or 40 days after intraperitoneal injection of TSIPs or single cells (SCs) obtained from PDX#1 and PDX#2 expressing luciferase.

(b) Peritoneal metastases growth curves from mice injected intraperitoneally with TSIPs or single cells (SCs) obtained from PDX#1 and PDX#2 expressing luciferase (5 mice for each group). The bioluminescence signal was measured every week for each individual mouse. P-values are calculated using unpaired two-sided T-test at 40 days (**p=0.005).

(c) Quantification of cohesive and isolated tumour cells in metastases and ascites formed by the injection of TSIP-PDX#1 and TSIP-PDX#2 in mice peritoneal cavity. Tumour cells were identified by MHC class-I antibody specifically recognizing the human isoform and respectively represent n= 880, 1795, 2985 cells from 3 different mice.

(d) Representative images of histological sections of metastases from 5 mice collected 40 days after intraperitoneal injection of TSIP-PDX#1 and TSIP-PDX#2 (3 different mice of TSIP-PDX#1 ascites). Top panels: tumour section were stained using Hematoxylin/Eosin/Saffron (HES) and bottom panels show high magnification of the boxed regions (i ii and iii) immunostained for Ezrin (red), Scribble (green) and DAPI. Red stars indicate TSIPs, arrowheads point to their outward apical pole.

(e) Representative images of histological sections of metastases from 5 mice injected with TSIP-PDX#1 or TSIP-PDX#2 stained using antibodies against human MHC class-I (purple), Vimentin (green) and EpCam (red). Boxed regions (i, ii and iii) are shown at high magnification to reveal markers expressed by single cells. Red stars indicate TSIPs. The quantification is displayed in panel (f).

(f) Bar graph showing the proportions of EpCam and Vimentin expressing tumour cells (identified by human MHC class-I staining) among the isolated or cohesive population of the ascites or metastases. From the left to the right of the graph, n= 510, 270, 1771, 24, 2964, 61 cells respectively from 3 different mice.

Scale bars 50 µm unless otherwise specified.

All graphs represent Mean±SEM from 5 mice or 3 biologically independent experiments unless otherwise specified.

peritoneal metastases retain a robust epithelial architecture and an inverted apico-basolateral polarity (see Graphical Summary in Fig. 8).

While we cannot exclude the possibility that a small fraction of the vimentin positive cells found in some peritoneal effusions contribute to the disease, these cells rapidly die in isolation (as has been reported for circulating tumour cell-clusters in the bloodstream [46]) and do not generate multicellular structures *ex vivo*. Moreover, our results are in agreement with recent mice models of breast and pancreas carcinomas demonstrating the formation of distant metastases independently of EMT activation [9,10]. TSIPs form and propagate in specific histological subtypes of CRCs with dismal outcome and increased occurrence of peritoneal metastases[30,31]. To date, mice models of these cancers, which evolve from the CIMP/serrated pathway, are lacking. Nevertheless, our results are in line with the phenotypes of *TGFβRI* and *SMAD3* knockout mice which induce respectively the differentiation of goblet cells and mucinous intestinal malignancies [47,48]. In addition, the low level of TGFβ activation is likely related to the lack of EMT activation in these tumours [49-51].

Our findings contradict the prevailing consensus that carcinoma progression is accompanied by the loss of epithelial architecture and polarity [52,53]. Yet, while the normal apico-basolateral polarity is maintained at the cellular level, the neoplastic tissue organisation is profoundly altered, with the protective apical pole contacting patients' peritoneal fluids and tissues. This may enable the TSIPs to survive in multiple environments and help them evade immune surveillance. Interestingly, TSIPs invade tissues using a unique mode of collective invasion that does not involve the formation of adhesion-based protrusions [54,55] but is reminiscent of propulsive amoeboid single cell migration [56], a process never reported for collectives. Moreover, collective apical budding does not occur from normal epithelia. While we have seen cancer formation and progression as the result of improper reactivation of normal developmental processes, TSIP biology rather suggests that neoplastic epithelia may develop

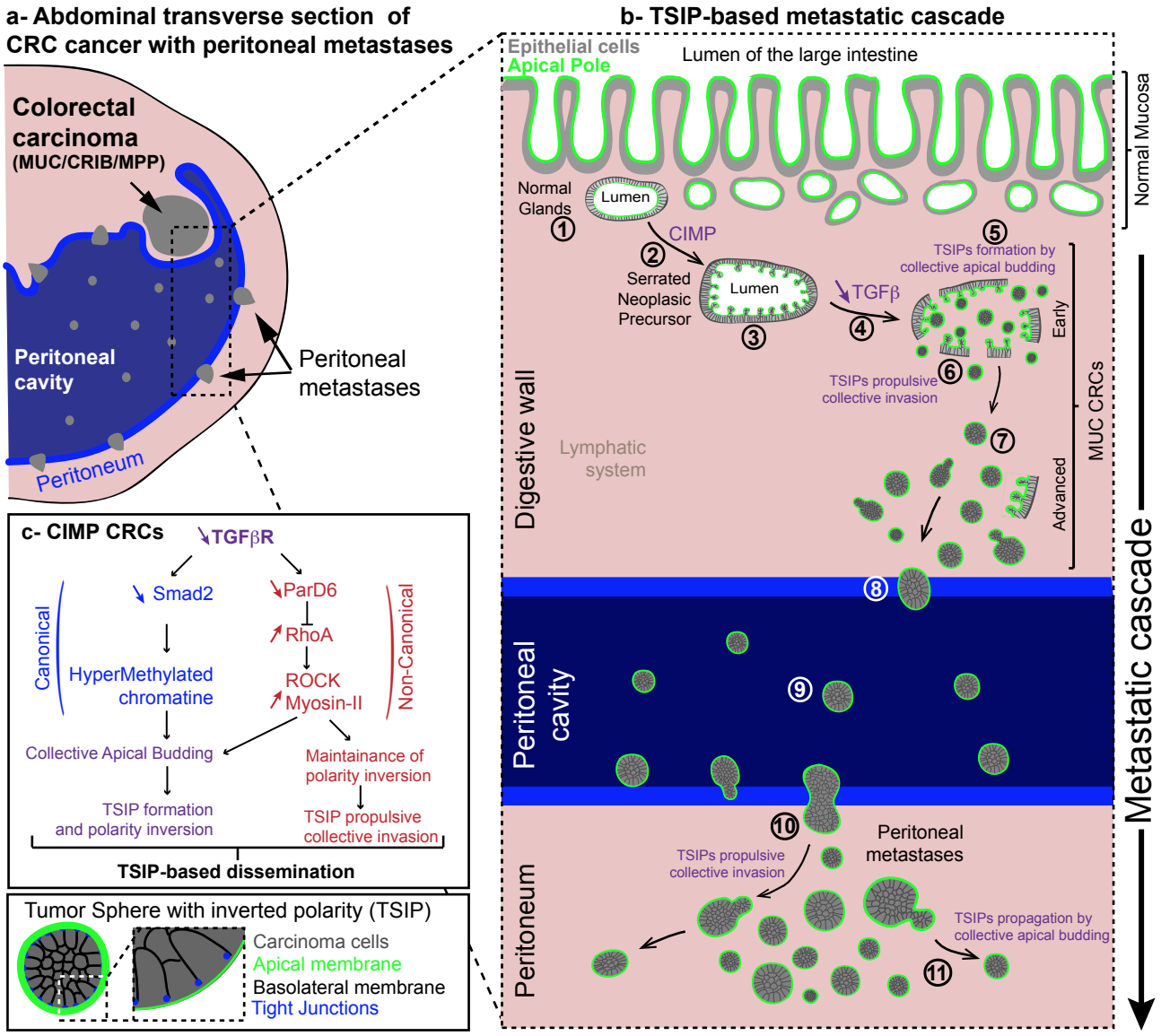

Figure 8. TSIP-based metastatic dissemination to the peritoneal cavity in patients with CIMP CRCs
(a)- Schematic representation of the abdominal transverse section of CRCs patients with peritoneal metastases.
(b)- TSIP-based metastatic cascade: (1) In the normal intestinal mucosa, the epithelial cell monolayer positions its apical pole toward the lumen, corresponding to the inside space of the gastrointestinal tube or the luminal cavity of glandular sections. (2) The CpG island methylator phenotype (CIMP) induces the development of glandular precursor lesions with a serrated morphology. (3) Serrated neoplastic glands display a saw-tooth pattern corresponding to serial events of bulging toward the apical pole. (4) Decrease in canonical and non-canonical TGFβ signalling (see (c) for details) promotes the progression to MUC CRCs and triggers TSIPs formation and their polarity inversion by collective apical budding, now independent tumour collectives surrounded by an outward apical pole (See also Fig. 3i). TSIPs are initially released into the luminal space of the neoplastic gland. (5) As collective apical budding develops, the CIMP glands breach, displaying numerous areas of rupture. TSIPs and mucus, initially segregated within the epithelial monolayer, are now in contact with the microenvironment. (6) TSIPs reach and spread in the stroma using collective invasion and the acto-myosin contractility (See (c) for details). (7) As MUC CRCs progress, TSIPs accumulate and the glandular architecture is lost, leading to tumours with an inverted topology, mainly composed by TSIPs with their apical pole in contact with the microenvironment. (8) TSIPs can directly exfoliate into the peritoneal space, seeding the peritoneal cavity (9). (10) TSIPs invade the peritoneum and underlying tissues using the same mode of collective invasion in their inverted topology. (11) Along the metastatic cascade, in primary tumours and in metastases, TSIPs propagate by alternating collective invasion and collective apical budding to generate new TSIPs.
(c)- Molecular mechanism underlying TSIP-based dissemination in CIMP CRCs associated with increased rate of somatic mutations in genes encoding TGFβ receptors and Smad2/3/4 and a decreased expression level of downstream effectors such as Smad co-factors and ParD6A.

specific strategies to colonize the body. This clinical cell biology research provides an alternative conception of cancer dissemination and is therefore vital if we are to use an understanding of the biology of tumour progression to the benefit of cancer patients.

REFERENCES

1. Bilder, D. Epithelial polarity and proliferation control: links from the Drosophila neoplastic tumor suppressors. *Genes Dev*. **18,** 1909–1925 (2004).
2. Huang, L. & Muthuswamy, S. K. Polarity protein alterations in carcinoma: a focus on emerging roles for polarity regulators. *Curr. Opin. Genet. Dev*. **20,** 41–50 (2010).
3. Muthuswamy, S. K. & Xue, B. Cell polarity as a regulator of cancer cell behavior plasticity. *Annu. Rev. Cell Dev. Biol*. **28,** 599–625 (2012).
4. Nieto, M. A., Huang, R. Y.-J., Jackson, R. A. & Thiery, J. P. EMT: 2016. *Cell* **166,** 21–45 (2016).
5. Thiery, J. P., Acloque, H., Huang, R. Y. J. & Nieto, M. A. Epithelial-mesenchymal transitions in development and disease. *Cell* **139,** 871–890 (2009).
6. Friedl, P. & Alexander, S. Cancer invasion and the microenvironment: plasticity and reciprocity. *Cell* **147,** 992–1009 (2011).
7. Liu, Y.-J. *et al*. Confinement and low adhesion induce fast amoeboid migration of slow mesenchymal cells. *Cell* **160,** 659–672 (2015).
8. Paluch, E. K., Aspalter, I. M. & Sixt, M. Focal Adhesion-Independent Cell Migration. *Annu. Rev. Cell Dev. Biol*. (2016). doi:10.1146/annurev-cellbio-111315-125341
9. Fischer, K. R. *et al*. Epithelial-to-mesenchymal transition is not required for lung metastasis but contributes to chemoresistance. *Nature* (2015). doi:10.1038/nature15748
10. Zheng, X. *et al*. Epithelial-to-mesenchymal transition is dispensable for metastasis but induces chemoresistance in pancreatic cancer. *Nature* (2015). doi:10.1038/nature16064
11. Friedl, P., Locker, J., Sahai, E. & Segall, J. E. Classifying collective cancer cell invasion. *Nat. Cell Biol*. **14,** 777–783 (2012).
12. Cheung, K. J., Gabrielson, E., Werb, Z. & Ewald, A. J. Collective invasion in breast cancer requires a conserved Basal epithelial program. *Cell* **155,** 1639–1651 (2013).
13. Montell, D. J., Yoon, W. H. & Starz-Gaiano, M. Group choreography: mechanisms orchestrating the collective movement of border cells. *Nat. Rev. Mol. Cell Biol*. **13,** 631–645 (2012).
14. Friedl, P. & Gilmour, D. Collective cell migration in morphogenesis, regeneration and cancer. *Nat. Rev. Mol. Cell Biol*. **10,** 445–457 (2009).
15. Pino, M. S. & Chung, D. C. *The chromosomal instability pathway in colon cancer*. *Gastroenterology* **138,** 2059–2072 (2010).
16. Vogelstein, B. *et al*. Genetic alterations during colorectal-tumor development. *N. Engl. J. Med*. **319,** 525–532 (1988).
17. Cancer Genome Atlas Network. Comprehensive molecular characterization of human colon and rectal cancer. *Nature* **487,** 330–337 (2012).
18. Guinney, J. *et al*. The consensus molecular subtypes of colorectal cancer. *Nat. Med*. (2015). doi:10.1038/nm.3967
19. Marisa, L. *et al*. Gene expression classification of colon cancer into molecular subtypes: characterization, validation, and prognostic value. *PLoS Med*. **10,** e1001453

(2013).
20. Juo, Y. Y. *et al*. Prognostic value of CpG island methylator phenotype among colorectal cancer patients: a systematic review and meta-analysis. *Ann. Oncol.* **25,** 2314–2327 (2014).
21. Weisenberger, D. J. *et al*. CpG island methylator phenotype underlies sporadic microsatellite instability and is tightly associated with BRAF mutation in colorectal cancer. *Nat. Genet.* **38,** 787–793 (2006).
22. Phipps, A. I. *et al*. Association between molecular subtypes of colorectal cancer and patient survival. *Gastroenterology* **148,** 77–87.e2 (2015).
23. Ward, R. L. *et al*. Adverse prognostic effect of methylation in colorectal cancer is reversed by microsatellite instability. *J. Clin. Oncol.* **21,** 3729–3736 (2003).
24. Bettington, M. *et al*. The serrated pathway to colorectal carcinoma: current concepts and challenges. *Histopathology* **62,** 367–386 (2013).
25. O'Brien, M. J., Zhao, Q. & Yang, S. Colorectal serrated pathway cancers and precursors. *Histopathology* **66,** 49–65 (2015).
26. van Gestel, Y. R. B. M. *et al*. Patterns of metachronous metastases after curative treatment of colorectal cancer. *Cancer Epidemiol* **38,** 448–454 (2014).
27. Segelman, J. *et al*. Incidence, prevalence and risk factors for peritoneal carcinomatosis from colorectal cancer. *Br J Surg* **99,** 699–705 (2012).
28. Sugarbaker, P. H. Peritoneal carcinomatosis: natural history and rational therapeutic interventions using intraperitoneal chemotherapy. *Cancer Treat. Res.* **81,** 149–168 (1996).
29. Franko, J. *et al*. Prognosis of patients with peritoneal metastatic colorectal cancer given systemic therapy: an analysis of individual patient data from prospective randomised trials from the Analysis and Research in Cancers of the Digestive System (ARCAD) database. *Lancet Oncol.* **17,** 1709–1719 (2016).
30. Hugen, N., van de Velde, C. J. H., de Wilt, J. H. W. & Nagtegaal, I. D. Metastatic pattern in colorectal cancer is strongly influenced by histological subtype. *Ann. Oncol.* **25,** 651–657 (2014).
31. Numata, M. *et al*. The clinicopathological features of colorectal mucinous adenocarcinoma and a therapeutic strategy for the disease. *World J Surg Oncol* **10,** 109 (2012).
32. Goéré, D. *et al*. Is there a possibility of a cure in patients with colorectal peritoneal carcinomatosis amenable to complete cytoreductive surgery and intraperitoneal chemotherapy? *Ann. Surg.* **257,** 1065–1071 (2013).
33. Mohamed, F., Cecil, T., Moran, B. & Sugarbaker, P. A new standard of care for the management of peritoneal surface malignancy. *Curr Oncol* **18,** e84–96 (2011).
34. Subramanian, A. *et al*. Gene set enrichment analysis: a knowledge-based approach for interpreting genome-wide expression profiles. *Proc. Natl. Acad. Sci. U.S.A.* **102,** 15545–15550 (2005).
35. Davidowitz, R. A. *et al*. Mesenchymal gene program-expressing ovarian cancer spheroids exhibit enhanced mesothelial clearance. *J Clin Invest* (2014). doi:10.1172/JCI69815
36. Tom, B. H. *et al*. Human colonic adenocarcinoma cells. I. Establishment and description of a new line. *In Vitro* **12,** 180–191 (1976).
37. Julien, S. *et al*. Characterization of a large panel of patient-derived tumor xenografts representing the clinical heterogeneity of human colorectal cancer. *Clin. Cancer Res.* **18,** 5314–5328 (2012).
38. Sato, T. *et al*. Long-term expansion of epithelial organoids from human colon, adenoma, adenocarcinoma, and Barrett's epithelium. *Gastroenterology* **141,** 1762–1772

(2011).
39. Laiho, P. *et al*. Serrated carcinomas form a subclass of colorectal cancer with distinct molecular basis. *Oncogene* **26,** 312–320 (2007).
40. de Miranda, N. F. C. C. *et al*. Transforming Growth Factor β Signaling in Colorectal Cancer Cells With Microsatellite Instability Despite Biallelic Mutations in TGFBR2. *Gastroenterology* **148,** 1427–37.e8 (2015).
41. Brown, K. A., Pietenpol, J. A. & Moses, H. L. A tale of two proteins: differential roles and regulation of Smad2 and Smad3 in TGF-beta signaling. *J. Cell. Biochem.* **101,** 9–33 (2007).
42. Maiuri, P. *et al*. The first World Cell Race. *Curr. Biol.* **22,** R673–5 (2012).
43. Alexander, S., Koehl, G. E., Hirschberg, M., Geissler, E. K. & Friedl, P. Dynamic imaging of cancer growth and invasion: a modified skin-fold chamber model. *Histochem. Cell Biol.* **130,** 1147–1154 (2008).
44. Giampieri, S., Pinner, S. & Sahai, E. Intravital imaging illuminates transforming growth factor beta signaling switches during metastasis. *Cancer Res.* **70,** 3435–3439 (2010).
45. O'Brien, L. E. *et al*. Rac1 orientates epithelial apical polarity through effects on basolateral laminin assembly. *Nat. Cell Biol.* **3,** 831–838 (2001).
46. Aceto, N. *et al*. Circulating tumor cell clusters are oligoclonal precursors of breast cancer metastasis. *Cell* **158,** 1110–1122 (2014).
47. McCauley, H. A. *et al*. TGFβ signaling inhibits goblet cell differentiation via SPDEF in conjunctival epithelium. *Development* **141,** 4628–4639 (2014).
48. Zhu, Y., Richardson, J. A., Parada, L. F. & Graff, J. M. Smad3 mutant mice develop metastatic colorectal cancer. *Cell* **94,** 703–714 (1998).
49. Lamouille, S., Xu, J. & Derynck, R. Molecular mechanisms of epithelial-mesenchymal transition. *Nat. Rev. Mol. Cell Biol.* **15,** 178–196 (2014).
50. Ozdamar, B. *et al*. Regulation of the polarity protein Par6 by TGFbeta receptors controls epithelial cell plasticity. *Science* **307,** 1603–1609 (2005).
51. Giampieri, S. *et al*. Localized and reversible TGFbeta signalling switches breast cancer cells from cohesive to single cell motility. *Nat. Cell Biol.* **11,** 1287–1296 (2009).
52. Bilder, D., Li, M. & Perrimon, N. Cooperative regulation of cell polarity and growth by Drosophila tumor suppressors. *Science* **289,** 113–116 (2000).
53. Zhan, L. *et al*. Deregulation of scribble promotes mammary tumorigenesis and reveals a role for cell polarity in carcinoma. *Cell* **135,** 865–878 (2008).
54. Wang, X., He, L., Wu, Y. I., Hahn, K. M. & Montell, D. J. Light-mediated activation reveals a key role for Rac in collective guidance of cell movement in vivo. *Nat. Cell Biol.* **12,** 591–597 (2010).
55. Hegerfeldt, Y., Tusch, M., Bröcker, E.-B. & Friedl, P. Collective cell movement in primary melanoma explants: plasticity of cell-cell interaction, beta1-integrin function, and migration strategies. *Cancer Res.* **62,** 2125–2130 (2002).
56. Callan-Jones, A. C. & Voituriez, R. Actin flows in cell migration: from locomotion and polarity to trajectories. *Curr. Opin. Cell Biol.* **38,** 12–17 (2016).

METHODS

Recovery and characterization of peritoneal effusions from colorectal cancer patients:

The human study protocols followed all relevant ethical regulations in accordance with the declaration of Helsinki principles. The study was approved by the ethic committee (CPP IDF 10), under protocol NI-2015-06-03, at Gustave Roussy and lariboisière Hospitals. Written informed consent was obtained from all patients. Peritoneal effusions from a total of 59 patients with colorectal cancer were collected. The patients received neoadjuvant chemotherapy 2 to 3 weeks before surgery. The peritoneal effusion samples were collected at the onset of Hyperthermic Intraperitoneal Chemotherapy treatment (HIPEC). Immediately after laparotomy, and before cytoreductive surgery, serous fluid was collected by addition and reabsorption of 500 ml of saline solution. The fluids were processed in the laboratory within 2 hours after collection for characterization and functional experiments. The freshly isolated samples were transferred to sterile tubes and centrifuged at 1500 rpm for 10 min. The Peritoneal Cancer Index (PCI)[33] was evaluated during surgery. Counting and characterization of cells in peritoneal effusion total fraction was done after *Ficoll-Paque* PLUS (GE HealthCare, 17144002) centrifugation following the manufacturer's protocol. A part of the interphase was removed and cells were cytospined at 1500 rpm for 5 min on a Superfrost plus glass slide (Thermo Scientific, 10149870). Then, the cells were fixed in 4% paraformaldehyde (PFA) (Electron microscopy science, 15710) during 5 min and washed with Phosphate-buffered saline (PBS). The cells count was performed on the cytospin slides.

Separation of tumour clusters and single cells: The rest of the interphase was carefully collected and transferred to a new sterile tube. DMEM containing 4.5 g/l glucose, glutaMAX (Life Technologies, 31966021) and 1% Penicillin-Streptomycin (Life Technologies, 15140-122) was added to a final volume of 10 ml. Differential centrifugations, spin down until 2000 rpm, were performed at least 4 times. During these centrifugations, the supernatants were

saved for the single tumour cells enrichment and analyses procedures. The clusters present in the pellet were counted, some of them were fixed in 4% PFA for 45 min and immobilized for immunofluorescence and characterization, the other part directly used for functional studies. TSIPs were defined as tumour clusters with spherical shape and smooth surface and irregular clusters were defined by their uneven shape and rim. In parallel, single cells were pulled-down by centrifugation at 1500 rpm 5 min and resuspended in fresh medium. The total number of single-cells was counted in a Neubauer chamber and viability was accessed with Trypan Blue (Life Technologies), an aliquot was used for cytospin (total single-cell fraction, see description below). Prior to functional studies (proliferation, aggregation, survival), to exclude any small aggregates that would have formed during the manipulation, the single cell suspension was filtered with a pre-separation filter (20 μm) (Miltenyi Biotec, 130-101-812). Single cells were used as such or enriched for CRC cells using EpCam-coated microbeads and MS columns (Miltenyi Biotec 130-061-101 and 130-041-301) or after exclusion of CD45 positive population using EasySepTM Human CD45 Depletion Kit (Stemcell, 18259) following manufacturer's protocol.

Animal studies:

Animal experiments were compliant with French legislation and EU Directive 2010/63. The project was validated by the Ethical Committe (CEEA) n°26 and was then granted French government authorizations under number 517-2015042114005883 and 2734-2015111711418501. Mice were obtained from Charles River, housed and bred at the Gustave Roussy animal core facility (accreditation number E-94-076-11). Animals were humanely euthanized according to endpoints that were validated by the Ethical Commitee and the French government (Ministère de l'Enseignement Supérieur, de la Recherche et de l'Innovation).

Organoids retrieval and preparation from Patient-Derived Xenograft (TSIP-PDX): Two human colorectal tumours (PDX#1 corresponding to LRB-0009C and PDX#2 corresponding to IGR-0012P) from the CReMEC tumour collection were maintained in NSG mice (NOD-scid IL2Rgamma^{null}, from Charles River, France) as previously described by Julien et al.[37]. Briefly, small tumour fragments were subcutaneously engrafted on the flank of anesthetized mice (2.5% isoflurane). Tumour growth was measured at least once a week. When the volume reach 1500 mm^3, mice were sacrificed and tumours were used for ex vivo experiments and 50 mm^3 fragments engrafted on the flank of new mice. Organoids were prepared according to Sato et al.[38]. and adapted for muco-secreting tumours as follows: The PDX#1 or PDX#2 tumours between 1000-1500 mm^3 were retrieved from the mice, minced into small fragments using a sterile scalpel and were incubated for 1h30 at 37°C in a final volume of 5 to 10 ml of culture medium (DMEM) without FBS and with 2 mg/ml collagenase (Sigma, C2139). The samples were then mixed with 20 ml of DMEM and filtered on 100 µm mesh size cell strainers (EASYstrainer, 542000). Digested tumour clusters were pelleted in by 4 pulse-centrifugations at 1500 rpm. The tumour fragments, free of single cells, were maintained 3 days in ultra-low attachment plates (Corning, CLS3471) in culture medium. Then, organoids were pelleted at 1500 rpm and characterized (staining with apico-basolateral polarity markers demonstrated the organoids display the characteristics of TSIPs, Ext. Fig. 6a-b). TSIPs-PDX were used for survival and invasion experiments as well as for mice intraperitoneal injection.

Mice intraperitoneal injections: TSIPs and single cells obtained from PDX#1 and PDX#2 (above) were transduced using GFP-Luciferase lentiviruses (see below for lentiviral particle production). Immediately after PDX tumour dissociation and mucin removal, tumour fragments were incubated with lentiviruses at the concentration of 600 000 virus per ml in a 6 wells ultra-low attachment plate. The medium was changed after 2 days and single cells obtained by trypsinization. 1.10^4 of transduced TSIPs, or the equivalent number of single

cells, were resuspended into 100 µl culture media and injected intraperitoneally using 25G needle. The mice were monitored by imaging bioluminescence every 7 days until 40 days post- injection.

Bioluminescence imaging: All bioluminescence imaging (BLI) experiments were performed using an IVIS Spectrum CT pre-clinical in vivo imaging system (PerkinElmer Life Sciences, Hopkinton, MA, USA). Mice were anesthetized with 2.5% isoflurane, received caudal intravenous injection of 150 mg/kg of D-Luciferin (Promega, E1605), and were imaged after 2 min. The settings (acquisition time, f/stop and binning) were applied differently from one experiment to another taking into account the metastasis development and the consecutive increasing levels of emitted photons.

Invasion assays:

Collagen-I assays: rat-tail Collagen-I (Corning, 354236) was neutralized with 1.0 M NaOH and 10x MEM (Life Technologies, 21430-02) according to the ratio: 1.0:0.032:0.1 (vol/vol/vol). The concentration was then adjusted to 1.3-2 mg/ml with DMEM 1X and the collagen was incubated on ice for 1-1h15. The TSIPs embedded in neutralized Collagen-I were added on top of the pre-coated well at a concentration of 1-2 TSIPs per microliter (ibidi 8-well chamber). The gel was allowed to polymerize for 45 min at 37°C. TSIPs were then cultured in culture medium supplemented with FBS 10 % for up to 6 days (3 days for TGFβ (R&D System, P01137, 20 ng/ml), SB431542 (Sellekchem, S1067, 10 µM) alone or in combination with lentivirus encoding shRNA Smad2 and ParD6A) and fixed for staining. Medium were supplemented with FAK inhibitor (Sigma, 869288-64-2, 10 μM), NSC-23766 (Tocris, 2161, 50 µM), integrin α2 function-blocking antibody (Santa Cruz, sc-13346, 5 µg/ml), Y27632 (Calbiochem, 688000, 25 µM) and Blebbistatin (Calbiochem, 203391, 10 µM).

Matrigel assays: TSIPs were embedded into 3 mg/mL Matrigel (BD, 354230) and incubated in a pre-coated 8-well chamber (Ibidi). After polymerization, culture medium supplemented with FBS 10 % was added.

TSIP Polarity assessment: After incubation into collagen-I or Matrigel, the apico-basolateral polarity of TSIPs was quantified after immunostaining using anti-Ezrin. TSIPs are considered with inverted polarity when at least 75% of the total peripheral cells displayed an outward apical pole in one confocal Z-section.

Ex vivo peritoneum invasion assay:

During surgery, peritoneal fragments were excised in non-tumoural region (confirmed by histology preparation). Patient peritoneum explants were immediately sealed at the bottom of a transwell insert (Millipore, PIEP12R48, the PET membrane was removed) using collagen-I. after insertion in 24-well culture plates, the insert was filled with culture medium. The side that lines the peritoneum cavity faces the upper chamber. TSIPs collected in matching patients are seeded on top of the peritoneum in the upper chamber. TSIPs collected in matching patients are seeded on top of the peritoneum in the upper chamber.. The invasion assay lasted for 3 days, then, the peritoneal tissue was washed in PBS supplemented with Ca^{2+} $Mg^{2+,}$ and fixed in PFA 4%.

LS174T budding assay:

24h after plating LS174T cell line (4.10^5 cells in a 22 cm^2 tissue culture dish or 1.10^5 in 10 $cm^{2\ dish}$ for Fig 3g), the medium was changed and the cells incubated with normal medium or treated as follows: TGFβ (10 ng/ml) , SB431542 (10 µM), H1152 (Tocris, 2414, 2 µM), Blebbistatin (10 µM) or Noggin (Peprotech, 120-10C, 100 ng/ml). At day 7, 8 and 9 the plates were hit 20 times on the bench, the medium collected and centrifuged for 8 sec at 500g to

pellet the TSIPs and the supernatant transferred back to the plates. TSIPs-LS174T were then counted under light microscope and TSIPs counts added for 3 consecutive days.

LS174T morphogenesis assay:

LS174T 2D cell cultures were partially dissociated with trypsin (0.25%)-EDTA and filtered through 20 uM pre-seperation filters (Milteny Biotech). The harvested clusters (<5 cells) were embedded in a mix of collagen-I (Rat-tail neutralized as described in the invasion assay and used at a final concentration of 1.3 mg/ml) and Matrigel (final concentration of 4.5mg/ml) in an Ibidi plate. Single cells died, but small clusters survived and were grown for 7 days at 37°C. Their polarity was assessed after fixation and Ezrin immunostaining. Most clusters developed as cysts, with the apical pole surrounding 1 to 3 lumens. The polarity was considered inverted (apical pole facing the ECM-gel when more than 50% of the cells displayed a peripheral Ezrin staining (and no lumen). The non-polar structures show a diffuse Ezrin localization.

Single cell assays from patients' primary samples and cell lines:

Single cells obtention: Single-cells from patients' peritoneal effusions were isolated as described above. Dissociated single-cell (dSC) suspensions were obtained from TSIPs, PDX#1 and PDX#2, LS174T and SW620 by dissociation using Trypsin (0.25%)-EDTA for 7-10 minutes, and filtered through 20 μm pre-separation filters. As controls, TSIPs from patients, PDX#1, PDX#2 and LS174T were incubated in similar conditions. Survival and proliferation in suspension were addressed by plating single-cells in ultra-low attachment 96-well plates at 10-100 cells/ml. Proliferation was followed by light-microscopy, survival was assessed with Trypan Blue and propidium iodide at day zero and every three days. Hoechst

was used to count nuclei. LS174T aggregation was promoted by increasing cell concentration at 4000 cells/ml.

ECM gels assays: single cells were obtained by dissociation as described above, and embedded in either Matrigel (Corning, 354238 diluted, with medium, to a final concentration of 3.5 μg/mL) with or without Y27632 at a concentration of 25 μM or collagen-I (Rat-tail collagen-I neutralized and polymerized as described for invasion assays). They were seeded in an Ibidi plate at 37°C and cultured with adequate supplemented medium. Survival was assessed throughout a period of 9 days.

TSIP mitotic index was calculated as the ratio between mitotic cells and total cell number, expressed in percentage. Mitotic and interphasic nuclei were stained with DAPI and identified by their morphology.

Cell lines culture condition and transfection:

LS174T (Sigma) were grown in EMEM medium supplemented with 1% non-essential amino acids (NEAA) 10% foetal bovine serum (FBS) and 50 μg/ml penicillin, 50 μg/ml streptomycin (P/S). Colo205 (ATCC) were cultured in RPMI-1640 supplemented with 1 mM sodium pyruvate (SP), 10% FBS and P/S. SW620 and Caco-2 (ATCC) were grown in DMEM supplemented with 1 mM SP, 10% FBS and P/S. HCT-15 and LS1034 (ATCC) were grown in RPMI-1640 supplemented with 10% FBS and P/S. All cell lines were maintained in a humidified incubator at 37ºC under a 5 % CO2 atmosphere. SiRNA transfection into LS174T was achieved using Dharmafect#1 according to the manufacturer's instructions. SiRNA were purchased from Dharmacon: siGENOME Human Smad2 (D-003561-04 (#2)), Smad3 (D-020067-01 (#1) and D-020067-04 (#2)), Smad4 (D-003902-05 (#1) and D-003902-07 (#2)) and non targetting #2 (D-001206-14-05), ON-TARGETplus Human ParD3 (L-015602-00), Scribble ((L-010500-00), Llgl2 (L-019812-01) and TGFβRI (M-003929-02).

Virus production, shRNA sequences, and infection:

Virus production: GFP-Luciferase, shParD6A and shSmad2 Lentiviruses were obtained by co-transfecting the lentiviral vector pFUGW-Pol2-ffLuc2-eGFP (Addgene, 71394), pRRL.TRE3GdsRed-ShParD6A and pRRL.TRE3GdsRed-Smad2 (Fellmann et al. 2013)[57] with the packaging vectors pMD2G (Addgene) and pCMVdR8,74 (Addgene) into HEK293T cells with the tranfection reagent JetPrime (Polyplus, 114-15). Lentiviruses-containing supernatants were collected on days 2 and 3 following transfection, concentrated by ultracentrifugation (50000g, 2h) and stored at −80 °C.

ShRNA sequences: cDNA sequences used to make shRNA lentiviruses are as follows:
Smad2#1:5'GAACAAACCAGGTCTCTTG3',
Smad2#2:5'GGTGTTCGATAGCATATTA3',
ParD6A#1:5'GCCAGGTTTCCTCAGTCATAGA3'
ParD6A#2:5'AACAGCCATAACCTCATTGTCA3'.
Hybridized complementary oligonucleotides were inserted in the XhoI/EcoRI sites of the pRRL.TRE3GdsRed.

Infection: LS174T (5.10^4 cells) were transduced using lentiviruses, amplified and sorted by FACS on a double GFP (infection) and DsRed (ShRNA induction) positive signal following induction of ParD6A and Smad2 shRNA expression (TetON regulated) by addition of 100 ng/ml doxycycline (Sigma-Aldrich, D9891). A shRNA Renilla construct cell line was made as a control in parallel. For organoids infection, see the *« Mice intraperitoneal injections » section above*.

Immunoblot:

Cells were lysed with SDS sample buffer [62.5 mM Tris-HCl (pH 6.8), 10% glycerol, 0.002% bromophenol blue, 2% SDS, and 5% β-mercaptoethanol] and lysates were boiled for 10 min. The samples were subjected to SDS-PAGE and proteins were transferred to nitrocellulose membranes (GE healthcare). Membranes were incubated for 30 min in Blocking Solution [Tris-buffered saline (TBS) containing 0.1% Tween-20, 3% BSA] and further incubated with the appropriate primary antibody overnight at 4°C. The following primary antibodies were used at the indicated dilutions: Smad2 (1:1000, Cell Signalling Technology, 5339S), Smad3 (1:1000, Cell Signalling Technology, 9523S), Smad4 (1:1000, Sigma-Aldrich, HPA019154), TGFβRI (1:500, Bioworld Technologies, BS3257), Phospho-Smad2 (1:1000, Cell Signalling Technology, 3101S), Phospho-T18/S19-MLC (1:1000, Cell Signalling Technology, 3674S), HSC70 (1:4000, Santa Cruz, sc-7298), RhoA (1:2000, 26C4 gift from J. Bertoglio) and Scribble (1:1000, Santa Cruz, sc-28737). The membranes were then washed three times with 0.1% Tween-20/TBS and incubated for 45 min with secondary antibody conjugated to horseradish peroxidase; anti-mouse HRP (1:10000, GE Healthcare NA931V) or anti-rabbit-HRP (1:3000, Cell Signalling Technology, 7074S). Bound antibodies were detected with enhanced chemiluminescence.

Quantitative reverse transcription–PCR:

The total RNA fraction was isolated using RNeasy Mini Kit 50 (Qiagen) and applied to reverse transcription using High capacity RNA-to-cDNA Kit (Applied Biosystems). The cDNA was analysed by qPCR using GoTaq qPCR Master Kit (Promega) with QuantiStudio 7Flex Real-Time PCR System (Applied Biosystems). Reaction parameters were 95°C for 1 min, followed by 45 cycles of 95°C for 10 sec, 60°C for 10 sec and 72°C for 20 sec. The triplicate mean values were calculated using GAPDH gene transcription as reference for normalization. For RT-PCR the following primers are used:

Smad2Fwd: 5'GCTTGAGAAAGCCATCACCACT3';

Smad2Rev: 5'AGGCCTGTTGTATCCCACTGA3';

ParD6AFwd: 5'CGCGCAGTCCCGATAGCATC3';

ParD6ARev: 5'AGAACTCCTGGAAGCCGCTC3';

ParD3Fwd: 5'TGTATGCCCAAGTCAAGAAGCC3';

ParD3Rev: 5'TGCCTCAGACGCTGTATCCG3';

Llgl2Fwd: 5'GCAACTGGCGTTCACATCGA3';

Llgl2Rev: 5'AGTAGTGTGTGCTCATCGCG3';

GAPDHFwd: 5'CTTTTGCGTCGCCAGCCGAG3';

GAPDHRev: 5'CCAGGCGCCCAATACGACCA3'.

Immunofluorescence, immunohistochemistry, antibodies and histology:

Immunofluorescence: Samples were washed twice in PBS supplemented with calcium (0.1 mM) and magnesium (1 mM) and fixed in PFA 4% for 45 min (TSIPs, peritoneum) or 10 min (cytospins and single cells). Permeabilization was performed in PBS supplemented with 0.5% TritonX-100 during 45 min (5 min for cytospins, single cells and slides from mice metastasis). Primary antibodies were incubated overnight at 4°C at the dilutions listed below in antibody diluent, PBS with 10% serum supplemented by 0.1% TritonX-100. Secondary antibodies (Cy™3-conjugated or Fluorescein (FITC) conjugated anti-Mouse or anti-Rabbit, Alexa Fluor 488 anti-rabbit 1:100, Jackson ImmunoResearch) and DAPI (1 μg/ml) were incubated overnight at 4°C or 2h at room temperature. Slides were mounted using Fluoromont-G (Southern Biotech).

Antibodies: The following primary antibodies were used at the indicated dilutions: EpCam (1:100, Thermofisher, MA5-12436), cytokeratin 20 (1:100, Dako, M7019), vimentin (1:500, Thermofisher, PA1-16759), calretinin (1:50, Life Technologies, 180211), CD133 (1:100,

Miltenyi Biotech, 130-090-422), CD45 (1:100, Thermofisher, MA5-13197), E-cadherin (1:100, Abcam, ab1416), E-cadherin (1:100, Cell Signalling Technology, 3195S), phospho-ERM (1:100, Cell Signalling Technology, 3149), Ezrin (1:100, BD Biosciences, 610603), GM130 (1:100, Novus Biologicals, NBP1-89757), ZO1 (1:200, Invitrogen, 40-2300), β1 integrin (1:100, Abcam, ab24693), occludin (1:100, Thermofisher, 33-1500), cleaved caspase 3 (1:100, Cell signalling Technology, 9661), GALT (1:50, Santa cruz, G-1) or Cytochrome C (1:100, BD Pharmigen, 556432), NERFH1 (Thermo Scientific, A5-17045), villin (1:100, Cell Signalling Technology, R814) beta-catenin (1:100, Thermo Scientific, MA1-300) alpha-catenin (1:100, Sigma Aldrich, C2081), Scribble (1:100, Santa Cruz, sc-28737), CMH-I (1:200, Abcam, Ab52922), aPKC (1:100, Santa Cruz, sc-216-G), Phospho-T18/S19-MLC (1:100, Cell Signalling Technology, 3674S), alexafluor 647 phalloidin (1:200, Life Technologies, A22287). Secondary antibodies used were from Jackson Immuno Research: FITC-chicken, 703-545-155, 1:200; Cy3-mouse, 715-165-151, 1:200; FITC-mouse, 715-545-150, 1:100; Cy3-rabbit, 711-165-152, 1:200; FITC-rabbit, 711-545-152, 1:100.

Histology: Colorectal cancer and peritoneum specimens obtained after chirurgical resection were formalin-fixed and paraffin embedded (FFPE) according to routine protocols. Peritoneal effusions were concentrated by centrifugation and fixed in formalin, then embedded for cytoblock. 3 μm sections of FFPE samples were deparaffinised, unmasked (Ph8) and rehydrated prior Hematoxylin Eosin Saffron (HES) or Alcian Blue staining, immunohistochemistry or immunofluorescence.

Immunohistochemistry: Sections were immunostained with Ezrin (1:100, BD Biosciences, 610603) or CK20 specific mouse monoclonal antibody, (clone Ks20.8, Dako, Glostrup, Denmark). Stainings were performed with Ventana BenchMark XT immunostainer (ventana Medical Systems, Tucson, AZ) utilizing UltraView DABv3 kit (Ventana). The chromogene was 3,3'-diaminobenzidine (DAB) in all the stainings. Histochemical staing of Alcian Blue

pH 2.5 were performed with Ventana BenchMark Special Stains (ventana Medical Systems, Tucson, AZ) utilizing V1.00.0010 process. Peritoneal effusions smears were coloured using May-Grünwald-Giemsa.

Live imaging, electron microscopy, images treatment and analyses

Microscopy acquisition and live imaging: images were acquired using an Olympus Epifluorescence inverted X73 microscope or a SpinningDisk CSU-W1 (Yokogawa) with a ZylasCMOC camera piloted with an Olympus X83. TSIPs behaviours in 3D culture were imaged by DIC time lapse microscopy, motorized stage, temperature and CO_2 controllers. Images were recorded every 30 min for 6 days for patients samples, every 2 days for organoids. *Sphericity, shape factor and perimeter* were measured using the Cellsens Dimension software (Olympus) from DIC images. *TSIPs polarity* was assessed by calculating the ratio between peripheral cells with or without Ezrin staining from one median section. *Analyses of TSIP trajectories from DIC timelapse sequences*: the TSIP perimeter was delineated manually and TSIP centroid position calculated using ImageJ. TSIP centroids displacement was automatically tracked using ImageJ and verified by visual inspection before further quantification. The speed (µm/day) is calculated with the total distance travelled over 6 days, the displacement (µm) means the length between the centroid positions at D0 and D6 and the directionality is the ratio between the distance and the displacement.

Images for display were processed using Metamorph or imageJ softwares.

Electron microscopy: Isolated TSIPs were fixed in 2 % glutaraldehyde in 0.1 M phosphate buffer pH 7.3 and deposited in drops of neutralized collagen (2 mg/ml) allowed to polymerize 10 min at room temperature laid on a glass coverslip. TSIPs were washed 30 min in phosphate buffer, post-fixed with 2% osmic acid at room temperature and rinsed in water. Samples were dehydrated in ethanol and embedded in Epon. Polymerization was complete

after 48 hours at 60°C. Ultrathin sections were collected on 100-mesh grids coated with Formvar and carbon, stained with uranyl acetate and lead citrate and observed with a FEI Technai Spirit transmission electron microscope at 80 Kv. Digital images were taken with a SIS MegaviewIII CCD camera.

Expression Profiles and sample phenotype definitions:

CIT: The gene expression profile from 15 Mucinous (MUC), 188 Lieberkuhnian (LBK) and 19 normal samples were obtained from the CIT collection of patient samples by Marisa et al. 2013[19] (GSE39582). Analyses of differential expression were done using t-test from the ClassComparison package in R.

TCGA expression data: TCGA RNASeq raw counts data were obtained from GSE62944[58]. *We retrieved 41 normal colon, 61 MUC CRC and 389 LBK*. Analyses of differential expression were performed using the limma voom procedure[59].

TGFBeta pathway: The Reactome signalling TGFbeta receptor complex and activin receptors have been classified according to the function of genes into three categories: receptors / canonical component/ non-canonical components.

TCGA mutation data: Somatic mutations were retrieved from the cBioPortal website using the dataset of 276 samples corresponding to the TCGA publication (TCGA, Nature 2012)[17] available from cbioportal: http://www.cbioportal.org/study?id=coadread_tcga_pub#summary. The significance of the differential prevalence of mutations per gene or per set of genes between Mucinous (n=26) and Lieberkuhnian (n=174) groups was calculated with a Fisher Exact Test.

Cell lines: We obtained gene expression profiles for ovarian cancer cell lines from GSE26805. We retrieved 9 clearance competent (invasive high) and 6 clearance incompetent (invasive low) cell lines as defined in the original publication Davidowitz et al.[35]. The EMT

signature was broken into a mesenchymal gene set and an epithelial gene set according to the direction of expression changes in the cell lines.

Gene set activity computation: The activity of a gene set in a sample was computed the following way: we first z-transformed the gene expression profiles to normalize the expression of each gene across samples. We then computed the enrichment score (ES) of a gene set using this z-transformed matrix of expression, as described in the Gene Set Enrichment Analysis original publication by Subramanian et al. [34]. The ES corresponds to the relative activity of a gene set in a sample as compared to all others. Hence, samples with high ES are the samples with the highest relative expression of the genes belonging to this set among the samples belonging to the gene expression matrix.

GSEA: Gene set enrichment analysis was implemented in R and follows the method described in Subramanian et al.[34]. Null distribution was obtained by 1,000 sample-shuffling. Gene signatures were obtained by ranking the genes according to the sign of the statistics (S) and the p-value (p) of the test with the following metric: $-1\times(S)\times \log(p, 10)$.

MUC vs LBK pathway enrichment analysis: Pathways were obtained from the KEGG and REACTOME pathways from the C2 collection of the MSigDB database. In order to identify pathways enriched in CIT and TCGA datasets, we first analysed the 2 datasets independently. The GSEA p-values were then integrated using the Stouffer method and corrected for multiple hypothesis testing with a False Discovery Rate (FDR) following the Benjamini-Hochberg procedure. Significant pathways were defined as those satisfying FDR < 0.2.

Statistics and reproducibility:

Peritoneal effusions have been collected from independent patients. The exact number of effusions analyzed is indicated in the figure legend. All experiments were repeated at least three times with similar results unless a different number of repeats is stated in the

legend.Values are represented as Means±SEM (Standard Error of the Mean), unless otherwise specified in the legend.

Statistical significance was tested with unpaired two-tailed Student's t-test (p_{TT}), one-way analysis of variance (ANOVA) (p_A), Linear regression (p_{LR}) using GRaphPad Prism or one-sided and two-sided Fisher Exact test ($p_{F,}$ using R and http://www.socscistatistics.com/tests/fisher/Default2.aspx)
with level of significance alpha = 0.05 (confidence interval 95%). Method used, P values and N numbers are indicated in the figure legends. P values of statistical significance are represented as ****P <0.0001, ***P <0.001, **P <0.01, *P <0.05. The exact value is indicated when possible.

No statistical method was used to predetermine sample size. No animals were excluded from the study. No method of randomization was used. The investigators were not blinded to allocation during experiments or outcome assessment.

Data availability

The human colon cancer RNA-seq and mutation datasets used to support the findings of this study are both derived from the TCGA Research Network (http://cancergenome.nih.gov/) and are respectively available from GSE62944 and cbioportal (http://www.cbioportal.org/study?id=coadread_tcga_pub#summary). The human colon cancer microarray data from the CIT cohort is available from GSE39582. The gene expression profiles for ovarian cancer cell lines are available from GSE26805.

Source data for Fig. 4a and 4b are provided in Supplementary Table 2 and 3 and Source data for Fig. 3h and Supp. Fig. 5C are provided in Supplementary movie 1 and 2 available in the

supporting the findings of this study are available from the corresponding author upon reasonable request.

Methods References

57. Fellmann, C. *et al*. An optimized microRNA backbone for effective single-copy RNAi. *Cell Rep* **5,** 1704–1713 (2013).
58. Rahman, M. *et al*. Alternative preprocessing of RNA-Sequencing data in The Cancer Genome Atlas leads to improved analysis results. *Bioinformatics* **31,** 3666–3672 (2015).
59. Law, C. W., Chen, Y., Shi, W. & Smyth, G. K. voom: Precision weights unlock linear model analysis tools for RNA-seq read counts. *Genome Biol*. **15,** R29 (2014).

ACKNOWLEDGMENTS

We express our gratitude to all the patients who participated in this study and thank the medical staff for assistance with acquisition of primary human specimens. We thank the members of the Jaulin lab and Digestive Cancer Unit for discussion; B. Baum for mentoring and support, S. Deborde, B. Goud, and G. Kreitzer for critical reading of the manuscript. We thank the Plateforme Anticorps Recombinant (Curie Institute), DSHB (University of Iowa) and Joannes Zuber for reagents and the technical services provided by PFIC core facility, module HCP (F. Drusch, V. Marty), Olivia Bawa, Valerie Roufiac, S. Piterboth, I. Villa, D. Vignjevic, S. Guilmeau. This work was supported by the CNRS (ATIP-AVENIR program), the Gustave Roussy foundation (Roulons pour le colon, Natixis) and Canceropole (Emergence).

AUTHOR CONTRIBUTIONS:

OZ, JR, FL, DS, SS, GP, IM, PR, CB, PA and J-LP designed research, performed experiments and analysed the data. LB, M Polrot and PG carried mice experiments. CL

analysed the microarray and RNAseq data. DE, DG, CE, M Pocard and DM provided clinical samples. PD, JYS performed the histological analyses. FJ conceived the project, designed research and wrote the manuscript. All provided intellectual input.

COMPETING FINANCIAL INTERESTS

The authors declare no competing financial interests.

Supplementary Table 1 : Pathological an molecular charateristics of primary tumours and peritoneal effusions of CRC patients with (a) or without (b) peritoneal carcinomatosis

1.a / Patients with peritoneal carcinomatosis of colorectal origin (PC+)

							Tumor cell clusters			Single cells	
	Cancer Type	**Primary tumour location**	**PCI**	**TNM Stage**	**KRAS/BRAF**	**MSS/MSI**	**Y/N**	**Number**	**Shapes**	**Y/N**	**Number**
1	LBK	Recto-Sigmoïd jonction	4	pT3N0	N/A	N/A	N	/	/	N	/
2	SRC	Sigmoïd/rectum	20	pT3N2aM1b	N/A	N/A	N	/	/	Y	75
3	CRIB	N/A	10	pT4aN2	BRAF	N/A	Y	100	S	N	/
4	LBK	Colon	6	pT4N2M1	N/A	N/A	N	/	/	N	/
5	MUC-cmp + SRC	Sigmoïd	10	pT4aN0M1b	KRAS	MSS	Y	10	S	N	/
6	MUC-cmp	caecum	18	pT3N2bM0	KRAS	MSS	Y	65	S	N	/
7	MUC	Rectum	6	pT4N2a	WT	N/A	N	/	/	Y	45
8	CRIB, MPP-cmp	Recto-Sigmoïd jonction	6	pT4aN2	WT	MSS	Y	1000	S	Y	1000
9	MUC	Colon Left	17	pT4N2M1b	N/A	N/A	Y	6	S	N	/
10	MUC-cmp	Colon Left+Right	20	pT4aN1aM1b	KRAS	N/A	Y	70	S	Y	175
11	MUC	Colon	16	pT4N2a	N/A	MSS	Y	100	S	N	/
12	MUC-cmp	Colon	20	pT4N1M1b	N/A	MSS	Y	1000	S	Y	2000
13	CRIB, MPP-cmp	Colon Right	17	pT3N2M0	KRAS	MSS	Y	100	S	Y	250
14	MUC-cmp	Colon	14	pT4bN1bM1b	KRAS	N/A	Y	15	S	N	/
15	LBK	Colon	4	pT3N0	N/A	N/A	N	/	/	N	/
16	LBK	Colon Right	15	pT3N1M0	N/A	N/A	N	/	/		
17	MUC	Recto-Sigmoïd jonction	19	ypT3N2	KRAS	N/A	Y	20	S		
18	MUC	transverse	27	pT4bN2aM1b	BRAF	N/A	Y	40	S		
19	LBK	Colon	4	pT3N1M1	WT	N/A	N	/	/		
20	LBK	Colon Left	13	pT4aN0M1	KRAS	N/A	Y	2	N/A		
21	MUC	Caecum	31	pT4bN2M1	KRAS	MSS	Y	300	S		
22	MUC-cmp	Transverse	9	pT4N0	WT	MSS	Y	5	S		
23	MUC	Sigmoïd	14	pT4aN2aM1	KRAS	MSS	Y	300	S		
24	LBK	Rectum	16	ypT3N1	KRAS	MSS	Y	100	I		
25	SRC	Caecum	4	N/A	WT	N/A	N	/	/		
26	CRIB	Transverse right colon	27	ypT3N2	BRAF	MSS	Y	220	S		
27	LBK	Colon Sigmoïd	5	pT4aN1M1M0	KRAS	N/A	N	/	/		
28	LBK	Colon Right	10	pT4N1	N/A	N/A	N	/	/		
29	LBK	Rectum	14	pT3N1	KRAS	N/A	Y	15	I		
30	LBK	Colon	4	pT4aN2aM0	WT	N/A	N	/	/		
31	MUC-cmp	Sigmoïd	27	pT4N2	WT	N/A	Y	30	I		
32	MUC-cmp	Transverse	8	pT4N0M1	KRAS	MSS	Y	30	S		
33	MPP	Sigmoïd	19	ypT4aN1aM1b	KRAS	N/A	Y	20	S		
34	LBK	Colon Right	4	pT3N1M0	KRAS	N/A	Y	1	N/A		
35	LBK	Sigmoid/rectum	4	pT4N2M1	N/A	N/A	N	/	/		
36	MUC	Sigmoïd	11	pT4N2M1	BRAF	MSS	Y	5	S		
37	MUC	Appendice (GCC)	35	pT4N0M1a	N/A	MSS	Y	500	S		
38	MUC-cmp	Colon	6	pT4aN2b	WT	N/A	N	/	/		
39	SRC	Colon Left	15	pT4bN0M1b	KRAS	N/A	N	/	/		
40	LBK	Colon Right	8	pT4N0	KRAS	N/A	N	/	/		
41	LBK	Colon Right	22	pT4aN0	N/A	N/A	Y	30	S		
42	MUC	Recto-Sigmoïd jonction	14	ypT3N1	WT	MSS	N	/	/		
43	MUC	Colon Right (+Appendix)	27	pT4	N/A	N/A	Y	20	S		

Statistics:

Clusters
- **Positive peritoneal effusions 68%**
- **Co-detection of single cells 40%**
- **Average number of clusters 152**
- **Clusters with spherical shape 88%**
- **Number of cells (average ± SEM) 257± 45** (n=31 spheres from 6 patients)

Single Cells
- **Positive peritoneal effusions 40%**
- **Co-detection clusters 67%**
- **Number (average ± SEM) 591± 316**

Peritoneal effusions containing no EpCam(+) or CK20(+) tumour cells: 33%

TSIP(+) associated tumours statistic :
- **Primary tumour stage: pT3 18%**
- **pT4 82%**
- **KRAS Mutation 62,5%**
- **BRAF Mutation 25%**
- **WT 12,5%**

1.b / Patients without peritoneal carcinomatosis of colorectal origin (PC-)

							Tumor cell clusters			single cells	
	Cancer Type	**Primary tumour location**	**PCI**	**TNM Stage**	**KRAS/BRAF**	**MSS/MSI**	**Y/N**	**Number**	**Shapes**	**Y/N**	**Number**
1	MUC	Colon Left	2	T3N2M1	N/A	N/A	N	/	/	N	/
2	MUC	Colon Right	2	T3N1M0	N/A	N/A	N	/	/	N	/
3	LBK	Sigmoïd	0	pT4aN2a	WT	N/A	Y	35	I	Y	10
4	N/A	Colon	0	pT3N2b	N/A	N/A	N	/	/	N	/
5	LBK	Left sigmoïd	2	pT3N0M1	WT	N/A	N	/	/		
6	LBK	Sigmoïd	0	pT4a N2a M1b	N/A	N/A	N	/	/		
7	MUC	Caecum	0	ypT3N0M0	N/A	N/A	N	/	/		
8	LBK	Rectum	0	ypT3N1aM1	WT	*MSS*	N	/	/		
9	LBK	Caecum	0	ypT3N2bM1b	WT	N/A	N	/	/		
10	LBK	Colon	2	pT4aN0M1b	KRAS	N/A	N	/	/		
11	MUC	Transverse right colon	2	pT3N1	KRAS	*MSI*	N	/	/		
12	MUC	Appendix	2	N/A	N/A	N/A	N	/	/		
13	LBK	Recto-Sigmoïd jonction	0	pT3N0M0	N/A	N/A	N	/	/		

LBK: Lieberkuhnian, SRC: Signet Ring Cells, CRIB: Cribriform, MUC: Mucinous, cmp: component, MPP: Micropapillary, S: Sphere, I : Irregular, PCI: Peritoneal Cancer Index (PCI + > 3, PCI - < 3), GCC: Goblet cell carcinoid, N/A: non available, /: not applicable, WT : Wild Type.

Supplementary Figure 1

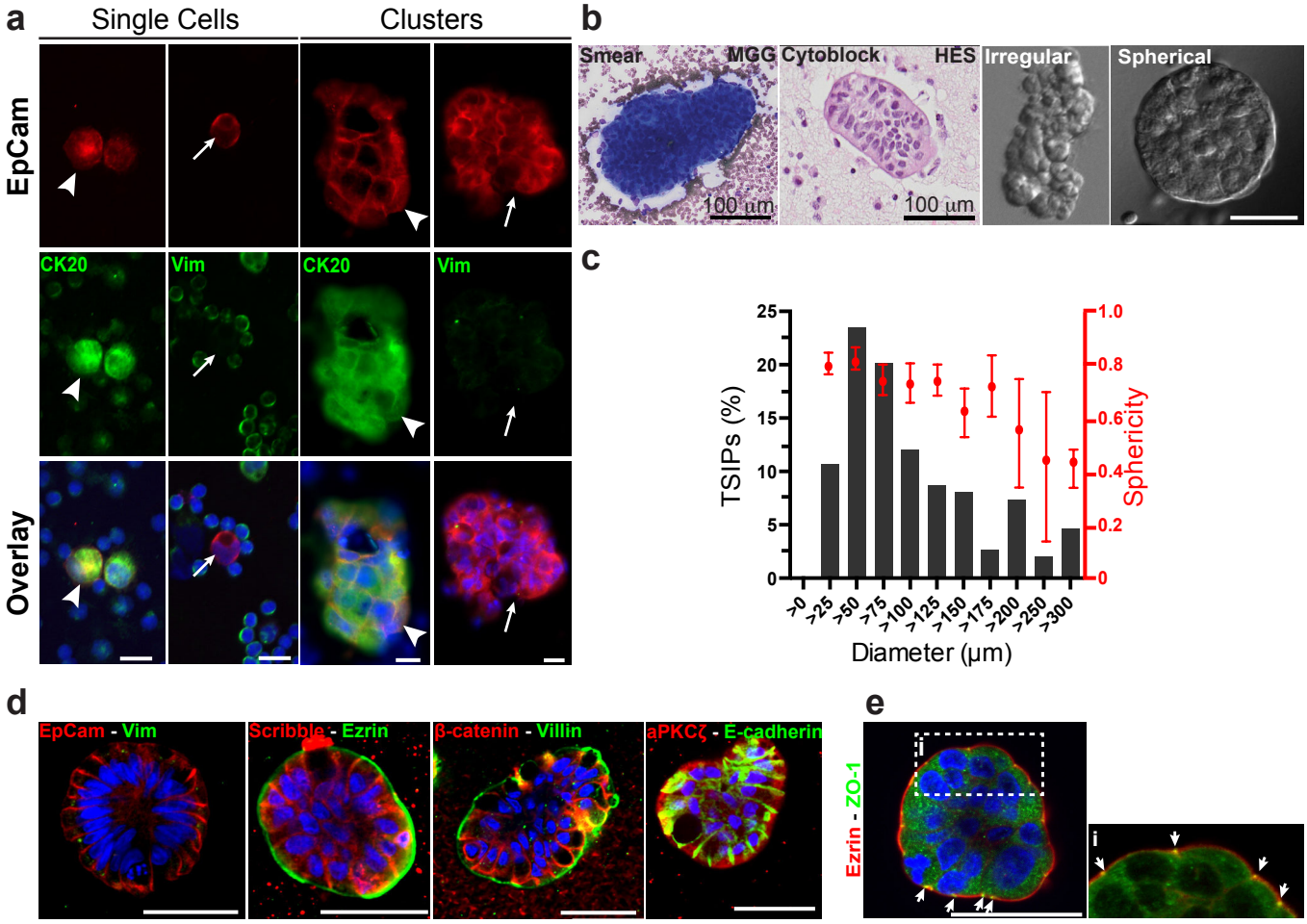

Supplementary Figure 1. Characterization of tumour single cells and clusters in peritoneal effusions of CRC patients with PC
(**a**) Cytospin of peritoneal effusions total fractions immunostained for Epithelial Cell Adhesion Molecule (EpCam), Cytokeratin 20 (CK20), Vimentin (Vim), and DAPI (only shown in overlay images). Arrowheads show co-staining of EpCam-CK20 and arrows show the absence of co-staining EpCam-Vim. Scale bar: 100 µm. (**b**) Smears and cytoblocks from peritoneal effusions of MUC CRC were processed and stained either by May-Grunwald Giemsa (MGG) or Hematoxylin/Eosin/ Saffron (HES). Live DIC images of patient tumour clusters with irregular or spherical (TSIP) morphology. (**c**) Distribution of TSIPs, mean diameters (µm) and sphericity (represented as mean ± SEM), calculated for 150 TSIPs from 7 effusions based on DIC images. (**d**) TSIPs from patients' peritoneal effusions were immunostained for Epithelial Cell Adhesion Molecule (EpCam), Vimentin (Vim), Scribble, Ezrin, β-catenin, Villin, aPKCζ and E-cadherin together with DAPI (one median section of confocal z-stack is displayed). (**e**) TSIP co-stained with Ezrin and ZO-1. The boxed region (i) is shown at high magnification. Arrows point to discrete ZO-1 puncta between the apical and the basolateral membranes.
Scale Bars: 50 µm unless otherwise specified.

Supplementary Figure 2

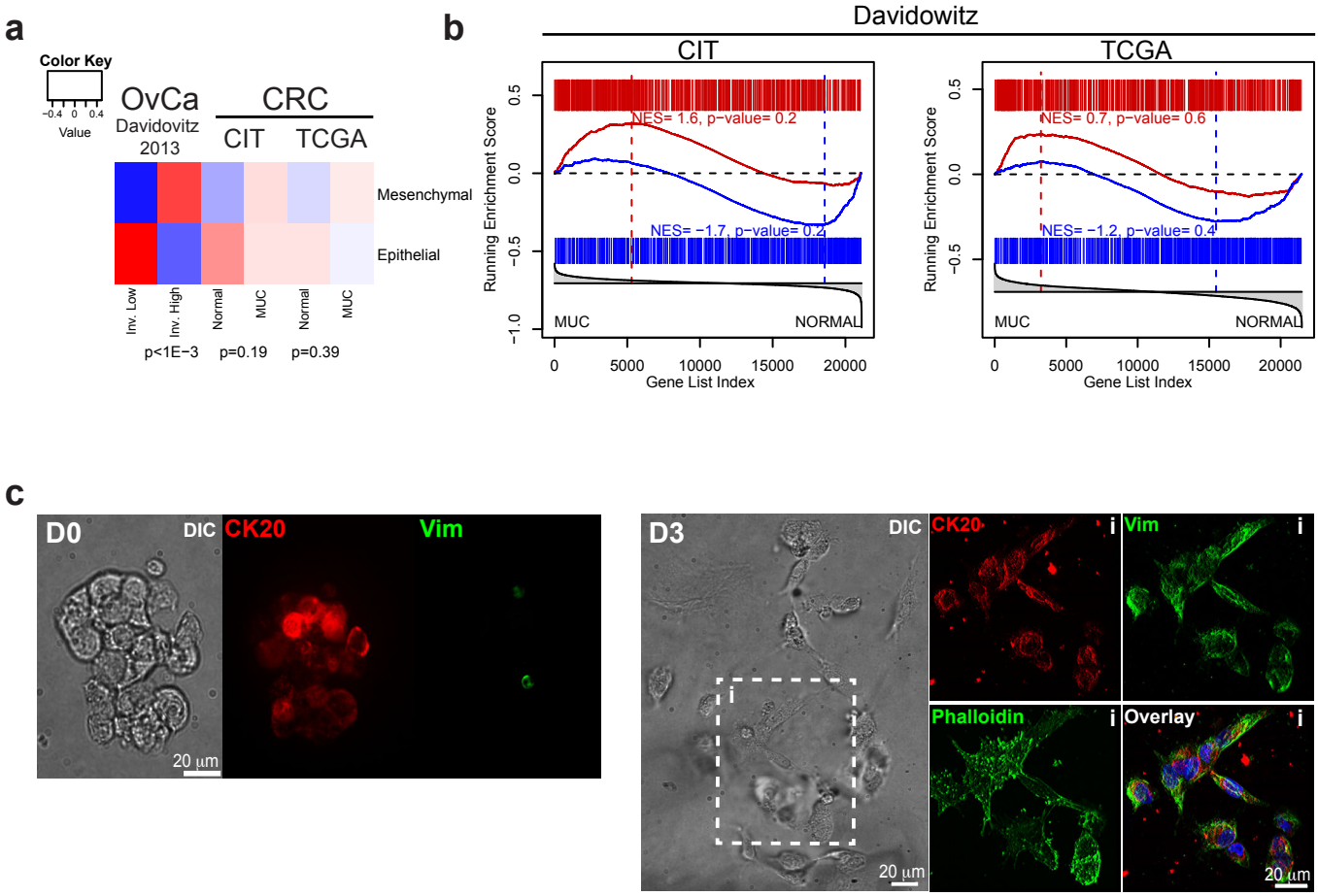

Supplementary Figure 2. The Epithelial-to-Mesenchymal Transition does not drive the dissemination of MUC CRCs
(**a**) Heatmap of mesenchymal and epithelial gene sets activity in the Davidovitz, CIT and TCGA gene expression profiles. Gene sets were extracted from the Davidowitz et al.[12]. The color corresponds to the average of the activity (calculated as an Enrichement Score) of each gene set among samples from specified phenotypes. Inv. Low and Inv. High refer to clearance incompetent and competent cell lines as defined in Davidowitz et al.[12].CIT Normal and MUC refer to normal and mucinous samples as defined in Marisa et al.[12].TCGA Normal and MUC refer to The Cancer Genome Atlas tumor-adjacent normal and mucinous samples[9]. The p-value refers to the significance of the Gene Set Enrichment Analysis of the mesenchymal and epithelial gene sets expression in invasive low or normal samples as compared to invasive high or mucinous samples. (**b**) Gene set enrichment analysis of the Davidowitz gene sets in the MUC CRC versus normal tissue gene signature from the CIT and TCGA datasets. GSEA was run with the mesenchymal and epithelial gene sets as defined in the Davidowitz original publication, respectively represented in red and blue. The reference list of genes was sorted using the significance of the test comparing gene expression in mucinous and normal samples from the CIT (left) and TCGA (right) datasets. The comparisons were not significantly different as reported by their p-values. (**c**) Representative images of irregular clusters collected from peritoneal effusions associated with Lieberkuhnian (LBK) CRCs embedded in collagen-I gel for 3 days. DIC microscopy shows cluster dissociation over time (compare D0 and D3) and mesenchymal cell invasion. Maximum projection of confocal z-stack revealed the upregulation of vimentin and decreased expression of Cytokeratin 20 at D3 when compared to D0.

Supplementary Figure 3

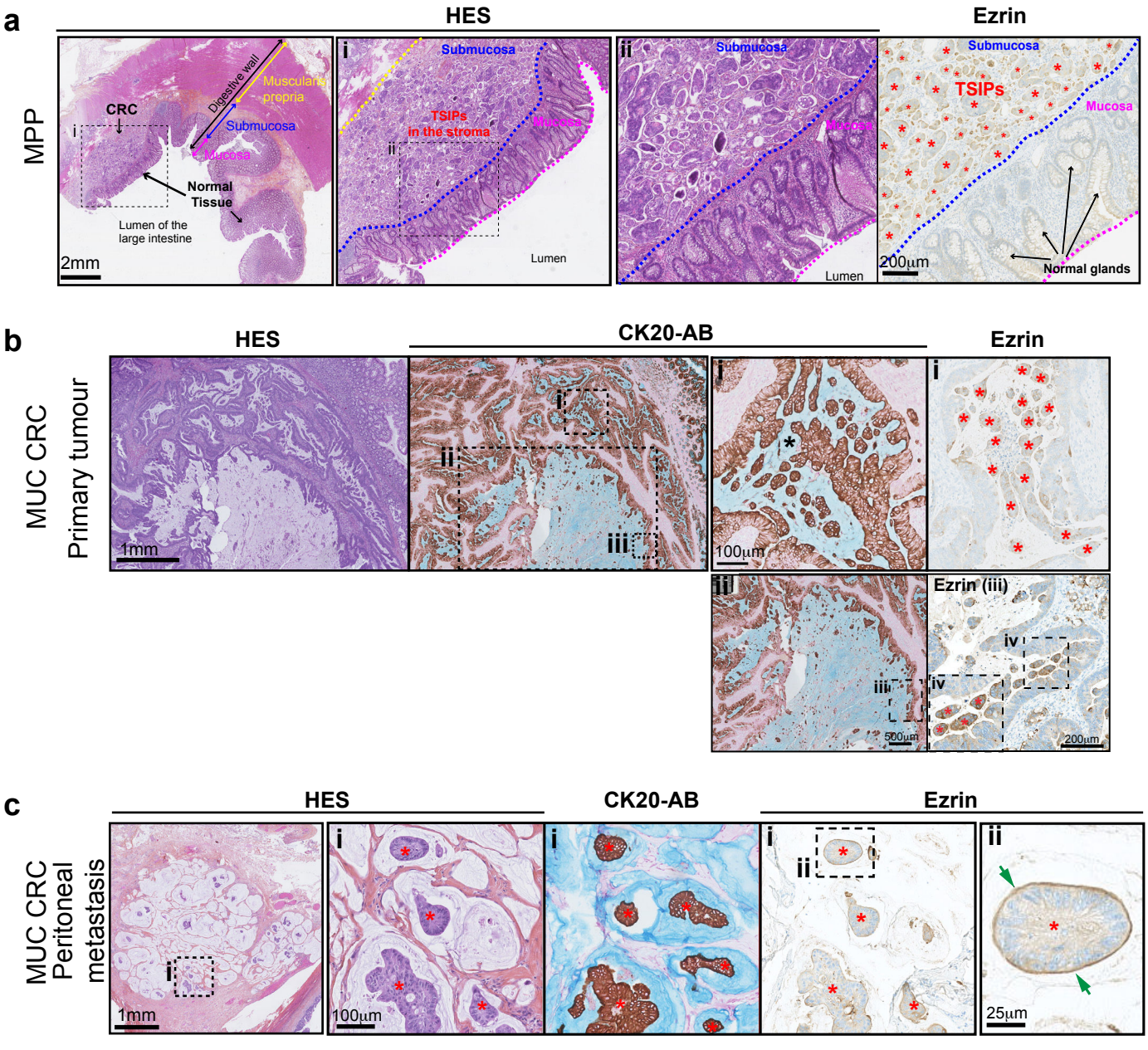

Supplementary Figure 3. TSIPs are present within Micropapillary and Mucinous CRC primary tumours and peritoneal metastases
(**a**) Representative tumour specimens of micropapillary (MPP) CRC primary tumour stained using Hematoxylin/Eosin/Saffron (HES) or anti-Ezrin. The left panel is a low magnification of the tissue, showing normal mucosa in contact with the intestinal lumen, the submucosa where the CRC is localized (in boxed region (i)) and the muscularis propria. The boxed regions (i and ii) are shown at high magnification to reveal the presence of tumour cells collectives with and outward Ezrin staining (TSIPs, designated by red stars) in the stroma of the submucosa. The apical pole highlighted by the Ezrin staining shows an inward polarity in the glands of the normal mucosa and an outward orientation on the tumoral component. (**b-c**) Representative tumour specimens of mucinous (MUC) CRC primary tumours and peritoneal metastases stained with Hematoxylin/Eosin/Saffron (HES), anti-Cytokeratin 20 (CK20) combined with Alcian Blue (AB, staining the mucus) and anti-Ezrin. The left panels represent low magnification of the tumours. Boxed regions are shown at high magnification. Black star indicates the lumen of a tumoral gland and the red stars designate TSIPs, CK20(+) tumour cell clusters surrounded with an outward Ezrin staining (pointed by green arrows in cii). Note that the MUC CRC primary tumour (in b) presents a glandular compartment where TSIPs accumulate in the luminal cavities of neoplastic glands (see boxed region (i)) as well as a large region where the glandular organisation is lost (see boxed region (ii)), TSIPs and Mucus blending in the stroma. The peritoneal metastasis (in c) is exclusively composed of TSIPs.

Supplementary Figure 4

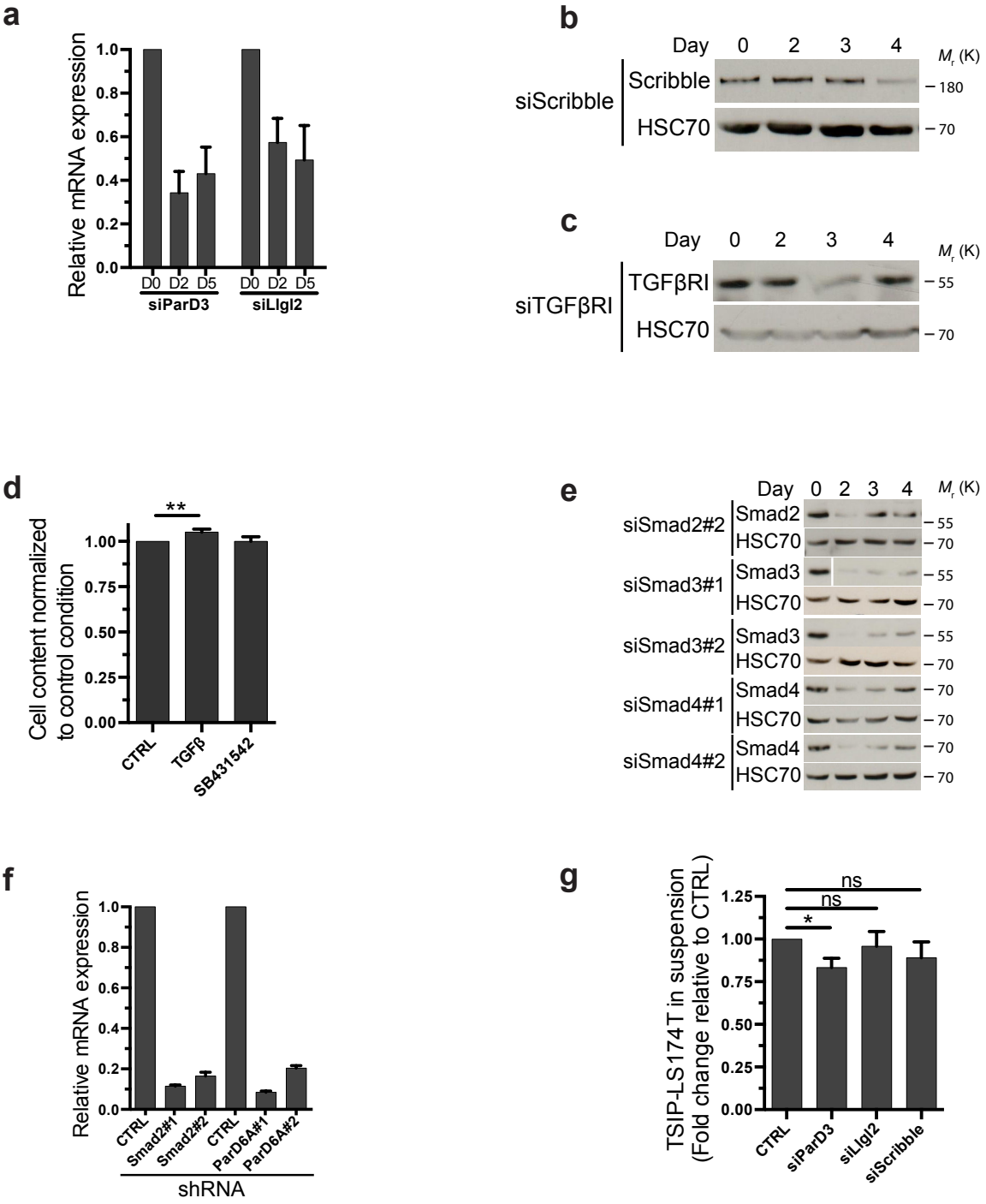

Supplementary Figure 4. The MUC CRC cell line LS174T produces TSIPs by collective apical budding

(**a**)Total RNA from cells transfected with siParD3 and siLlgl2 were analysed by qRT–PCR at the indicated time for ParD3 and Llgl2 mRNA expression, respectively, and normalized to GAPDH. (**b**) Immunoblot analysis of LS174T cell line transfected during the indicated time with siScribble and revealed with anti-Scribble antibody. HSC70 was used as a loading control. (**c**) Immunoblot analysis of LS174T cell line transfected during the indicated time with siTGFβRI and revealed with TGFβRI antibody. HSC70 was used as a loading control. (**d**) LS174T cells were grown for 9 days in the indicated condition, lysed in 2% SDS and the cell content was quantified using BCA protein assay. For each condition, data are displayed as means ± SEM from n=5 experiments. p-values were calculated using unpaired t-test (**p<0.01). (**e**) Immunoblot analysis of LS174T cell line transfected during the indicated time with siSmad2, siSmad3 or siSmad4, lysed after 2, 3 or 4 days and revealed with the appropriate antibody. HSC70 was used as a loading control. (**f**) LS174T cells were infected by lentiviruses encoding two independent hairpins against Smad2 and ParD6A. Total RNA from the infected cells were analysed by qRT–PCR for Smad2 or ParD6A mRNA expression relative to control cells and normalized to GAPDH. (**g**) Bar graph representing the number of TSIPs released by 2D LS174T cultures transfected with the indicated siRNA and normalized to control siRNA. For each condition, data are displayed as means ± SEM from n=3-5 experiments. p-values were calculated using unpaired t test (*p<0.05).

Supplementary Figure 5

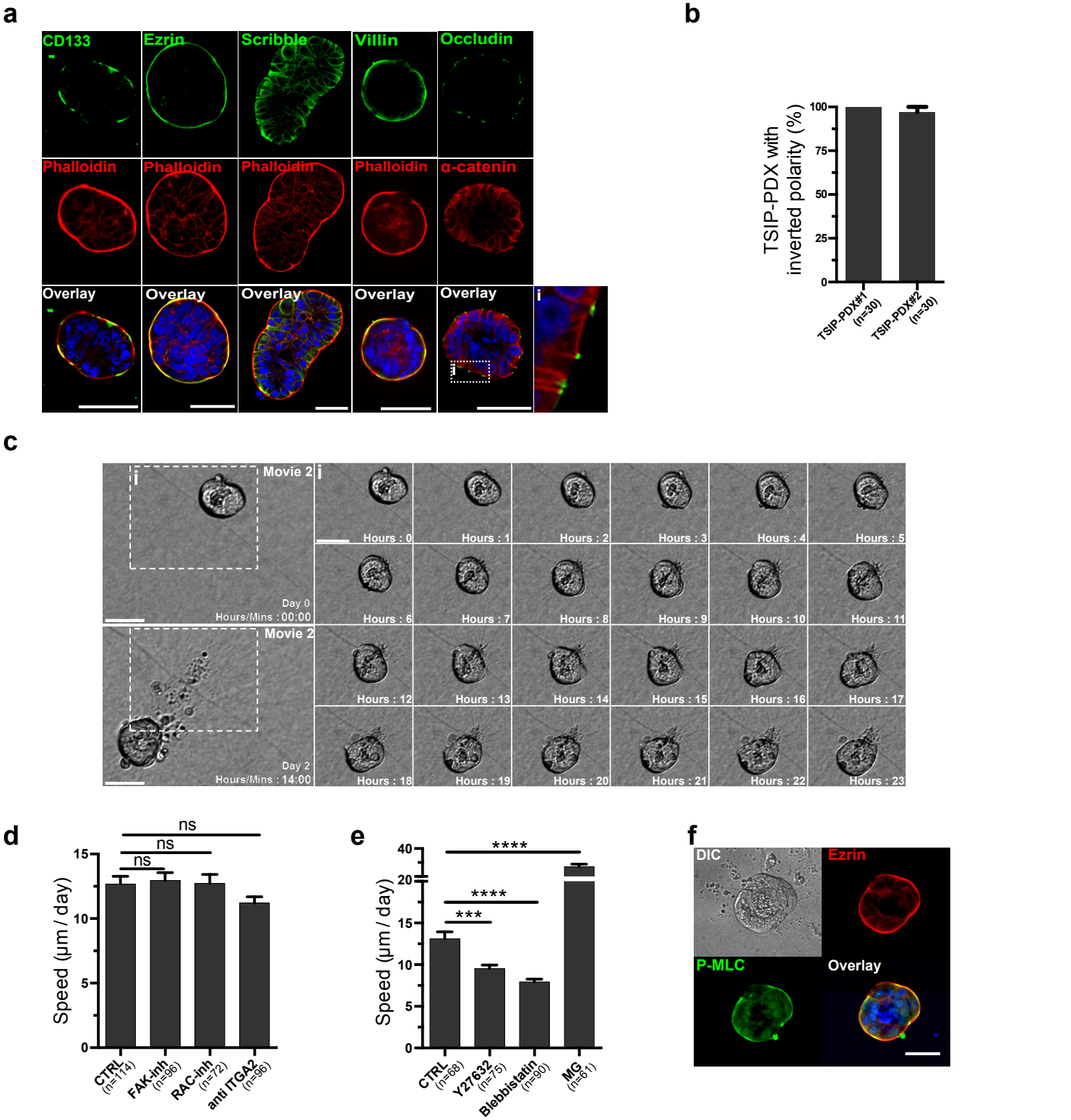

Supplementary Figure 5. TSIP collective invasion occurs independently of protrusions and adhesion but relies on actomyosin contractility

(**a**) TSIPs obtained from PDX#1 and PDX#2, maintained in suspension and immunostained for Scribble, Ezrin, Villin, α-catenin, CD133, Occludin, Phalloidin and DAPI (one median section of confocal z-stack is shown). The boxed region (i) is magnified showing tight junctions. (**b**) Bar graph showing the quantification of TSIPs from PDX#1 and PDX#2 displaying an outward apical pole in suspension. TSIPs are considered with inverted polarity when at least 75% of the total peripheral cells displayed an outward Ezrin staining in one confocal Z-section. Results are represented as mean ± SEM from 3 independent experiments with 10 TSIPs per experiment. (**c**) Time lapse sequences of TSIP-PDX#1 collectively invading into collagen-I by DIC microscopy (corresponding to Supplementary movie 2). Time is displayed as day and hh:mm. Boxed region (i) is displayed at 1 hour interval time-points to show the lack of protrusions at the leading edge during the 24 hours displacement. (**d**) Quantification of TSIP-PDX#1 average speed in collagen-I in control condition or treated with inhibitors of FAK (FAK-Inh, PF-573228) and Rac (Rac-Inh, NSC23766) or integrin alpha 2 function-blocking antibody (anti-ITGA2). The number of TSIPs analysed (n) is indicated in the graph for each condition and has been calculated from 3 experiments. Values represent means ± SEM, p values are calculated using unpaired t test (ns: p>0.05). (**e**) Quantification of TSIP-PDX#1 average speed in collagen-I in control condition or treated with inhibitors of ROCK (Y27632) and Myosin-II (Blebbistatin). TSIP-PDX#1 were also embedded into 3mg/ml of matrigel (MG) instead of collagen to perturb the transmembrane apical proteins. Average speeds of all TSIP were calculated from 3 experiments and the number of TSIPs analysed (n) is indicated in the graph for each condition. Values represent means ± SEM, p-values are calculated using unpaired t test (****p<0.0001, ***p<0.001). (**f**) Representative image of TSIP-PDX#1 after 3 days in collagen-I in control conditions stained using anti-Ezrin, anti-P-MLC and DAPI.

Scale bars: 50 µm.

Supplementary Figure 6

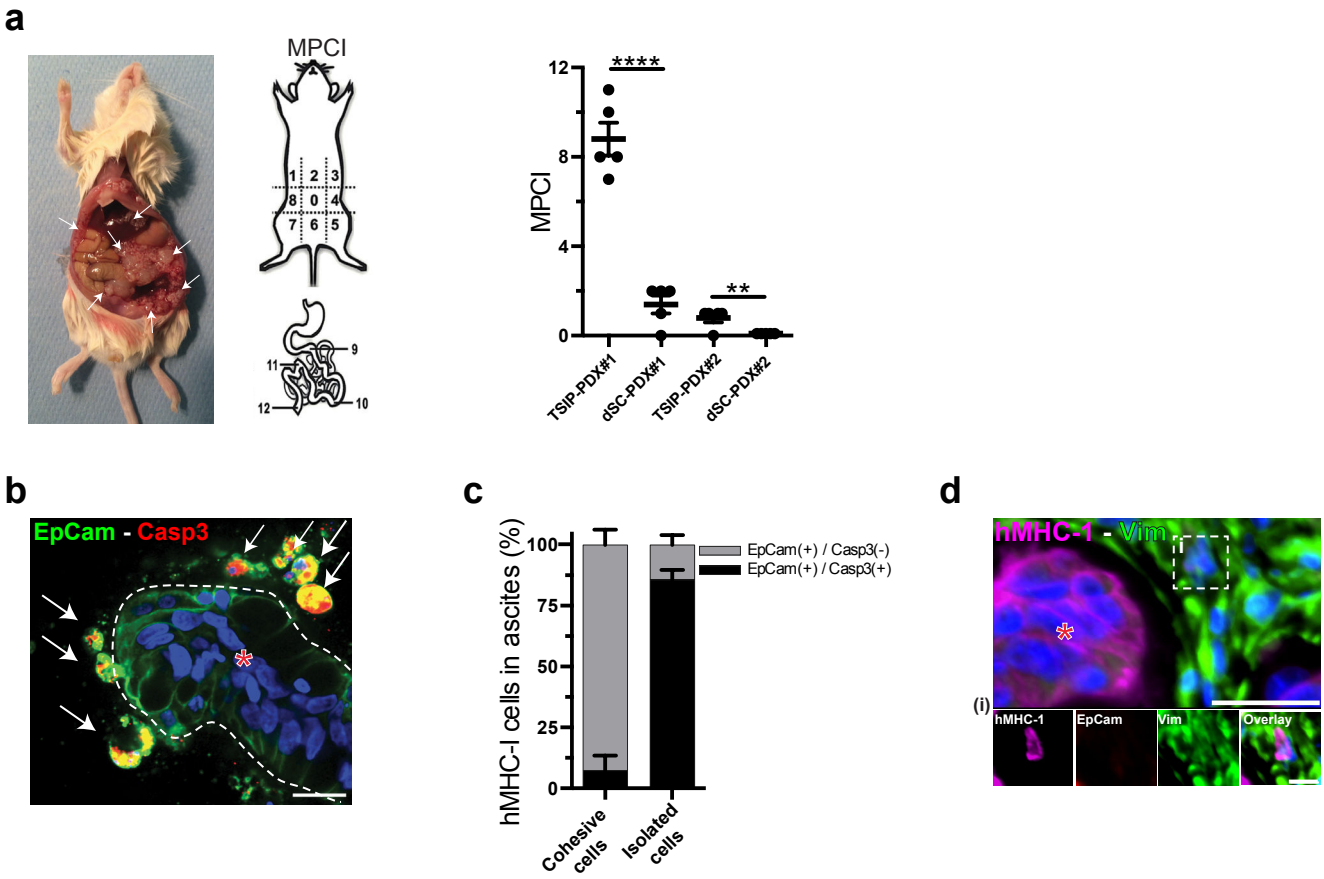

Supplementary Figure 6. Intraperitoneal injection of TSIPs produce metastases that retain the epithelial and polarised architecture
(**a**) Macroscopic aspect of mice peritoneal cavity 40 days after injection of TSIP-PDX#1. Arrows point to numerous metastases. The schematic represents the regions used to calculate the modified Peritoneal Cancer Index (mPCI) for mice adapted from Mohamed et al. {Mohamed:2011ux}. The bar graph displays the mPCI for each group (n= 5 mice per group). (**b**) Immunofluorescence of tumour intermediates found in ascites stained for EpCam and cleaved Caspase 3 (Casp3). Red star and white line highlight TSIPs (with no Casp3 positive cells), arrows point to isolated cells expressing cleaved caspase 3. (**c**) Bar graph representing the proportions of EpCam(+) cells, positive or negative for cleaved caspase 3 (Casp3), in the isolated and cohesive tumour cell fractions (identified by human MHC class-I staining). Respectively, n= 345 and 836 cells from 3 different mice injected with TSIP-PDX#1 were counted (results are represented as Mean ± SEM). (**d**) Immunofluorescence of metastasis from mice injected with TSIP-PDX#1 using antibodies against human MHC class-I and Vimentin (Vim). Boxed region is shown at high magnification and displays Vim(+) and EpCam(-) tumour cell. Scale bars: 50 µm.

CHAPTER 3: DISCUSSION

Peritumoral invasion is the first step to the deadly metastatic cascade of cancer, and fully understanding the mechanisms that control this process is a prerequisite to the identification of relevant therapeutic strategies. The studies I contributed to during my PhD program revealed that CRC cancer cells disseminated as cohesive cluster, which maintained the architecture of the epithelial tissue they arise from. Two epithelium-based architectures were found in patient specimens, 1) a glandular architecture in which the cell clusters maintained a normal apico-basolateral axis with a luminal cavity and 2) an inverted architecture in which the cell clusters, named TSIPs (tumor spheres with inverted polarity), displayed an inverted polarity axis, with the apical pole of cells facing the extracellular matrix. These clusters employed two distinct collective invasion strategies to disseminate, 1) a protrusive mode and 2) a propulsive mode respectively, which relied on distinct actin dynamics. We revealed a major contribution of the small Rho GTPases signaling pathway to both modes of invasion. We first identified a mechanism by which KIF17 kinesin motor protein promoted RhoA-GTP activity at cell-cell junction to insure epithelial cohesivness. We then revealed that ROCK inhibition triggers collective of glandular CRC clusters by inducing Leader cell formation through the activation of the GEF, FARP2 combined to the inhibition of Myosin-II. In an opposite way, we showed that ROCK and Myosin-II activity is required for the invasion of TSIPs. All our results illustrate the plasticity of CRC collective mode of invasion and show that, as it was shown years ago for single cell mode of invasion, there are distinct contributions of RhoA/ROCK signaling to the collective invasion of CRC.

CRC cancer cells keep their epithelial architecture to invade collectively

EMT is not required for CRC invasion

In the past decades, most of the biomedical research investigations have focused on the EMT transcriptional program, seen as the main driver of cancer cell dissemination (Chaffer et al., 2016). Here we show that CRCs invasion can occur collectively and does not automatically require carcinoma cell individualization. Our analysis of patients' FFPE samples of CRCs invading into the submucosa demonstrates that most of the tumor area remains cohesive, consistent with recent observation in breast carcinomas (Khalil et al.,

2017). Our results are in line with the growing body of experimental evidences supporting the contribution of collective behaviour to carcinoma invasion (Cheung and Ewald, 2016; Friedl et al., 2012). Accordingly, our time-lapse imaging of CRC specimens collected from the peritoneal cavity of metastatic patients provides dynamic evidences that large tumour cell cohorts are highly invasive and collectively conquer their environment, without the contribution of an EMT/MET conversion. This dynamic collective behaviour has now been reported from several cancer types originating from patients or mice models, at early or late stages of cancer progression (Aceto et al., 2014; Cheung et al., 2013; Giampieri et al., 2009). In addition, it has recently been demonstrated that pancreas and breast cancer metastases form without activation of the EMT transcription factors in mice (Fischer et al., 2015; Zheng et al., 2015). Furthermore it was demonstrated that tumour clusters are the most efficient if not the only metastasis seeders (Aceto et al., 2014; Cheung and Ewald, 2016).

Alternatively, EMT contribution to cell invasion may not be through complete loss of epithelial features and carcinoma cell individualization. Indeed in the study of Zajac et al., we demonstrate that maintenance of cell-cell junctions is required for cell survival. Instead, EMT may contribute to the dampening of epithelial features, such as cell-cell junction relaxing and/or acquisition of mesenchymal features, sufficient for cell clusters invasion. The mesenchymal features may be acquisition of motile morphology as observed at the invasive front of patients with carcinoma (Brabletz et al., 2001; Bronsert et al., 2014). In another way, EMT may contribute to carcinoma progression by insuring cancer cell survival in different environments and by promoting resistance to anti-tumoral therapies.

Epithelial architecture contributeV to cancer cell invasion

Inter and intra-tumoral heterogeneity, together with cancer cell plasticity, imply that dissemination strategies can be multiple and possibly complementary (Alexander and Friedl Cell 2011). By investigating specimens from metastatic CRC patients we have identified two new collective and epithelial modes of cancer dissemination. The first one arises from well-differentiated adenocarcinoma primary tumors, which represent 80% of CRC (Fleming et al., 2012). They generate clusters invading as glandular structures into the peritumoral stroma *in vivo* or the collagen-I gel *in vitro* (Bronsert et al., 2014; Prall et al., 2009). In this case the CRC clusters are composed of epithelial cell cohorts organized around central lumens, meaning they have retained their epithelial polarity and architecture. Although this mode of

migration was reported during normal development and organogenesis (Donà et al., 2013; Durdu et al., 2014) its contribution to carcinoma invasion was only suggested from analysis of fixed histology specimen form CRC patient lacking a supportive dynamic insight (Christiansen and Rajasekaran, 2006; Prall et al., 2009). In fact, in prostate and breast specimens from patient glandular clusters of cancer cells were found in the peritumoral stroma. We provide here a live reporting of the invasion of such structures, which keep their lumen along with the rest of the epithelial features. We demonstrate that the switch from non-invasive to invasive was triggered by leader cell formation that retained epithelial markers. However, it was shown that leader cells in other collectively invading cancer cells models harbor a mesenchymal morphology along with mesenchymal markers such as integrins or metalloproteases (Hegerfeldt et al., 2002; Nabeshima et al., 2000), while maintaining epithelial markers expression. This epithelial-mesenchymal phenotype of the leader cell is necessary to generate the traction forces necessary to move the cohort and may result from a partial EMT, which contributes to epithelial cell plasticity (Brabletz et al., 2001; Bronsert et al., 2014; Chaffer et al., 2016)

Differently the second identified mode of collective invasion, generated by collective apical budding, generates TSIPs that retain a robust epithelial architecture and an inverted apico-basolateral polarity and do not necessitate the formation of leader cells to move, instead they use their apical acto-myosin contractility to generate the forces to move. Their ability to navigate through the matrix without any protrusive leader cell completely excludes a potential contribution of EMT program.

Why and how keep epithelial features?

Collective invasion is typically the slowest migratory mode (Weigelin et al., 2012). Intravasation into lymphatic vessels can be efficiently performed by cell groups or clusters (Byers et al., 1995; Giampieri et al., 2009; Hashizume et al., 1996; Madhavan et al., 2001) which is supported by the existence of circulating tumour clusters from patient peripheral blood samples (Aceto et al., 2014; Brandt et al., 1996; Hart, 2009; Hou et al., 2011; Kats-Ugurlu et al., 2009; Khoja et al., 2014). The organization as a heterogeneous cell mass could be an advantage, as in the case of TSIPs: the protective apical pole contacting the extra-cellular matrix may protect inner cells from immune clearing from microenvironment harsh

conditions. We come to that conclusion as in physiological conditions, the apical pole lines the lumen of the intestine, protecting inner tissues from aggression contained in the intestinal bowl. In the case of glandular protrusive collective invasion, the more migratory leader cells promote invasion of less motile cells (the followers), thereby increasing overall tumor invasion (Friedl and Wolf, 2003). The collective mass may provide a signaling advantage, as in developmental models it was shown that a self-generated gradient generated by the group promoted efficient invasion (Donà et al., 2013) or the presence of the lumen may create a signaling hub (Durdu et al., 2014). Indeed, it was shown that microluminal concentration of the FGF (fibroblast growth factor) in the rosette-like structure of collectively migrating pLL regulated the movement of the whole group of cell (Durdu et al., 2014).

ROCK triggers collective invasion of glandular CRC

We identified ROCK2 as an essential kinase controlling the transition from non-invasive to collectively invasive CRCs glandular models such as cysts and tumoroids. We have shown that glandular collective invasion was allowed by a leader/follower polarization of the cohort. Leader cells are the protrusive cells at the front that adhere to the matrix and generate traction forces transmitted to the followers to insure the group motion (Cai et al., 2014; Wang et al., 2010). ROCK2 inhibition promoted collective invasion through the formation of leader cells based on a dual mechanism involving the reduction of acto-myosin contractility to unchain the collective and the activation of Rac1 through the GEF FARP2 to generate the protrusive force. Interestingly inhibition of ROCK in the whole cysts was inducing only one or two leader cells, raising the question of whether ROCK was contributing to the leader cell identity or if it was instead helping to reveal it.

ROCK2 inhibition is necessary in the leader cells

Using the mosaic expression of dominant negative protein, we targeted ROCK2 inhibition in a restricted number of cells within our models of non invasive glandular CRC model. Cells with inhibited ROCK2 became leaders, demonstrating that low ROCK2 activity determined the leader cell identity. This demonstrated that, unlike in breast and lung carcinomas, in our CRC models, leaders are not predetermined by a transcriptional program (Cheung et al., 2013; Konen et al., 2017; Lebreton and Casanova, 2014). Our model of leader cell generation is similar to the collective migration of Border cells in Drosophila, in which

any high levels of Rac1 determines the leader cell fate. While the high level or Rac1 in Leader cells of the Border cell results from upstream chemokine signaling through RTK receptor, we haven't determined how this low level of ROCK2 kinase activity would come about *in vivo.* My hypothesis would be that low level of ROCK2 activity in the CRC cluster is the requirement for subsequent leader cell formation as ROCK inhibition in the whole cyst is sufficient to generate only few leaders. This is in line with a recent study conducted in patients that has associated a ROCK2 variant in its coiled-coil domain with development of CRC (Sari et al., 2013). The localization of this nucleotide polymorphism may impede ROCK2 activity 1) either by preventing the dimerization of the protein 2) or by mis-localization of the kinase domain as suggested by the protein's models of regulation (Truebenstein et al., 2015; Yamaguchi et al., 2006). The formation of a leader cell would be a stochastic event occurring at site of lower acto-myosin tension (Reffay et al., 2014) or would be in response to external cues that should be further determined. Nonetheless we further demonstrated that in addition to Myosin-II dependent F-actin contraction, ROCK controls the Rac1 dependent F-actin polymerization to form leader cells.

ROCK inhibition promotes Rac1 activation in the leader cell

Rac1 activation is a common determinant of leader cell formation (Wang et al., 2010; Yamaguchi et al., 2015). We show that ROCK inhibition is sufficient to induce Rac1 activation and that Rac1 activity was necessary for leader cell formation. The ROCK/Rac1 balance is a core mechanism controlling all migratory processes. In single cell invasion it controls the switch between the amoeboid propulsive invasion and the mesenchymal protrusive mode of invasion (Sahai and Marshall, 2003; Sanz-Moreno et al., 2008). Similar to the protrusive leader cell it induces in our CRC model, ROCK inhibition also promotes the switch to the protrusive mesenchymal invasion of amoeboid invading cell which also requires Rac1 activation (Sadok and Marshall, 2014; Sanz-Moreno et al., 2008). In melanoma cells, the ROCK/Rac1 crosstalk was shown to be mediated by ARHGAP22, a GAP for Rac1, which is activated by ROCK and inhibits Rac1 activation (Sanz-Moreno et al., 2008). In breast cancer cells, this cross talk is mediated by FilGAP, also a GAP for Rac1 which is phosphorylated and activated by ROCK (Ohta et al., 2006; Saito et al., 2012). As highlighted by these studies, the GEFs and GAPs governing small RhoGTPases spatiotemporal activation vary with cell types and stimuli. In fact the Rac1 activity polarization required for actin-rich protrusive structures formation can be induced by different GEFs. While DOCK180 was shown

to induce the protrusion of Border cells, Beta-Pix, Tiam1 and Vav1 are the GEFs required for protrusive leader cells in collectively moving monolayers (Goicoechea et al., 2014; Osmani et al., 2006, 2010; Zaritsky et al., 2017).

To identify the GEF or GAP mediating the ROCK/Rac1 crosstalk in the collective invasion of our CRC, we performed a siRNA screen targeting all the GEFs and GAPs of the mammalian RhoGTPases. We found 3 pairs of homologous GEFs whose depletion prevented ROCK dependent collective invasion. Of these, two were described as GEFs for RhoA-GTPase and only one pair was reported to be a GEF for Rac1 or Cdc42 (FARP1/FARP2). Therefore we considered FARPs as candidates to the support of the ROCK/Rac1 crosstalk in the CRC collective invasion (Cheadle and Biederer, 2012; Fukuhara et al., 2004; He et al., 2013; Kubo et al., 2002). We further demonstrated that FARP2 and not FARP1 was necessary for ROCKs inhibition induced leader cell formation. The screening approach seemed to us an unbiased privileged approach to identify relevant candidates in the regulation of CRC collective invasion. None of the already well described Beta-Pix, Tiam1 Vav2 or DOCK180 in the regulation of collective migration or the GAPs for RhoA such as p190RhoGAP or MyosinXIA were among our hits (Bianco et al.,2007; Ellenbroek et al., 2012; Osmani et al., 2006) (Hidalgo-Carcedo et al., 2011; Omelchenko and Hall, 2012). Moreover, a recent study using the same screen approach looking for GEF regulating the collective invasion of brochial epithelial cells identified several candidates such as SOS1, Beta-Pix and RhoA GEFs (Zaritsky et al., 2017). Different hypotheses may explain these discrepancies, 1) collective invasion in different environment may use different processes; for example, %eta-Pix contribution was mainly studied in 2D collective migration (Ellenbroek et al., 2012; Osmani et al., 2006). 2) Physiological collective migration such as of Drosophila Border cell, normal wound healing epithelial cells or neuronal cells do not use the same signaling pathways (Montell et al., 2012; Osmani et al.,2006, 2010; Zaritsky et al., 2017). Therefore, we suggest that FARP2 dependent collective mechanism may be specific of CRC collective invasion. Although we have demonstrated that ROCK inhibition induced collective invasion of organoids from PDX, a more physiological model of CRC, making it a broad mechanism of CRC invasion, the requirement of FARP2 remains to be shown in further physiological models.

Beta-Pix and Tiam1 are activated by integrins at the front row of wounded astrocytes monolayers and DOCK180 responds to growth factors stimulation in drosophila %order cells (Bianco et al., 2007; Ellenbroek et al., 2012; Osmani et al., 2006). In collective invasion of our CRC model FARP2 activation downstream of ROCK inhibition seems to activate Rac1.

FARP2 mediates ROCK/Rac1 crosstalk in leader cell

We found that FARP2 but not FARP1 was necessary for the collective invasion of CRC. Although both FARP1 and FARP2 were shown to regulate cytoskeleton dynamics in neuronal development, (Cheadle and Biederer, 2012, 2014; Kubo et al., 2002; Mlechkovich et al., 2014; Toyofuku et al., 2005; Zhuang et al., 2009), they are downstream of distinct signaling pathways and are also found to regulate additional distinct cellular processes (Koyano et al., 2001; Takegahara et al., 2010). FARP2 is the only one described to regulate cell motility in an endothelin dependent manner (Miyamoto et al., 2003). In this study, the effect of FARP2 on cell motility relies on the Cdc42 GEF activity of the protein. Instead, our results suggest FARP2 to be a GEF for Rac1 given its new role as regulator of collective invasion of CRC. However, as previously mentioned in the introduction of this dissertation, the specificity of FARP2 GEF activity towards a specific Rho-GTPase is not yet clear and may be context dependent, in fact specificity towards Rac1 is claimed (He et al., 2013; Kubo et al., 2002; Takegahara et al., 2010; Toyofuku et al., 2005) while others report it as a GEF for Cdc42 (Fukuhara et al., 2004; Fukuyama et al., 2005; Miyamoto et al., 2003). Our demonstration of FARP2-Rac1 link remains factual: ROCK inhibition induces Rac1 activation and Rac1 activation as well as FARP2 are necessary for ROCK inhibition to induce collective invasion. Further experiments should be conducted to prove that FARP2 is necessary and sufficient to induce Rac1 activation. To confirm FARP2 GEF's activity towards Rac1 and not Cdc42, further experiments should be done in a way that exclude a potential role of Cdc42 in Rac1 activation, as it was shown that Cdc42 can induce polarized Rac1 activation (Kawakatsu et al., 2005; Nishimura et al., 2005; Omelchenko et al., 2014; Osma ni et al., 2006). I will discuss these experiments in the following paragraph.

How does ROCK regulate FARP2 activity?

FARP2 is known to adopt an autoinhibited conformation (He et al., 2013). How could ROCK inhibition contribute to release that conformation to promote FARP2 activation? Although FARP2 sequence contained the consensus sequence of ROCK kinase substrate, we failed to identify phosphorylation induced by ROCK activation, excluding direct phosphorylation by ROCK. Two distinct labs have reported that FARP2 could be phosphorylated by the Src tyrosine kinase; we therefore propose that regulation of FARP2 by ROCK may be indirect

(Fukuhara et al., 2004; Miyamoto et al., 2003). ROCK was shown to control the activity of GEFs for Rac1 such as Tiam1/2 through relocalization either by direct phosphorylation or by indirect phosphorylation of interactors (Nakayama et al., 2008; Nishimura et al., 2005; Takefuji et al., 2007). Similarly in our CRC Caco-2 cells, upon ROCK inhibition FARP2 protein was rapidly relocalized and enriched at the membrane of cell-cell contacts. We propose that ROCK prevents FARP2 localization at the membrane to prevent its activity. This is supported by different studies which demonstrate that activation of FARP2 can be mediated by interaction with transmemebranar proteins via its FERM domain or with membranar lipids through its PH domains thereby promoting an activated conformation of the protein (He et al., 2013; Toyofuku et al., 2005). In support to this model in which the FERM domain and the PH domain play an inhibitory role on the DH-PH domain, most of the *in vitro* studies of FARP2 activity were conducted with a DH PH construct lacking FERM domain and PH domain, suggesting that they may impede FARP activation (Fukuhara et al., 2004; Fukuyama et al., 2005; Kubo et al., 2002; Miyamoto et al., 2003). Moreover, the FERM construct was shown to have negative effect on FARP2 activation (Miyamoto et al., 2003).

As there were no available specific antibodies that allowed us to monitor FARP2 endogenous localization we followed the localization of overexpressed FARP2 construct. We therefore cannot exclude a potential bias brought by the TAG or the amount of overexpressed proteins in localization and activation of FARP2. Further approaches should be used to have a better view on how ROCK regulates FARP2 activity.

We were able to show that ROCK inhibition was promoting FARP2 relocalization from the cytoplasm to cell-cell contacts. How does this promotes Leader cells fate? As FARP2 was shown to activate Rac1 at cell-cell junction (Fukuhara et al., 2004; Kawakatsu et al., 2005) and we know that Rho/ROCK promotes cell-cell junction stabilization (Priya et al., 2015, 2017), ROCK/Rac1 antagonism at cell-cell junction regulates the tension to coordinate collective invasion, therefore FARP2 may participate to cell-cell junction relaxation necessary for collective invasion (Hidalgo-Carcedo et al., 2011; Omelchenko and Hall, 2012).

The most expected role FARP is Rac1 dependent actin polymerization necessary to induce the protrusive Leader cell. While activation of Rac1 alone is sufficient to drive the collective migration of Border cells, we found FARP2 activation alone to be ineffective at triggering Caco-2 collective invasion, but combining it to relaxing acto-myosin contractility was

sufficient to induce collective invasion in agreement with the regulatory role of ROCK on two effectors, FARP2 and Myosin to induce collective invasion of CRC.

ROCK restricts leader cell formation through the acto-myosin contractility

While activation of FARP2 alone was not sufficient to induce protrusive leader cell, combining it to acto-myosin relaxation promoted leader cell formation. This is in agreement with previous reports from 2D cultures, where breaking up the supracellular marginal actin bundle and/or loosening acto-myosin tension at cell-cell junctions both contribute to collective migration (Omelchenko and Hall, 2012; Reffay et al., 2014; Riahi et al., 2015). Similarly, in the border cells the peripheral cortical actin, stabilized by moesin and myosin restricted ectopic leader cell formation (Combedazou et al., 2017; Ramel et al., 2013).

We found that Myosin-II inhibition was not sufficient to induce collective invasion. Instead high levels of myosin-II inhibition induced thin protrusions out of the caco-2 cyst as previously reported (Ivanov et al., 2008). These structures are distinct from protrusion of leader cells as they lacked the rich actin filament. In single cells they are considered to be by-products associated to the collapse of the cell body due to loss of acto-myosin contractility and their appearance functionally translates into the loss of all types of invasion either protrusive or propulsive (Sadok et al., 2015; Sahai and Marshall, 2003; Sanz-Moreno et al., 2008).
In fact, all types of invasions require acto-myosin contractility. Moreover acto-myosin contractility can be regulated by other kinases different from ROCK, such as the Ca-2+ dependent MLCK and the Cdc42 dependent MRCK (Wilkinson et al., 2005). The use of the Myosin-II inhibitor Blebbistatin does not discriminate between the targets of ROCK2 and may therefore induce a decrease of acto-myosin that is not observed when using ROCK inhibitors. To prevent the complete loss of acto-myosin contractility and the formation of these dendrites, we realized a dose response experiment and found 10 µM concentration of the blebbistatin the maximum concentration of inhibitor we could use to allow relaxing of acto- myosin without major impedment of the Caco-2 cysts morphology. This acto-myosin relaxation combined to FARP2 activation was sufficient to induce protrusive leader cell.

Interestingly, relaxing of the acto-myosin cortical network was also shown to promote migration of non-motile cells. In that study, authors demonstrated that disruption of acto-myosin network was releasing G-actin monomer which were efficiently used to polymerize F-actin filament necessary for protrusive forces (Lomakin et al., 2015)

All in all ROCK dependent acto-myosin contractility prevents Rac1 dependent actin polymerization required for protrusive invasive structures, that in our case are necessary for the leader cell formation. Therefore ROCK inhibition induces collective invasion by relaxation of the acto-myosin cable and the unleashing of ROCK antagonism towards Rac1.

ROCK regulates tension at cell-cell junctions

Acto-myosin contractility contributes to collective invasion by regulation of cell-cell junction contractility. In the work in collaboration with the Kretzer lab, we described a new signaling pathway involving RhoA-ROCK activation downstream of the microtubule dependent motor protein Kif17 which contributed to junction stabilization. This is in agreement with the well known pathway of RhoA/ROCK activation at cell-cell junction (Ivanov et al., 2008; Priya et al., 2015, 2017). To allow efficient collective movement, acto-myosin tension at cell-cell junctions need to be relaxed (Hidalgo-Carcedo et al., 2011; Omelchenko and Hall, 2012). ROCK inhibition may contribute to that relaxation of cell-cell junction in our CRC model, a role maybe mediated by FARP2. In fact, we demonstrated that FARP2 was relocalized at cell-cell junctions upon ROCK inhibition and previous studies have shown that FARP2 activated Cdc42 and Rac1 there (Fukuhara et al., 2004; Fukuyama et al., 2005). As it exists an antagonism between Rac1 and ROCK, this suggests that it could be involved in the relaxation of cell-cell junction.

Conclusion:
Together, our results show that ROCK activity synchronize the cytoskeleton to harness CRC invasive behavior. ROCK inhibitors are already used in the clinic for the treatment of several cardiovascular conditions; the rationale at the basis of this is to prevent or reduce invasion and metastasis formation by blocking ROCK activity.(Croft et al., 2004; Narumiya et al., 2009; Sadok and Marshall, 2014). However our research points out that this might not always be the case, as CRC invasiveness could be actually triggered by ROCK inhibition.

ROCK2 but not ROCK1 inhibition triggers collective invasion of CRC

While the majority of work studying ROCK kinases contribution to cell invasion fail to discriminate the respective contribution of each isoform, using dominant negative

constructs and shRNA depletions we find that ROCK2 and not ROCK1 was inducing collective invasion from our CRC model (Amano et al., 1999). Our results are in agreement with described role of the ROCK2 isoform in the single cell invasion of fibroblasts. In several reports, authors demonstrated that ROCK2 activity controlled mesenchymal protrusive migration by antagonizing Rac1 activity, by promoting acto-myosin stability and contractility phosphorylation of Lim Kinase and MLC phosphorylation (Newell-Litwa et al., 2015). ROCK1 is responsible of large low contractile myosin bundles at the rear of the cell, which were shown to polarize the cell and to localize GEFs for Rac1 at front rear of the cell (Newell-Litwa et al., 2015; Vicente-Manzanares et al., 2011). However, in the collective invasion, only ROCK1 isoform was described so far in the regulation of the acto-myosin contractility at cell-cell junctions (Hidalgo-Carcedo et al., 2011) where PDK1 competes with RhoE for ROCK1 binding thereby inducing its activation to regulate single cell invasion of melanoma.

ROCK activity promotes collective propulsive mode of invasion

The TSIPs use a mode of collective invasion that does not require the formation of leader cells, which reminds the mode of invasion used by amoeboid single cells (Paluch and Raz, 2013). As these clusters displayed an inverted apico-basolateral polarity axis, we asked whether these features were specifically required for their movement. We found that polarity proteins expression were not responsible for that phenotype as depleting them in normally polarized clusters cell had no effect. Instead, ECM signaling by the laminin rich ECM was sufficient to induce loss of apical membranar identity without impeding cluster invasion. Instead inhibiting contractility of the apical acto-myosin network was sufficient to prevent TSIPs invasion. Adding to this the fact that Rac inhibitors or Integrin inhibitors had no effect on TSIP invasion, we concluded that TSIP were using a propulsive, adhesion mode of invasion which relied on acto-myosin contractility.

ROCK as a therapeutic target to prevent CRC metastatic dissemination?

ROCK activity regulation in cancer

Although most of the studies focus on a promoting role of ROCK activity in cancer progression (Croft et al., 2004; Itoh et al., 1999; Wei et al., 2016), contradictory studies are

emerging, presenting ROCK activity as a negative regulator of cancer progression and more importantly studies show a promotion of invasion induced by ROCK inhibition. Most interestingly these studies are conducted in colon carcinoma (Sari et al., 2013).
How does this translate into the human pathology remain to be determined. How is ROCK activity and acto-mysoin regulated *in vivo*? In the TSIP, we identified a signalling dependent on TGF beta. This non canonical signalling downstream of TGFbeta negatively regulated RhoA/ROCK activity through ParD6. Another hypothesis would be regulation by the JAK/Stat signalling pathway as previously reported for the amoeboid mode of invasion.

Yet, it remains essential to elucidate the tumor specific context enabling pro or anti-invasive functions of this kinase in order to propose relevant therapeutic strategies to patients and avoid paradoxical effects.

Different requirement of ROCK to different modes of invasion

Here we show that collective invasion of CRC makes different use of the Rho signalling pathway. We show that while ROCK activation is required to promote collective invasion of TSIPs which rely on acto-myosin contractility and does not need adhesion to the matrix, ROCK downregulation induces a Rac1 dependent protrusive collective mode of invasion which is related to the single mesenchymal mode of invasion that requires adhesion to the matrix (Sahai and Marshall, 2003; Sanz-Moreno et al., 2008). Therefore as for single cell mode of invasion, ROCK is a major determinant of collective invasion plasticity making it a poor therapeutic target to prevent cancer cell invasion. To overcome this dual contribution of ROCKs to cell invasion it was proposed, for single cells, to combine ROCK inhibition to either adhesion inhibition or to proteolysis inhibition (Sahai and Marshall, 2003; Sanz-Moreno et al., 2008). Although we did not assess the contribution of integrin based adhesion to the protrusive collective mode of invasion, it is well know that integrins are expressed by leader cells and are essential for these cells to insure the traction necessary to move the cohort (Etienne-Manneville and Hall, 2001; Hegerfeldt et al., 2002; Yamaguchi et al., 2015). Alternatively, a recent study revealed efficient blockade of melanoma invasion by potent ROCK inhibition *in vitro* and *in vivo* (Sadok et al., 2015*)*. They propose that the switch to different more efficient modes of invasion rather than the inhibition of cell invasion induced

by the ROCK inhibition in previous studies was due to the low efficiency of the drugs used, namely Y27632 and H1152 or Blebbistatin. These drugs were not sufficient to induce total collapse of the acto-myosin cytoskeleton whose contractility is well known to contribute to all modes of invasion (Combedazou et al., 2017; Lomakin et al., 2015; Pandya et al., 2017; Sanz-Moreno et al., 2011). Its total shut down should be sufficient to prevent switch to another mode as Sadok and al. proved using potent new drugs (Sadok et al., 2015)

Xenograft of cancer cell lines into mice peritonea (Itoh et al., 1999) or subcutaneously (Croft et al., 2004) revealed that the ROCK mutant CAT promoted tumour progression, Sadok et al. demonstrated that ROCK inhibition could impede tumor growth and therefore prevent tumor progression. All these studies suggest that ROCK may have a pro-tumoral effect that would be nonetheless independent of its role in cell invasion. In support of that, it was shown that in transgenic mice models of skin cancer, expression of an active form of ROCK2 increases proliferation, but not invasion (Samuel et al., 2011).
More specific tools should be used in the future to study the pro-invasive role of ROCK *in vivo*. In fact, the CAT effect on ROCK specific substrate can be questioned as the construct lacks the ROCK C-term domain which is essential to ensure correct localization of the kinase at the membrane (Chen et al., 2002; Truebestein et al., 2015).
Although we cannot exclude that the anti-invasive function of ROCK2 are restricted to the early step of collective invasion studied in our in vitro experimental system, our results are in agreement with the recent large scale in vivo RNAi screen revealing that loss of Myosin-II triggers the formation of invasive squamous cell carcinomas (Schramek et al., 2014).

Whether in 2D or 3D, amoeboid or mesenchymal, collective leader-follower or collective propulsive, ROCK contribution to cell invasion varies depending on the conditions. Therefore, targeting ROCK activity does not appear to be an efficient strategy to prevent invasion of CRC (Lomakin et al., 2015; Sanz-Moreno et al., 2008).

REFERENCES

Aceto, N., Bardia, A., Miyamoto, D.T., Donaldson, M.C., Wittner, B.S., Spencer, J.A., Yu, M., Pely, A., Engstrom, A., Zhu, H., et al. (2014). Circulating Tumor Cell Clusters Are Oligoclonal Precursors of Breast Cancer Metastasis. Cell *158*, 1110–1122.

Acharya, B.R., Espenel, C., and Kreitzer, G. (2013). Direct Regulation of Microtubule Dynamics by KIF17 Motor and Tail Domains. J. Biol. Chem. *288*, 32302–32313.

Alan, J.K., and Lundquist, E.A. (2013). Mutationally activated Rho GTPases in cancer. Small GTPases *4*, 159–163.

Alexander, S., Weigelin, B., Winkler, F., and Friedl, P. (2013). Preclinical intravital microscopy of the tumour-stroma interface: invasion, metastasis, and therapy response. Curr. Opin. Cell Biol. *25*, 659–671.

Amado-Azevedo, J., Reinhard, N.R., van Bezu, J., de Menezes, R.X., van Beusechem, V.W., van Nieuw Amerongen, G.P., van Hinsbergh, V.W.M., and Hordijk, P.L. (2017). A CDC42-centered signaling unit is a dominant positive regulator of endothelial integrity. Sci. Rep. *7*, 10132.

Aman, A., and Piotrowski, T. (2008). Wnt/beta-catenin and Fgf signaling control collective cell migration by restricting chemokine receptor expression. Dev. Cell *15*, 749–761.

Amano, M., Ito, M., Kimura, K., Fukata, Y., Chihara, K., Nakano, T., Matsuura, Y., and Kaibuchi, K. (1996). Phosphorylation and Activation of Myosin by Rho-associated Kinase (Rho-kinase). J. Biol. Chem. *271*, 20246–20249.

Amano, M., Chihara, K., Kimura, K., Fukata, Y., Nakamura, N., Matsuura, Y., and Kaibuchi, K. (1997). Formation of actin stress fibers and focal adhesions enhanced by Rho-kinase. Science *275*, 1308–1311.

Amano, M., Chihara, K., Nakamura, N., Kaneko, T., Matsuura, Y., and Kaibuchi, K. (1999). The COOH Terminus of Rho-kinase Negatively Regulates Rho-kinase Activity. J. Biol. Chem. *274*, 32418–32424.

Amano, M., Kaneko, T., Maeda, A., Nakayama, M., Ito, M., Yamauchi, T., Goto, H., Fukata, Y., Oshiro, N., Shinohara, A., et al. (2003). Identification of Tau and MAP2 as novel substrates of Rho-kinase and myosin phosphatase. J. Neurochem. *87*, 780–790.

Amano, M., Hamaguchi, T., Shohag, M.H., Kozawa, K., Kato, K., Zhang, X., Yura, Y., Matsuura, Y., Kataoka, C., Nishioka, T., et al. (2015). Kinase-interacting substrate screening is a novel method to identify kinase substrates. J Cell Biol *209*, 895–912.

Arimura, N., Inagaki, N., Chihara, K., Ménager, C., Nakamura, N., Amano, M., Iwamatsu, A., Goshima, Y., and Kaibuchi, K. (2000). Phosphorylation of Collapsin Response Mediator Protein-2 by Rho-kinase EVIDENCE FOR TWO SEPARATE SIGNALING PATHWAYS FOR GROWTH CONE COLLAPSE. J. Biol. Chem. *275*, 23973–23980.

Bacallao, R., Antony, C., Dotti, C., Karsenti, E., Stelzer, E.H., and Simons, K. (1989). The subcellular organization of Madin-Darby canine kidney cells during the formation of a polarized epithelium. J. Cell Biol. *109*, 2817–2832.

Bianco, A., Poukkula, M., Cliffe, A., Mathieu, J., Luque, C.M., Fulga, T.A., and Rørth, P. (2007). Two distinct modes of guidance signalling during collective migration of border cells. Nature *448*, 362–365.

Bilder, D., Li, M., and Perrimon, N. (2000). Cooperative regulation of cell polarity and growth by Drosophila tumor suppressors. Science *289*, 113–116.

Bishop, A.L., and Hall, A. (2000). Rho GTPases and their effector proteins. Biochem. J. *348*, 241–255.

Blanchoin, L., Boujemaa-Paterski, R., Sykes, C., and Plastino, J. (2014). Actin Dynamics, Architecture, and Mechanics in Cell Motility. Physiol. Rev. *94*, 235–263.

Brabletz, T., Jung, A., Reu, S., Porzner, M., Hlubek, F., Kunz-Schughart, L.A., Knuechel, R., and Kirchner, T. (2001). Variable β-catenin expression in colorectal cancers indicates tumor progression driven by the tumor environment. Proc. Natl. Acad. Sci. *98*, 10356–10361.

Brandt, B., Junker, R., Griwatz, C., Heidl, S., Brinkmann, O., Semjonow, A., Assmann, G., and Zänker, K.S. (1996). Isolation of prostate-derived single cells and cell clusters from human peripheral blood. Cancer Res. *56*, 4556–4561.

Bronsert, P., Enderle-Ammour, K., Bader, M., Timme, S., Kuehs, M., Csanadi, A., Kayser, G., Kohler, I., Bausch, D., Hoeppner, J., et al. (2014). Cancer cell invasion and EMT marker expression: a three-dimensional study of the human cancer-host interface. J. Pathol. *234*, 410–422.

Brouhard, G., and Sept, D. (2012). Microtubules: sizing up the GTP cap. Curr. Biol. CB *22*, R802-803.
Bryant, D.M., Datta, A., Rodríguez-Fraticelli, A.E., Peränen, J., Martin-Belmonte, F., and Mostov, K.E. (2010). A molecular network for de novo generation of the apical surface and lumen. Nat. Cell Biol. *12*, 1035–1045.
Buckley, C.D., Tan, J., Anderson, K.L., Hanein, D., Volkmann, N., Weis, W.I., Nelson, W.J., and Dunn, A.R. (2014). Cell adhesion. The minimal cadherin-catenin complex binds to actin filaments under force. Science *346*, 1254211–1254211.
Bustelo, X.R. (2014). Vav family exchange factors: an integrated regulatory and functional view. Small GTPases *5*, 9.
Byers, S.W., Sommers, C.L., Hoxter, B., Mercurio, A.M., and Tozeren, A. (1995). Role of E-cadherin in the response of tumor cell aggregates to lymphatic, venous and arterial flow: measurement of cell-cell adhesion strength. J. Cell Sci. *108 (Pt 5)*, 2053–2064.
Cai, D., Chen, S.-C., Prasad, M., He, L., Wang, X., Choesmel-Cadamuro, V., Sawyer, J.K., Danuser, G., and Montell, D.J. (2014a). Mechanical Feedback through E-Cadherin Promotes Direction Sensing during Collective Cell Migration. Cell *157*, 1146–1159.
Cai, D., Chen, S.-C., Prasad, M., He, L., Wang, X., Choesmel-Cadamuro, V., Sawyer, J.K., Danuser, G., and Montell, D.J. (2014b). Mechanical Feedback through E-Cadherin Promotes Direction Sensing during Collective Cell Migration. Cell *157*, 1146–1159.
Camand, E., Peglion, F., Osmani, N., Sanson, M., and Etienne-Manneville, S. (2012). N-cadherin expression level modulates integrin-mediated polarity and strongly impacts on the speed and directionality of glial cell migration. J Cell Sci *125*, 844–857.
Campbell, I.D., and Humphries, M.J. (2011). Integrin Structure, Activation, and Interactions. Cold Spring Harb. Perspect. Biol. *3*, a004994.
Cancer Genome Atlas Research Network (2014). Comprehensive molecular characterization of gastric adenocarcinoma. Nature *513*, 202–209.
Cano, A., Pérez-Moreno, M.A., Rodrigo, I., Locascio, A., Blanco, M.J., Barrio, M.G. del, Portillo, F., and Nieto, M.A. (2000). The transcription factor Snail controls epithelial–mesenchymal transitions by repressing E-cadherin expression. Nat. Cell Biol. *2*, ncb0200_76.
Chaffer, C.L., Juan, B.P.S., Lim, E., and Weinberg, R.A. (2016). EMT, cell plasticity and metastasis. Cancer Metastasis Rev. *35*, 645–654.
Charras, G., and Sahai, E. (2014). Physical influences of the extracellular environment on cell migration. Nat. Rev. Mol. Cell Biol. *15*, 813–824.
Chausovsky, A., Bershadsky, A.D., and Borisy, G.G. (2000). Cadherin-mediated regulation of microtubule dynamics. Nat. Cell Biol. *2*, 797–804.
Cheadle, L., and Biederer, T. (2012). The novel synaptogenic protein Farp1 links postsynaptic cytoskeletal dynamics and transsynaptic organization. J. Cell Biol. *199*, 985–1001.
Cheadle, L., and Biederer, T. (2014). Activity-Dependent Regulation of Dendritic Complexity by Semaphorin 3A through Farp1. J. Neurosci. Off. J. Soc. Neurosci. *34*, 7999–8009.
Chen, X., Tan, I., Ng, C.H., Hall, C., Lim, L., and Leung, T. (2002a). Characterization of RhoA-binding Kinase ROKα Implication of the Pleckstrin Homology Domain in ROKα Function Using Region-specific Antibodies. J. Biol. Chem. *277*, 12680–12688.
Chen, X., Tan, I., Ng, C.H., Hall, C., Lim, L., and Leung, T. (2002b). Characterization of RhoA-binding kinase ROKalpha implication of the pleckstrin homology domain in ROKalpha function using region-specific antibodies. J. Biol. Chem. *277*, 12680–12688.
Chen, Z., Borek, D., Padrick, S.B., Gomez, T.S., Metlagel, Z., Ismail, A.M., Umetani, J., Billadeau, D.D., Otwinowski, Z., and Rosen, M.K. (2010). Structure and control of the actin regulatory WAVE complex. Nature *468*, 533–538.
Cheung, K.J., and Ewald, A.J. (2016). A collective route to metastasis: Seeding by tumor cell clusters. Science *352*, 167–169.
Cheung, K.J., Gabrielson, E., Werb, Z., and Ewald, A.J. (2013). Collective invasion in breast cancer requires a conserved basal epithelial program. Cell *155*, 1639–1651.
Cheung, K.J., Padmanaban, V., Silvestri, V., Schipper, K., Cohen, J.D., Fairchild, A.N., Gorin, M.A., Verdone, J.E., Pienta, K.J., Bader, J.S., et al. (2016). Polyclonal breast cancer metastases arise from collective

dissemination of keratin 14-expressing tumor cell clusters. Proc. Natl. Acad. Sci. *113*, E854–E863.
Christiansen, J.J., and Rajasekaran, A.K. (2006). Reassessing epithelial to mesenchymal transition as a prerequisite for carcinoma invasion and metastasis. Cancer Res. *66*, 8319–8326.
Clark, A.G., and Vignjevic, D.M. (2015). Modes of cancer cell invasion and the role of the microenvironment. Curr. Opin. Cell Biol. *36*, 13–22.
Cohen, P.T.W. (2002). Protein phosphatase 1--targeted in many directions. J. Cell Sci. *115*, 241–256.
Coleman, M.L., Sahai, E.A., Yeo, M., Bosch, M., Dewar, A., and Olson, M.F. (2001). Membrane blebbing during apoptosis results from caspase-mediated activation of ROCK I. Nat. Cell Biol. *3*, 339–345.
Combedazou, A., Choesmel-Cadamuro, V., Gay, G., Liu, J., Dupré, L., Ramel, D., and Wang, X. (2017). Myosin II governs collective cell migration behaviour downstream of guidance receptor signalling. J Cell Sci *130*, 97–103.
Côté, J.-F., and Vuori, K. (2002). Identification of an evolutionarily conserved superfamily of DOCK180-related proteins with guanine nucleotide exchange activity. J. Cell Sci. *115*, 4901–4913.
Couzens, A.L., Saridakis, V., and Scheid, M.P. (2009). The hydrophobic motif of ROCK2 requires association with the N-terminal extension for kinase activity. Biochem. J. *419*, 141–148.
Croft, D.R., Sahai, E., Mavria, G., Li, S., Tsai, J., Lee, W.M.F., Marshall, C.J., and Olson, M.F. (2004). Conditional ROCK activation in vivo induces tumor cell dissemination and angiogenesis. Cancer Res. *64*, 8994–9001.
Dang, I., Gorelik, R., Sousa-Blin, C., Derivery, E., Guérin, C., Linkner, J., Nemethova, M., Dumortier, J.G., Giger, F.A., Chipysheva, T.A., et al. (2013). Inhibitory signalling to the Arp2/3 complex steers cell migration. Nature *503*, 281–284.
Das, T., Safferling, K., Rausch, S., Grabe, N., Boehm, H., and Spatz, J.P. (2015). A molecular mechanotransduction pathway regulates collective migration of epithelial cells. Nat. Cell Biol. *17*, 276–287.
Donà, E., Barry, J.D., Valentin, G., Quirin, C., Khmelinskii, A., Kunze, A., Durdu, S., Newton, L.R., Fernandez-Minan, A., Huber, W., et al. (2013). Directional tissue migration through a self-generated chemokine gradient. Nature *503*, 285–289.
Duchek, P., Somogyi, K., Jékely, G., Beccari, S., and Rørth, P. (2001). Guidance of cell migration by the Drosophila PDGF/VEGF receptor. Cell *107*, 17–26.
Durdu, S., Iskar, M., Revenu, C., Schieber, N., Kunze, A., Bork, P., Schwab, Y., and Gilmour, D. (2014). Luminal signalling links cell communication to tissue architecture during organogenesis. Nature *515*, 120–124.
Dusek, R.L., Godsel, L.M., and Green, K.J. (2007). Discriminating roles of desmosomal cadherins: beyond desmosomal adhesion. J. Dermatol. Sci. *45*, 7–21.
Eden, S., Rohatgi, R., Podtelejnikov, A.V., Mann, M., and Kirschner, M.W. (2002). Mechanism of regulation of WAVE1-induced actin nucleation by Rac1 and Nck. Nature *418*, 790–793.
Ellenbroek, S.I.J., Iden, S., and Collard, J.G. (2012). The Rac activator Tiam1 is required for polarized protrusional outgrowth of primary astrocytes by affecting the organization of the microtubule network. Small GTPases *3*, 4–14.
Emmert, D.A., Fee, J.A., Goeckeler, Z.M., Grojean, J.M., Wakatsuki, T., Elson, E.L., Herring, B.P., Gallagher, P.J., and Wysolmerski, R.B. (2004). Rho-kinase-mediated Ca2+-independent contraction in rat embryo fibroblasts. Am. J. Physiol. Cell Physiol. *286*, C8-21.
Etienne-Manneville, S. (2013). Microtubules in cell migration. Annu. Rev. Cell Dev. Biol. *29*, 471–499.
Etienne-Manneville, S. (2014). Neighborly relations during collective migration. Curr. Opin. Cell Biol. *30*, 51–59.
Etienne-Manneville, S., and Hall, A. (2001). Integrin-mediated activation of Cdc42 controls cell polarity in migrating astrocytes through PKCzeta. Cell *106*, 489–498.
Etienne-Manneville, S., and Hall, A. (2002). Rho GTPases in cell biology. Nature *420*, 629–635.
Farooqui, R., and Fenteany, G. (2005). Multiple rows of cells behind an epithelial wound edge extend cryptic lamellipodia to collectively drive cell-sheet movement. J Cell Sci *118*, 51–63.
Fearon, E.R. (2011). Molecular genetics of colorectal cancer. Annu. Rev. Pathol. *6*, 479–507.
Fearon, E.R., and Vogelstein, B. (1990). A genetic model for colorectal tumorigenesis. Cell *61*, 759–767.
Feng, J., Ito, M., Ichikawa, K., Isaka, N., Nishikawa, M., Hartshorne, D.J., and Nakano, T. (1999). Inhibitory Phosphorylation Site for Rho-associated Kinase on Smooth Muscle Myosin Phosphatase. J. Biol. Chem. *274*,

37385–37390.
Ferlay, J., Soerjomataram, I., Dikshit, R., Eser, S., Mathers, C., Rebelo, M., Parkin, D.M., Forman, D., and Bray, F. (2015). Cancer incidence and mortality worldwide: Sources, methods and major patterns in GLOBOCAN 2012. Int. J. Cancer *136*, E359–E386.
Fischer, K.R., Durrans, A., Lee, S., Sheng, J., Li, F., Wong, S.T.C., Choi, H., El Rayes, T., Ryu, S., Troeger, J., et al. (2015). Epithelial-to-mesenchymal transition is not required for lung metastasis but contributes to chemoresistance. Nature *527*, 472–476.
Fleming, M., Ravula, S., Tatishchev, S.F., and Wang, H.L. (2012). Colorectal carcinoma: Pathologic aspects. J. Gastrointest. Oncol. *3*, 153–173.
van der Flier, L.G., and Clevers, H. (2009). Stem cells, self-renewal, and differentiation in the intestinal epithelium. Annu. Rev. Physiol. *71*, 241–260.
Fojo, A.T., and Menefee, M. (2005). Microtubule targeting agents: basic mechanisms of multidrug resistance (MDR). Semin. Oncol. *32*, S3-8.
de Forges, H., Bouissou, A., and Perez, F. (2012). Interplay between microtubule dynamics and intracellular organization. Int. J. Biochem. Cell Biol. *44*, 266–274.
Friedl, P. (2004). Prespecification and plasticity: shifting mechanisms of cell migration. Curr. Opin. Cell Biol. *16*, 14–23.
Friedl, P., and Alexander, S. (2011a). Cancer Invasion and the Microenvironment: Plasticity and Reciprocity. Cell *147*, 992–1009.
Friedl, P., and Alexander, S. (2011b). Cancer invasion and the microenvironment: plasticity and reciprocity. Cell *147*, 992–1009.
Friedl, P., and Gilmour, D. (2009). Collective cell migration in morphogenesis, regeneration and cancer. Nat. Rev. Mol. Cell Biol. *10*, 445–457.
Friedl, P., and Wolf, K. (2008). Tube Travel: The Role of Proteases in Individual and Collective Cancer Cell Invasion. Cancer Res. *68*, 7247–7249.
Friedl, P., and Wolf, K. (2010). Plasticity of cell migration: a multiscale tuning model. J. Cell Biol. *188*, 11–19.
Friedl, P., Noble, P.B., Walton, P.A., Laird, D.W., Chauvin, P.J., Tabah, R.J., Black, M., and Zänker, K.S. (1995). Migration of Coordinated Cell Clusters in Mesenchymal and Epithelial Cancer Explants in Vitro. Cancer Res. *55*, 4557–4560.
Friedl, P., Locker, J., Sahai, E., and Segall, J.E. (2012). Classifying collective cancer cell invasion. Nat. Cell Biol. *14*, 777–783.
Fukata, Y., Oshiro, N., Kinoshita, N., Kawano, Y., Matsuoka, Y., Bennett, V., Matsuura, Y., and Kaibuchi, K. (1999). Phosphorylation of Adducin by Rho-Kinase Plays a Crucial Role in Cell Motility. J. Cell Biol. *145*, 347–361.
Fukuhara, T., Shimizu, K., Kawakatsu, T., Fukuyama, T., Minami, Y., Honda, T., Hoshino, T., Yamada, T., Ogita, H., Okada, M., et al. (2004). Activation of Cdc42 by trans interactions of the cell adhesion molecules nectins through c-Src and Cdc42-GEF FRG. J. Cell Biol. *166*, 393–405.
Fukuyama, T., Ogita, H., Kawakatsu, T., Fukuhara, T., Yamada, T., Sato, T., Shimizu, K., Nakamura, T., Matsuda, M., and Takai, Y. (2005a). Involvement of the c-Src-Crk-C3G-Rap1 signaling in the nectin-induced activation of Cdc42 and formation of adherens junctions. J. Biol. Chem. *280*, 815–825.
Fukuyama, T., Ogita, H., Kawakatsu, T., Fukuhara, T., Yamada, T., Sato, T., Shimizu, K., Nakamura, T., Matsuda, M., and Takai, Y. (2005b). Involvement of the c-Src-Crk-C3G-Rap1 Signaling in the Nectin-induced Activation of Cdc42 and Formation of Adherens Junctions. J. Biol. Chem. *280*, 815–825.
Gadea, G., and Blangy, A. (2014). Dock-family exchange factors in cell migration and disease. Eur. J. Cell Biol. *93*, 466–477.
Garcia-Mata, R., Boulter, E., and Burridge, K. (2011). The “invisible hand”: regulation of RHO GTPases by RHOGDIs. Nat. Rev. Mol. Cell Biol. *12*, nrm3153.
Gardner, M.K., Hunt, A.J., Goodson, H.V., and Odde, D.J. (2008). Microtubule assembly dynamics: new insights at the nanoscale. Curr. Opin. Cell Biol. *20*, 64–70.
Gassama-Diagne, A., Yu, W., ter Beest, M., Martin-Belmonte, F., Kierbel, A., Engel, J., and Mostov, K. (2006). Phosphatidylinositol-3,4,5-trisphosphate regulates the formation of the basolateral plasma membrane in epithelial cells. Nat. Cell Biol. *8*, 963–970.

Giampieri, S., Manning, C., Hooper, S., Jones, L., Hill, C.S., and Sahai, E. (2009). Localized and reversible TGFβ signalling switches breast cancer cells from cohesive to single cell motility. Nat. Cell Biol. *11*, 1287–1296.
Goicoechea, S.M., Awadia, S., and Garcia-Mata, R. (2014). I'm coming to GEF you: Regulation of RhoGEFs during cell migration. Cell Adhes. Migr. *8*, 535–549.
Goldstein, B., and Macara, I.G. (2007). The PAR proteins: fundamental players in animal cell polarization. Dev. Cell *13*, 609–622.
Goto, H., Kosako, H., Tanabe, K., Yanagida, M., Sakurai, M., Amano, M., Kaibuchi, K., and Inagaki, M. (1998). Phosphorylation of vimentin by Rho-associated kinase at a unique amino-terminal site that is specifically phosphorylated during cytokinesis. J. Biol. Chem. *273*, 11728–11736.
Guasch, R.M., Scambler, P., Jones, G.E., and Ridley, A.J. (1998). RhoE regulates actin cytoskeleton organization and cell migration. Mol. Cell. Biol. *18*, 4761–4771.
Gupta, G.P., and Massagué, J. (2006). Cancer metastasis: building a framework. Cell *127*, 679–695.
Haas, P., and Gilmour, D. (2006). Chemokine signaling mediates self-organizing tissue migration in the zebrafish lateral line. Dev. Cell *10*, 673–680.
Hahmann, C., and Schroeter, T. (2010). Rho-kinase inhibitors as therapeutics: from pan inhibition to isoform selectivity. Cell. Mol. Life Sci. CMLS *67*, 171–177.
Hart, I.R. (2009). New evidence for tumour embolism as a mode of metastasis. J. Pathol. *219*, 275–276.
Hashizume, R., Koizumi, H., Ihara, A., Ohta, T., and Uchikoshi, T. (1996). Expression of beta-catenin in normal breast tissue and breast carcinoma: a comparative study with epithelial cadherin and alpha-catenin. Histopathology *29*, 139–146.
Hayer, A., Shao, L., Chung, M., Joubert, L.-M., Yang, H.W., Tsai, F.-C., Bisaria, A., Betzig, E., and Meyer, T. (2016). Engulfed cadherin fingers are polarized junctional structures between collectively migrating endothelial cells. Nat. Cell Biol. *18*, 1311–1323.
He, X., Kuo, Y.-C., Rosche, T.J., and Zhang, X. (2013). Structural Basis for Autoinhibition of the Guanine Nucleotide Exchange Factor FARP2. Structure *21*, 355–364.
Hegerfeldt, Y., Tusch, M., Bröcker, E.-B., and Friedl, P. (2002). Collective Cell Movement in Primary Melanoma Explants: Plasticity of Cell-Cell Interaction, β1-Integrin Function, and Migration Strategies. Cancer Res. *62*, 2125–2130.
Hidalgo-Carcedo, C., Hooper, S., Chaudhry, S.I., Williamson, P., Harrington, K., Leitinger, B., and Sahai, E. (2011). Collective cell migration requires suppression of actomyosin at cell-cell contacts mediated by DDR1 and the cell polarity regulators Par3 and Par6. Nat. Cell Biol. *13*, 49–58.
Hodge, R.G., and Ridley, A.J. (2016). Regulating Rho GTPases and their regulators. Nat. Rev. Mol. Cell Biol. *17*, 496–510.
Hou, J.-M., Krebs, M., Ward, T., Sloane, R., Priest, L., Hughes, A., Clack, G., Ranson, M., Blackhall, F., and Dive, C. (2011). Circulating tumor cells as a window on metastasis biology in lung cancer. Am. J. Pathol. *178*, 989–996.
Ichikawa, K., Ito, M., and Hartshorne, D.J. (1996). Phosphorylation of the large subunit of myosin phosphatase and inhibition of phosphatase activity. J. Biol. Chem. *271*, 4733–4740.
Ihara, K., Muraguchi, S., Kato, M., Shimizu, T., Shirakawa, M., Kuroda, S., Kaibuchi, K., and Hakoshima, T. (1998). Crystal structure of human RhoA in a dominantly active form complexed with a GTP analogue. J. Biol. Chem. *273*, 9656–9666.
Ishizaki, T., Maekawa, M., Fujisawa, K., Okawa, K., Iwamatsu, A., Fujita, A., Watanabe, N., Saito, Y., Kakizuka, A., Morii, N., et al. (1996). The small GTP-binding protein Rho binds to and activates a 160 kDa Ser/Thr protein kinase homologous to myotonic dystrophy kinase. EMBO J. *15*, 1885–1893.
Ishizaki, T., Naito, M., Fujisawa, K., Maekawa, M., Watanabe, N., Saito, Y., and Narumiya, S. (1997). p160ROCK, a Rho-associated coiled-coil forming protein kinase, works downstream of Rho and induces focal adhesions. FEBS Lett. *404*, 118–124.
Itoh, K., Yoshioka, K., Akedo, H., Uehata, M., Ishizaki, T., and Narumiya, S. (1999). An essential part for Rho–associated kinase in the transcellular invasion of tumor cells. Nat. Med. *5*, 221–225.
Ivanov, A.I., Hopkins, A.M., Brown, G.T., Gerner-Smidt, K., Babbin, B.A., Parkos, C.A., and Nusrat, A. (2008). Myosin II regulates the shape of three-dimensional intestinal epithelial cysts. J. Cell Sci. *121*, 1803–1814.

Izawa, T., Fukata, Y., Kimura, T., Iwamatsu, A., Dohi, K., and Kaibuchi, K. (2000). Elongation factor-1 alpha is a novel substrate of rho-associated kinase. Biochem. Biophys. Res. Commun. *278*, 72–78.
Jacobs, M., Hayakawa, K., Swenson, L., Bellon, S., Fleming, M., Taslimi, P., and Doran, J. (2006). The Structure of Dimeric ROCK I Reveals the Mechanism for Ligand Selectivity. J. Biol. Chem. *281*, 260–268.
Janke, C., and Kneussel, M. (2010). Tubulin post-translational modifications: encoding functions on the neuronal microtubule cytoskeleton. Trends Neurosci. *33*, 362–372.
Jaulin, F., and Kreitzer, G. (2010). KIF17 stabilizes microtubules and contributes to epithelial morphogenesis by acting at MT plus ends with EB1 and APC. J. Cell Biol. *190*, 443.
Jaulin, F., Xue, X., Rodriguez-Boulan, E., and Kreitzer, G. (2007). Polarization-dependent selective transport to the apical membrane by KIF5B in MDCK cells. Dev. Cell *13*, 511–522.
Juanes-García, A., Llorente-González, C., Vicente-Manzanares, M., Juanes-García, A., Llorente-González, C., and Vicente-Manzanares, M. (2016). Molecular control of non-muscle myosin II assembly. Oncotarget *7*, 5092–5093.
Julian, L., and Olson, M.F. (2014). Rho-associated coiled-coil containing kinases (ROCK): Structure, regulation, and functions. Small GTPases *5*.
Julien, S., Merino-Trigo, A., Lacroix, L., Pocard, M., Goéré, D., Mariani, P., Landron, S., Bigot, L., Nemati, F., Dartigues, P., et al. (2012). Characterization of a large panel of patient-derived tumor xenografts representing the clinical heterogeneity of human colorectal cancer. Clin. Cancer Res. Off. J. Am. Assoc. Cancer Res. *18*, 5314–5328.
Kaneko, T., Amano, M., Maeda, A., Goto, H., Takahashi, K., Ito, M., and Kaibuchi, K. (2000). Identification of calponin as a novel substrate of Rho-kinase. Biochem. Biophys. Res. Commun. *273*, 110–116.
Kats-Ugurlu, G., Roodink, I., de Weijert, M., Tiemessen, D., Maass, C., Verrijp, K., van der Laak, J., de Waal, R., Mulders, P., Oosterwijk, E., et al. (2009). Circulating tumour tissue fragments in patients with pulmonary metastasis of clear cell renal cell carcinoma. J. Pathol. *219*, 287–293.
Katzav, S., Cleveland, J.L., Heslop, H.E., and Pulido, D. (1991). Loss of the amino-terminal helix-loop-helix domain of the vav proto-oncogene activates its transforming potential. Mol. Cell. Biol. *11*, 1912–1920.
Kawabata, S., Usukura, J., Morone, N., Ito, M., Iwamatsu, A., Kaibuchi, K., and Amano, M. (2004). Interaction of Rho-kinase with myosin II at stress fibres. Genes Cells Devoted Mol. Cell. Mech. *9*, 653–660.
Kawakatsu, T., Ogita, H., Fukuhara, T., Fukuyama, T., Minami, Y., Shimizu, K., and Takai, Y. (2005). Vav2 as a Rac-GDP/GTP Exchange Factor Responsible for the Nectin-induced, c-Src- and Cdc42-mediated Activation of Rac. J. Biol. Chem. *280*, 4940–4947.
Kawano, Y., Fukata, Y., Oshiro, N., Amano, M., Nakamura, T., Ito, M., Matsumura, F., Inagaki, M., and Kaibuchi, K. (1999). Phosphorylation of myosin-binding subunit (MBS) of myosin phosphatase by Rho-kinase in vivo. J. Cell Biol. *147*, 1023–1038.
Kawasaki, Y., Senda, T., Ishidate, T., Koyama, R., Morishita, T., Iwayama, Y., Higuchi, O., and Akiyama, T. (2000). Asef, a link between the tumor suppressor APC and G-protein signaling. Science *289*, 1194–1197.
Kemphues, K.J., Priess, J.R., Morton, D.G., and Cheng, N.S. (1988). Identification of genes required for cytoplasmic localization in early C. elegans embryos. Cell *52*, 311–320.
Khalil, A.A., Ilina, O., Gritsenko, P.G., Bult, P., Span, P.N., and Friedl, P. (2017). Collective invasion in ductal and lobular breast cancer associates with distant metastasis. Clin. Exp. Metastasis 1–9.
Khoja, L., Lorigan, P., Dive, C., Keilholz, U., and Fusi, A. (2015). Circulating tumour cells as tumour biomarkers in melanoma: detection methods and clinical relevance. Ann. Oncol. Off. J. Eur. Soc. Med. Oncol. *26*, 33–39.
Kimura, K., Fukata, Y., Matsuoka, Y., Bennett, V., Matsuura, Y., Okawa, K., Iwamatsu, A., and Kaibuchi, K. (1998). Regulation of the association of adducin with actin filaments by Rho-associated kinase (Rho-kinase) and myosin phosphatase. J. Biol. Chem. *273*, 5542–5548.
Koch, S., and Nusrat, A. (2009). Dynamic regulation of epithelial cell fate and barrier function by intercellular junctions. Ann. N. Y. Acad. Sci. *1165*, 220–227.
Konen, J., Summerbell, E., Dwivedi, B., Galior, K., Hou, Y., Rusnak, L., Chen, A., Saltz, J., Zhou, W., Boise, L.H., et al. (2017). Image-guided genomics of phenotypically heterogeneous populations reveals vascular signalling during symbiotic collective cancer invasion. Nat. Commun. *8*, 15078.
Kosako, H., Amano, M., Yanagida, M., Tanabe, K., Nishi, Y., Kaibuchi, K., and Inagaki, M. (1997).

Phosphorylation of glial fibrillary acidic protein at the same sites by cleavage furrow kinase and Rho-associated kinase. J. Biol. Chem. *272*, 10333–10336.
Kosako, H., Goto, H., Yanagida, M., Matsuzawa, K., Fujita, M., Tomono, Y., Okigaki, T., Odai, H., Kaibuchi, K., and Inagaki, M. (1999). Specific accumulation of Rho-associated kinase at the cleavage furrow during cytokinesis: cleavage furrow-specific phosphorylation of intermediate filaments. Oncogene *18*, 2783–2788.
Koyano, Y., Kawamoto, T., Shen, M., Yan, W., Noshiro, M., Fujii, K., and Kato, Y. (1997). Molecular cloning and characterization of CDEP, a novel human protein containing the ezrin-like domain of the band 4.1 superfamily and the Dbl homology domain of Rho guanine nucleotide exchange factors. Biochem. Biophys. Res. Commun. *241*, 369–375.
Koyano, Y., Kawamoto, T., Kikuchi, A., Shen, M., Kuruta, Y., Tsutsumi, S., Fujimoto, K., Noshiro, M., Fujii, K., and Kato§, Y. (2001). Chondrocyte-derived ezrin-like domain containing protein (CDEP), a rho guanine nucleotide exchange factor, is inducible in chondrocytes by parathyroid hormone and cyclic AMP and has transforming activity in NIH3T3 Cells. Osteoarthritis Cartilage *9*, *Supplement 1*, S64–S68.
Krebs, A.M., Mitschke, J., Lasierra Losada, M., Schmalhofer, O., Boerries, M., Busch, H., Boettcher, M., Mougiakakos, D., Reichardt, W., Bronsert, P., et al. (2017). The EMT-activator Zeb1 is a key factor for cell plasticity and promotes metastasis in pancreatic cancer. Nat. Cell Biol. *19*, 518–529.
Kubo, T., Yamashita, T., Yamaguchi, A., Sumimoto, H., Hosokawa, K., and Tohyama, M. (2002). A novel FERM domain including guanine nucleotide exchange factor is involved in Rac signaling and regulates neurite remodeling. J. Neurosci. Off. J. Soc. Neurosci. *22*, 8504–8513.
Lawson, C.D., and Burridge, K. (2014). The on-off relationship of Rho and Rac during integrin-mediated adhesion and cell migration. Small GTPases *5*, e27958.
Lebreton, G., and Casanova, J. (2014). Specification of leading and trailing cell features during collective migration in the Drosophila trachea. J. Cell Sci. *127*, 465–474.
Leung, T., Manser, E., Tan, L., and Lim, L. (1995). A Novel Serine/Threonine Kinase Binding the Ras-related RhoA GTPase Which Translocates the Kinase to Peripheral Membranes. J. Biol. Chem. *270*, 29051–29054.
Leung, T., Chen, X.Q., Manser, E., and Lim, L. (1996). The p160 RhoA-binding kinase ROK alpha is a member of a kinase family and is involved in the reorganization of the cytoskeleton. Mol. Cell. Biol. *16*, 5313.
Ligon, L.A., and Holzbaur, E.L.F. (2007). Microtubules tethered at epithelial cell junctions by dynein facilitate efficient junction assembly. Traffic Cph. Den. *8*, 808–819.
Liu, K.D., Datta, A., Yu, W., Brakeman, P.R., Jou, T.-S., Matthay, M.A., and Mostov, K.E. (2007). Rac1 is required for reorientation of polarity and lumen formation through a PI 3-kinase-dependent pathway. Am. J. Physiol. Renal Physiol. *293*, F1633-1640.
Liu, X., Yu, X., Zack, D.J., Zhu, H., and Qian, J. (2008). TiGER: A database for tissue-specific gene expression and regulation. BMC Bioinformatics *9*, 271.
Lomakin, A.J., Lee, K.-C., Han, S.J., Bui, D.A., Davidson, M., Mogilner, A., and Danuser, G. (2015). Competition for actin between two distinct F-actin networks defines a bistable switch for cell polarization. Nat. Cell Biol. *17*, 1435–1445.
Lyle, K., Kumar, P., and Wittmann, T. (2009a). SnapShot: Microtubule Regulators I. Cell *136*, 380, 380.e1.
Lyle, K., Kumar, P., and Wittmann, T. (2009b). SnapShot: Microtubule regulators II. Cell *136*, 566, 566.e1.
Madaule, P., and Axel, R. (1985). A novel ras-related gene family. Cell *41*, 31–40.
Madhavan, M., Srinivas, P., Abraham, E., Ahmed, I., Mathew, A., Vijayalekshmi, N.R., and Balaram, P. (2001). Cadherins as predictive markers of nodal metastasis in breast cancer. Mod. Pathol. Off. J. U. S. Can. Acad. Pathol. Inc *14*, 423–427.
Maekawa, M., Ishizaki, T., Boku, S., Watanabe, N., Fujita, A., Iwamatsu, A., Obinata, T., Ohashi, K., Mizuno, K., and Narumiya, S. (1999a). Signaling from Rho to the actin cytoskeleton through protein kinases ROCK and LIM-kinase. Science *285*, 895–898.
Maekawa, M., Ishizaki, T., Boku, S., Watanabe, N., Fujita, A., Iwamatsu, A., Obinata, T., Ohashi, K., Mizuno, K., and Narumiya, S. (1999b). Signaling from Rho to the actin cytoskeleton through protein kinases ROCK and LIM-kinase. Science *285*, 895–898.
Martin-Belmonte, F., Gassama, A., Datta, A., Yu, W., Rescher, U., Gerke, V., and Mostov, K. (2007). PTEN-Mediated Apical Segregation of Phosphoinositides Controls Epithelial Morphogenesis through Cdc42. Cell *128*, 383–397.

Mason, S.D., and Joyce, J.A. (2011). Proteolytic networks in cancer. Trends Cell Biol. *21*, 228–237.
Matsui, T., Amano, M., Yamamoto, T., Chihara, K., Nakafuku, M., Ito, M., Nakano, T., Okawa, K., Iwamatsu, A., and Kaibuchi, K. (1996). Rho-associated kinase, a novel serine/threonine kinase, as a putative target for small GTP binding protein Rho. EMBO J. *15*, 2208.
Matsui, T., Maeda, M., Doi, Y., Yonemura, S., Amano, M., Kaibuchi, K., Tsukita, S., and Tsukita, S. (1998). Rho-Kinase Phosphorylates COOH-terminal Threonines of Ezrin/Radixin/Moesin (ERM) Proteins and Regulates Their Head-to-Tail Association. J. Cell Biol. *140*, 647–657.
Meller, N., Merlot, S., and Guda, C. (2005). CZH proteins: a new family of Rho-GEFs. J. Cell Sci. *118*, 4937–4946.
Meng, W., Mushika, Y., Ichii, T., and Takeichi, M. (2008). Anchorage of Microtubule Minus Ends to Adherens Junctions Regulates Epithelial Cell-Cell Contacts. Cell *135*, 948–959.
Meşe, G., Richard, G., and White, T.W. (2007). Gap junctions: basic structure and function. J. Invest. Dermatol. *127*, 2516–2524.
Miki, H., Suetsugu, S., and Takenawa, T. (1998). WAVE, a novel WASP-family protein involved in actin reorganization induced by Rac. EMBO J. *17*, 6932–6941.
Miki, T., Smith, C.L., Long, J.E., Eva, A., and Fleming, T.P. (1993). Oncogene ect2 is related to regulators of small GTP-binding proteins. Nature *362*, 462–465.
Miller, N.L.G., Kleinschmidt, E.G., and Schlaepfer, D.D. (2014). RhoGEFs in cell motility: Novel links between Rgnef and focal adhesion kinase. Curr. Mol. Med. *14*, 221–234.
Miyamoto, Y., Yamauchi, J., and Itoh, H. (2003). Src kinase regulates the activation of a novel FGD-1-related Cdc42 guanine nucleotide exchange factor in the signaling pathway from the endothelin A receptor to JNK. J. Biol. Chem. *278*, 29890–29900.
Miyamoto, Y., Torii, T., Yamamori, N., Ogata, T., Tanoue, A., and Yamauchi, J. (2013). Akt and PP2A reciprocally regulate the guanine nucleotide exchange factor Dock6 to control axon growth of sensory neurons. Sci. Signal. *6*, ra15.
Mlechkovich, G., Peng, S.-S., Shacham, V., Martinez, E., Gokhman, I., Minis, A., Tran, T.S., and Yaron, A. (2014a). Distinct Cytoplasmic Domains in Plexin-A4 Mediate Diverse Responses to Semaphorin 3A in Developing Mammalian Neurons. Sci. Signal. *7*, ra24.
Mlechkovich, G., Peng, S.-S., Shacham, V., Martinez, E., Gokhman, I., Minis, A., Tran, T.S., and Yaron, A. (2014b). Distinct cytoplasmic domains in Plexin-A4 mediate diverse responses to semaphorin 3A in developing mammalian neurons. Sci. Signal. *7*, ra24.
Montell, D.J., Yoon, W.H., and Starz-Gaiano, M. (2012). Group choreography: mechanisms orchestrating the collective movement of border cells. Nat. Rev. Mol. Cell Biol. *13*, 631–645.
Mori, K., Amano, M., Takefuji, M., Kato, K., Morita, Y., Nishioka, T., Matsuura, Y., Murohara, T., and Kaibuchi, K. (2009). Rho-kinase Contributes to Sustained RhoA Activation through Phosphorylation of p190A RhoGAP. J. Biol. Chem. *284*, 5067–5076.
Moritz, M., and Agard, D.A. (2001). Gamma-tubulin complexes and microtubule nucleation. Curr. Opin. Struct. Biol. *11*, 174–181.
Murata, T., Ohnishi, H., Okazawa, H., Murata, Y., Kusakari, S., Hayashi, Y., Miyashita, M., Itoh, H., Oldenborg, P.A., Furuya, N., et al. (2006). CD47 Promotes Neuronal Development through Src- and FRG/Vav2-Mediated Activation of Rac and Cdc42. J. Neurosci. Off. J. Soc. Neurosci. *26*, 12397–12407.
Nabeshima, K., Inoue, T., Shimao, Y., Okada, Y., Itoh, Y., Seiki, M., and Koono, M. (2000). Front-Cell-specific Expression of Membrane-Type 1 Matrix Metalloproteinase and Gelatinase A during Cohort Migration of Colon Carcinoma Cells Induced by Hepatocyte Growth Factor/Scatter Factor. Cancer Res. *60*, 3364–3369.
Nagtegaal, I.D., and Hugen, N. (2015). The Increasing Relevance of Tumour Histology in Determining Oncological Outcomes in Colorectal Cancer. Curr. Colorectal Cancer Rep. *11*, 259–266.
Nagumo, H., Ikenoya, M., Sakurada, K., Furuya, K., Ikuhara, T., Hiraoka, H., and Sasaki, Y. (2001). Rho-associated kinase phosphorylates MARCKS in human neuronal cells. Biochem. Biophys. Res. Commun. *280*, 605–609.
Nakagawa, O., Fujisawa, K., Ishizaki, T., Saito, Y., Nakao, K., and Narumiya, S. (1996). ROCK-I and ROCK-II, two isoforms of Rho-associated coiled-coil forming protein serine/threonine kinase in mice. FEBS Lett. *392*, 189–193.

Nakayama, M., Goto, T.M., Sugimoto, M., Nishimura, T., Shinagawa, T., Ohno, S., Amano, M., and Kaibuchi, K. (2008). Rho-Kinase Phosphorylates PAR-3 and Disrupts PAR Complex Formation. Dev. Cell *14*, 205–215.
Narumiya, S., Tanji, M., and Ishizaki, T. (2009). Rho signaling, ROCK and mDia1, in transformation, metastasis and invasion. Cancer Metastasis Rev. *28*, 65–76.
Nelson, W.J. (2003). Adaptation of core mechanisms to generate cell polarity. Nature *422*, 766–774.
Newell-Litwa, K.A., Badoual, M., Asmussen, H., Patel, H., Whitmore, L., and Horwitz, A.R. (2015). ROCK1 and 2 differentially regulate actomyosin organization to drive cell and synaptic polarity. J. Cell Biol. *210*, 225–242.
Niessen, C.M. (2007). Tight junctions/adherens junctions: basic structure and function. J. Invest. Dermatol. *127*, 2525–2532.
Nieto, M.A., Huang, R.Y.-J., Jackson, R.A., and Thiery, J.P. (2016). EMT: 2016. Cell *166*, 21–45.
Nishimura, T., and Takeichi, M. (2008). Shroom3-mediated recruitment of Rho kinases to the apical cell junctions regulates epithelial and neuroepithelial planar remodeling. Dev. Camb. Engl. *135*, 1493–1502.
Nishimura, T., Yamaguchi, T., Kato, K., Yoshizawa, M., Nabeshima, Y., Ohno, S., Hoshino, M., and Kaibuchi, K. (2005). PAR-6-PAR-3 mediates Cdc42-induced Rac activation through the Rac GEFs STEF/Tiam1. Nat. Cell Biol. *7*, 270–277.
Nobes, C.D., and Hall, A. (1995). Rho, rac, and cdc42 GTPases regulate the assembly of multimolecular focal complexes associated with actin stress fibers, lamellipodia, and filopodia. Cell *81*, 53–62.
Nobes, C.D., Lauritzen, I., Mattei, M.G., Paris, S., Hall, A., and Chardin, P. (1998). A new member of the Rho family, Rnd1, promotes disassembly of actin filament structures and loss of cell adhesion. J. Cell Biol. *141*, 187–197.
O'Brien, L.E., Jou, T.S., Pollack, A.L., Zhang, Q., Hansen, S.H., Yurchenco, P., and Mostov, K.E. (2001). Rac1 orientates epithelial apical polarity through effects on basolateral laminin assembly. Nat. Cell Biol. *3*, 831–838.
Ohashi, K., Nagata, K., Maekawa, M., Ishizaki, T., Narumiya, S., and Mizuno, K. (2000). Rho-associated Kinase ROCK Activates LIM-kinase 1 by Phosphorylation at Threonine 508 within the Activation Loop. J. Biol. Chem. *275*, 3577–3582.
Ohta, Y., Hartwig, J.H., and Stossel, T.P. (2006). FilGAP, a Rho- and ROCK-regulated GAP for Rac binds filamin A to control actin remodelling. Nat. Cell Biol. *8*, 803–814.
Omelchenko, T., and Hall, A. (2012). Myosin-IXA regulates collective epithelial cell migration by targeting RhoGAP activity to cell-cell junctions. Curr. Biol. CB *22*, 278–288.
Omelchenko, T., Vasiliev, J.M., Gelfand, I.M., Feder, H.H., and Bonder, E.M. (2003). Rho-dependent formation of epithelial "leader" cells during wound healing. Proc. Natl. Acad. Sci. *100*, 10788–10793.
Omelchenko, T., Rabadan, M.A., Hernández-Martínez, R., Grego-Bessa, J., Anderson, K.V., and Hall, A. (2014a). β-Pix directs collective migration of anterior visceral endoderm cells in the early mouse embryo. Genes Dev. *28*, 2764–2777.
Omelchenko, T., Rabadan, M.A., Hernández-Martínez, R., Grego-Bessa, J., Anderson, K.V., and Hall, A. (2014b). β-Pix directs collective migration of anterior visceral endoderm cells in the early mouse embryo. Genes Dev. *28*, 2764–2777.
Orgaz, J.L., Pandya, P., Dalmeida, R., Karagiannis, P., Sanchez-Laorden, B., Viros, A., Albrengues, J., Nestle, F.O., Ridley, A.J., Gaggioli, C., et al. (2014). Diverse matrix metalloproteinase functions regulate cancer amoeboid migration. Nat. Commun. *5*, 4255.
Osmani, N., Vitale, N., Borg, J.-P., and Etienne-Manneville, S. (2006). Scrib controls Cdc42 localization and activity to promote cell polarization during astrocyte migration. Curr. Biol. CB *16*, 2395–2405.
Osmani, N., Peglion, F., Chavrier, P., and Etienne-Manneville, S. (2010a). Cdc42 localization and cell polarity depend on membrane traffic. J. Cell Biol. *191*, 1261–1269.
Osmani, N., Peglion, F., Chavrier, P., and Etienne-Manneville, S. (2010b). Cdc42 localization and cell polarity depend on membrane traffic. J. Cell Biol. *191*, 1261–1269.
Paluch, E.K., and Raz, E. (2013). The role and regulation of blebs in cell migration. Curr. Opin. Cell Biol. *25*, 582–590.
Pandya, P., Orgaz, J.L., and Sanz-Moreno, V. (2017). Actomyosin contractility and collective migration: may the force be with you. Curr. Opin. Cell Biol. *48*, 87–96.
Pearce, L.R., Komander, D., and Alessi, D.R. (2010). The nuts and bolts of AGC protein kinases. Nat. Rev. Mol.

Cell Biol. *11*, 9–22.
Perez-Moreno, M., Jamora, C., and Fuchs, E. (2003). Sticky business: orchestrating cellular signals at adherens junctions. Cell *112*, 535–548.
Pinner, S., and Sahai, E. (2008). PDK1 regulates cancer cell motility by antagonising inhibition of ROCK1 by RhoE. Nat. Cell Biol. *10*, 127–137.
Plutoni, C., Bazellieres, E., Borgne-Rochet, M.L., Comunale, F., Brugues, A., Séveno, M., Planchon, D., Thuault, S., Morin, N., Bodin, S., et al. (2016a). P-cadherin promotes collective cell migration via a Cdc42-mediated increase in mechanical forces. J Cell Biol *212*, 199–217.
Plutoni, C., Bazellières, E., and Gauthier-Rouvière, C. (2016b). P-cadherin-mediated Rho GTPase regulation during collective cell migration. Small GTPases *7*, 156–163.
Pollard, T.D. (2016). Actin and Actin-Binding Proteins. Cold Spring Harb. Perspect. Biol. *8*, a018226.
Porter, A.P., Papaioannou, A., and Malliri, A. (2016). Deregulation of Rho GTPases in cancer. Small GTPases *7*, 123–138.
Prall, F., Ostwald, C., and Linnebacher, M. (2009). Tubular invasion and the morphogenesis of tumor budding in colorectal carcinoma. Hum. Pathol. *40*, 1510–1512.
Priya, R., Gomez, G.A., Budnar, S., Verma, S., Cox, H.L., Hamilton, N.A., and Yap, A.S. (2015). Feedback regulation through myosin II confers robustness on RhoA signalling at E-cadherin junctions. Nat. Cell Biol. *17*, ncb3239.
Priya, R., Liang, X., Teo, J.L., Duszyc, K., Yap, A.S., and Gomez, G.A. (2017a). ROCK1 but not ROCK2 contributes to RhoA signaling and NMIIA-mediated contractility at the epithelial zonula adherens. Mol. Biol. Cell *28*, 12–20.
Priya, R., Liang, X., Teo, J.L., Duszyc, K., Yap, A.S., and Gomez, G.A. (2017b). ROCK1 but not ROCK2 contributes to RhoA signaling and NMIIA-mediated contractility at the epithelial zonula adherens. Mol. Biol. Cell *28*, 12–20.
Radu, M., Semenova, G., Kosoff, R., and Chernoff, J. (2014). PAK signalling during the development and progression of cancer. Nat. Rev. Cancer *14*, 13–25.
Ramel, D., Wang, X., Laflamme, C., Montell, D.J., and Emery, G. (2013). Rab11 regulates cell-cell communication during collective cell movements. Nat. Cell Biol. *15*, 317–324.
Reffay, M., Parrini, M.C., Cochet-Escartin, O., Ladoux, B., Buguin, A., Coscoy, S., Amblard, F., Camonis, J., and Silberzan, P. (2014a). Interplay of RhoA and mechanical forces in collective cell migration driven by leader cells. Nat. Cell Biol. *16*, 217–223.
Reffay, M., Parrini, M.C., Cochet-Escartin, O., Ladoux, B., Buguin, A., Coscoy, S., Amblard, F., Camonis, J., and Silberzan, P. (2014b). Interplay of RhoA and mechanical forces in collective cell migration driven by leader cells. Nat. Cell Biol. *16*, 217–223.
Riahi, R., Sun, J., Wang, S., Long, M., Zhang, D.D., and Wong, P.K. (2015). Notch1–Dll4 signalling and mechanical force regulate leader cell formation during collective cell migration. Nat. Commun. *6*, ncomms7556.
Ridley, A.J. (2015). Rho GTPase signalling in cell migration. Curr. Opin. Cell Biol. *36*, 103–112.
Ridley, A.J., and Hall, A. (1992). The small GTP-binding protein rho regulates the assembly of focal adhesions and actin stress fibers in response to growth factors. Cell *70*, 389–399.
Ridley, A.J., Paterson, H.F., Johnston, C.L., Diekmann, D., and Hall, A. (1992). The small GTP-binding protein rac regulates growth factor-induced membrane ruffling. Cell *70*, 401–410.
Ridley, A.J., Schwartz, M.A., Burridge, K., Firtel, R.A., Ginsberg, M.H., Borisy, G., Parsons, J.T., and Horwitz, A.R. (2003). Cell Migration: Integrating Signals from Front to Back. Science *302*, 1704–1709.
Riento, K., Guasch, R.M., Garg, R., Jin, B., and Ridley, A.J. (2003). RhoE Binds to ROCK I and Inhibits Downstream Signaling. Mol. Cell. Biol. *23*, 4219–4229.
Rohatgi, R., Ma, L., Miki, H., Lopez, M., Kirchhausen, T., Takenawa, T., and Kirschner, M.W. (1999). The interaction between N-WASP and the Arp2/3 complex links Cdc42-dependent signals to actin assembly. Cell *97*, 221–231.
Rossman, K.L., Der, C.J., and Sondek, J. (2005). GEF means go: turning on RHO GTPases with guanine nucleotide-exchange factors. Nat. Rev. Mol. Cell Biol. *6*, 167–180.
Rowe, R.G., and Weiss, S.J. (2008). Breaching the basement membrane: who, when and how? Trends Cell Biol. *18*, 560–574.

Rowe, R.G., and Weiss, S.J. (2009). Navigating ECM barriers at the invasive front: the cancer cell-stroma interface. Annu. Rev. Cell Dev. Biol. *25*, 567–595.
Sadok, A., and Marshall, C.J. (2014). Rho GTPases: masters of cell migration. Small GTPases *5*, e29710.
Sadok, A., McCarthy, A., Caldwell, J., Collins, I., Garrett, M.D., Yeo, M., Hooper, S., Sahai, E., Kuemper, S., Mardakheh, F.K., et al. (2015). Rho Kinase Inhibitors Block Melanoma Cell Migration and Inhibit Metastasis. Cancer Res. *75*, 2272–2284.
Sahai, E., and Marshall, C.J. (2003). Differing modes of tumour cell invasion have distinct requirements for Rho/ROCK signalling and extracellular proteolysis. Nat. Cell Biol. *5*, 711–719.
Saito, K., Ozawa, Y., Hibino, K., and Ohta, Y. (2012). FilGAP, a Rho/Rho-associated protein kinase–regulated GTPase-activating protein for Rac, controls tumor cell migration. Mol. Biol. Cell *23*, 4739–4750.
Samuel, M.S., Lopez, J.I., McGhee, E.J., Croft, D.R., Strachan, D., Timpson, P., Munro, J., Schröder, E., Zhou, J., Brunton, V.G., et al. (2011). Actomyosin-mediated cellular tension drives increased tissue stiffness and β-catenin activation to induce epidermal hyperplasia and tumor growth. Cancer Cell *19*, 776–791.
Sanz-Moreno, V., and Marshall, C.J. (2010). The plasticity of cytoskeletal dynamics underlying neoplastic cell migration. Curr. Opin. Cell Biol. *22*, 690–696.
Sanz-Moreno, V., Gadea, G., Ahn, J., Paterson, H., Marra, P., Pinner, S., Sahai, E., and Marshall, C.J. (2008). Rac Activation and Inactivation Control Plasticity of Tumor Cell Movement. Cell *135*, 510–523.
Sanz-Moreno, V., Gaggioli, C., Yeo, M., Albrengues, J., Wallberg, F., Viros, A., Hooper, S., Mitter, R., Féral, C.C., Cook, M., et al. (2011). ROCK and JAK1 Signaling Cooperate to Control Actomyosin Contractility in Tumor Cells and Stroma. Cancer Cell *20*, 229–245.
Sari, I., Berberoglu, B., Ozkara, E., Oztuzcu, S., Camci, C., and Demiryurek, A.T. (2013). Role of rho-kinase gene polymorphisms and protein expressions in colorectal cancer development. Pathobiol. J. Immunopathol. Mol. Cell. Biol. *80*, 138–145.
Sasaki, Y., Suzuki, M., and Hidaka, H. (2002). The novel and specific Rho-kinase inhibitor (S)-(+)-2-methyl-1-[(4-methyl-5-isoquinoline)sulfonyl]-homopiperazine as a probing molecule for Rho-kinase-involved pathway. Pharmacol. Ther. *93*, 225–232.
Schramek, D., Sendoel, A., Segal, J.P., Beronja, S., Heller, E., Oristian, D., Reva, B., and Fuchs, E. (2014). Direct in vivo RNAi screen unveils myosin IIa as a tumor suppressor of squamous cell carcinomas. Science *343*, 309–313.
Sebbagh, M., Renvoizé, C., Hamelin, J., Riché, N., Bertoglio, J., and Bréard, J. (2001). Caspase-3-mediated cleavage of ROCK I induces MLC phosphorylation and apoptotic membrane blebbing. Nat. Cell Biol. *3*, 346–352.
Sebbagh, M., Hamelin, J., Bertoglio, J., Solary, E., and Bréard, J. (2005). Direct cleavage of ROCK II by granzyme B induces target cell membrane blebbing in a caspase-independent manner. J. Exp. Med. *201*, 465–471.
Shao, J., Welch, W.J., Diprospero, N.A., and Diamond, M.I. (2008). Phosphorylation of profilin by ROCK1 regulates polyglutamine aggregation. Mol. Cell. Biol. *28*, 5196–5208.
Sin, W.C., Chen, X.Q., Leung, T., and Lim, L. (1998). RhoA-binding kinase alpha translocation is facilitated by the collapse of the vimentin intermediate filament network. Mol. Cell. Biol. *18*, 6325–6339.
Steeg, P.S. (2006). Tumor metastasis: mechanistic insights and clinical challenges. Nat. Med. *12*, 895–904.
Sumi, T., Matsumoto, K., and Nakamura, T. (2001). Specific activation of LIM kinase 2 via phosphorylation of threonine 505 by ROCK, a Rho-dependent protein kinase. J. Biol. Chem. *276*, 670–676.
Takefuji, M., Mori, K., Morita, Y., Arimura, N., Nishimura, T., Nakayama, M., Hoshino, M., Iwamatsu, A., Murohara, T., Kaibuchi, K., et al. (2007). Rho-kinase modulates the function of STEF, a Rac GEF, through its phosphorylation. Biochem. Biophys. Res. Commun. *355*, 788–794.
Takegahara, N., Kang, S., Nojima, S., Takamatsu, H., Okuno, T., Kikutani, H., Toyofuku, T., and Kumanogoh, A. (2010). Integral roles of a guanine nucleotide exchange factor, FARP2, in osteoclast podosome rearrangements. FASEB J. *24*, 4782–4792.
Tambe, D.T., Corey Hardin, C., Angelini, T.E., Rajendran, K., Park, C.Y., Serra-Picamal, X., Zhou, E.H., Zaman, M.H., Butler, J.P., Weitz, D.A., et al. (2011). Collective cell guidance by cooperative intercellular forces. Nat. Mater. *10*, 469–475.
Tanaka, T., Nishimura, D., Wu, R.-C., Amano, M., Iso, T., Kedes, L., Nishida, H., Kaibuchi, K., and Hamamori,

Y. (2006). Nuclear Rho kinase, ROCK2, targets p300 acetyltransferase. J. Biol. Chem. *281*, 15320–15329.
Tepass, U., Theres, C., and Knust, E. (1990). crumbs encodes an EGF-like protein expressed on apical membranes of Drosophila epithelial cells and required for organization of epithelia. Cell *61*, 787–799.
Tominaga, T., Ishizaki, T., Narumiya, S., and Barber, D.L. (1998). p160ROCK mediates RhoA activation of Na-H exchange. EMBO J. *17*, 4712–4722.
Toyofuku, T., Yoshida, J., Sugimoto, T., Zhang, H., Kumanogoh, A., Hori, M., and Kikutani, H. (2005). FARP2 triggers signals for Sema3A-mediated axonal repulsion. Nat. Neurosci. *8*, 1712–1719.
Truebestein, L., Elsner, D.J., Fuchs, E., and Leonard, T.A. (2015). A molecular ruler regulates cytoskeletal remodelling by the Rho kinases. Nat. Commun. *6*, 10029.
Truebestein, L., Elsner, D.J., and Leonard, T.A. (2016). Made to measure – keeping Rho kinase at a distance. Small GTPases *7*, 82.
Uehata, M., Ishizaki, T., Satoh, H., Ono, T., Kawahara, T., Morishita, T., Tamakawa, H., Yamagami, K., Inui, J., Maekawa, M., et al. (1997). Calcium sensitization of smooth muscle mediated by a Rho-associated protein kinase in hypertension. Nature *389*, 990–994.
Vicente-Manzanares, M., Ma, X., Adelstein, R.S., and Horwitz, A.R. (2009). Non-muscle myosin II takes centre stage in cell adhesion and migration. Nat. Rev. Mol. Cell Biol. *10*, 778–790.
Vicente-Manzanares, M., Newell-Litwa, K., Bachir, A.I., Whitmore, L.A., and Horwitz, A.R. (2011). Myosin IIA/IIB restrict adhesive and protrusive signaling to generate front-back polarity in migrating cells. J. Cell Biol. *193*, 381–396.
Wang, H.-W., and Nogales, E. (2005). Nucleotide-dependent bending flexibility of tubulin regulates microtubule assembly. Nature *435*, 911–915.
Wang, X., He, L., Wu, Y.I., Hahn, K.M., and Montell, D.J. (2010a). Light-mediated activation reveals a key role for Rac in collective guidance of cell movement in vivo. Nat. Cell Biol. *12*, 591–597.
Wang, X., He, L., Wu, Y.I., Hahn, K.M., and Montell, D.J. (2010b). Light-mediated activation reveals a key role for Rac in collective guidance of cell movement in vivo. Nat. Cell Biol. *12*, 591–597.
Ward, Y., Yap, S.-F., Ravichandran, V., Matsumura, F., Ito, M., Spinelli, B., and Kelly, K. (2002). The GTP binding proteins Gem and Rad are negative regulators of the Rho-Rho kinase pathway. J. Cell Biol. *157*, 291–302.
Watanabe, N., Madaule, P., Reid, T., Ishizaki, T., Watanabe, G., Kakizuka, A., Saito, Y., Nakao, K., Jockusch, B.M., and Narumiya, S. (1997). p140mDia, a mammalian homolog of Drosophila diaphanous, is a target protein for Rho small GTPase and is a ligand for profilin. EMBO J. *16*, 3044–3056.
Watanabe, N., Kato, T., Fujita, A., Ishizaki, T., and Narumiya, S. (1999). Cooperation between mDia1 and ROCK in Rho-induced actin reorganization. Nat. Cell Biol. *1*, 136–143.
Weber, G.F., Bjerke, M.A., and DeSimone, D.W. (2012). A mechanoresponsive cadherin-keratin complex directs polarized protrusive behavior and collective cell migration. Dev. Cell *22*, 104–115.
Wei, L., Surma, M., Shi, S., Lambert-Cheatham, N., and Shi, J. (2016). Novel Insights into the Roles of Rho Kinase in Cancer. Arch. Immunol. Ther. Exp. (Warsz.) *64*, 259–278.
Wennerberg, K., and Der, C.J. (2004). Rho-family GTPases: it's not only Rac and Rho (and I like it). J. Cell Sci. *117*, 1301–1312.
Wennerberg, K., Forget, M.-A., Ellerbroek, S.M., Arthur, W.T., Burridge, K., Settleman, J., Der, C.J., and Hansen, S.H. (2003). Rnd Proteins Function as RhoA Antagonists by Activating p190 RhoGAP. Curr. Biol. *13*, 1106–1115.
Westcott, J.M., Prechtl, A.M., Maine, E.A., Dang, T.T., Esparza, M.A., Sun, H., Zhou, Y., Xie, Y., and Pearson, G.W. (2015). An epigenetically distinct breast cancer cell subpopulation promotes collective invasion. J. Clin. Invest. *125*, 1927–1943.
Wilkinson, S., Paterson, H.F., and Marshall, C.J. (2005). Cdc42–MRCK and Rho–ROCK signalling cooperate in myosin phosphorylation and cell invasion. Nat. Cell Biol. *7*, 255–261.
Willis, A.L., Sabeh, F., Li, X.-Y., and Weiss, S.J. (2013). Extracellular matrix determinants and the regulation of cancer cell invasion stratagems. J. Microsc. *251*, 250–260.
Wolf, K., and Friedl, P. (2011). Extracellular matrix determinants of proteolytic and non-proteolytic cell migration. Trends Cell Biol. *21*, 736–744.
Wolf, K., Mazo, I., Leung, H., Engelke, K., Andrian, U.H. von, Deryugina, E.I., Strongin, A.Y., Bröcker, E.-B.,

and Friedl, P. (2003). Compensation mechanism in tumor cell migration. J. Cell Biol. *160*, 267–277.
Wolf, K., Wu, Y.I., Liu, Y., Geiger, J., Tam, E., Overall, C., Stack, M.S., and Friedl, P. (2007). Multi-step pericellular proteolysis controls the transition from individual to collective cancer cell invasion. Nat. Cell Biol. *9*, 893–904.
Woodcock, S.A., Rooney, C., Liontos, M., Connolly, Y., Zoumpourlis, V., Whetton, A.D., Gorgoulis, V.G., and Malliri, A. (2009). SRC-induced disassembly of adherens junctions requires localized phosphorylation and degradation of the rac activator tiam1. Mol. Cell *33*, 639–653.
Woods, A., Wang, G., and Beier, F. (2007). Regulation of chondrocyte differentiation by the actin cytoskeleton and adhesive interactions. J. Cell. Physiol. *213*, 1–8.
Yamada, S., and Nelson, W.J. (2007). Localized zones of Rho and Rac activities drive initiation and expansion of epithelial cell-cell adhesion. J. Cell Biol. *178*, 517–527.
Yamaguchi, H., Kasa, M., Amano, M., Kaibuchi, K., and Hakoshima, T. (2006). Molecular mechanism for the regulation of rho-kinase by dimerization and its inhibition by fasudil. Struct. Lond. Engl. 1993 *14*, 589–600.
Yamaguchi, N., Mizutani, T., Kawabata, K., and Haga, H. (2015). Leader cells regulate collective cell migration via Rac activation in the downstream signaling of integrin β1 and PI3K. Sci. Rep. *5*, srep07656.
Yoneda, A., Multhaupt, H.A.B., and Couchman, J.R. (2005). The Rho kinases I and II regulate different aspects of myosin II activity. J Cell Biol *170*, 443–453.
Yu, B., Martins, I.R.S., Li, P., Amarasinghe, G.K., Umetani, J., Fernandez-Zapico, M.E., Billadeau, D.D., Machius, M., Tomchick, D.R., and Rosen, M.K. (2010). Structural and energetic mechanisms of cooperative autoinhibition and activation of Vav1. Cell *140*, 246–256.
Zaritsky, A., Tseng, Y.-Y., Rabadán, M.A., Krishna, S., Overholtzer, M., Danuser, G., and Hall, A. (2017). Diverse roles of guanine nucleotide exchange factors in regulating collective cell migration. J Cell Biol *216*, 1543–1556.
Zhao, Z., and Manser, E. (2005). PAK and other Rho-associated kinases--effectors with surprisingly diverse mechanisms of regulation. Biochem. J. *386*, 201–214.
Zheng, X., Carstens, J.L., Kim, J., Scheible, M., Kaye, J., Sugimoto, H., Wu, C.-C., LeBleu, V.S., and Kalluri, R. (2015). Epithelial-to-mesenchymal transition is dispensable for metastasis but induces chemoresistance in pancreatic cancer. Nature *527*, 525–530.
Zhuang, B., Su, Y.S., and Sockanathan, S. (2009). FARP1 promotes the dendritic growth of spinal motor neuron subtypes through transmembrane Semaphorin6A and PlexinA4 signaling. Neuron *61*, 359–372.

RESUME DU TRAVAIL DE THESE

La progression métastatique des cancers est responsable de 90% des décès liés à la maladie. Cette cascade est initiée par l'invasion des cellules cancéreuses du stroma péritumoral, et conduit à leur dissémination dans l'organisme. Mon travail de thèse a eu pour but d'identifier les mécanismes moléculaires et cellulaires régulant l'invasion des cancers colorectaux (CRC), qui est le 2ème cancer le plus répandu dans le monde. Grâce à une analyse réalisée sur des échantillons humains de tumeurs primaires, nous avons révélé que les cellules de CRC utilisent un mode d'invasion collective dans lequel elles gardent une architecture glandulaire spécifique des épithelia. Cette observation va à l'encontre du dogme selon lequel les carcinomes perdent leur architecture épithéliale et s'individualisent grâce à un programme transcriptionnel de la transition épithélio-mesenchymateuse, pour pouvoir envahir. Durant ma thèse, j'ai donc étudié les mécanismes régulant ce mode d'invasion collective des CRC.

Pour cela, nous avons utilisé des modèles organotypiques non invasives récapitulant l'architecture épithéliale des glandes de CRC (cystes de Caco-2 et organoïdes de xénogreffes dérivées de patients) dans des tests d'invasion utilisant du collagène-I. L'évaluation des phénotypes invasives a été faite par microscopie.

Du fait de son rôle central dans la régulation de la motilité cellulaire, nous avons émis l'hypothèse que la voie des RhoGTPases pouvait réguler l'invasion collective des CRCs. Cette voie est composée des petites Rho qui sont de petites moléculaire « interrupteurs », qui cyclent entre une forme inactive liée à un GDP et une forme active liée au GTP. On trouve également dans cette voie de signalisation leurs activateurs, les guanines nucleotide exchange factors (GEFs), et leurs inactivateurs les GTPase activtors proteins, les (GAPs). Les GEFs activent les Rho en catalysant l'échange de leur GDP en GTP, tandis que les GAPs les inactivent en promouvant leur activité GTPase.. Sous leur forme active, les RhoGTPases interagissent avec leurs effecteurs et régulent leur activité. Rac1, Cdc42 et RhoA sont les trois Rho les plus étudiés et régulent principalement la dynamique du cytosquelette d'actine. Rac1 et Cdc42 promeuvent la polymérisation d'actine, tandis que RhoA induit sa contractilité par l'intermédiaire de son effecteur ROCK et de la Myosin-II.

Afin de déterminer quels acteurs de la voie des RhoGTPases pouvait réguler l'invasion collective, nous avons réalisé un criblage utilisant des siRNA ciblant tous les effecteurs connus des RhoGTPases. Seule la déplétion des protéines ROCK, principaux effecteurs de RhoA a déclenché l'invasion collective dans notre système expérimental. Afin de confirmer le

résultat du crible, nous avons utilisé deux drogues ciblant les ROCK kinases, Y27632 et H1152. En accord avec le résultat du crible, le traitement des cystes non invasives induisait l'invasion collective. De façon à exclure un effet lignées cellulaire dépendant, nous avons réalisé des test d'invasion avec des organoïdes, qui sont par ailleurs des modèles plus physiologiques. Comme pour les cystes, nous avons observé l'induction de l'invasion par Y27632 et H1152 dans les organoides.

Deux isoformes de ROCK existent : ROCK1 et ROCK2. Pour savoir lequel des deux ou si les deux isoformes étaient impliqués dans l'invasion collective des CRC nous avons utilisé une approche shRNA nous permettant de cibler chaque isoforme de façon indépendante. La déplétion de ROCK2 et non celle de ROCK1 était suffisante à l'induction de l'invasion collective des cystes.

Pour se mouvoir de façon collective, les cohortes de cellules sont organisées en deux sous-populations fonctionnellement distincts qui induisent la polarisation du groupe invasif, avec les cellules « leader » protrusives à l'avant et les cellules « follower » à l'arrière. Pour déterminer à quelle sous-population l'inhibition de ROCK2 contribue, nous avons utilisé un mutant dominant négatif spécifique de ROCK2 et ne ciblant pas ROCK1 pour transduire des cystes non invasives de façon mosaïque. Les cellules exprimant le dominant négatif avaient trois fois plus de chance de devenir leader. De ce fait, l'inhibition de ROCK2 est suffisante pour la formation des cellules « leader ».

Sachant que Rac1 promeut la polymérisation d'actine dans les protrusion cellulaires nous avons voulu déterminer si son activité était nécessaire à la formation des cellules « leader » dans l'invasion collective. Pour cela nous avons inhibé Rac1 par NSC23766 dans des conditions d'inhibition des ROCKs. Cela conduit à une diminution de 2 à 3 fois de l'invasion induite par ROCKs. Cela démontre la nécessité de l'activation de Rac1 dans l'invasion collective en aval de ROCK2. Pour déterminer le médiateur du dialogue entre ROCK2 et Rac1, nous avons réalisé un crible utilisant des siARN ciblant toutes les GEFs de la voie des RhoGTP. Nous avons identifié les protéines FARPs comme, étant nécessaires à l'invasion collective induite par l'inhibition de ROCK. Nous avons démontré que FARP2 et non FARP1 était nécessaire pour l'invasion collective dépendant de l'inhibition de ROCK2. La surexpression de mutants actifs de FARP2 n'induisent pas d'invasion des Caco-2 : FARP2 est donc nécessaire mais non-suffisant à l'induction de l'invasion collective. Nous avons émis l'hypothèse que la Myosin-II pouvait empêcher la formation de cellule leader en maintenant le réseau cortical d'acto-myosin sous tension. L'inhibition de la Myosin-II seule n'est pas suffisante à induire l'invasion collective, cependant, la combinaison de l'activation

de FARP2 et de l'inhibition de Myosin-II est suffisante à induire l'invasion collective des cystes de Caco-2. En conclusion l'inhibition de ROCK2 induit l'invasion collective des cystes Caco-2 via son effet sur deux voies parallèles : une levée d'inhibition sur la voie FARP/Rac1 et l'inhibition de la voie Myosin-II

Durant ma thèse j'ai décrit une nouvelle voie de régulation de l'invasion collective de glandes de CRC dépendante de ROCK2. De façon intéressante, notre étude révèle un rôle anti-invasif de ROCK2 contredisant son rôle pro-invasif précédemment décrit dans l'invasion individuelle des cellules. Cela suggère que ROCK2 assure des rôles distincts en fonction du mode d'invasion adopté par les cellules cancéreuses. Ceci remet en question le bénéfice thérapeutique de l'inhibition de ROCK proposé par ces précédentes études pour prévenir l'invasion des cellules cancéreuses.

université PARIS-SACLAY | ÉCOLE DOCTORALE Cancérologie, biologie, médecine, santé (CBMS)

Etude de la contribution des voies de signalisation Rho-GTPase dépendantes à l'invasion collective des carcinomes colorectaux

Mots clés : Invasion collective, Rho-GTPases, Colorectal carcinoma

Résumé : La progression métastatique des cancers est responsable de 90% des décès liés à la maladie. Cette cascade est initiée par l'invasion des cellules cancéreuses du stroma péritumoral, et conduit à leur dissémination dans l'organisme. Mon travail de thèse a eu pour but d'identifier les mécanismes moléculaires et cellulaires régulant l'invasion du cancer colorectal (CRC), qui est le 2ème cancer le plus répandu dans le monde. Grâce à une analyse réalisée sur des échantillons humains de tumeurs primaires, nous avons révélé que les cellules de CRC utilisent un mode d'invasion collective dans lequel elles gardent une architecture glandulaire spécifique des épithelia. Afin d'étudier les voies de signalisation régulant cette invasion, nous avons utilisé des modèles organotypiques récapitulant l'architecture des glandes de CRC (cystes de Caco-2 et organoïdes de xénogreffes dérivées de patients) dans des tests d'invasion utilisant du collagène-I. Du fait de son rôle central dans la régulation de la motilité cellulaire, nous avons émis l'hypothèse que la voie des RhoGTPases pouvait réguler l'invasion collective des CRCs. Dans un criblage utilisant des siRNA ciblant tous les effecteurs connus des RhoGTPases, seule la déplétion des protéines ROCK a déclenché l'invasion collective dans notre système expérimental. Nous avons démontré que l'inhibition de ROCK2 et non de ROCK1 était suffisante pour induire la formation de cellules leader, permettant la polarisation leader/follower requise pour l'invasion collective. Nos résultats montrent que l'inhibition de ROCK2 déclenche l'invasion collective par l'inhibition de la myosine II combinée à l'activation du facteur d'échange de guanine FARP2 et Rac1. Notre étude permet donc d'identifier FARP2 comme un nouvel effecteur de ROCK2 et le positionne comme un nouveau médiateur de la signalisation croisée entre RhoA et Rac1 dans la régulation de l'invasion collective des CRC. En conclusion, nous avons décrit une nouvelle voie de signalisation dépendante de ROCK2 dans la régulation de l'invasion collective de glandes de CRC. De façon intéressante, notre étude révèle un rôle anti-invasif de ROCK2 contredisant son rôle pro-invasif dans l'invasion de cellules individuelles. Cela suggère que ROCK2 assure des rôles distincts en fonction du mode d'invasion adopté par les cellules cancéreuses et remet en question le bénéfice thérapeutique de l'inhibition de ROCK proposé pour bloquer l'invasion des cellules cancéreuses.

Deciphering the contribution of Rho-GTPases dependent signaling pathways to the collective invasion of colorectal carcinoma

Keywords : collective invasion, Rho-GTPases, Colorectal Carcinoma

Abstract : Metastatic progression of cancer is responsible for 90% of the disease related deaths. It is a multi-step process initiated by invasion of the peritumoral stroma by cancer cells which leads to their dissemination throughout the organism.
My PhD work aimed at identifying the molecular and cellular processes driving colorectal carcinoma (CRC) invasion, the 2nd most frequent cancer worldwide. Our live analysis of human primary cancer specimens revealed that CRC cells used a collective mode of invasion to disseminate, in which cells retain an epithelium specific -glandular architecture. To investigate the signaling pathways regulating this mode of invasion, we used 3D organotypic models recapitulating the features of CRC glands (Caco-2 cysts and Patient derived Xenografts (PDX) organoids) in collagen-I based organotypic invasion assays and in microscopy-based analyses. Because of their central role in the regulation of cell motility, we postulated that Rho-GTPases signaling pathways could control the collective invasion of CRC. In a siRNA based screen targeting all the known effectors of Rho-GTPases we found that only ROCK kinases down-regulation induced collective invasion in our experimental settings. We demonstrated that ROCK2 but not ROCK1 inhibition was sufficient to promote Leader cell formation, which induced the leader/follower polarization necessary for collective invasion. Our results revealed that ROCK2 inhibition triggered collective invasion through the concomitant inhibition of Myosin-II and activation of the guanine exchange factor FARP2 and RAC1. We therefore have identified FARP2 as a new effector of ROCK2 and a mediator of the RhoA-RAC1 crosstalk in the regulation of collective invasion. In conclusion our study proposes a new ROCK dependent-signaling pathway in the regulation of collective invasion of highly polarized CRC glands models. Importantly, we found ROCK2 to be an anti-invasive protein which is in contradiction with its described pro-invasive role in single cell invasion. This suggests distinct roles of ROCK which may depend on the mode of invasion adopted by the cells and questions the benefit of proposed ROCK inhibition strategies to block cancer cell invasion.

Université Paris-Saclay
Espace Technologique / Immeuble Discovery
Route de l'Orme aux Merisiers RD 128 / 91190 Saint-Aubin, France